Universidad Autónoma de Madrid

UAM
UNIVERSIDAD AUTONOMA
DE MADRID

Estudio del aparato de Golgi y del segmento inicial del axón de neuronas corticales en el cerebro normal y en la enfermedad de Alzheimer

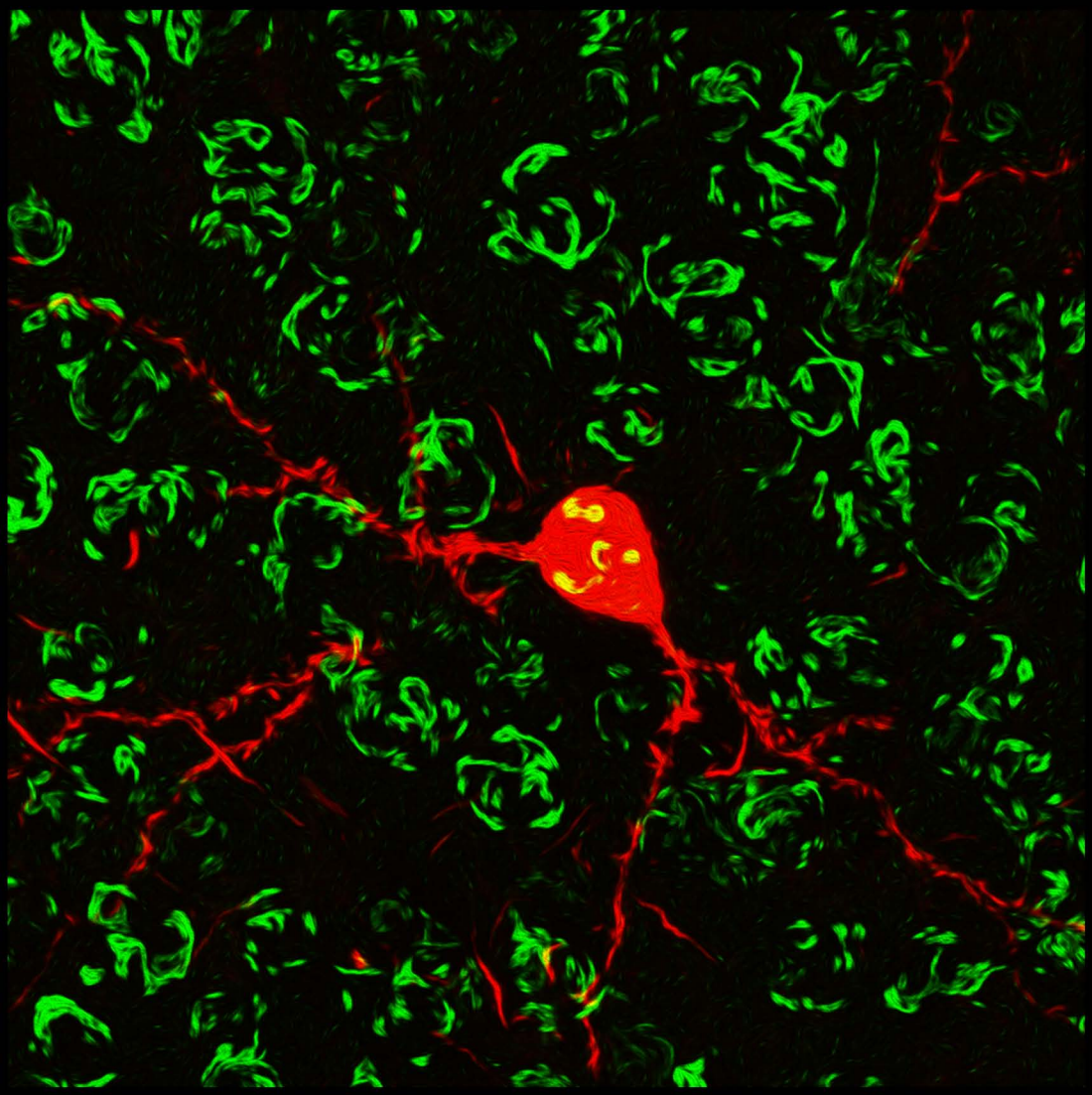

Alejandro Antón Fernández

Tesis Doctoral

2018

Universidad Autónoma de Madrid

Facultad de Medicina

Departamento de Anatomía, Histología y Neurociencia

Estudio del aparato de Golgi y del segmento inicial del axón de neuronas corticales en el cerebro normal y en la enfermedad de Alzheimer

Tesis Doctoral 2018

Alejandro Antón Fernández

Dirigida por Alberto Muñoz Céspedes y Javier DeFelipe Oroquieta

Universidad Autónoma de Madrid

Facultad de Medicina

Departamento de Anatomía, Histología y Neurociencia

Estudio del aparato de Golgi y del segmento inicial del axón de neuronas corticales en el cerebro normal y en la enfermedad de Alzheimer

Memoria presentada por

Alejandro Antón Fernández

Para optar al grado de Doctor en Neurociencias

Realizada en el Laboratorio Cajal de Circuitos Corticales (CSIC-UPM) bajo la dirección del Dr. Alberto Muñoz Céspedes y el Dr. Javier DeFelipe Oroquieta

Fdo.: Alberto Muñoz

Fdo.: Javier DeFelipe

Agradecimientos

El recorrido que ha sido necesario para llegar hasta este momento ha sido largo y se ha visto nutrido con aportaciones de todo tipo y de mucha gente diversa. En todo caso debo en primer lugar agradecer muy especialmente a Javier y a Alberto por haberme permitido participar del trabajo de un laboratorio donde la productividad y la rigurosidad no están reñidas. Me siento realmente muy afortunado y me hace mucha ilusión que mi tesis pueda llevar la firma como co-director de alguien como Javier, cuya generosidad y honradez son difíciles de encontrar en investigadores de su talla y genialidad. Nunca ha dudado un solo instante en apoyarme y darme todo lo que he podido necesitar a lo largo de estos años. Por otro lado, la productividad de estos años durante el desarrollo de esta tesis, no habría sido posible sin el concienzudo y eficiente trabajo de mi director, Alberto. Trabajar a diario con él ha sido tremendamente fácil y enriquecedor, siempre abierto y receptivo a tomar sendas de investigación inesperadas, siendo este trabajo reflejo de ello. No tengo palabras para agradecerle a ambos lo afortunado que me siento de haber podido trabajar con ellos todos estos años en los distintos proyectos en los que nos hemos embarcado. Sinceramente espero en los próximos años poder seguir trabajando de una forma u otra con vosotros.

A continuación quiero agradecer mucho a todo el Laboratorio Cajal de Circuitos Corticales por su calidad humana, cuyo ambiente y trabajo diario han permitido y facilitado enormemente el mío, que culmina ahora en esta tesis. Muchas gracias a tod@s (más los que me haya podido haber dejado por las prisas…): Ángel, Isa, Lidia Alonso, Ruth, Lidia Blázquez, Asta, Rodri, Gonzalo, Ana, Montse, Pilar, Yago, Carmen, Silvia, Diana (Sánchez), Juncal, Laura, Marta (Barbado), Mónica, Débora, Miguel...

Hoy en día el laboratorio está conformado por muchísima gente, siendo tantos ya que hay gente incluso a la que ni he podido llegar apenas a conocer. Todavía recuerdo, al principio, cuando con la excepción de Lore y de vez en cuando de Diana, era el jovenzuelo del laboratorio. Luego llegó Andrea, y después comenzaron a venir gente también de TFGs, que luego fueron TFMs y luego Tesis... (desplazándome progresivamente hacia el cambio de década): Guille, las Martas, Mamen, Sandra (y demás gente que ha pasado más fugazmente por el labo como Ernesto, Patri, Andrea…). Tengo que agradecer especialmente a Lore, por su ayuda con el trabajo experimental, sobre todo al principio cuando era un recién llegado, y por su infinita cultura Simpsons que siempre hace ameno el trabajo de poyata; a Diana y a Andrea con las que desde el principio he podido trabajar a gusto, pudiéndome apoyar siempre en ellas y aprender juntas todo lo que íbamos descubriendo; a las Martas (Turégano o chicken-girl, Domínguez o >8-girl y Montero, FPU-girl) y a Guille, con l@s que he compartido mesa y purés día tras día, y de donde tantas veces han surgido debates y fantasías hilarantes y absurdas que han hecho olvidarnos por un rato de los malos momentos del día; a Sean por introducir el *Oscurity*; y a Débora por nutrirme con víveres azucarados en las últimas horas del día y sugerirme siempre ante cualquier molestia, hielo en la rodilla.

No puedo olvidarme tampoco de las personas que me introdujeron en el mundo de la investigación y a las que estaré siempre agradecido: Paz Viveros y, sobretodo, Meritxell López-

Gallardo. Vosotras me disteis una oportunidad que he intentado no desaprovechar. Sin olvidarme de Pablo Rubio, ni de Jesús López-Redondo, quienes me introdujeron de lleno en la investigación neuroanatómica y por cuyo apoyo al principio de mi carrera siempre les estaré agradecido. Tampoco me olvido de la gente con la que trabajé en mi Facultad de Biología de la Complu y con la que compartí además una parte importante de la carrera: Patri, Virginia, Aida… y sobretodo Marcos. Con él he coincidido en todas y cada una de las distintas etapas de mi vida. Parece que el destino nos quiere decir algo…

Aunque fuéramos poca cosa, junto a Pacho (aunque él no lo supiera), he de mencionar aquí a mis compañerísimas del Máster, sin las cuales esos dos años hubieran parecido diez: Rebeca, Elisa, Carol y Tamara, a la que debo lo poco que sé todavía de estadística. Todas juntas aprendimos que comer mucho dulce nunca es malo, si el examen se acerca. Hay veces que *todo da, todo da lo mismo*…

Quiero también aprovechar para agradecer a Teresa Gómez-Isla por haberme acogido en su laboratorio durante mi estancia en Boston, y haberme tratado tan bien. Gracias a su generosidad pude aprender mucho acerca de la enfermedad de Alzheimer y conocer a gente maravillosa como María Calvo, Marta Marquie, Nil Sáez, Anurag o Juan. Ellos hicieron de mi estancia allí un verano especial.

También quiero reconocer y agradecer a aquellos roedores (ratas, ratones y hámster) y donantes humanos, de quienes hemos obtenido los cerebros y que han sido imprescindibles para que todos los estudios de esta tesis hayan podido tener lugar.

Aunque ya fuera del ámbito académico, no puedo dejar de citar a gente a la que quiero y que me hacen la vida más feliz: a mis amigos de siempre, aunque siempre anden lejos (Alfonso, César y Pablo); a Susan Saranton (la santísima trinidad de la prensa gratuita y el pipeteo); a Gorka (mi hermano de vermú); a Isa y sebas, por ser una amistad ajena al tiempo y a la distancia; a María López y a Euge, que aunque a veces odien Madrid, en el fondo la aman; a Aida Llauró (para que no me regañe más en mis sueños); a los Osos Amorosos, aunque ahora ganen sin mi (eso se va a acabar ya); a mi familia en general, y a mis hermanos (Nono y Borja) y mis padres en particular, cuyo esfuerzo, en todos los sentidos, hizo posible que pudiera estudiar lo que más me gustaba, y que acabara siendo Doctor en el área que siempre me fascinó desde que veía el programa de Punset en las madrugadas de los Domingos, antes de haber acabado mis deberes del colegio: la neurociencia. Por último y especialmente a María, por la felicidad que me aporta y de la que aprendo algo nuevo todos los días.

Gracias a todos y a toda la gente que no he citado pero de la que he podido aprender algo a lo largo de mi vida o, al menos, de cuyos impuestos han salido las becas o contratos públicos de las que he podido disfrutar este tiempo para poder investigar. Mi desagradecimiento en este caso sería para aquellas entidades y personas, más o menos públicas y muchas veces intensamente patrióticas, cuyos esfuerzos por lucrarse a costa del resto, están saliendo caro para el conjunto de la sociedad, y que en última instancia están hipotecando el futuro de la Ciencia española.

A mis abuelos Pilar y Antonio,

y a mis padres Ana y Jose

¡Cuán grande es el daño causado inconscientemente por los biógrafos de sabios ilustres al achacar las grandes conquistas científicas al genio antes que al trabajo y la paciencia!

Santiago Ramón y Cajal

ÍNDICE

RESUMEN DE LA TESIS DOCTORAL

La hipótesis inicial de esta tesis doctoral ha sido si la hiperfosforilación de la proteína tau, evento crucial en ciertas patologías del sistema nervioso como la enfermedad de Alzheimer (EA), podría inducir o estar asociado con la aparición de alteraciones microanátomicas en estructuras fundamentales para la neurona. En concreto, hemos estudiado el aparato de Golgi (AG), necesario para la correcta maduración y direccionamiento de las proteínas, y el segmento inicial del axón (SIA), una región esencial en la regulación de la excitabilidad neuronal y la generación de potenciales de acción. Para este estudio hemos empleado técnicas de inmunofluorescencia, microscopia confocal y técnicas de cuantificación en tres dimensiones y en tejido cerebral procedente de autopsias de pacientes con la EA, así como material de ratones transgénicos P301S, modelo murino de taupatía. Además, hemos estudiado los cambios que se producen en el AG y en los SIA durante el ciclo de hibernación del hámster sirio, caracterizado por la acumulación reversible de tau hiperfosforilado durante la fase de torpor y, por tanto, reproduce algunas aspectos de la EA. Los resultados obtenidos indican que durante la enfermedad de Alzheimer el aparato de Golgi de las neuronas que acumulan tau hiperfosforilado sufre alteraciones estructurales, como la fragmentación y una disminución importante de su tamaño (directamente relacionado con el nivel de actividad celular). Asimismo, hemos observado cambios plásticos en la longitud y la posición del SIA en aquellas células que desarrollan agregados de tau hiperfosforilado en la EA. La asociación de estas alteraciones estructurales del AG y el SIA y la presencia de patología tau, ha sido corroborada o apoyada por los resultados obtenidos en los modelos animales de hiperfosforilación de tau. Los resultados de este estudio evidencian a nivel celular la importancia de la patología tau en el desarrollo de la enfermedad. Las alteraciones morfológicas observadas sugieren repercusiones en el procesamiento de proteínas y en el control de la excitabilidad y de las respuestas de las neuronas donde se produce la hiperfosforilación y posterior agregación de la proteina tau. La posible disfunción de los circuitos neuronales en los que participan las neuronas con tau hiperfosforilado podría desempeñar un papel importante en el desarrollo de la enfermedad.

I - INTRODUCCIÓN

1. Neuroanatomía de la corteza cerebral

La corteza cerebral es la región del sistema nervioso que controla las funciones cognitivas superiores (Geschwind y Rakic, 2013) y cuya expansión durante la evolución explica el gran aumento del tamaño del cerebro de mamíferos (Finlay y Darlington, 1995). El tamaño de la corteza cerebral varía mucho entre las especies de mamíferos aunque el ratio entre la masa corporal y el tamaño del cerebro no correlaciona siempre con la complejidad en el comportamiento y la inteligencia.

La corteza cerebral está conformada por neuronas cuyas prolongaciones axonales y dendríticas ocupan un espacio denominado neuropilo que ocupa alrededor del 90% del volumen total (Alonso-Nanclares y cols., 2008), así como de células gliales, axones procedentes de regiones subcorticales y vasos sanguíneos.

Respecto al conjunto de neuronas presentes en la corteza, existe una amplísima diversidad de tipos cuya clasificación está constantemente en revisión (DeFelipe y cols., 2005). Una de las primeras clasificaciones de las neuronas data de los tiempos de Cajal, cuando se clasificaron según fueran células de axón largo, hoy en día neuronas de proyección, o células de axón corto, hoy en día denominadas como interneuronas (Cajal, 1892). Actualmente otro tipo de clasificación cataloga los tipos neuronales corticales según tengan o no espinas dendríticas. Las neuronas con espinas incluirían las células piramidales y las células estrelladas con espinas. Las neuronas piramidales son el tipo neuronal más importante en número de toda la corteza, representando entre el 70 y el 85% del total de neuronas. Estas son neuronas denominadas "excitadoras" al utilizar glutamato como neurotransmisor, y dan lugar a la mayoría de las sinapsis excitadoras corticales (White, 1989; Jones, 1984; Lund, 1984; revisado en DeFelipe y Fariñas, 1992). Las células estrelladas son en general células de axón corto y presentan una gran heterogeneidad morfológica. Las neuronas sin espinas por el contrario representan entre el 15 y el 30% de la población neuronal, siendo todas ellas interneuronas o neuronas de axón local. Estas utilizan de forma mayoritaria el neurotransmisor GABA (Houser y cols., 1984) lo que las convierte en células fundamentalmente inhibidoras, aunque existen algunas excepciones (Peters y cols., 1990; Gonchar y cols., 1995; Fabri y Manzoni, 1996). Se han descrito una gran variedad

de tipos de interneuronas con diferentes características morfológicas, bioquímicas y fisiológicas (DeFelipe, 1993). Respecto a la morfología por ejemplo, se pueden hallar células neurogliaformes, células en cesto pequeñas y células en candelabro cuya arborización axónica está restringida dentro del área ocupada por el campo dendrítico. Las células en cesto grandes, las neuronas Cajal-Retzius y las neuronas bipenachadas horizontales se caracterizan por tener colaterales axónicas y/o dendritas largas y horizontales. Por último las células de doble bouquet, las células de Martinotti, las neuronas con arcadas axonales, las células bipolares y las células tipo II se caracterizan por poseer colaterales axónicas y/o dendritas largas y verticales.

El otro gran grupo celular de la corteza cerebral sería el correspondiente a las células de glía que se dividen en macroglía (astrocitos, oligodendrocitos y células ependimales) y microglía. A la glía se le atribuye multitud de funciones de soporte, fagocíticas, neurotróficas, de formación de mielina, de recaptación de neurotransmisores liberados al espacio extracelular por neuronas o de servir como guía durante los procesos de migración neuronal. Los astrocitos además, intervienen directamente en el procesamiento de información habiéndose establecido el término de sinapsis tripartita, para explicar el papel activo de estos en la trasmisión de información sináptica (Perea y Araque, 2010).

Evolutivamente la corteza cerebral de los mamíferos ha surgido a partir de la región dorsal de las vesículas telencefálicas, denominada palio, con el aporte adicional de células procedentes de la región ventral de las vesículas telencefálicas, también llamada subpalio (Puelles, 2001; Molnár y cols., 2006). De acuerdo con criterios filogénicos, ontogénicos y funcionales, la corteza cerebral se ha dividido en tres regiones principales: paleocorteza, arquicorteza y neocorteza. La paleocorteza se encuentra en la base de los hemisferios y, junto con el bulbo olfatorio, constituye el cerebro olfatorio o rinencéfalo. La arquicorteza está representada primariamente por la formación del hipocampo que contiene el giro dentado, hipocampo propio o asta de Ammón (campos CA1-CA3/4) y el subículo.

La neocorteza es la región que más se ha expandido a largo de la evolución, particularmente en primates, llegando a representar por ejemplo en el hombre al menos el 85% del peso total de los hemisferios cerebrales (Jenkins y Truex, 1963). En

ella se pueden subdividir funcional y anatómicamente, diferentes regiones especializadas en el procesamiento de distintos tipos de información, contenidos en los distintos lóbulos cerebrales. Las áreas que están directamente relacionadas con el movimiento y la sensación perceptiva se denominan respectivamente áreas motoras o sensoriales, y pueden ser primarias o secundarias. Las áreas primarias son las que procesan la información tanto de entrada (aferencias sensoriales) como de salida (eferencias motoras) de forma más rápida. Las áreas sensoriales primarias por ejemplo, procedente de los distintos sentidos, reciben información de receptores periféricos con sólo unas pocas sinapsis intermedias. Así mismo la corteza motora primaria contiene neuronas que proyectan directamente a la médula espinal. Rodeando estas áreas primarias se encuentran las áreas sensoriales y motoras secundarias, en las que la información procedente de los diferentes sistemas aferentes corticales y de asociación es finalmente elaborada en complejas respuestas de aprendizaje, memoria y comportamiento. Estas áreas, denominadas también como de asociación, procesan aspectos más complejos que una única modalidad sensorial o una única función motora, como hacen las áreas primarias.

La innovación en las técnicas de tinción celular permitió a investigadores como Meynert, Lewis o Betz dar las primeras descripciones anatómicas de la corteza cerebral, apreciando una laminación cortical. Ellos observaron en mamíferos que esta, generalmente, estaba constituida por seis láminas o capas, establecidas en paralelo a la superficie pial, siendo diferenciable en base a la morfología y al tamaño de las células que los componen (Jones, 1984; Rakic, 1988; Creutzfeldt, 1995). Esta disposición laminada o estratificada de la corteza es característica de mamíferos, pero no es exclusiva de estos, dándose en varias especies de vertebrados no mamíferos.
Teniendo en cuenta el patrón de dicha laminación, la corteza de los mamíferos puede dividirse en tres tipos fundamentales (Cajal 1909-1911; Brodmann, 1919; Vogt y Vogt, 1919): isocorteza, alocorteza y mesocorteza. La isocorteza (o neocorteza) correspondería a aquella parte de la corteza que coincide con las primeras descripciones de laminación de seis capas distintas, vislumbradas a mediados del siglo XIX. La denominación de isocorteza proviene de la relativa uniformidad en el número de capas entre distintas áreas y corresponde a la corteza del neopalio. La alocorteza

por otra parte comprende la arquicorteza y la palecorteza, exhibiendo una estructura laminar más simple, compuesta de tres capas, que varía además mucho de un área a otra. La formación del hipocampo (giro dentado, el asta de Ammón y subículo) por ejemplo cuenta con tres capas de células, la capa polimórfica, la capa piramidal y la capa molecular. La mesocorteza (también llamada perialocorteza o corteza paralímbica) representa una corteza de transición entre la alocorteza y la isocorteza, con características intermedias entre estos dos tipos de cortezas. La mesocorteza se localiza en el giro parahipocámpico (pre- y parasubiculum, corteza entorrinal y corteza parahipocámpica posterior), en zonas paraolfatorias (corteza prepiriforme correspondiente a la peripaleocorteza) y en la circunvolución cingular o del cuerpo calloso (corteza cingular).

Partiendo de la descripción general de la isocorteza, las seis capas que pueden llegar a desarrollar la estructura laminar de un área cortical, serían las siguientes: la capa I o capa plexiforme externa, donde la presencia de células es muy escasa mientras que la densidad de neuropilo es muy alta, al encontrarse numerosas fibras horizontales y terminales de las células piramidales de capas subyacentes. Las capas II (capa granular externa) y III están conformadas por células piramidales pequeñas y medianas, respectivamente, y son responsables de gran parte de las conexiones cortico-corticales. La capa IV, o capa granular interna, contiene células piramidales de tamaño semejante a las de la capa II y variedades de pequeñas células estrelladas. Esta capa está ausente en la corteza motora y es el estrato fundamental de ramificación de las fibras aferentes corticales, sobretodo procedente de núcleos talámicos. Las capas infragranulares V y VI contienen las células piramidales que proyectan al tálamo, así como a otros núcleos subcorticales extratalámicos y otras áreas corticales (Feldman, 1984; Jones, 1984; White, 1989).

Aunque esta descripción de la estratificación sea general y simplista, muchas de estas características estructurales se repiten en todas las áreas corticales de todos los mamíferos; sin embargo, como formulara Lorente de Nó (Lorente de Nó, 1949), muchas áreas de la corteza cerebral poseen rasgos anatómicos específicos, no habiendo un patrón estructural único que sea aplicable a todas las regiones corticales.

2. Proteína tau

2.1 - Estructura e isoformas

La proteína tau fue descubierta por Marc Kirschner y colaboradores en 1975 (Weingarten y cols., 1975) durante la búsqueda de factores que promovieran el ensamblaje de los microtúbulos. Tau pertenece a la familia de las proteínas asociadas a microtúbulos (MAP) tipo II, que son exclusivas de células nerviosas de mamíferos (Chapin y Bulinski, 1991). Su estructura proteica se puede subdividir fundamentalmente en dos dominios unidos por una región rica en residuos de prolina. Uno de esos dominios es el extremo carboxilo terminal, denominado dominio de ensamblaje y que presenta una alta homología entre ratones y humanos, y el otro es el extremo amino terminal o dominio de proyección que difiere notablemente entre ambas especies (Wang y Mandelkow, 2015). En el dominio de ensamblaje se encuentra la región de unión a microtúbulos, que está formada por 3 o 4 secuencias repetidas (lo que da lugar a las isoformas 3R o 4R), siendo esta la región filogenéticamente más conservada y la que desempeña su función más conocida, la de unión y estabilización de microtúbulos. Dicha función es regulada por fosforilaciones en residuos de serina y treonina dentro del dominio de ensamblaje o en zonas adyacentes. El dominio de proyección está cargado negativamente, lo que repele electroestáticamente al otro dominio, facilitando la unión de la proteína a componentes de distintos tipos de membrana como la plasmática o la de orgánulos intracelulares. Esta estructura otorga a la proteína una conformación no plegada en forma de clip y con cierta tendencia a agregarse a través de las regiones de unión a microtúbulos en circunstancias en las cuales estas estén al descubierto.

La proteína tau está codificada por un único gen situado en el cromosoma 17 que incluye 16 exones y que se expresan diferencialmente en distintas isoformas por *splicing* alternativo (Neve y cols., 1986; Goedert y cols., 1989; Himmler, 1989). Se diferencian primero, según la presencia de ninguno (0N), uno (1N) o dos (2N) insertos de 29 aminoácidos en el extremo amino-terminal, así como de 3 (3R) o 4 (4R)

repeticiones de la región de unión a microtúbulos en el carboxilo terminal, según tengan o no el fragmento de repetición número 2 (R2), contenido en el exón 10 (figura 1). De esta forma se dan 6 combinaciones que dan lugar a las 6 isoformas presentes en el ser humano: 0N3R, 1N3R, 2N3R, 0N4R, 1N4R y 2N4R (Goedert y cols., 1989b). A diferencia del hombre, en el ratón adulto únicamente se expresan las tres isoformas 4R de tau (0N4R, 1N4R y 2N4R), expresándose tau 3R solamente de forma transitoria en etapas perinatales (Wang 2015). Las isoformas de tau 3R y 4R se encuentran en la misma proporción en el cerebro humano adulto y alteraciones en su ratio se han relacionado con taupatías como la demencia frontotemporal con parkinsonismo, asociadas al cromosoma 17 (FTDP-17; Blennow y cols., 2006; Ballatore y cols., 2007; Iqbal y cols., 2009). La vulnerabilidad existente en ciertas regiones implicadas en las distintas taupatías podría deberse a las diferencias regionales que se dan en el splicing alternativo.

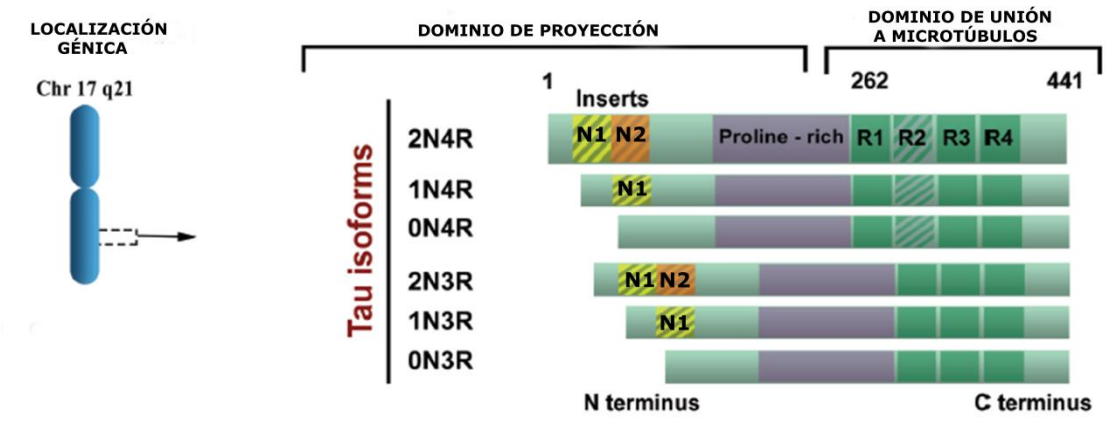

Figura 1: Esquema de las distintas isoformas de la proteína tau. Modificado de Simic (2016).

2.2 - Localización celular

La localización diferencial de la proteína tau dentro de la célula parece estar regulada mediante la fosforilación de determinados residuos peptídicos (LaPointe y cols., 2009; Xia y cols., 2015), variando además según el tipo de isoforma que sea (Wang y Mandelkow, 2015). Tau se puede encontrar tanto libre en el citosol como en el núcleo

(Sultan y cols., 2011) y asociada a microtúbulos o a distintos tipos de membrana (Arrasate y cols., 2000). Ésta es además capaz de asociarse a la membrana plasmática a través de una secuencia rica en prolina localizada en el amino terminal (Brandt y cols., 1995). Se ha descrito también a tau como una proteína periférica asociada a la membrana del aparato de Golgi (Farah y cols., 2006), habiéndose observado además en la membrana externa mitocondrial (Jung y cols., 1993).

Su distribución subcelular está regulada durante el desarrollo neuronal, habiéndose observado cómo en neuronas inmaduras la proteína tau se distribuye por todo el cuerpo celular y las neuritas. Una vez que el axón emerge y la neurona se polariza, tau acaba predominando en el dominio axonal sobre el somatodendrítico, situación que se mantiene durante el estado adulto en condiciones normales (Papasozomenos y cols., 1987). Esta distribución diferencial se ve alterada en las distintas taupatías en las que se rompe la compartimentalización mayoritaria de tau en el dominio axonal, contribuyendo probablemente a la degeneración de la neurona afectada. Los mecanismos reguladores que subyacen a la distribución diferencial de tau dentro de la neurona se desconocen en gran medida, aunque se ha observado por ejemplo que el ARN mensajero que la codifica parece tener cierta tendencia a ser trasladado al axón (Garner y cols., 1988; Aronov y cols., 2002). A su vez, a nivel proteico hay distintos factores que podrían intervenir en esta polaridad, como una mayor tasa de renovación de la proteína en el dominio somatodendrítico que en el axón, una mayor afinidad de tau por los microtúbulos axonales que los dendríticos (Hirokawa y cols., 1996; Nakata y Hirokawa, 2003; Konishi y Setou, 2009) o la formación del segmento inicial del axón como barrera contra la difusión retrógrada de tau hacia las dendritas (Li y cols., 2011).

2.3 – Funciones

La proteína tau participa en funciones diversas dependiendo del dominio neuronal en el que se encuentre. La primera función descrita de la proteína tau fue la de ensamblar y regular la dinámica de formación de los microtúbulos, permitiendo la organización del citoesqueleto y manteniendo así la morfología neuronal apropiada (Drubin y

Kirschner, 1986; Caceres y Kosik, 1990; Panda y cols., 1999). Dicha función está regulada por un proceso post-traduccional de fosforilación en residuos de serina o treonina que modulan la afinidad de unión a los microtúbulos (Drewes y cols., 1995). Además de la interacción de tau con los microtúbulos, su relación con proteínas motoras como la quinesina o dineina, explicarían su función en el transporte axonal, sobretodo en la liberación de factores tróficos y otros componentes celulares desde la terminal presináptica (Dixit y cols., 2008), así como en el trasporte de orgánulos membranosos (Drewes y cols., 1998; Stamer y cols., 2002). Parece tener además un papel relevante en la maduración neuronal durante la formación de neuritas, dado que el descenso o aumento de los niveles de expresión de tau parecen inhibir e incrementar respectivamente el número de neuritas formadas (Cáceres y Kosik, 1990).
En relación a su presencia en el núcleo celular, se ha descrito en estudios en cultivos e *in vivo* como parece jugar un papel relevante en el mantenimiento de la integridad genómica nuclear, facilitada por la capacidad que tiene de unirse tanto al ARN como al ADN (Wang y Mandelkow, 2015).

Respecto al dominio dendrítico, se ha sugerido la presencia de tau dentro de las espinas dendríticas (Ittner y cols., 2010). Aunque su papel aquí no está todavía claro, estudios in vitro sugieren que podría estar implicada en la regulación de la plasticidad sináptica, dado que la activación a nivel sináptico parece inducir su translocación desde el tallo dendrítico hacia las espinas, que son las regiones postsinápticas. Se ha observado también cómo tau parece asociarse a la quinasa FYN para enviarla a las espinas dendríticas donde fosforilaría a la subunidad 2 del receptor NMDA, estabilizando su interacción con la proteína PSD95 y potenciando así la señalización glutamatérgica (Wang y Mandelkow, 2015).

Por último, dado que se ha comprobado recientemente en estudios in vitro e in vivo cómo tau es secretada de forma fisiológica al medio extracelular, siendo además regulado por la actividad neuronal (Pooler y cols., 2013), algunos estudios han tratado de encontrar posibles funciones de ésta fuera de las células. Se ha observado por ejemplo que la proteína tau tiene una afinidad por ciertos receptores como los muscarínicos de acetilcolina M1 y M3 (Gómez-Ramos y cols., 2008), mayor incluso que el mismo ligando clásico. Se ha llegado a sugerir entonces que la función extracelular

de tau en condiciones fisiológicas podría estar relacionada con la de la comunicación celular (Wang y Mandelkow, 2015). En otro sentido, un aumento patológico de los niveles de tau en el medio extracelular como el que se da en pacientes con la enfermedad de Alzheimer (EA), podría entonces incrementar los niveles de calcio intracelular a través de la activación de receptores como los muscarínicos, lo que en determinados contextos puede inducir un efecto citotóxico. Además es interesante señalar que la distribución de estos receptores se encuentra preferentemente en neuronas localizadas en regiones muy vulnerables en la EA como la corteza entorrinal y el hipocampo.

2.4 - La fosforilación de tau y otras modificaciones post- traduccionales

La funcionalidad de tau está regida por su compleja regulación a nivel post transcripcional mediante modificaciones en distintos residuos peptídicos. Estas modificaciones pueden suponer la fosforilación, isomerización, glicación, nitración, la adición de N-acetilglucosaminas, acetilación, oxidación, poliaminación, sumoilación o la ubiquitinación de distintos residuos (Biernat y cols., 1993; Reynolds y cols., 2008; Usardi y cols., 2011; Noble y cols., 2013; Morris y cols., 2015). Algunas de estas modificaciones, como la acetilación, la glicación de tau, y sobre todo la fosforilación, parecen ser relevantes para la alteración en la funcionalidad normal de tau en taupatías como la EA.

La fosforilación es la principal y más común modificación post transcripcional de la proteína tau, la cual contiene 85 residuos peptídicos potencialmente fosforilables, que incluyen 45 serinas, 35 treoninas y 5 tirosinas, la mayoría de ellas situadas en la región rica en prolinas que flanquea la región de unión a microtúbulos (Hanger y cols., 2009). Esta fosforilación está regulada fisiológicamente durante el desarrollo, siendo muy intensa hacia el final de la sinaptogénesis, para entonces disminuir de forma importante (Bramblett y cols., 1993; Goedert y cols., 1993; Brion y cols., 1993). El complejo control de la fosforilación de tau es un mecanismo rápido para modular la dinámica de unión a microtúbulos afectando a su ensamblaje. Normalmente, la

fosforilación de residuos tanto dentro de la región de unión a microtúbulos (serinas 262, 293, 324 y 356) como fuera de ella (treoninas 214 o 231; serina 235), suponen la separación de la proteína de los microtúbulos (Lindwall y Cole, 1984; Drechsel y cols., 1992; Bramblett y cols.,1993; Yoshida y Ihara, 1993; Biernat y cols., 1993; Drewes y cols., 1995; Ksiezak-Reding y cols., 2003; Sengupta y cols., 1998), aunque no siempre es así ya que por ejemplo se ha visto que la fosforilación de la treonina en posición 50 facilita dicha unión (Feijoo y cols., 2005).

Además de la unión a microtúbulos, la fosforilación de tau regula su distribución subcelular y las interacciones moleculares con distintas proteínas como las implicadas en la regulación del transporte axonal (LaPointe y cols., 2009; Xia y cols., 2015), en el transporte de las proteínas cargo a la espinas dendríticas (Ebneth y cols., 1998) o de su asociación con la membrana plasmática (Maas y cols., 2000; Pooler y cols., 2012; Sontag y Sontag., 2013).

El estado de fosforilación de cualquier fosfoproteína como tau, depende del balance entre la actividad de quinasas y fosfatasas. Las quinasas como la glucógeno sintasa quinasa 3 (GSK-3) y la quinasa dependiente de ciclina 5 (cdk5) parecen estar implicadas en la fosforilación fisiológica de tau en el cerebro normal (Mandelkow y cols., 1992; Baumann y cols., 1993; Kobayashi y cols., 1993; Singh y cols., 1995; Muñoz-Montaño y cols., 1997; Hong y cols., 1997; Cohen, 1999). Por otro lado se ha visto cómo las fosfatasas PP1, PP2A, PP2B, PP2C, PP3 y PP5 pueden desfosforilar tau bajo condiciones in vitro (Buée y cols., 2000; Liu y cols., 2005a; Martin y cols., 2013). De entre éstas, la PP2A es la que muestra un mayor efecto sobre el estado de fosforilación de tau, suponiendo alrededor del 70% de la actividad fosfatasa relacionada con tau (Liu y cols., 2005a; Martin y cols., 2013; Sontag y Sontag, 2014). El desequilibrio en la actividad o en la expresión entre quinasas y fosfatasas puede conducir a la hiperfosforilación de tau, definido así cuando tiene alrededor del triple del nivel de fosforilación que el que tiene la proteína tau en el cerebro humano adulto normal, que son habitualmente unos 2 o 3 grupos fosfato por molécula (Köpke y cols., 1993). La hiperfosforilación de tau es de hecho un fenómeno común a todas de las taupatías, incluida la EA. En esta enfermedad se han descrito numerosas fosforilaciones patológicas en múltiples epítopos de la proteína tau reconocidos por anticuerpos como AT8 (S199/S202/T205),

AT100 (T212/S214/T217), AT180 (T231/235) y PHF-1 (S396/S404), así como en sitios individuales como S262 o S422 (figura 2). Aunque se cree que la hiperfosforilación en tau ocurriría de forma secuencial con un patrón temporal preciso, todavía no está claro cómo esta se da (Bertrand y cols., 2010). Aun así, un estudio reciente ha sugerido que las fosforilaciones en la región carboxilo terminal, concretamente en el epítopo PHF-1, se produciría desde estadios tempranos de la patología, incrementándose progresivamente a medida que se suceden estadios más tardíos, cuando la fosforilación en el epítopo AT8 es también muy relevante (Mondragón-Rodriguez y cols., 2014). La fosforilación de este epítopo podría jugar además un rol central en la regulación de otras fosforilaciones de tau en otros residuos vinculados también con la patología, dado que se ha visto como su fosforilación puede inducir una cascada de múltiples fosforilaciones en paralelo, llevadas a cabo por las quinasas GSK3-β y Cdk5 (Bertrand y cols., 2010).

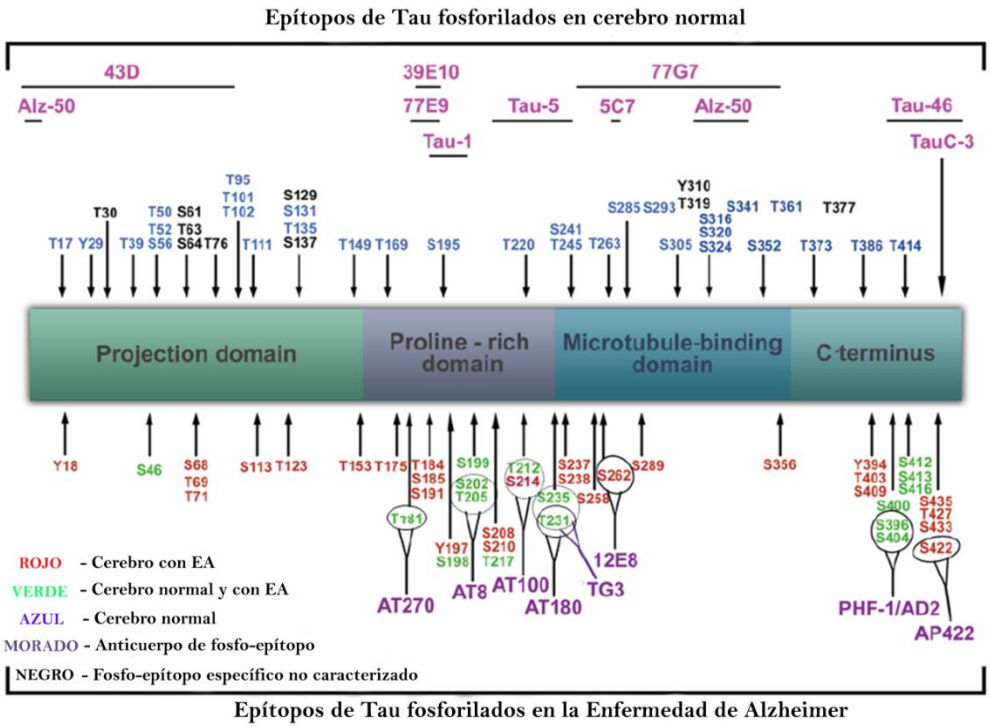

Figura 2: Esquema de los distintos epítopos fosforilables en cerebro normal y en cerebro de paciente con EA. Modificado de Simic (2016).

Los mecanismos precisos que provocan la hiperfosforilación de tau se desconocen en gran medida, pero todos ellos producen un desequilibrio del balance fosforilación/desfosforilación, debido fundamentalmente a cambios conformacionales de la proteína tau que la convierten en mejor diana para las quinasas y peor sustrato para las fosfatasas, cambios que conducen a la activación de las quinasas que fosforilan tau o a la inhibición de las proteínas fosfatasas (PP) implicadas en su desfosforilación, como PP1, PP2A, PP2B y PP2C. En línea con esta hipótesis del desequilibrio entre quinasas y fosfatasas, algunos estudios han descrito en la EA una reducción en la expresión y en la actividad de PP2A (Gong y cols., 1993; Vogelsberg-Ragaglia y cols., 2001). Junto a ello la supresión de la actividad de las fosfatasas PP1 y PP2A por el ácido okadaico reprodujo la patología tau en roedores, implicándolas también en la enfermedad (Guo y cols., 2017).

La GSK-3, la cdk5, la proteína quinasa A (PKA), la quinasa dependiente de calcio y calmodulina tipo II (CaMKII), la proteína activadora de mitógenos (MAP), la quinasa ERK1/2 o las quinasas activadas por estrés han sido también implicadas en la hiperfosforilación de tau. Las dos quinasas más relevantes en la patología de la EA son la GSK3 y la cdk5, habiéndose relacionado con todas los estadios de la patología neurofibrilar durante la enfermedad. La sobreexpresión de GSK-3 por ejemplo en células de cultivos y en animales transgénicos indujo la hiperfosforilación de tau en muchos de los sitios observados en la EA (Lucas y cols., 2001), mientras que la inhibición de su actividad a través del uso del litio, atenuó la fosforilación de tau en dichos modelos (Hong y cols., 1997).

Se han encontrado diversas modificaciones postraduccionales inductoras de cambios conformacionales que hacen más probable la hiperfosforilación de tau (Blennow y cols., 2006; Ballatore y cols., 2007; Iqbal y cols., 2009). Por ejemplo la acetilación de ciertas lisinas parecen proteger a tau de su hiperfosforilación y de su agregación en fibrillas, habiéndose visto en cerebros de pacientes con EA cómo los niveles de lisina en esos mismos residuos estaban reducidos respecto a cerebros control (Cook y cols., 2014). Sin embargo, la presencia de acetilaciones en otras lisinas de la cadena peptídica de tau se ha vinculado con procesos patológicos, habiéndose hallado éstas modificaciones en tejido procedente de pacientes con EA, que no se encuentran en

tejido control (Irwin y cols., 2013; Min y cols., 2013). Respecto a las glicosilaciones, producidas fundamentalmente en el aparato de Golgi (Stanley, 2011), la amino-glicosilación (N-glicosilación) puede facilitar la fosforilación anómala de tau al inhibir reacciones de desfosforilación (Liu y cols., 2002), mientras que la adición de grupos O-gluco-N-acetilos (O-GlcNAc), que se da en serinas y treoninas, pueden protegerla frente a la fosforilación de estos mismos residuos, dado que son potencialmente fosforilables. De hecho se ha visto como la O-GlucosilNAcetilación puede suprimir la agregación de tau hiperfosforilado, habiéndose encontrado en tejido de pacientes con EA una reducción en los niveles de estos grupos O-GlcNAc en tau (Liu y cols., 2004). Otras modificaciones conformacionales pueden ser producidas por escisiones de fragmentos peptídicos llevadas a cabo por caspasas o calpaínas, que pueden por sí solas inducir la hiperfosforilación de tau (Kovacech y Novak, 2010). Estudios recientes en cultivos primarios de neuronas y en tejido de cerebral de pacientes con taupatías, indican que las especies de tau que sufren escisiones por parte de caspasas-3 suelen tener tendencia a fosforilarse, viéndose además que tras la escisión y la hiperfosforilación, la molécula adquiere propensión a agregarse en fibrillas y en última instancia en ovillos (Zilkova y cols., 2011). Respecto a las consecuencias funcionales de la hiperfosforilación de tau, se ha comprobado en numerosas ocasiones una relación entre su fosforilación anormal y su auto-agregación, dándose el primer suceso siempre antes que la agregación. El tau disociado de los microtúbulos por su hiperfosforilación, sería más vulnerable a sufrir un proceso de auto-agregación, formando oligómeros y posteriormente agregados de tau. De hecho estudios in vitro han descrito cómo, una vez que la proteína tau se hiperfosforila, ésta es capaz de autoagregarse, sugiriendo que la hiperfosforilación puede directamente inducir agregación (Avila, 2006). Para este proceso de agregación parece que son clave unos hexapéptidos que se encuentran en los dominios repetidos R2 y R3, los cuales tienen propensión a formar estructuras de lámina beta (Mukrasch y cols., 2005). El desenmascaramiento de éste segmento peptídico sería el primer paso en el proceso de formación de las fibrillas de tau, al poderse dar la conformación en lámina beta y permitir entrelazarse con otras láminas. Para ello, los cambios conformacionales inducidos por variaciones postraduccionales como la hiperfosforilación, podrían ser clave en dicho

desenmascaramiento al alterar la estructura conformacional de la proteína, de forma que dichos hexapéptidos se quedaran al descubierto.

En las taupatías dichas fibrillas se van agregando en haces largos que al enrollarse van formando filamentos helicoidales pareados dentro de la neurona. Cuando las fibrillas se agregan una sobre otra de forma paralela, forman los denominados filamentos rectos (Crowther, 1991). Los distintos filamentos se van auto ensamblando en proporciones variables, según el tipo de taupatía, formando los ovillos neurofibrilares. En un estudio previo realizado en nuestro laboratorio (Blázquez-Llorca et al., 2010) se clasificó a las neuronas de pacientes con EA en tipo I y II en base a la cantidad intraneuronal de filamentos de tau hiperfosforilado. El tipo I se caracterizaría por la presencia de un marcaje difuso citoplasmático que no llega a formar ovillos neurofibrilares, visualizándose en las dendritas y el axón proximal un intenso marcaje fibrilar de tau hiperfosforilado. Las neuronas con un patrón de tipo II, se observa la presencia de un ovillo neurofibrilar más o menos avanzado (IIa o IIb según el grado de desarrollo del mismo, en base a la clasificación de Merino-Serrais y cols, 2013), mostrándose además, a diferencia del patrón I, una menor intensidad de marcaje fibrilar en el árbol dendrítico de la neurona.

Por último, además de la agregación y la formación de fibrillas y agregados, la separación de tau de los microtúbulos, inducida por su hiperfosforilación, facilitaría su deslocalización del dominio axonal hacia el dominio somatodendrítico y a los terminales sinápticos. Esto podría comprometer la integridad de los microtúbulos del axón así como la funcionalidad sináptica. La hiperfosforilación podría afectar también a la tasa intracelular de degradación de la proteína. Por ejemplo, la fosforilación de tau en la serina de la posición 262 o 356, hace que no sea reconocida por la proteína de choque térmico (HSP), protegiéndose así de la degradación proteosomal (Dickey y cols., 2007), lo que potenciaría su toxicidad en la célula. Por último, la hiperfosforilación podría alterar la asociación de tau con las distintas proteínas con las que interactúa en la membrana plasmática o en el aparato de Golgi, en las espinas dendríticas con la quinasa Fyn o en el núcleo con la molécula de ADN, alterando así, posiblemente, las funciones fisiológicas de ésta proteína en multitud de vías de señalización en las que está implicada (Hanger y cols., 2009).

2.5 - Secreción de tau y sus propiedades priónicas

Dado el patrón espacio temporal descrito por Braak en la evolución de la EA, donde a medida que la evolución de la enfermedad avanza, la presencia de patología tau se extiende por distintas regiones cerebrales de acuerdo a los estadios que él mismo definió (Braak y Braak, 1991), se formuló la posibilidad de que la proteína tau alterada pudiera propagarse de unas zonas a otras. Esta teoría se apoya en el hecho de que tau se ha encontrado en el medio extracelular, viéndose por ejemplo cómo en cultivos primarios de neuronas, formas fosforiladas y desfosforiladas de tau pueden secretarse de forma fisiológica (Karch y cols., 2012). Esta liberación además se puede potenciar si las neuronas, por ejemplo, son excitadas sinápticamente mediante neurotransmisión glutamatérgica (Pooler y cols., 2013). Para que tau se pueda secretar es esencial el terminal amino de la proteína, que es el que interactúa con la membrana plasmática así como con proteínas de membrana. Diversos estudios han descrito que las neuronas son capaces de liberar tau por exocitosis o mediante la secreción de exosomas derivados de cuerpos multivesiculares (Gendreau y Hall, 2013). Se observó de hecho, que el tau humano fosforilado en la treonina 181 que se secreta en exosomas de neuronas en cultivo, también se han encontrado en exosomas obtenidos del fluido cerebroespinal de pacientes en fases tempranas de la EA (Saman y cols., 2012). Se ha descrito además que dicho tau extracelular puede ser internalizado por otras neuronas mediante endocitosis, mediada o no por receptor (Wang y Mandelkow, 2015).

Se han propuesto dos posibles mecanismos de propagación de tau entre regiones distintas mediante comunicación trans-sináptica. En el primero, la degeneración de la neurona presináptica causada por factores citotóxicos asociadas a la enfermedad, podría conducir a la liberación de tau desde la membrana presináptica, permitiendo al tau difundir a través del espacio sináptico. El otro mecanismo, que se daría de forma fisiológica, consiste en la liberación de tau del terminal presináptico por exocitosis o mediante la vía exosomal o incluso por vesículas sinápticas, que podrían ser recogidas por las neuronas postsinápticas. Aunque la liberación trans-sináptica parecería la opción más lógica, se discute si la liberación de tau puede darse a través de mecanismos distintos a la transferencia directa por neuronas conectadas

sinápticamente. Por ejemplo se ha visto que la activación microglial precede la liberación de tau entre áreas conectadas anatómicamente hipocampales, indicando que la propagación de tau podría seguir a la progresión de neuroinflamación (Wang y Mandelkow, 2015).

La otra característica de tau que sustenta la hipótesis de la propagación de tau patológico como causa de la evolución espacio temporal de la EA, consiste en las propiedades de tipo priónico de tau descritas en los últimos años. Dichas propiedades se basan en el hecho de que el tau huésped puede ser inducido a agregarse en filamentos por la inyección intracerebral de extractos de cerebro con tau patológico procedente de muestras cerebrales de pacientes de Alzheimer, de ratones que expresan tau mutado en estadios tardíos o por la simple administración intraperitoneal de tau patológico (Alonso y cols., 2016). La formación de patología tau en forma de ovillos y distrofias neuríticas se pueden dar localmente en el área de inyección así como en regiones conectadas anatómicamente a dicha área (Hu y cols., 2016). Además se ha observado cómo la hiperfosforilación de tau parece determinar la propagación y la morfología de las lesiones de tau, dado que en el estudio de Hu y cols (2016), cuando el extracto aislado de tau hiperfosforilado se desfosforilaba in vitro previamente a su administración, la patología tau se reducía drásticamente modificándose incluso la morfología de los agregados de tau patológico.

3. Enfermedad de Alzheimer

La enfermedad de Alzheimer (EA) es hoy en día la principal causa de demencia asociada al envejecimiento, representando entre el 50% y el 75% de los casos de demencia senil (Morishima-Kawashima e Ihara, 2002). Según la Fundación Alzheimer España (FAE), se encuentran afectados entre el 5-7% de la población mayor de 65 años y este porcentaje aumenta alcanzando el 25% en personas mayores de 85 años. Cerca de 650.000 personas están afectadas en España y se prevé que el número de enfermos llegue casi a triplicarse en 2050 según la Sociedad Española de Neurología.

Como demencia se caracteriza por un deterioro cognitivo progresivo que no sólo afecta a la pérdida de las funciones de memoria, orientación y lenguaje, sino también a otros componentes funcionales más complejos, tales como la personalidad, el raciocinio o la resolución de problemas. En los estadios más avanzados, la dependencia mental y física del enfermo acaba siendo absoluta (Jucker y cols., 2006). Las principales características histopatológicas de la enfermedad son, primero, la presencia de placas seniles que están formadas fundamentalmente a partir de acumulaciones extracelulares del péptido β-amiloide que puede agregar, según el tipo de placa, prolongaciones dendríticas y axónicas degeneradas (neuritas distróficas) y prolongaciones gliales alteradas. En segundo lugar están los ovillos neurofibrilares intracelulares de tau hiperfosforilado (figura 3), además de otras lesiones neurofibrilares como las mismas neuritas distróficas o los llamados "hilos de neuropilo" presentes en las prolongaciones neuronales (Tolnay y Probst, 1999; Duyckaerts y Dickson, 2003).

La presencia de estas lesiones asociadas a la proteína tau, hacen que se considere a la EA como integrante del grupo de enfermedades denominadas como "taupatías". Aunque hoy en día un gran número de enfermedades están agrupadas dentro de esta categoría, en un principio Emil Kraepelin pensó que la patología neurofibrilar era exclusiva de lo que acabó denominando como EA, en homenaje a su discípulo Alois Alzheimer quien, en 1907, fue el primero en describirla (Alzheimer, 1907). Poco tiempo después se empezó a observar que la presencia de dichos agregados no era tan específica de la EA como se había asumido hasta entonces (Hübner, 1908, 1910; Alzheimer, 1911; Fuller, 1911; Schnitzler, 1911; Simchowicz, 1911; Ley, 1922; Rothschild y Kasanin, 1936; von Braunmühl, 1957).

Con el estudio en 1986 de Pollock y colaboradores (1986) se hizo patente que la patología fibrilar de tau no se restringía a la EA, al comprobarse que al igual que en la EA, los agregados filamentosos en la enfermedad de Pick y en la parálisis supranuclear progresiva, estaban también asociados con la proteína tau.

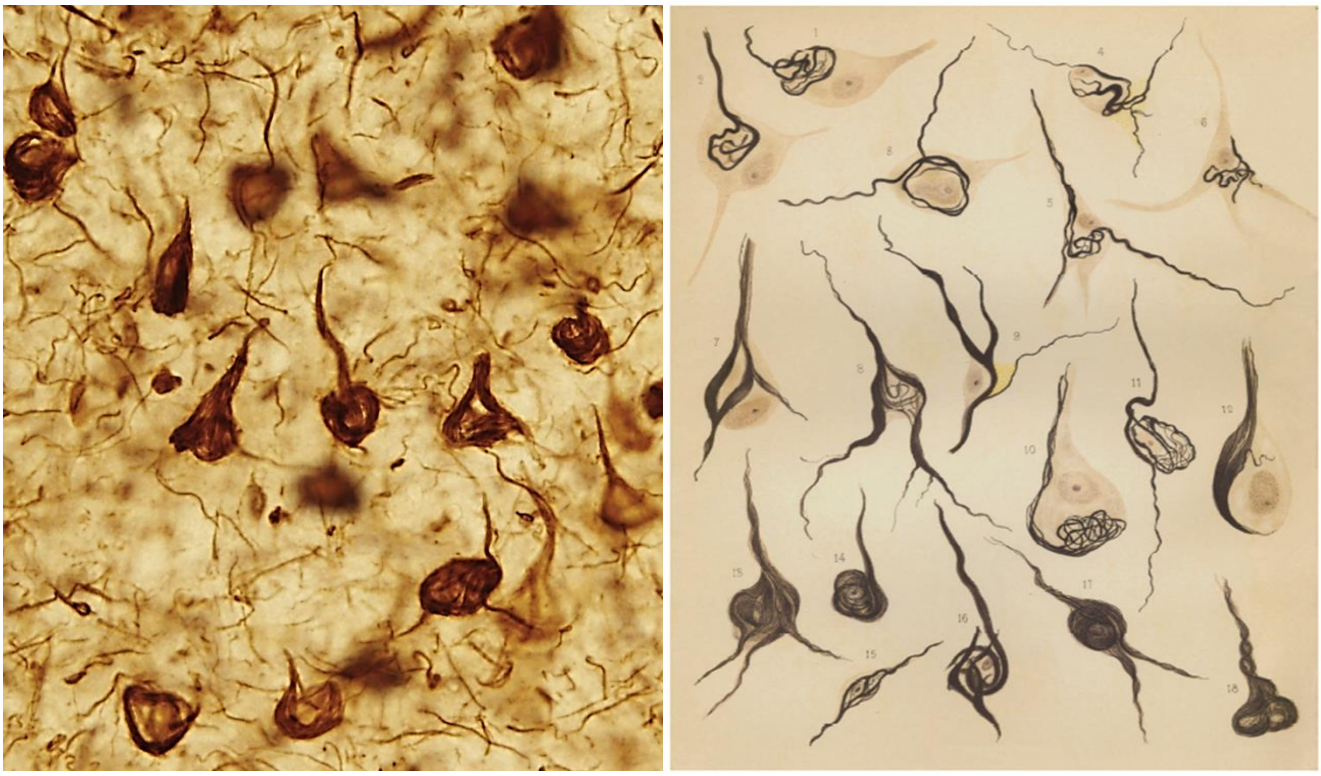

Figura 3: A la izquierda, microfotografía obtenida en nuestro laboratorio a partir de tejido *post mortem* procedente de la necorteza temporalde un paciente con EA, donde se observa la patología tau presente en la enfermedad, caracterizada fundamentalmente por la presencia de ovillos neurofibrilares. A la derecha se observan las ilustraciones de ovillos neurofibrilares realizadas por G. Sala, discípulo de Ramón y Cajal. Tomado de DeFelipe (2009).

Spillantini y colaboradores (1997) fueron los primeros en usar el término de "taupatías" para describir a la familia de enfermedades que presentan acumulaciones filamentosas de tau hiperfosforilado en neuronas y células gliales, junto con la aparición en el paciente de signos de demencia (Chin y Goldman, 1996; Spillantini y Goedert, 1998, 2013; Ballatore y cols., 2007; Ferrer y cols., 2014).

Hoy en día las taupatías se agrupan en base a distintos factores patológicos, como el papel exclusivo o no de la patología tau en la enfermedad, las isoformas de tau mayoritarias presentes en la patología o el tipo de célula afectada. En base al primer rasgo, las taupatías se clasifican como primarias o secundarias, dependiendo de si la patología tau es considerada como el mayor factor contribuyente a la neurodegeneración o si está asociada con otras patologías, respectivamente

(Williams, 2006; Dickson y cols., 2011; Kovacs, 2016). La EA pertenecería a este último grupo, dado que en esta enfermedad se sabe al menos de la presencia de patología amiloide. Respecto al segundo rasgo de clasificación, según el ratio de las isoformas 3R y 4R de tau presentes en las lesiones neurofibrilares, se han clasificado cuatro clases distintas de taupatías (Spillantini y Goedert, 1998; Williams, 2006; Dickson y cols., 2011; Kovacs, 2016). La EA pertenecería a la clase I de taupatías donde las seis isoformas de tau se presentan en un número equilibrado entre las isoformas con 3 repeticiones y las de 4. Por último, las taupatías se clasifican también según afecte a neuronas y/o a células gliales (Braak y Braak, 1991; Duyckaerts y cols., 2009; Kovacs y Budka, 2010; Montine y cols., 2012). Hay taupatías en las que la acumulación patológica de tau se da preferentemente en neuronas, como en la EA o en la enfermedad de Pick, otras mixtas en las que se puede observar dicha acumulación tanto en neuronas como en células gliales, como en la parálisis supranuclear progresiva, la degeneración cortico-basal o la argirofilia granulosa, y por último otras donde la patología tau se da preferentemente en glía como la taupatía glial globular (Kovacs, 2016). En base a las distintas clasificaciones, la EA por lo tanto se considera una taupatía secundaria de clase I y neuronal.

Precisamente en base a considerar la EA como una taupatía, Braak y Braak (1991) establecieron hace ya más de 20 años, seis estadios para describir el avance de la EA. Para ello se basaron en la presencia o ausencia de los ovillos neurofibrilares a lo largo de distintas regiones cerebrales, cuya distribución espacio-temporal sigue un patrón estereotipado y predecible (Arnold y cols. 1991; Braak y Braak 1991; Braak y cols. 2006) que aunque correlaciona con el deterioro cognitivo, no así con la demencia clínicamente diagnosticada, al darse esta solamente en los últimos estadios de la clasificación de Braak y Braak. Los primeros estadios de Braak cursan de forma asintomática, pudiendo tener la enfermedad pero sin mostrar signos de demencia. La evolución de la patología tau se puede resumir en tres fases: entorrinal, límbica e isocortical (figura 4). Los primeros ovillos neurofibrilares se observan en la corteza transentorrinal o peririnal seguido de la corteza entorrinal (estadíos I y II). En una fase posterior se observa ya una abundante presencia de patología tau en la región CA1 del hipocampo, propagándose y acumulándose en otras estructuras límbicas como el subículo de la formación hipocampal (estadio III) y la amígdala, tálamo y claustro

(estadio IV). Finalmente se observa patología tau en todas las isocortezas, siendo las áreas asociativas las primeras y más severamente afectadas (estadio V) y posteriormente las primarias sensoriales, motoras y visuales (estadio VI). Las alteraciones histopatológicas que se dan a lo largo de la EA son además muy selectivas y poco aleatorias. Por ejemplo existen áreas adyacentes a la corteza entorrinal, el subículo o la región CA1 del hipocampo, como por ejemplo el pre- y el parasubículo o el giro dentado, que carecen prácticamente de ovillos neurofibrilares (Hyman y cols., 1984;Hyman y cols., 1986; Arendt y cols., 1998; Braak y cols., 2006). Además parece haber también una selectividad de tipo celular ya que en general los ovillos neurofibrilares suelen encontrarse en células piramidales grandes más que en piramidales pequeñas o interneuronas (Hirano y Zimmerman, 1962; Mountjoy y cols., 1983; Pearson y cols., 1985; Braak y Braak, 1986; Braak y cols. 1989; Iwamoto y Emson, 1991). En la corteza entorrinal por ejemplo parecen verse afectadas preferentemente neuronas estrelladas de capa II y III, así como neuronas multipolares grandes de capa IV. En las áreas de CA1 y del subículo de la formación hipocampal, sólo se desarrolla patología tau en el estrato piramidal, y en áreas isocorticales estaría preferentemente asociada a neuronas piramidales de capa III y capa V (Hyman y cols. 1984; Arnold y cols. 1991; Braak y Braak 1991).

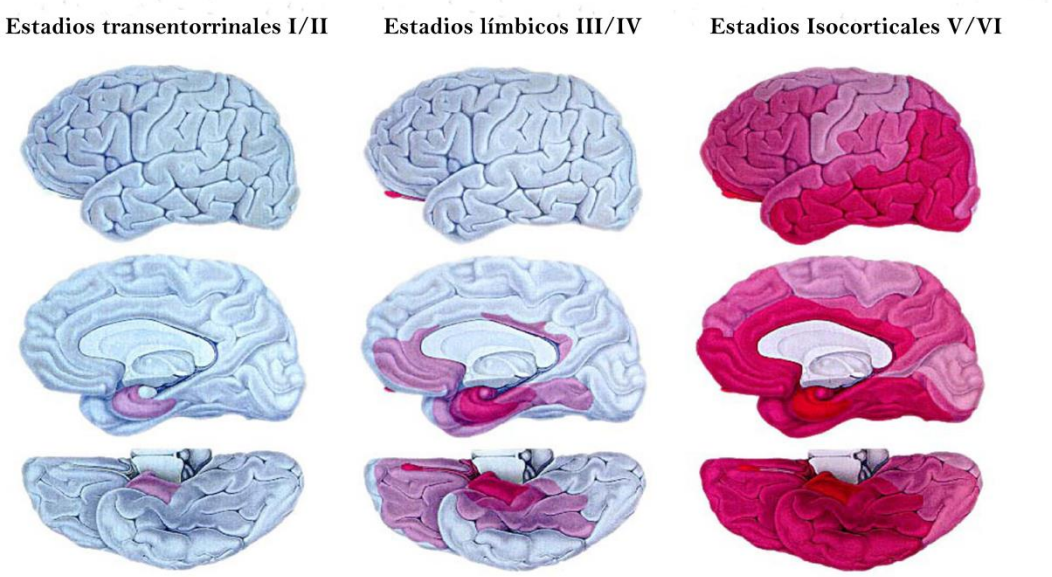

Figura 4: Esquema de los estadios neuropatológicos de la EA de acuerdo con Braak y Braak (1991). Modificado de Arendt y cols (2016).

4. Modelos de hiperfosforilación de tau

4.1 – La hibernación como modelo de fosforilación fisiológica de la proteína tau

La hibernación es un proceso fisiológico que permite a ciertos organismos sobrevivir en condiciones ambientales adversas, desarrollando la capacidad de sobrevivir durante extensos periodos con temperaturas extremas y de escasa disponibilidad de alimentos, mediante distintos mecanismos que permiten un ahorro energético muy considerable en el metabolismo de dicho animal (Von der Ohe y cols., 2006). Durante la hibernación de los mamíferos se produce un descenso generalizado de la temperatura corporal, la tasa metabólica (Buck y Barnes, 2000), la actividad neural (Strumwasser, 1959; South, 1972; Walker y cols., 1977; Igelmund, 1996), así como en procesos fundamentales para el mantenimiento celular como la transcripción, la traducción o las modificaciones postraduccionales (Frerichs y cols., 1998; van Breukelen y Martin, 2002). En pequeños mamíferos como el hámster Sirio (*mesocricetus auratus*), la hibernación es facultativa, lo que significa que entra en hibernación solo si se dan las circunstancias ambientales propicias, como que la temperatura ambiental caiga por debajo de los 5ºC y que se den largos periodos de oscuridad. La fase en la cual el animal entra en un estado de consumo de mínima energía se denomina torpor y en el caso del hámster suele durar entre 3 y 4 días. Durante este periodo la temperatura corporal llega a caer hasta los 0.5-3ºC (Strumwasser, 1959b), llegando muchas veces incluso a alcanzar temperaturas por debajo del punto de congelación (Barnes, 1989). Estos periodos de torpor son interrumpidos por cortos periodos de vigilia ("*arousal*" en inglés) donde el animal vuelve a tener una actividad cerebral y una temperatura corporal normal durante unas breves horas (Geiser, 2013; Geiser y Martin, 2013). Pasadas esas horas el hámster volvería a entrar en el estado de torpor nuevamente durante otros 3 o 4 días. Estos ciclos torpor-vigilia se repiten sucesivamente durante la hibernación, pudiendo alargarse durante meses, hasta que las condiciones ambientales mejoran y el animal entonces vuelva a un estado de eutermia.

Los animales hibernantes, como el hámster Sirio, han sido usados como modelo para estudios sobre la plasticidad de distintos procesos que se dan en el metabolismo en general, y en la fisiología y microanatomía neuronal en particular, dada la reversibilidad de estos cambios que se producen en intervalos de tiempo muy cortos (Arendt y cols., 2003). En consonancia con el descenso generalizado del metabolismo proteico, se ha observado en el tejido cerebral durante la hibernación modificaciones morfológicas relevantes como la reducción del área del cuerpo neuronal, de la complejidad del árbol dendrítico y la densidad de espinas (Popov y cols., 1992; Popov y Bocharova, 1992; von der Ohe y cols., 2006), así como del número de poliribosomas de la superficie del retículo endoplásmico rugoso, junto al aparente desensamblaje de la estructura del aparato de Golgi durante la fase de torpor (Popov y cols., 1999; Bocharova y cols., 2011).

Dado que la proteína tau es un elemento central en la remodelación del citoesqueleto durante la plasticidad sináptica y neuronal (Grubb y cols., 2011) se pensó que éste podría desempeñar un papel importante durante la hibernación y ser por tanto objeto también de modificaciones reversibles durante este proceso. Así, por ejemplo, se llegó a comprobar durante la fase de torpor que en animales hibernantes como el *suslik* europeo, la ardilla de tierra europea (Griffith y cols., 1983; Rodriguez y cols., 2003) o el hámster Sirio, la proteína tau sufre una hiperfosforilación reversible. Esto ha hecho que la hibernación en estas especies se esté utilizando como modelo de estudio de los mecanismos que regulan los procesos de fosforilación y desfosforilación de esta proteína (Arendt y cols., 2003; Hartig y cols., 2005, 2007).

El comienzo en la hiperfosforilación de tau no se da hasta que el hámster, previamente en estado de eutermia, no entra en la fase de torpor, y una vez en ella, a las pocas horas comienza a producirse un importante incremento de la fosforilación de tau (figura 5). Este incremento progresa de forma continuada durante toda la fase de torpor (Stieler y cols., 2011) hasta que el animal despierta y entra en una breve fase de vigilia, donde la fosforilación de tau se revierte completamente en pocas horas (Arendt y cols., 2003). Los epítopos fosforilados durante la hibernación son equivalentes a los que se dan en la formación de los denominados filamentos helicoidales pareados (siglas “PHF” en inglés) que conforman los ovillos neurofibrilares en la EA (Arendt y

cols., 2003; Hartig y cols., 2007; Stieler y cols., 2009; Stieler y cols., 2011; Su y cols., 2008). De hecho en las neuronas corticales donde se da esta hiperfosforilación, llega a conformarse un patrón de agregación de tau hiperfosforilado equivalente al denominado como de "preovillo" observable en pacientes de la EA. Como su propio nombre indica, este patrón sería un estadio previo a la formación de los ovillos neurofibrilares, que durante la hibernación no llega a darse y por tanto no se seguiría la evolución patológica de la EA.

Las áreas en las cuales se observa una mayor hiperfosforilación de tau durante la fase de torpor son el hipocampo ventral, la corteza entorrinal y la isocorteza, habiendo aparentemente poblaciones neuronales con distinta sensibilidad a desarrollar acúmulos de tau hiperfosforilado dentro de las mismas áreas. Por ejemplo en el hipocampo, las células piramidales de CA3 muestran una densidad de células con tau hiperfosforilado mucho mayor que en CA1, mientras que en el giro dentado no ocurre dicha hiperfosforilación (Arendt y cols., 2003).

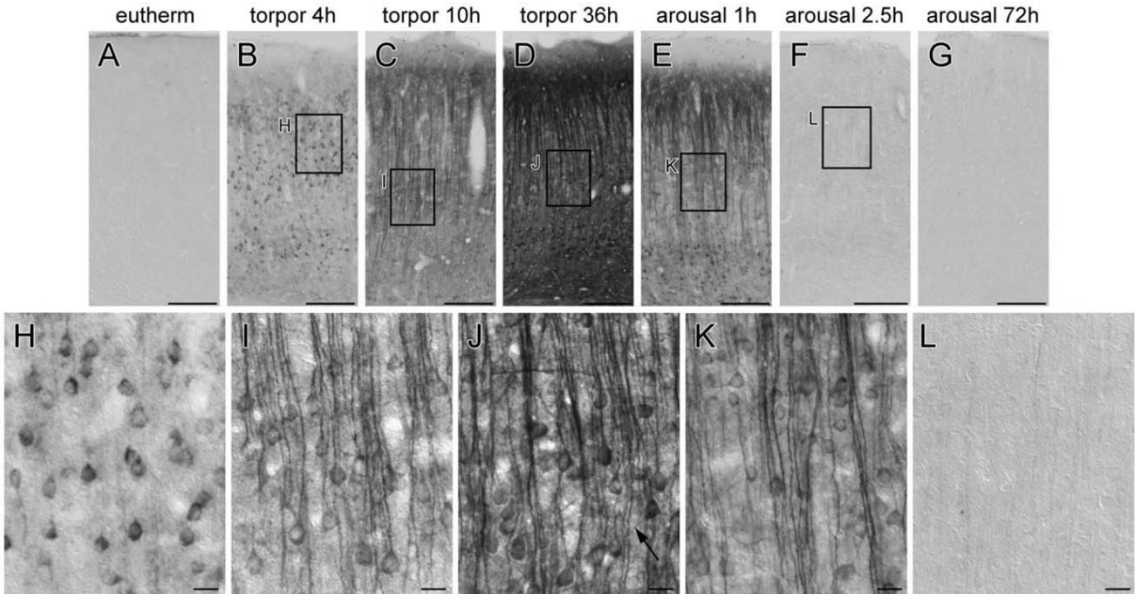

Figura 5: Microfotografías obtenidas de la corteza cerebral del hámster Sirio durante los distintos estadios de la hibernación (eutermia, torpor, vigilia) a distintos tiempos. El marcaje inmunorreactivo que se observa en las dendritas apicales y en algunos somas durante el torpor es tau hiperfosforilado en el epítopo reconocido por el anticuerpo AT8. Dicha hiperfosforilación desaparece una vez el animal despierta del torpor en fase de vigilia. Modificado de Stieler y cols (2011).

La fosforilación de tau que se da durante la hibernación, es un proceso fisiológico que la célula utiliza en procesos plásticos para hacer más dinámica la red de microtúbulos, siendo un evento fundamental, por ejemplo, durante la plasticidad neuronal y la sinaptogénesis en el desarrollo cerebral (Goedert y cols., 1993). Se ha sugerido que la regulación de la hiperfosforilación de tau estaría preservada en el cerebro mamífero adulto como un proceso natural vinculado con la neuroprotección y la plasticidad, que no tiene por qué estar asociado con efectos patológicos. La hiperfosforilación, al conferir a tau por ejemplo resistencia contra proteasas, podría ser entonces un mecanismo para estabilizar su estructura durante la fase de torpor. Del mismo modo, se ha sugerido que la fosforilación de tau en la EA podría inicialmente representar una reacción fisiológica con una función protectora que en el curso de la patogénesis eventualmente se vuelve dañina para la célula. Por lo tanto la hibernación podría representar un modelo de neuroprotección frente a condiciones de estrés (Zhou y cols., 2001) y se ha propuesto que los mecanismos neuroprotectores durante la hibernación podrían jugar una función importante también en las primeras etapas de enfermedades neurodegenerativas como la EA u otras taupatías (Arendt, 2004; Su y cols., 2008).

4.2 – El ratón transgénico P301S como modelo de agregación de tau hiperfosforilado

La mutación MAPT P301S es una de las más de 30 mutaciones encontradas en el gen de tau en pacientes con demencia frontotemporal con parkinsonismo asociado al cromosoma 17 (FTPD-17). Estas mutaciones mostraron por primera vez cómo alteraciones en la proteína tau podían llegar a ser suficientes para inducir neurodegeneración. El modelo de ratón mutante P301S (PS19), desarrollado por Virginia Lee (Yoshiyama y cols., 2007) y utilizado en el presente trabajo, sobreexpresa ese mismo gen mutado de tau, asociado a un promotor de la proteína priónica de ratón (Prnp). Este transgen incluye los cuatro dominios de unión a microtúbulos y un inserto amino-terminal (4R/1N). Su expresión en estos ratones es 5 veces mayor que el de la proteína endógena de tau, lo que lleva, a partir de los 6 meses de edad, a la

formación de ovillos neurofibrilares similares a los observados en la EA en algunas neuronas de la neocorteza, amígdala, hipocampo, tronco encéfalo y médula espinal (Yoshiyama y cols., 2007). Estos ovillos pueden ser reconocidos utilizando anticuerpos como AT8, que reconoce la serina 202 y treonina 205 fosforiladas, PHF1 en las serinas fosforiladas en 396 y 404, o AT270 en la treonina fosforilada en la posición 205. Entre los 8 y 10 meses de edad la patología tau se incrementa notablemente, decreciendo a partir de entonces dada la pérdida progresiva de neuronas que se da en esa edad. Ésta pérdida se da principalmente en el hipocampo y en corteza entorrinal, pero también en otras áreas como la neocorteza o la amígdala, donde la pérdida es más severa alrededor de los 12 meses (Yoshiyama y cols., 2007). Comportamentalmente estos ratones muestran signos de deterioro cognitivo incluyendo déficits selectivos en el aprendizaje espacial y en la habilidad de memoria asociada al laberinto de agua de Morris (Takeuchi y cols., 2011). Junto al déficit cognitivo se observan déficits motores que progresan hacia la parálisis a partir de los 10 meses, asociados normalmente con posturas encorvadas y dificultad en la ingesta, siendo la tasa de mortalidad de alrededor de un 80% hacia los 12 meses con una mediana de supervivencia de 9 meses (Yoshiyama y cols., 2007).

Por último, la patología tau y la pérdida neuronal que probablemente sean los mayores inductores de los déficits comportamentales descritos, vienen acompañados por microgliosis y astrocitosis, así como de daños en la función sináptica a partir de los 3 meses de edad. Sin embargo no se ha descrito patología amiloide en ningún área cerebral, lo que convierte a estos ratones en un buen modelo para estudiar específicamente los efectos que la patología tau en exclusiva podría tener sobre la neurona en la EA, ya que no presentan el otro elemento fundamental de la histopatología de dicha enfermedad, las placas de β-amiloide (Yoshiyama y cols., 2007).

5. Aparato de Golgi

5.1 – Descubrimiento e identificación

Aunque hoy en día está asumido que el aparato de Golgi (AG) es un orgánulo presente en todas las células eucariotas, la tarea para confirmar su existencia así como su presencia en todo tipo de células eucariotas se dilató por más de medio siglo. Su descubrimiento y primeras descripciones se realizaron en células nerviosas por investigadores muy relevantes en la historia de la neurociencia. La existencia de estructuras equivalentes al aparato de Golgi se observaron pocos años antes de su descubrimiento por Camilo Golgi y sus discípulos en 1898 (figura 6). Sin embargo estas estructuras no fueron reconocidas como pertenecientes a la misma entidad morfológica, y fueron considerados fenómenos relacionados con la división celular y con el núcleo. No fue hasta los estudios en tejido nervioso de Camilo Golgi, de quien acabó adquiriendo su nombre el orgánulo, que éste se describiría por primera vez como una entidad estructuralmente independiente. Para llegar a su visualización y descripción fue necesario que el científico italiano llegara a modificar la técnica que usaba habitualmente para teñir el tejido nervioso, denominada "*reazione nera*", mientras trataba de demostrar frente a Cajal su teoría de la *"rete nervosa diffusa*".

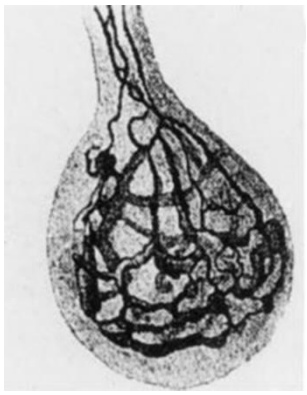

Figura 6: Primera ilustración publicada del "*Apparato reticolare interno*" realizada por Camilo Golgi. Corresponde al aparato de Golgi de una célula de Purkinje de la lechuza común. El tejido fue fijado con osmio y bicromato, usando la "*reazione nera*" junto a nitrato de plata. Tomado de Dröscher (1998).

Precisamente el neurocientífico español escribió en su autobiografía (Cajal, 1917) que en 1891 él observó mediante una reducción selectiva con sales de oro en pirámides cerebrales, la estructura que años después describiría Camilo Golgi como aparato endocelular o reticular. Sin embargo, como no pudo reproducir estos hallazgos, decidió no publicarlo. Cuando Golgi comprobó que sus observaciones eran consistentes, decidió presentar sus hallazgos en la conferencia de medicina y cirugía de la Sociedad de Pavía el 19 de abril de 1898. Aquí el científico italiano describió el "aparato reticular interno" (el término "Aparato de Golgi" fue introducido posteriormente por Nusbaum en 1913) como una estructura intracelular con una compleja organización tridimensional, independiente de la membrana celular y que normalmente se encontraba alrededor del núcleo. En las primeras décadas del siglo XX se publicaron numerosos artículos acerca del aparato de Golgi, tratando de desentrañar su naturaleza e incluso debatiendo su existencia. Hasta que, siguiendo el consejo de Palade de usar tetróxido de osmio (Palade, 1952), Dalton y Felix en 1954 (Dalton y Felix, 1954) proveyeron mediante la microscopía electrónica, la primera descripción de la estructura del aparato de Golgi en células del epidídimo. En las primeras descripciones ultraestructurales del AG, éste se describió como un apilamiento de cisternas (llamadas también lamelas) cuya superficie era curvada y lisa, rodeados por vacuolas de tamaño variable (Dröscher, 1998).

5.2 - Estructura y composición

La estructura del aparato de Golgi (AG) se compone de distintos apilamientos de cisternas de alrededor de 1 µm de diámetro (Rabouille y cols. 1995; Pelletier y cols. 2002) dispuestas unas sobre otras de forma muy próxima, así como de vesículas, que se localizan perinuclearmente y alrededor del centro de organización de microtúbulos (figura 7) (Képès y cols., 2005; Egea y cols., 2006; Yadav y Linstedt, 2011). Normalmente cada apilamiento consta de entre 4 y 11 cisternas en mamíferos, siendo característico de cada tipo celular (Rambourg, 1997). La integridad de todo el complejo estructural del orgánulo es mantenido por distintos sistemas estructurales. El espacio

que hay entre cisternas, que es además regular a lo largo de todo el apilamiento (~20 nm), está ocupado por lo que se denomina como la matriz de Golgi, que es un complejo proteico resistente a detergente y sales, donde la asociación de distintas proteínas de membrana, sobre todo las denominadas *coiled-coil* o de tipo hélice enrollada, facilitan la compactación de dicho apilamiento y hacen de soporte estructural de todo el conjunto (Franke y cols. 1972; Cluett y Brown 1992; Slusarewicz y cols. 1994; Sinka y cols. 2008). Además, el mantenimiento de la estructura está íntimamente relacionado con el citoesqueleto, tanto con los microtúbulos como con los filamentos de actina (Thyberg y Moskalewski 1985; Weidman y cols. 1993; Thyberg y Moskalewski 1999; Egea y cols. 2006; Kondylis y cols. 2007). Estas interacciones facilitan su posicionamiento y movimiento dentro de la célula, aunque también parecen ayudar a determinar la morfología del orgánulo. De hecho su morfología y localización celular se puede alterar de forma crítica cuando ambos citoesqueletos se despolimerizan. Por último, junto al soporte citoesquelético, parece ser también muy importante para la integridad del orgánulo las proteínas que regulan la dirección y la fusión de vesículas procedentes del retículo endoplásmico en las membranas de las cisternas del AG, como las proteínas de fusión de membranas (tipo SNARE).

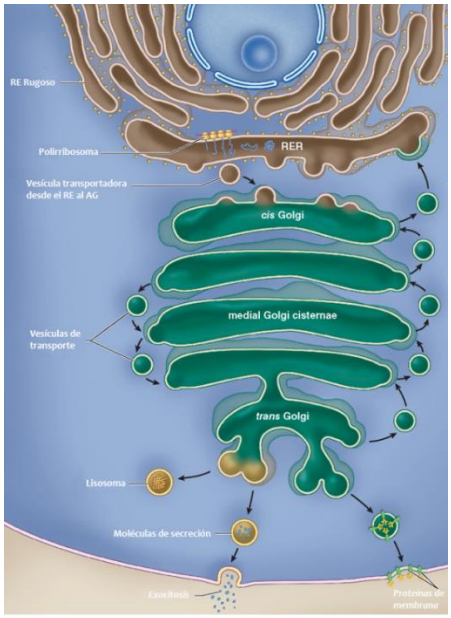

Figura 7: Esquema de la organización estructural y de las funciones celulares más conocidas del aparato de Golgi (AG). Las proteínas recién sintetizadas en el retículo endoplásmico sufrirán modificaciones post-transcripcionales a lo largo de su transporte por los distintos

compartimentos del AG, hasta la cara trans, desde donde se secretarán hasta su destino final. Tomado de Mescher (2013).

Los apilamientos de cisternas propios del AG están conservados a lo largo de la evolución eucariota. Dentro de cada tipo celular además, el volumen del AG puede variar dependiendo del nivel de síntesis proteico que suela requerir ese tipo, y se ha visto por ejemplo que un incremento en la síntesis puede llevar a un incremento en el volumen del AG, de hecho las células con una mayor tasa de actividad suelen tener orgánulos de mayor tamaño (Clermont y cols. 1993; Salehi y cols., 1995; Noske y cols. 2008). Además del volumen, la morfología del Golgi varía mucho entre tipos celulares. Por ejemplo en leucocitos o en células plasmáticas la estructura del aparato de Golgi es muy sencilla, con una morfología compacta y esférica (Rambourg 1997). Sin embargo en neuronas, el AG cubre un área muy grande del citoplasma y su morfología suele ser compleja adquiriendo muchas circunvoluciones que se distribuyen a lo largo de todo el soma alrededor del núcleo, soliéndose incluso extender parcialmente por la dendrita apical. Ésta morfología es característica de los mamíferos y se basa en la extensión lateral de túbulos desde las cisternas, hacia cisternas de otros apilamientos adyacentes, fusionando así cisternas tanto de la misma posición dentro del apilamiento, como de distintas posiciones (Rambourg 1997). Estas redes tubulares que se forman entre apilamientos se denominan zonas no compactas.

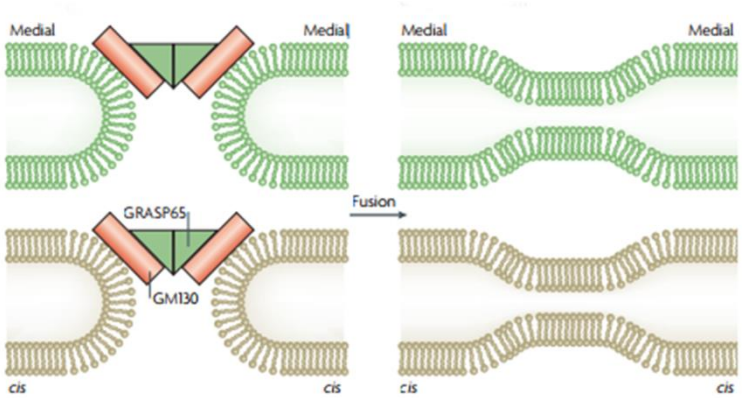

Figura 8: Esquema de las fusiones laterales del aparato de Golgi a través de la asociación de proteínas como GRASP65 y GM130, que posibilitan la formación de los denominados Golgi *ribbon*. Tomado de Voeltz y Prinz (2007).

La conjunción de los distintos apilamientos lateralmente unidos formando una red membranosa, es lo que se conoce como el Golgi *ribbon* (figura 8) y permitiría un incremento en la eficiencia de los procesos enzimáticos, particularmente en los de glicosilación (Storrie y cols., 1998; Storrie y Yang, 1998). Cada AG, o unidad de apilamiento, está polarizada constando en ambos extremos de dos redes membranosas, que serían la entrada y salida de éste. En la puerta de entrada del AG, el compartimento cis, se encuentran los denominados agrupamientos de vesículas tubulares (VTCs) que median el transporte entre el retículo endoplásmico y el AG. En la salida del AG, en la cara trans, se encuentra la red trans Golgi (TGN) que recibe proteínas que llegan desde la cisterna cis y que han pasado de forma secuencial a través de las cisternas del compartimento medial hasta llegar al compartimento trans, desde donde finalmente se distribuirán hacia distintas localizaciones celulares o se secretarán al exterior de la célula (Klumperman, 2011). Existen dos modelos distintos del funcionamiento del AG: el del transporte vesicular y el de la maduración cisternal. En el primero las moléculas son transportadas mediante vesículas a lo largo del orgánulo transportándose de cisterna en cisterna por los distintos compartimentos que conforman el AG. En este modelo las enzimas residentes del AG estarían localizadas en cada cisterna de forma permanente. Sin embargo, en el modelo de maduración las moléculas a transportar irían siendo retenidas en cisternas en maduración y por lo tanto estas serían estructuras dinámicas donde la nueva cisterna es continuamente ensamblada en el lado cis y la cisterna madura es continuamente desensamblada en el lado trans (Lowe y cols., 2002).

A pesar del alto grado de organización del AG y de lo que se pensaba hasta hace no mucho, se ha demostrado que este orgánulo es muy dinámico. Por una parte, experimentos en 1990 fueron los que comenzaron a cambiar la noción de que las cisternas del AG eran compartimentos estáticos. Para empezar se observó cómo las proteínas residentes del AG rotan a lo largo de distintos compartimentos, pudiendo moverse rápidamente entre diferentes cisternas. A lo largo de su estructura se da además un balance de flujo tanto anterógrado, hacia la cara trans, como retrogrado, de vuelta hacia el retículo endoplásmico desde el compartimento cis. Junto a esto, en distintos procesos fisiológicos como la división mitótica, en respuesta al estrés

ambiental, bajo el efecto de ciertos fármacos como la brefeldina A o en distintas condiciones patológicas, se pueden dar distintas alteraciones que pueden afectar tanto al transporte a través de las membranas del orgánulo como a su morfología. De forma que bajo estas circunstancias pueden redistribuirse las distintas proteínas residentes del AG y además desensamblarse y reensamblarse la estructura entera del AG de manera reversible en cuestión de apenas unas pocas horas (Levine y cols., 1995; Glick, 2002; Fan y cols., 2008).

5.3 - Función celular en neuronas

Tras el descubrimiento de la existencia del AG como entidad autónoma celular, pronto se apuntó desde el mismo laboratorio de Golgi su posible función en la vía secretora de la célula (Bentivoglio, 1998). Desde hace ya un tiempo este orgánulo está considerado un elemento fundamental de la vía secretora. Éste recibe desde el retículo endoplásmico prácticamente todas las moléculas de secreción recién sintetizadas, así como las proteínas transmembrana que se distribuirán a lo largo de toda la célula. Las proteínas a las que les falta una señal específica de destino, serán por defecto empaquetadas en vesículas de la vía constitutiva hacia la membrana plasmática (Mellman y Simons 1992; Bossard, 2007; De Matteis y Luini, 2008). En el caso de células polarizadas como las neuronas, emergen además rutas adicionales desde la red del compartimento trans del AG (TGN) para liberar proteínas de forma específica hacia el dominio axónico o hacia el dendrítico (Dotti y Simons 1990; Wandinger-Ness y cols. 1990). De hecho distintos estudios farmacológicos han demostrado que muchas de las proteínas destinadas al transporte axonal de vía rápida, como los neurotransmisores peptídicos (Purves, 2002), son procesadas a lo largo del AG desde donde son enviadas hacia el dominio axónico (Hammerschlag y cols., 1982). Este orgánulo tiene por tanto una función fundamental en el tráfico axónico, clave para el mantenimiento de las sinapsis, y la alteración de su funcionamiento por tanto tiene graves consecuencias para el correcto funcionamiento de la neurona.

Las moléculas que salen desde el AG a su destino final, han sido ya procesadas y modificadas de forma secuencial al atravesar los distintos compartimentos del orgánulo. Dentro de los mecanismos de procesamiento proteico se incluyen fundamentalmente la glicosilación, fosforilación, sulfación o el corte proteolítico de residuos peptídicos. Éstos varían dependiendo del destino final de la proteína, así como de su estructura y de la variedad de enzimas de procesamiento presentes en el AG, que variará según el tipo celular. La glicosilación es un proceso fundamental y muy común en el procesamiento de buena parte del conjunto de proteínas celulares, donde se da la síntesis y adición (o eliminación) de los carbohidratos de las glicoproteínas por parte de las glicosiltransferasas (o glicosilasas) residentes en la membrana del AG (Stanley, 2011). En éste orgánulo se sintetizan además glicolípidos y la esfingomielina procedentes de la ceramida, que es sintetizada previamente en el retículo endoplámico, y que son elementos muy relevantes para la fisiología del sistema nervioso (Jeckel y cols., 1990).

Hasta los años 90 del siglo pasado, las principales funciones que se atribuían al aparato de Golgi era la de participar en el procesamiento y secreción de las proteínas sintetizadas en la célula, y no había indicios de que tuviera alguna función en la señalización celular. Sin embargo, a comienzos de los años 90 distintos estudios encontraron en este orgánulo niveles muy altos de calcio, lo que sugirió la posibilidad de que tuviera un papel en la regulación del calcio intracelular. Hasta entonces, sólo el retículo endoplasmático y la mitocondria eran considerados como los únicos almacenes de calcio de la célula. A partir de dichos estudios comenzó a observarse que el AG era un almacén de calcio intracelular tan importante como los otros dos, dado que en condiciones normales las concentraciones de calcio en el AG son similares o incluso más altos que los del RE y significativamente mayores que las encontradas en la mitocondria (Chandra y cols., 1991; Xue y cols., 1994; Pezzati y cols., 1997).

Además, la localización de distintas proteínas reguladoras de los niveles de calcio en sus membranas como el canal receptor de calcio inositol-1,4,5 trifosfato (IP3R), la calcio ATPasa del retículo sarco (endo)plásmico (SERCA) y la calcio ATPasa de vías secretoras (SPCA), pusieron de relieve su importante papel en la regulación del calcio intracelular (Durr y cols., 1998; Porat y Elazar, 2000) y la importancia de su integridad

estructural para una homeostasis normal de calcio (Cifuentes y cols., 2001; Vanoevelen y cols., 2005).

5.4 - Proteínas estructurales principales

GM130 y GRASP65

Tanto la proteína de matriz del compartimento Cis (GM130), como la proteína de reensamblado y apilamiento del Golgi (GRASP65) serían parte de la matriz permanente del AG que mantiene la entidad e identidad del orgánulo. GM130 es una proteína periférica de membrana unida a la membrana celular y localizada principalmente en el compartimento cis del AG (Nakamura y cols., 1995). Fue de las primeras proteínas utilizadas como marcador del AG, siendo adscrito al grupo de proteínas denominadas "golginas". Éstas son proteínas ricas en estructuras enrolladas en espiral que se localizan específicamente en el AG (Munro, 2011). Está muy conservada en vertebrados y muestra incluso una amplia conservación dentro de todos los metazoos. GRASP65 por su parte es también una proteína periférica de membrana estrechamente unida a la membrana del Golgi, cuyo papel principal sería el de soporte estructural, al estar implicada en el apilamiento de las cisternas. Dada la estrecha asociación estructural entre ambas proteínas en la membrana del AG, las funciones descritas para ambas parecen ser equivalentes (Puthenveedu y cols., 2006). Ambas están estrechamente unidas en el lado cis de los apilamientos cisternales, así como en los espacios entre cisternas. GM130 es la que se uniría al segundo dominio tipo PDZ de GRASP65, mientras esta haría de puente de unión de GM130 a la membrana del AG. Esta estrecha asociación entre ambas proteínas formaría un complejo que, junto a otras proteínas, es clave en la unión de apilamientos de Golgi adyacentes que permiten la unión lateral de estos y que forman el llamado *Golgi ribbon* característico de mamíferos y que es fundamental por ejemplo para los procesos de glicosilación que se dan en este orgánulo (Putheenvedu y cols. 2006). La formación de estas uniones laterales gracias, a la formación de dicho complejo proteico, sirve además de punto de control para la progresión del ciclo celular, dado que la regulación de las

fosforilaciones en dichas proteínas es clave en el desensamblaje y reensamblaje de su estructura durante la mitosis (Barr y cols., 1997, 1998, Shorter y Warren, 1999; Puthenveedu y Linstedt 2001; Puthenveedu y cols., 2006; Nakamura y cols., 1995, 2010). El complejo que forman facilita además la fusión de vesículas a la membrana del Golgi, cumpliendo un papel fundamental en el transporte de vesículas entre el retículo endoplásmico y el AG, así como entre las cisternas de este último.

Golgina84

La golgina84 es una proteína integral de membrana no vinculada a la matriz del aparato del Golgi. Está además asociada con proteínas GTPasas tipo rab, y se encuentra en la cara cis del AG aunque en un gradiente que se incrementa hacia la cara trans (Bascom y cols., 1999; Diao y cols., 2003; Satoh y cols., 2003; Sohda y cols., 2010). Distintos estudios han demostrado el papel de esta proteína en el mantenimiento de la arquitectura del AG, destacando su papel en la promoción y el mantenimiento de las fusiones laterales entre cisternas que facilitan el ensamblaje del *Golgi ribbon* (Diao y cols., 2003). Se le ha asignado también un papel relevante en la regulación de la unión de vesículas a membranas, gracias a su asociación con proteínas rab (Waters y Hughson, 2000; Whyte y Munro, 2002). Para estudiar la funcionalidad de la proteína, se observó recientemente cómo la interferencia en la expresión normal de la golgina84 inducía la ruptura de las uniones laterales de las cisternas, así como la fragmentación del AG. Esta alteración de la estructura del AG vino además acompañado de la fosforilación de tau en distintos epítopos relevantes en taupatías como la enfermedad de Alzheimer (Jiang y cols., 2014).

MG160

La proteína medial del AG (MG160) es una sialoglicoproteína tipo I integral de membrana rica en cisteínas y muy conservada en la filogenia que está presente sobretodo en el compartimento medial del AG (Gonatas y cols., 1989; Gonatas y cols., 1995). Dada la elevada expresión de MG160 en neuronas durante el desarrollo temprano, se ha sugerido que esta proteína debe tener un papel importante en la biogénesis y en el funcionamiento del AG. Se ha descrito también su participación en la regulación del tráfico y procesamiento de factores de crecimiento fibroblástico (FGF),

siendo MG160 capaz de unirse a factores como FGF 1,2 y 4 (Burrus y cols., 1992). De hecho su secuencia aminoacídica es prácticamente idéntica a la de las proteínas receptoras de factores de crecimiento de pollo (CFR) y de la ligando de selectina 1 (ESL-1), que son receptores de factores de crecimiento (Burrus y cols., 1992; Gonatas y cols., 1995; Steegmaier y cols., 1995; Mourelatos y cols., 1996).

5.5 - Alteraciones estructurales en neuropatologías

El AG neuronal sufre una gran variedad de alteraciones estructurales en diversas enfermedades neurodegenerativas. Algunas de ellas suponen la pérdida de la configuración típica en red, que es reemplazada por elementos pequeños desconectados (fragmentación), o por una disminución en su tamaño (Mourelatos y cols., 1996; Fujita y cols., 2000, 2006; Baloyannis, 2014). La primera enfermedad humana en la que se describió la fragmentación o dispersión del AG fue en la esclerosis lateral amiotrófica esporádica (Gonatas y cols., 1992), si bien ya Cajal había descrito alteraciones en la estructura de este orgánulo en células situadas en los márgenes de lesiones mecánicas (figura 9; DeFelipe y Jones, 1991). De forma más reciente diversos estudios han descrito la fragmentación del AG en células apoptóticas (Aslan y Thomas, 2009) y tras procesos isquémicos (Hu y cols., 2007).

Respecto a las enfermedades neurodegenerativas en las que se ha descrito alteraciones del AG, se incluyen la EA (Salehi y cols., 1994), la enfermedad de Creutzfeldt-Jacob (Sakurai y cols., 2000), la ataxia espinocerebelar de tipo 2 (Huynh y cols., 2003), la atrofia sistémica múltiple (Takamine y cols., 2000), la enfermedad de Parkinson (Fujita y cols., 2006).

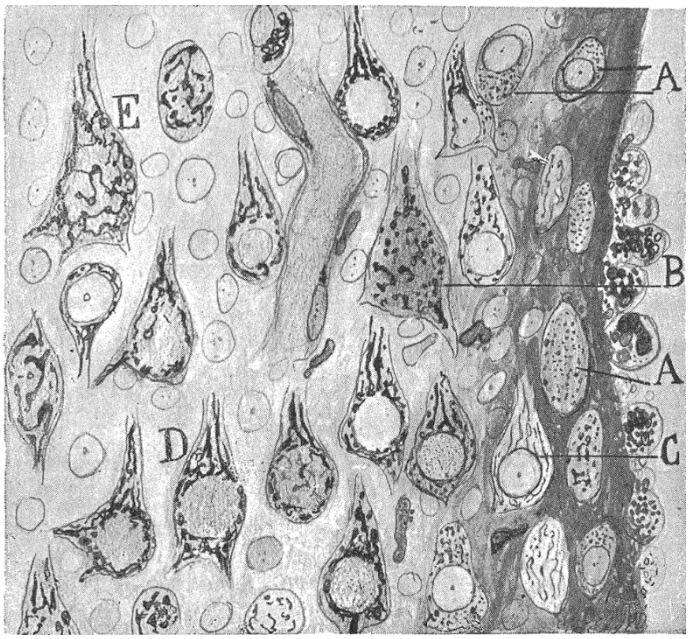

Figura 9: Ilustración de Ramón y Cajal en la que se representa el borde de una herida en el cerebro de un gato de 20 días de edad. En A y B se representan célula y neurona piramidal respectivamente, cuyo AG estaría fragmentado. En D y en E se ilustran células nerviosas con el AG en un estado normal. Tomado de Defelipe y Jones (1991).

Distintos estudios han sugerido que las alteraciones del AG que se observan en dichas patologías, como la fragmentación de su estructura, podría representar un evento temprano previo al inicio de los síntomas clínicos de dichas enfermedades (Karecla y Kreis, 1992; Mourelatos y cols., 1996; Bellouze y cols., 2014; Haase y Rabouille, 2015; Bexiga y Simpson, 2013), lo que podría convertir al AG en un hipotético índice de neurodegeneración celular (Stieber y cols., 1996). Es muy probable que la fragmentación del AG en estos procesos neurodegenerativos no tenga una única causa, sino que estén involucrados distintos mecanismos patológicos que puedan afectar a distintas proteínas del AG, como las involucradas en el mantenimiento de su estructura. En el caso de la EA distintos estudios llevados a cabo en modelos animales de la enfermedad han relacionado los dos principales eventos histopatológicos de la enfermedad, la acumulación de proteínas β-amiloide y la hiperfosforilación de tau, con la fragmentación del AG (Liazoghli y cols., 2005; Jiang y cols., 2014, Joshi y Wang, 2015). Sin embargo la secuencia temporal y la relación causal entre la acumulación de placas de amiloide o de ovillos neurofibrilares de tau y las alteraciones del AG a lo

largo de la evolución de la enfermedad no se ha caracterizado hasta el momento. Ambos eventos patológicos podrían afectar al AG y a su vez el estado de éste último podría influir sobre dichos procesos patológicos. Por ejemplo, estudios llevados a cabo principalmente en cultivos celulares han mostrado que el funcionamiento correcto del AG es necesario para la producción de Aβ y para el tráfico y la maduración de la proteína precursora de amiloide (APP) y sus enzimas de procesamiento (Burgos y cols., 2010; Choy y cols., 2012; Greenfield y cols., 1999; Huse y cols., 2002; Joshi y cols., 2015). A su vez se ha observado en un modelo murino que genera placas de amiloide (APPswe/PS1ΔE9), que la acumulación de los péptidos Aβ llevan a la fragmentación del AG, mediado por la fosforilación de GRASP65 a través de la quinasa cdk5, lo que a su vez parece que acelera el tráfico de APP y la producción de Aβ (Joshi y cols., 2015, Joshi y Wang, 2015). Junto a esto, un estudio realizado en neuronas en cultivo ha demostrado que la desorganización del AG, puede inducir la hiperfosforilación de tau (Jiang y cols., 2014). Por tanto ambos procesos patológicos parecen estar de una forma u otra interrelacionados con la alteración de la estructura del AG.

5.6 - Relación entre la fosforilación de tau y la fragmentación del aparato de Golgi

En los últimos años los resultados de distintos estudios han encontrado una estrecha relación entre la hiperfosforilación de tau, la organización de microtúbulos y la alteración estructural del AG. La presencia de la proteína tau, así como de numerosas quinasas relacionadas con su fosforilación, en las membranas del AG, hizo que se sugiriera el papel de tau como intermediario entre dicho orgánulo y los microtúbulos (Farah y cols., 2006). Se sabe que la integridad de la estructura del AG depende del citoesqueleto. De hecho la despolimerización de la actina o la ruptura de los microtúbulos, causa alteraciones estructurales en el AG como la fragmentación, cambios en su forma o en su localización dentro de la neurona (Egea y cols., 2006; Cole y cols., 1996). Por tanto, la afectación del esqueleto de microtúbulos causado por la hiperfosforilación de tau, podría alterar la estructura del AG. En todo caso, se ha visto cómo la afectación de los microtúbulos produce la hiperfosforilación de tau y la

fragmentación del orgánulo de una forma reversible. Por ejemplo, durante la división mitótica de diferentes tipos celulares, la fragmentación del AG se da de forma simultánea a la fosforilación general de tau en epítopos conocidos por estar fosforilados también en la enfermedad de Alzheimer como PHF1, AT8, AT100 or AT180 (Pope y cols., 1994; Preuss y cols., 1995; Illenberger y cols., 1998; Delobel y cols., 2002). Respecto a la relación directa entre ambos sucesos, distintos trabajos han descrito resultados que respaldan dicha vinculación, aunque en sentidos opuestos. Por un lado se ha propuesto que la hiperfosforilación de tau podría preceder a la fragmentación del AG. Para ello, primero, en cultivos primarios de neuronas se ha observado cómo la sobreexpresión de tau, normal o mutada, que en distintos estudios se ha visto que puede inducir su misma hiperfosforilación (Bertrand y cols., 2010), induciría la fragmentación del AG (Liazoghli y cols., 2005). Además estudios en modelos murinos que reproducen la patología tau, se vio cómo la presencia de tau hiperfosforilado parecía tener relación con la aparición de alteraciones estructurales en el AG de neuronas espinales (Lin y cols., 2003; Liazoghli y cols., 2005). Por otro lado, se ha observado cómo la fragmentación del AG en células de cultivo provocada por la administración de fármacos como brefeldina A o nocodazol o por la interrupción en la expresión de ciertas proteínas estructurales del orgánulo como la golgina84, inducían la hiperfosforilación de tau (Jiang y cols., 2014). Sugiriéndose por tanto que la hiperfosforilación de tau podría ser una consecuencia de la alteración estructural del AG (Elyaman y cols., 2002, Jiang y cols., 2014). Respecto a los estudios realizados en pacientes con EA, se ha descrito la fragmentación del AG en algunas poblaciones neuronales (Salehi y cols., 1995; Stieber y cols., 1996; Baloyannis, 2014). Sin embargo hay controversia respecto a la posible relación entre dicha fragmentación y la presencia intracelular de agregados de tau hiperfosforilado. En el estudio de Salehi *y* colaboradores se sostiene que la fragmentación del AG en neuronas de la región CA1 de la formación hipocampal, no parece estar asociada a la presencia de ovillos neurofibrilares intracelulares. Sin embargo, Stieber *y cols* sugirieron que en neuronas del subículo y de la corteza entorrinal, dichas alteraciones podrían estar asociadas de forma preferente con neuronas que no presentaban dichos ovillos de tau hiperfosforilado. Hay que tener en cuenta que la metodología empleada en estos estudios pioneros, presenta ciertas dificultades técnicas a tener en cuenta. Los

procedimientos de fijación usados en estos estudios, con intervalos de tiempo *post mortem* excesivamente largos (hasta más de 30 días) en los casos de pacientes, pudieron afectar la preservación del AG. A su vez el escaso grosor de las secciones histológicas llevado a cabo en el tejido (sólo 5 μm), así como los métodos de tinción usados, a través por ejemplo del uso de cromógenos combinados con tinciones de plata para su estudio en microscopia convencional de campo claro, podrían haber interferido en la medición del tamaño del AG o en la identificación de los niveles de agregación de tau hiperfosforilado que las neuronas podían tener. Los resultados obtenidos por tanto en estos estudios, y que han permanecido vigentes hasta hoy, no parecen resultar suficientemente fiables y sería necesario conocer mejor y de forma más fidedigna la posible relación entre la acumulación de tau hiperfosforilado y la alteración estructural del AG.

6. Segmento inicial del axón

6.1 - Funciones del SIA

El segmento inicial del axón (SIA) de neuronas de animales vertebrados es una estructura altamente especializada localizada en la zona más proximal del axón (figura 10). Esta estructura separa el dominio axonal del somatodendrítico y es la región en la que se inician los potenciales de acción (Palay y cols., 1968; Kole y cols., 2008), convirtiéndose en la región integradora de los potenciales sinápticos subumbrales provenientes del resto de dominios neuronales. Las características biofísicas y estructurales del SIA se consideran ideales para la iniciación de los potenciales de acción por contar con el umbral más bajo para su generación de toda la neurona. Esto se debe fundamentalmente a la alta densidad de canales de sodio dependientes de voltaje presentes en este dominio (Debanne y cols., 2011).

El SIA contribuiría además al mantenimiento de la polaridad neuronal de dos formas distintas. Por un lado el SIA constituye una barrera de difusión al inhibir la movilidad de proteínas de membrana entre los dominios somatodendrítico y axonal (Kobayashi y

cols., 1992; Winckler y cols., 1999). Por otro lado, el SIA contribuye al mantenimiento de la polaridad neuronal al actuar como filtro selectivo para el transporte de orgánulos y macromoléculas hacia el dominio axonal (Jones y Svitkina, 2016). La presencia de un filtro de este tipo explicaría por ejemplo que las proteínas motoras axonales de la superfamilia de quinesinas puedan entrar en el dominio axonal, mientras que proteínas cargo dendríticas o la proteína asociada a microtúbulos tipo 2 (MAP2) se encuentren exclusivamente en el dominio somatodendrítico de la neurona, estando excluidas del axón (Song y cols., 2009). Song y colaboradores (2009) propusieron que la interacción de la anquirina-G (AnK G), una de las proteínas principales del SIA, con los filamentos de actina, sería en buena parte responsable de dicho filtro selectivo dentro del citoplasma. El segmento inicial es por lo tanto una estructura crucial para el control de la polaridad y la excitabilidad neuronal (Grubb y cols., 2010). Además, tanto su longitud, como su composición en cuanto al tipo de canales iónicos que expresa, así como su posición en la región proximal del axón pueden variar considerablemente entre las distintas poblaciones neuronales, pudiendo ser responsables de parte de las diferencias electrofisiológicas existentes entre ellas (Grubb y cols., 2011).

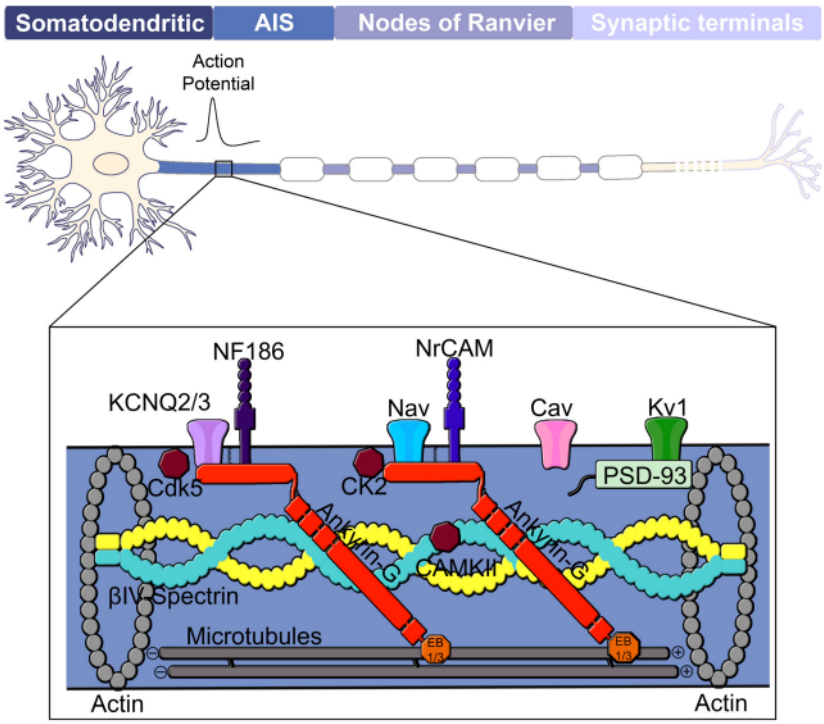

Figura 10: Esquema de la posición dentro de la célula y de la estructura del SIA, en la que se muestran las proteínas más relevantes de su conformación, organizadas por el citoesqueleto

de actina y el de los microtúbulos. La anquirina-G (en rojo) es considerada la principal organizadora de esta estructura, controlando la localización de proteínas asociadas a membrana como los canales de voltaje o moléculas de adhesión como NF186 y NrCAM. La anquirina-G está también asociada al citoesqueleto de actina mediante su interacción con la espectrina-IVβ. Tomado de Nelson y Jenkins, 2017.

6.2- Estructura del SIA

El SIA está constituido por haces de microtúbulos y filamentos de actina cubiertos por una red submembranosa de proteínas citoesqueléticas cuyos principales componentes son la anquirina-G y la espectrina-IVβ. Estas proteínas se asocian y forman complejos con proteínas que desempeñan importantes funciones en el SIA como la proteína de adhesión neurofascina 186 y la proteína de adhesión neuronal (NrCAM), canales de sodio, potasio y calcio dependientes de potencial y proteínas que los reclutan y unen al citoesqueleto de actina (Jones y cols., 2014). Todo ese complejo, forma una estructura densa observable mediante microscopía electrónica a la que se denominó como "undercoating" (Palay y cols., 1968). La anquirina-G, proteína responsable de la localización del resto de proteínas en estos complejos, es considerada como la principal organizadora del SIA dado que la supresión de su expresión produce el desensamblaje de toda la estructura (Hedstrom y cols., 2007, 2008; Jenkins y Bennett, 2001). Respecto a los canales dependientes de voltaje, los de sodio serían los principales responsables del bajo umbral existente en el SIA para la generación de los potenciales de acción. Estos se inician en la región más distal del SIA (Popovic y cols., 2011) en la que se expresan canales Nav1.6 con un umbral de activación menor que los de la región proximal (subtipo Nav1.2) (Hu y cols., 2009).

Recientemente un estudio realizado mediante microscopía de superresolución (microscopía de reconstrucción óptica estocástica o STORM) reveló que los filamentos de actina están organizados a lo largo de toda la extensión del SIA formando un patrón de anillos perpendiculares al eje longitudinal del axón y espaciados periódicamente cada 190 nanómetros (Figura 11; Xu y cols., 2013). En un estudio posterior, se observó

que, de la misma forma, tanto la espectrina-IVβ como la anquirina-G mostraban también una distribución periódica (Zhong y cols., 2014). Esta organización del citoesqueleto axonal submembranoso tiene un papel importante en el mantenimiento de la polarización axonal, influenciando el tráfico vesicular hacia y desde el axón y justificando por tanto el papel del SIA en el control de los mecanismos de transporte a lo largo del axón.

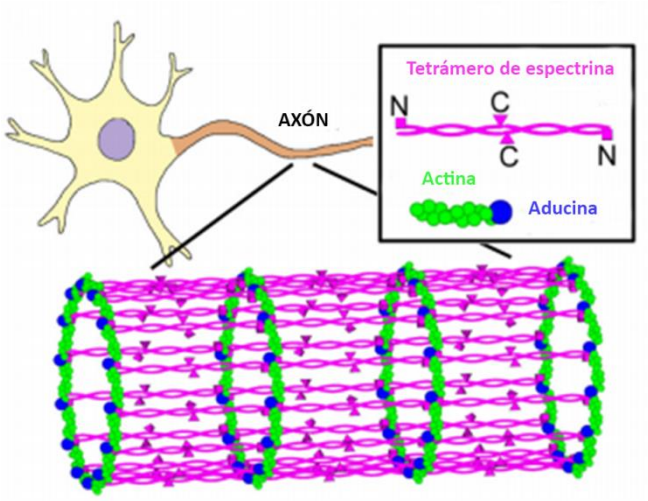

Figura 11: Esquema representativo de la organización anular de la estructura del SIA. Los filamentos de actina (verde), cubierta por la aducina (azul), forman estructuras en forma de anillo que envuelven la circunferencia del axón. Los tetrámeros de espectrina (magenta) conectan los anillos de actina/aducina a lo largo del axón, formando una malla que se repite de forma secuencial a lo largo del axón. Modificado de Xu y colaboradores (2013).

6.3 - Almacenamiento de Ca^{2+} en el SIA: Orgánulo de cisternas y orgánulo Sacular Gigante (OSG)

El orgánulo de cisternas (CO) es una estructura localizada dentro del SIA de neuronas de la corteza cerebral que fue descrita mediante microscopia electrónica en 1968 por S. Palay (Palay y cols., 1968) y que está formado por cisternas elongadas del retículo endoplasmático liso unidas por material electrodenso (Peters y cols., 1968; Kosaka, 1980; Spacek, 1985; Benedeczky y cols., 1994). La membrana más externa del CO está

además en aposición con la cara interna de la membrana plasmática (Palay y cols., 1968; Peters y cols., 1968; Peters, 1991). La formación del CO depende de la proteína asociada a actina denominada sinaptopodina (synpo), que es un excelente marcador para identificar el CO dentro del SIA y que interactúa con filamentos de F-actina y con la proteína α-actinina promoviendo la formación de haces y la elongación de filamentos de actina (Kremerskothen y cols., 2005; Bas Orth y cols., 2007; Sanchez-Ponce y cols., 2011). De hecho los ratones deficientes en sinaptopodina no son capaces de desarrollar el orgánulo de cisternas del SIA, aunque esto no afecta a la generación de potenciales de acción (Bas Orth y cols., 2007). El orgánulo de cisternas presenta similitudes estructurales con el aparato de la espina, un orgánulo localizado en una subpoblación de espinas dendríticas (Spacek, 1985) e implicado en la regulación de los niveles de calcio y en procesos de plasticidad en las espinas. Al igual que estos, el CO está considerado también como un regulador de los niveles de calcio en el SIA (Benedeczky y cols., 1994; Bas Orth y cols., 2007).

En un estudio anterior de nuestro grupo (Sánchez-Ponce y cols., 2011) se describió la presencia en el interior del SIA de algunas neuronas de la capa V de la neocorteza, de una estructura alargada que fue denominada como “orgánulo sacular gigante” (OSG). Este orgánulo está formado por estructuras membranosas saculares y tubulares que se orientan de forma paralela al eje del axón y se localiza en posición central dentro del SIA, extendiéndose a lo largo de toda su longitud, lo que hizo sugerir la posibilidad de que fuera un componente central del retículo endoplásmico liso. A nivel estructural, el OSG se asocia con microfilamentos asociados con microtúbulos adyacentes o con la cara citoplasmática de la membrana plasmática. Debido a que hasta el momento se desconocen las funciones que desempeñan el OSG así como la naturaleza y distribución de las subpoblaciones neuronales que lo poseen, en el presente estudio nos proponemos profundizar en el conocimiento de este orgánulo mediante técnicas de trazado axonal e inmunocitoquímicas.

6.4- Plasticidad del SIA

A pesar de la complejidad de la organización estructural del SIA, se han descrito fenómenos de plasticidad morfológica y funcional asociados a cambios en la longitud del SIA, en su localización y/o en la expresión de canales iónicos en su superficie, inducidos por variaciones en la actividad neuronal (Yamada y Kuba, 2016). Se ha sugerido que dicha plasticidad (figura 12) podría representar un mecanismo fisiológico para mantener la homeostasis neuronal, potenciando la actividad neuronal cuando hubiera una reducción de la actividad sináptica, o disminuyendo la excitabilidad neuronal tras una sobreestimulación (Grubb y cols., 2011).

Respecto a los cambios que se producen en la localización del SIA a lo largo del axón, se ha descrito como la estimulación de alta frecuencia desplaza distalmente el SIA alrededor de 45 µm en neuronas del núcleo laminar de la vía auditiva del pollo, al contrario de aquellas neuronas que recibieron estímulos de baja frecuencia (Kuba y cols., 2006). Además, estudios *in vitro* describieron cómo la despolarización crónica de neuronas hipocampales disociadas de hipocampo (Grubb y Burrone, 2010; Evans y cols., 2013) produce un desplazamiento distal del SIA a lo largo del axón asociado a un descenso en la excitabilidad de su membrana.

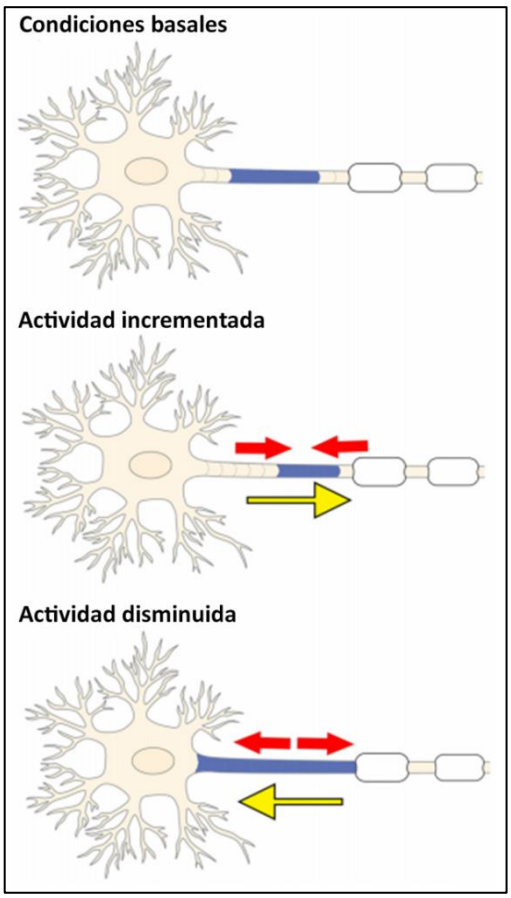

Figura 12: Esquema de la plasticidad asociada al SIA dependiente del nivel de actividad neuronal. Modificado de Nelson y Jenkins (2017).

En experimentos con cultivos de neuronas procedentes del bulbo olfatorio, se ha demostrado que la despolarización crónica causa diferentes tipos de desplazamientos en el SIA de neuronas excitadoras o inhibidoras; mientras que en interneuronas inhibidoras el SIA se desplaza proximalmente, en aquellas excitadoras se mueve distalmente (Chand y cols., 2015). Esto implicaría que existe cierta especificidad según el tipo de célula, respecto a la plasticidad del SIA. En modelos de enfermedades asociados con fenómenos de hiperexcitabilidad neuronal como la epilepsia (Harty y cols., 2013; Hamada y Kole, 2015), se producen desplazamientos del SIA. Dichas observaciones sugirieron de nuevo que la plasticidad del SIA podría ejercer de mecanismo orientado al mantenimiento de la homeostasis del circuito neural.

La plasticidad del SIA asociada a cambios en su longitud, se observó por primera vez en neuronas del núcleo coclear de aves en las que se demostró que la deprivación de estímulos auditivos produce una elongación del SIA al cabo de pocos días, incrementándose la superficie de membrana ocupada por los canales sensibles a voltaje. Esto potenciaría la excitabilidad de la membrana, permitiendo compensar la pérdida de actividad del nervio auditivo (Kuba y cols., 2010). Además, se ha observado que la llegada de información aferente durante los procesos de maduración cortical, produce también procesos de plasticidad en la longitud del SIA de neuronas corticales, en paralelo al refinamiento de los circuitos neurales durante el desarrollo (Cruz y cols., 2009; Gutzmann y cols., 2014; Kuba y cols., 2014; Schlüter y cols., 2017).

Por último, también se han descrito variaciones en la longitud del SIA en situaciones patológicas. Por ejemplo, se ha observado el alargamiento del SIA en un modelo animal del síndrome de Angelman, que es una alteración en el desarrollo neurológico asociado con el autismo (Kaphzan y cols., 2011), mientras que tras una isquemia o tras un daño traumático cerebral se ha observado un acortamiento del mismo (Baalman y cols., 2013; Harty y cols., 2013; Hamada y Kole, 2015).

6.5- Relación entre la proteína tau y el SIA

Dentro del SIA se describió lo que se denominó como barrera de difusión de tau, al ejercer el SIA como filtro que controla el tráfico retrógrado (del axón al soma) y anterógrado (del soma al axón) de la proteína asociada a microtúbulos tau (Li y cols., 2011). La disfunción de esta barrera en modelos de neurodegeneración debido a la presencia intracelular de tau hiperfosforilado (Li y cols., 2011), puso de relieve la posible implicación del SIA en las enfermedades neurodegenerativas como la EA. En un estudio reciente en un modelo murino para taupatías que expresa la proteína tau humana con la mutación P301L, se ha descrito cómo la hiperfosforilación de tau induce en neuronas hipocampales un aumento en el umbral de despolarización para la generación de potenciales de acción, reduciendo la tasa de disparo neuronal, en paralelo a un desplazamiento distal del SIA dependiente del nivel de fosforilación de tau (Hatch y cols., 2017). Los autores de este estudio propusieron que la reducción en la excitabilidad hipocampal observada en estos ratones transgénicos, podría ser debida a la recolocalización distal del SIA lo cual podría contribuir a la disfunción hipocampal descrita en la EA. Además, se ha observado que la suspensión de la expresión de proteínas constituyentes del SIA como la anquirina-G o la sobreexpresión de quinasas ligadas a la EA como la glucógeno sintasa quinasa-3β (GSK3β), alteran de manera notable la barrera de difusión de tau presente en el SIA (Zempel y cols., 2017). Por otro lado, también se ha observado que la exposición a oligómeros de β-amiloide altera tanto los filamentos de actina del SIA como la red de microtúbulos, dañando la barrera de difusión de tau del SIA y en consecuencia, provocando la difusión patológica de la proteína tau por todo el dominio somatodendrítico (Zempel y cols., 2017).

Todas estas observaciones, llevadas a cabo en modelos animales, sugieren que durante el desarrollo de la EA se podrían producir alteraciones estructurales del SIA asociadas a la hiperfosforilación de tau, lo cual podría influir sobre la excitabilidad neuronal. Sin embargo, hasta el momento no se han realizado observaciones en tejido procedente de pacientes de la EA. En el presente trabajo nos proponemos estudiar, mediante técnicas de inmunofluorescencia utilizando anticuerpos que reconocen el SIA y la proteína tau hiperfosforilada, las posibles alteraciones en la longitud y la

posición del SIA en neuronas piramidales, y su relación con el contenido neuronal en fosfo-tau, en tejido procedente de pacientes con la EA así como en el modelo murino P301S de taupatía.

II - MARCO GLOBAL Y OBJETIVOS

Aquellas enfermedades neurodegenerativas como la enfermedad de Alzheimer (EA) en las que se forman agregaciones proteicas intracelulares y donde se ha observado la fragmentación del aparato de Golgi (AG), suelen ir aparejadas a deficiencias en el transporte axonal (Sheetz y cols., 1998). Desde el AG se transportan una gran cantidad de moléculas destinadas al axón y a las dendritas, y en células polarizadas como las neuronas, la clasificación y el trasporte de proteínas a ambos dominios son cruciales para mantener su polaridad. Dado el importante papel que tanto el AG como el segmento inicial del axón (Leterrier y Dargent, 2013) tienen en la regulación del transporte axonal, su alteración podría tener efectos adversos sobre la funcionalidad del axón y de los terminales presinápticos. La posible relación entre la presencia de agregados de tau hiperfosforilado y la alteración del SIA y el AG no ha sido estudiada en profundidad. El objetivo de este trabajo ha sido estudiar esta relación en un intento de valorar la implicación de estas estructuras en la fisiopatología de la EA. Para ello primero hemos estudiado la morfometría del AG en neuronas de cerebros humanos controles y de pacientes con EA. En estos últimos hemos estudiado si las alteraciones del AG pudieran estar asociadas a la presencia de agregados de tau hiperfosforilado. Para profundizar en dicha asociación hemos utilizado además dos modelos animales de hiperfosforilación de tau: uno fisiológico como es el hámster Sirio durante los periodos de hibernación, y otro patológico usando al ratón transgénico P301S, portador del gen de tau humano mutado y que genera agregados de tau hiperfosforilado. De la misma forma en el presente trabajo se ha estudiado la organización del segmento inicial del axón, en cerebros normales y en cerebros de pacientes con la EA, así como en cerebros de hámster durante su hibernación y de ratones mutantes P301S, estudiándose de nuevo si la presencia de agregados proteicos de tau hiperfosforilado pudiera alterar dicha estructura o su localización dentro de la región proximal del axón.

III - RESUMEN DE RESULTADOS Y DISCUSIÓN

III- A Aparato de Golgi

A. I El aparato de Golgi en el cerebro humano

El aparato de Golgi en neuronas corticales de cerebros humanos procedentes de sujetos control

Para caracterizar las alteraciones del aparato de Golgi (AG) en pacientes con la enfermedad de Alzheimer (EA), quisimos estudiar primero sus características morfológicas en neuronas piramidales neocorticales e hipocampales a partir de tejido cerebral obtenido de autopsias humanas de sujetos control. En este trabajo se estudiaron secciones teñidas con DAPI e inmunoteñidas doblemente con anticuerpos que reconocen el marcador neuronal NeuN, así como MG160 que es una sialoglicoproteína utilizada normalmente como marcador del AG y que está localizada principalmente en el compartimento medial del mismo. Los elementos inmunoreactivos (-ir) del AG para el marcador MG160 se localizaron en el citoplasma neuronal, identificado mediante el marcado para la proteína NeuN, y situados usualmente en posición perinuclear. Los resultados obtenidos demostraron que la proteína MG160 se expresa ampliamente en el AG de neuronas neocorticales e hipocampales. Encontramos además una gran variabilidad respecto a las características morfológicas de los elementos del AG positivos para MG160. Esto nos llevó a subdividir cualitativamente el AG en tres estados o categorías morfológicas distintas: la primera correspondería a la apariencia normal “no fragmentada” en la que es visible una red de cisternas contorneadas que se distribuyen por todo el cuerpo celular, extendiéndose parcialmente por la dendrita apical. La segunda categoría correspondería al estado “fragmentado” del AG, en el que se deja de observar la red característica del AG normal, mostrando una apariencia globular dispersa por el soma. Este estado se encuentra más comúnmente en la región CA1 del hipocampo que en la

neocorteza. Por último, aquellos orgánulos cuya estructura estaba severamente alterada, mostrando normalmente escasa inmunoreactividad para MG160, se clasificaron como “muy alterados”.

El porcentaje de neuronas con un AG no fragmentado, o normal, fue mayor en la corteza temporal que en la región hipocampal CA1. Además, la morfología del AG en neuronas neocorticales mostró una menor complejidad que en las hipocampales, observándose una aparente disminución en la extensión de sus cisternas y en el número de circunvoluciones de las mismas. Posteriormente, con el fin de caracterizar mejor el AG de neuronas piramidales empleamos una herramienta de análisis en tres dimensiones (3D) del programa informático *Fiji* para poder cuantificar en cerebros de sujetos control, el volumen y la superficie de los elementos inmunoreactivos para MG160. Durante el análisis observamos un mayor volumen y superficie del AG en neuronas hipocampales de CA1 que en neuronas procedentes de la corteza temporal. Observamos la misma tendencia cuando los datos provenientes de los diferentes casos control fueron analizados individualmente. Se compararon además los valores promedio para la superficie y el volumen del AG entre los diferentes casos, tanto de células piramidales de la neocorteza como de CA1. Los resultados mostraron valores homogéneos entre casos, no encontrándose prácticamente diferencias significativas inter-individuales.

Por último, hay que destacar que observamos que casi el 10% de las neuronas neocorticales de los sujetos control mostraron un AG con una apariencia fragmentada o muy alterada, acompañada de una reducción en su volumen y superficie con respecto al AG normal. Consideramos que estas alteraciones del AG podrían estar relacionadas con el periodo *post mortem* (1.5-5 horas *post mortem*) previo a la fijación de las muestras. En el caso de las neuronas hipocampales de CA1, el porcentaje de neuronas con un AG alterado (fragmentado o muy alterado) fue de casi el 25%, marcadamente mayor que aquel encontrado en la corteza temporal. Esta diferencia entre ambas regiones podría ser debida a la posición más profunda de CA1 comparado con la neocorteza, localizada más superficialmente, lo cual supondría un periodo previo a la fijación más prolongado en el caso de CA1. Otra posibilidad podría

ser que las neuronas hipocampales fueran más sensibles a factores *post mortem* que las neocorticales.

El aparato de Golgi en cerebro de pacientes con EA

De acuerdo con estudios previos en cerebros de pacientes con la EA (Salehi y cols., 1995; Stieber y cols., 1996), el AG de ciertas neuronas se encuentra alterado, mostrando normalmente una apariencia fragmentada. En nuestro estudio hemos encontrado que la fragmentación del AG de ciertas neuronas piramidales, tanto de la neocorteza como de CA1, está asociada a una reducción en el tamaño del AG. La superficie y el volumen del AG con apariencia fragmentada y sobre todo del de aquellos cuya morfología estaba severamente alterada, se vieron generalmente reducidos en comparación con el volumen y la superficie de los AG normales o no fragmentados.

La posible relación entre la fragmentación del AG y la acumulación progresiva de la proteína tau hiperfosforilada no ha sido estudiada sistemáticamente hasta el momento. En este trabajo hemos analizado esta relación, tanto en neuronas piramidales de la corteza temporal como de la región CA1 en pacientes con EA, a partir de series de imágenes obtenidas mediante microscopía confocal a partir de secciones teñidas con inmunofluorescencia doble —usando anticuerpos frente a la proteína MG160, junto a anticuerpos AT8, que reconocen los epítopos fosforilados en la serina 202 y la treonina 205 de la proteína tau—, y contrateñidas con Dapi. Para poder estudiar la posible relación entre las alteraciones observadas en el AG y la acumulación de tau hiperfosforilado, nos hemos servido en este trabajo de la clasificación utilizada previamente en nuestro laboratorio (Merino-Serrais y cols., 2013), respecto a los distintos patrones de inmunoreactividad para AT8 que se observan en la EA. En dicho estudio se distinguieron dos patrones distintos para visualizar los filamentos helicoidales pareados cuya agregación forman las estructuras patológicas características de las taupatías. El patrón I o estadio de pre-ovillo, presenta un marcaje difuso fundamentalmente citoplásmico con agregados no fibrilares,

mientras que el patrón II sería aquel en el que la agregación de los filamentos helicoidales evoluciona hasta desarrollarse el ovillo neurofibrilar típico de la EA.

En un primer análisis de tipo cualitativo observamos en tejido procedente de pacientes que, al igual que vimos en los sujetos control, el porcentaje de neuronas con un AG fragmentado o muy alterado fue mayor en CA1 que en la neocorteza temporal. Además, el porcentaje de neuronas con el AG normal o no fragmentado, es menor en pacientes con EA que en los controles, lo que indica una alteración generalizada del AG en la enfermedad. Estos resultaron concuerdan con estudios previos en los que se describió la fragmentación del AG en neuronas de pacientes con la EA y que sugirieron un papel importante de la fragmentación del orgánulo en la neuropatología y patogénesis de la EA (Baloyannis, 2014, Salehi y cols., 1995, Stieber y cols., 1996).
Al comparar las neuronas negativas para el marcado con AT8 (AT8-) con aquellas que sí lo presentaban (AT8+), el porcentaje de neuronas neocorticales e hipocampales con AG muy alterados fue mayor en neuronas con tau hiperfosforilado (AT8+), tanto en las de tipo I como en aquellas con un patrón de hiperfosforilación más avanzado (tipo II). Asimismo, encontramos un descenso generalizado en la superficie y el volumen de los elementos inmunoreactivos para MG160 en neuronas neocorticales e hipocampales de pacientes con EA comparado con los casos control. Con el fin de determinar si existe un efecto perjudicial de la acumulación progresiva de tau hiperfosforilado sobre el AG en neuronas de pacientes, analizamos esos datos distinguiendo de nuevo entre células en estadio pre-ovillo y células con ovillo neurofibrilar (patrón de hiperfosforilación tipo II). Los resultados mostraron tanto en corteza temporal como en CA1, un aparente declive progresivo en los valores promedio de superficie y volumen del AG inmunoreactivos para MG160, al pasar de neuronas AT8- a neuronas AT8+ tipo I y AT8+ tipo II. Para evaluar la posible influencia de la variabilidad inter-individual en estos resultados, se analizaron separadamente los datos obtenidos en los distintos pacientes. Los resultados mostraron una tendencia similar en todos los pacientes.

Estos resultados respaldarían la idea de que la agregación de tau hiperfosforilado podría ejercer un efecto perjudicial sobre las características morfológicas del AG. Sin embargo, están parcialmente en desacuerdo con lo observado en estudios pioneros realizados en tejido también de pacientes con la EA. En dichos estudios se propuso que

las alteraciones del AG en neuronas (incluyendo fragmentación y reducción en tamaño) no están relacionadas con la presencia intracelular de ovillos neurofibrilares en la región CA1 del hipocampo (Salehi y cols., 1995) o incluso que estarían preferentemente asociados con neuronas carentes de ovillos neurofibrilares en el subículo y en la corteza entorrinal (Stieber y cols., 1996). Diversos factores pueden subyacer a estas discrepancias. Es posible que por ejemplo algunas neuronas AT8- con el AG fragmentado o alterado pudieran tener tau hiperfosforilado en residuos distintos a los reconocidos por el AT8. Por lo tanto, es necesario explorar en futuros estudios el grado en el que la acumulación de fosfo-tau, hiperfosforilado en distintos epítopos reconocidos por anticuerpos como PHF1 o AT180, se correlacionaría con alteraciones del AG (Goedert y cols., 1994). Por otro lado, estudios realizados por Salehi y cols., (1995) y por Stieber y cols., (1996) fueron realizados usando tejido cerebral incluido en parafina procedente de pacientes con periodos *post mortem* muy largos y muy heterogéneos, fijados en formaldehido durante tiempos por encima incluso del mes. Además, el tamaño del AG fue estimado en dos dimensiones en secciones de 5-6 micras de espesor, y por tanto el cuerpo celular de las neuronas piramidales no pudo ser probablemente estudiado al completo en la mayoría de los casos, dado que el diámetro del soma de la mayoría de las células piramidales es mayor de 5 micrómetros. En nuestro estudio, hemos realizado reconstrucciones completas en tres dimensiones (3D) usando microscopia confocal. En los estudios de Salehi y Stieber la identificación del AG mediante microscopía óptica convencional, se realizó mediante tinciones inmunocitoquímicas usando cromógenos opacos a la luz. Estos autores tiñeron los ovillos neurofibrilares de forma subsecuente (Salehi y cols., 1995) o simultánea (Stieber y cols., 1996) al marcaje del AG usando, respectivamente, la técnica de *Bodian* (con nitratos de plata reducidos) o métodos histoquímicos mediante el uso de distintos cromógenos coloreados. Los procedimientos de fijación usados en estos estudios podrían haber afectado por tanto a la preservación del AG, mientras que el tipo de seccionamiento y las metodologías de tinción usadas podrían haber interferido en la medición del tamaño del AG o con la valoración del grado de patología tau neuronal. A diferencia de dichos estudios, en este trabajo la segmentación en 3D del AG se basó en el análisis de la fluorescencia detectada mediante la selección de umbral que permite el software de análisis. El umbral fue

ajustado para cada serie de imágenes obtenidas mediante microscopía confocal y afectó de igual forma a las neuronas AT8- y AT8+ contenidas en cada campo microscópico. Dado que la intensidad del marcaje influye sobre las mediciones de superficie y volumen, la metodología utilizada en este trabajo podría inducir cierto sesgo en la medición de los valores absolutos de la superficie y el volumen del AG. Sin embargo, la principal observación de nuestro estudio, mostrando una reducción progresiva del tamaño del AG asociado al incremento en la acumulación de fosfo-tau, fue observada de manera consistente en todos los pacientes. Como ya se ha comentado, esto sugeriría que la acumulación de agregados de fosfo-tau podría dañar los AG de neuronas corticales en la EA. Los datos obtenidos se sustentan además en el hecho de que las alteraciones del AG en pacientes con la EA fueron más pronunciadas en neuronas piramidales de CA1 que de la corteza temporal, y de acuerdo con los estudios de Braak y Braak (1995) durante la progresión del patrón espaciotemporal de la EA, la patología tau se detecta antes en CA1 que en la neocorteza.

Alteraciones del aparato de Golgi en neuronas con tau hiperfosforilado en un sujeto control sin demencia

Para evaluar en tejido humano los efectos inducidos únicamente por la presencia de agregados de tau hiperfosforilado (presumiblemente sin otro factor patológico propio de la EA como las placas de β-amiloide), hemos estudiado las características morfológicas del AG neuronal en un sujeto de 45 años de edad que no presentaba ninguna enfermedad neurológica, psiquiátrica o psicológica (no diagnosticado con EA) y que murió como consecuencia de un tumor pulmonar. A pesar de no estar diagnosticado de EA ni de ninguna otra enfermedad neurológica, en distintas regiones del cerebro del paciente se encontró una cantidad considerable de neuronas AT8+. Estas se encontraron en distintas regiones corticales como la corteza temporal (áreas de Brodmann 20, 21, 22 y 38), prefrontal (áreas 9, 10 y 12) o frontal (áreas 44, 45, 46 y 47), mientras que no se detectó su presencia en otras áreas como la motora primaria (área 4), somatosensorial (área 3b) o visual (área 17) primaria. No se encontraron

placas de amiloide en ninguna de las regiones analizadas. Realizamos la cuantificación de la superficie y el volumen del AG (MG160-ir) en neuronas AT8-, y AT8+ (tipo I y II) en neuronas piramidales de CA1 y de las áreas 22 y 38 de la neocorteza temporal, donde la presencia de neuronas con tau hiperfosforilado fue más abundante. Los resultados en las tres regiones analizadas mostraron una reducción de la superficie y el volumen del AG en neuronas AT8+ respecto a las neuronas AT8-, que alcanzaron significación estadística únicamente en el caso de las neuronas AT8+ de tipo II. Estos resultados respaldan la posibilidad de que la agregación del tau hiperfosforilado ejerza un efecto perjudicial sobre la integridad estructural del AG en neuronas corticales. Cabe destacar que la fragmentación transitoria del AG durante la división mitótica es concomitante al incremento de la fosforilación de tau, revelada mediante la utilización de los mismos anticuerpos (AT8) que reconocen los ovillos neurofibrilares en la EA (Delobel y cols., 2002; Illenberger y cols., 1998; Pope y cols., 1994; Preuss y cols., 1995; Preuss y Mandelkow, 1998; Vincent y cols., 1996). En el caso de la EA, es probable que las alteraciones del AG neuronal observadas en este estudio contribuyan a la disfunción y degeneración neuronal propias de dicha enfermedad.

Efectos del envejecimiento y el tiempo *post mortem* sobre las características morfométricas del AG neuronal

Las diferencias observadas previamente respecto al tamaño y a las alteraciones morfológicas del AG entre los casos control y los pacientes con la EA, e incluso las diferencias inter-individuales encontradas dentro de cada grupo, podrían ser parcialmente debidas a diferencias en la edad de los pacientes empleados en este estudio y/o en el retraso del tiempo *post mortem* previo a la fijación del tejido cerebral. Para poder evaluar la potencial contribución de estos factores hemos estudiado ratones C57BL/6J con distintas edades (2, 8, 15 y 20 meses), así como otros de dos meses de edad cuyos cerebros fueron fijados por inmersión después de distintos tiempos *post mortem*. En estos animales medimos la superficie y el volumen del AG en neuronas piramidales de CA1 y CA3, así como de las capas supra e

infragranulares de la corteza somatosensorial. Como cabía esperar no observamos neuronas AT8+ en estas regiones en ninguno de estos animales y el AG de las neuronas observadas en todas las regiones y edades tuvieron una apariencia normal no fragmentada. El análisis cuantitativo reveló que no hubo diferencias entre los distintos grupos de edad en términos de superficie y volumen en los elementos MG160-ir de las neuronas piramidales supragranulares. Sin embargo, sí que se encontró una tendencia asociada al envejecimiento respecto a la reducción en el tamaño del AG, a la vista de la inmunoreactividad para MG160 en neuronas piramidales de capas infragranulares neocorticales y en la región CA3. Esta reducción fue más marcada aún en CA1. Finalmente encontramos que la superficie y el volumen de los elementos MG160-ir del AG de neuronas piramidales fue sensible al retraso en el periodo *post mortem*, dado que se vieron reducciones significativas en todas las regiones examinadas, en aquellos animales con un periodo *post mortem* de 2 y 5 horas, comparado con aquellas en las que había un periodo *post mortem* de 30 minutos previo a la fijación. Los resultados por tanto mostraron que el AG de neuronas neocorticales de ratones es sensible al envejecimiento y al retraso en el tiempo *post mortem* previo a la fijación, siendo mayor dicha sensibilidad en el caso de las neuronas hipocampales. El descenso en el volumen y en la superficie de los elementos del AG MG160-ir, fundamentalmente en la región hipocampal CA1, junto a la diferencia de edad entre el grupo control y los pacientes con la EA usados en nuestro estudio (controles, media ± DS: 50.6 ± 9.8 años; EA, media ± DS 83.1 ± 4.6 años), hacen que no se pueda descartar la posibilidad de que el descenso observado en el tamaño del AG de pacientes con la EA, especialmente en la región CA1, pudiera ser debido parcialmente al envejecimiento y no como consecuencia de la enfermedad por sí misma. Sin embargo, esto es improbable ya que también se ha descrito fragmentación del AG, en estudios en los que se usaros sujetos control y pacientes sin diferencias de edad (Salehi y cols., 1995). El incremento en el periodo *post mortem* previo a la fijación produjo disminuciones en la superficie y el volumen del AG en los ratones analizados. El material humano utilizado en nuestro estudio no presentó diferencias en el periodo *post mortem* entre el grupo control y los pacientes y por tanto no podemos considerarlo un factor que contribuya a las diferencias observadas en el volumen y superficie del AG. Sin embargo, nuestros resultados indican que tanto la edad como el periodo *post mortem* son factores que

deben tomarse en consideración cuando se analicen diferencias en el tamaño del AG entre neuronas procedentes de sujetos controles respecto al de pacientes con la EA o cuando se comparen modelos animales de la EA con pacientes humanos, dado que el tejido cerebral procedente de modelos animales está normalmente fijado mediante perfusión sin que haya tiempo *post mortem* previo a la fijación.

A. II El aparato de Golgi en el modelo murino de taupatía P301S

A continuación nos propusimos estudiar el efecto de la patología tau sobre la estructura del AG en ausencia de otros factores asociados al desarrollo de la EA como la patología amiloide. En este trabajo se han estudiado las características morfológicas del AG en neuronas piramidales de la corteza somatosensorial y de la región hipocampal CA1, en animales transgénicos P301S y controles de 2 y 36 semanas de edad, en relación a la acumulación de tau hiperfosforilado. De acuerdo con descripciones previas de este modelo animal (Yoshiyama y cols., 2007), tanto en el hipocampo como en la neocorteza de ratones de 2 semanas de edad, no observamos neuronas con tau hiperfosforilado a pesar de que todas las neuronas en estas regiones sobreexpresaran el gen humano mutado de tau MAPT P301S. Para comprobar esto último realizamos tinciones inmunocitoquímicas usando anticuerpos (T13) contra la proteína tau humana. En tejido procedente de ratones transgénicos observamos una intensa inmunoreactividad frente a la proteína tau de origen humano a lo largo de toda la corteza cerebral, al contrario que en los animales del grupo control en los que no se observó inmunoreactividad. Asimismo, estudiamos secciones inmunoteñidas con anticuerpos que reconocen MG160 o GRASP65, una proteína periférica de membrana localizada en el compartimento cis del AG, en combinación con anticuerpos AT8.

A las dos semanas de edad y a pesar de la expresión de tau de origen humano, el AG de las neuronas piramidales hipocampales y neocorticales presentó una morfología aparentemente normal en los animales transgénicos, semejante al grupo control,

consistente en una red de cisternas contorneadas distribuidas alrededor del cuerpo celular que se extendían parcialmente hacia la dendrita apical. Utilizando microscopía confocal y técnicas de cuantificación en tres dimensiones, no encontramos diferencias entre el grupo control y los animales transgénicos en cuanto a la superficie y volumen del AG de neuronas neocorticales e hipocampales, con ninguno de los marcadores del AG utilizados (GRASP65 y MG160). A las 36 semanas de edad, cuando hipotéticamente los niveles de tau humana mutada serían mayores, tampoco se encontraron diferencias en el tamaño del AG entre neuronas de ratones control y neuronas sin tau hiperfosforilado (AT8-) de los ratones transgénicos. Por tanto, estos datos indican que en este modelo animal la sobreexpresión de tau mutado P301S por sí solo no es suficiente para inducir alteraciones en el AG de neuronas corticales.

Alteraciones estructurales del AG en neuronas corticales con agregaciones de tau hiperfosforilado

En estudios previos realizados en cultivos de células HEK y de neuronas de médula espinal, se describió que la sobreexpresión de tau humana, tanto en su forma normal (isoforma 4R) como en su forma mutada (P301L), induce la fragmentación del AG (Liazoghli y cols., 2005). Por otro lado, se ha descrito que la sobreexpresión de tau *in vitro* puede conducir a su fosforilación (Bertrand y cols., 2010b). Sin embargo, hasta el momento no se ha demostrado la relación directa entre la hiperfosforilación de tau y la alteración del AG en neuronas corticales.

En este trabajo, al igual que en estudios previos (Yoshiyama y cols., 2007), encontramos en los ratones transgénicos P301S de 36 semanas de edad, una subpoblación de neuronas a lo largo de la corteza cerebral que presentaban acúmulos de fosfo-tau detectables con tinciones inmunocitoquímicas con anticuerpos AT8. Dichas neuronas AT8+ se encontraron fundamentalmente en el asta de Amón, el giro dentado, el subículo, la corteza insular, la corteza motora primaria y secundaria, la corteza visual primaria y secundaria, la corteza granular retroesplenial y diferentes

áreas de la corteza somatosensorial (área de barriles, área de representación de las patas, del tronco y de los labios).

Para estudiar las posibles alteraciones del AG en las neuronas AT8+ en el modelo P301S, nos hemos centrado en CA1 y en el área de representación de la pata trasera de la corteza somatosensorial primaria, por ser éstas las regiones donde el número de neuronas AT8+ fue mayor. La mayoría de ellas mostraron tanto el patrón de pre-ovillo (patrón I de acuerdo con Merino-Serrais y cols., 2013) como el patrón intermedio de ovillo neurofibrilar (patrón IIa), mientras que la presencia de neuronas con un patrón avanzado de ovillo neurofibrilar (IIb) fue escaso. El análisis del AG en algunas neuronas hipocampales y neocorticales, mostró una morfología alterada consistente en una retracción aparente de su estructura y en una disminución de estructuras tubulares mostrando a menudo una apariencia lobular y polarizada en un extremo del cuerpo celular. Utilizando dos marcadores del AG (MG160 y GRASP65) observamos que el porcentaje de neuronas con este tipo de alteración fue mucho mayor en neuronas con agregados de tau hiperfosforilado intracelular que en neuronas adyacentes AT8- (MG160: 73.2% de neuronas AT8+, frente al 19.1% de neuronas AT8-; GRASP65: 69.5% de neuronas AT8+, frente al 22.1% de neuronas AT8-). A continuación cuantificamos el volumen y la superficie de los elementos del AG inmunoreactivos para GRASP65 o MG160 en neuronas AT8+ y AT8- así como en animales del grupo control de la misma edad (AT8-). En las dos regiones analizadas, no se encontraron diferencias significativas entre neuronas de animales del grupo control y neuronas AT8- de ratones transgénicos. Sin embargo, en ambas regiones, observamos una reducción en la superficie y el volumen del AG en las neuronas piramidales AT8+ respecto a las neuronas AT8-. Esta reducción sin embargo no llegó a ser estadísticamente significativa en el caso de la superficie del AG de neuronas en la región CA1 marcadas con GRASP65, probablemente debido al escaso número de neuronas AT8+ encontradas en el tejido utilizado. Finalmente, calculamos el porcentaje de descenso en tamaño del AG en neuronas AT8+ comparado con las neuronas AT8- de su alrededor. La media de la reducción en porcentaje de la superficie y el volumen del AG, fue mayor cuando se analizó la inmunoreactividad para MG160 (26.4% y 28.3%, respectivamente) que

cuando dicha reducción se estimó con anticuerpos para GRASP65 (14.8% y 13.2%, respectivamente).

Todos estos resultados indican que la acumulación de fosfo-tau en las neuronas corticales está asociada con alteraciones estructurales del AG, dado que el porcentaje de neuronas con alteraciones morfológicas en el AG fue significativamente mayor en neuronas AT8+ que en neuronas adyacentes AT8-. Hay que destacar que en nuestro material no encontramos prácticamente evidencia de procesos de fragmentación del AG en neuronas AT8+ (ni tampoco en las AT8-). Esta observación difiere de la fragmentación descrita en motoneuronas de la médula espinal con tau hiperfosforilado en la serina 202 (CP13+), en un estudio que utilizó ratones mutantes JNPL3, donde se sobreexpresa el gen mutado de tau P301L (Liazoghli y cols., 2005).

El tipo de mutación en el gen de tau y el consecuente tipo de hiperfosforilación y agregación de la proteína, los anticuerpos usados para detectar el fosfo-tau, la población neuronal estudiada o la edad de los animales estudiados son algunos de los factores que podrían haber contribuido a las diferencias existentes entre nuestro estudio y el de Liazoghli y colaboradores (2005). Nuestros resultados en el modelo P301S también contrastan con la fragmentación del AG descrita en neuronas corticales de pacientes con la EA (Antón-Fernández y cols., 2017), lo que indica que las alteraciones del AG producidas en ratones P301S solo reproduciría parcialmente aquello que ocurre durante el desarrollo de la enfermedad. Estas diferencias podrían ser explicadas por la posible implicación de diferentes factores presentes durante el desarrollo de la EA y la preparación de las muestras histológicas, que podrían ser perjudiciales para la integridad del AG, como la presencia de oligómeros de amiloide (Jiang y cols., 2014; Joshi y cols., 2015 a,b) que están bidireccionalmente relacionados con la patología tau (Oddo y cols., 2004; Dai y cols., 2015, 2017), el envejecimiento y el retraso en el periodo *post mortem* previo al procesamiento del tejido (Antón-Fernández y cols., 2017), así como otros factores no conocidos que pudieran estar asociados con la progresión de la enfermedad. Los resultados obtenidos en este trabajo en el modelo murino de taupatía P301S, en el que el único factor patológico presente es la presencia de formas mutadas de la proteína tau y el desarrollo de agregados de tau hiperfosforilado (Yoshiyama y cols., 2015), respaldarían la idea de

que la acumulación de fosfo-tau está asociada con alteraciones estructurales del AG (Antón-Fernández y cols., 2017). Aunque ambos procesos aparecen de forma concomitante, la relación causal entre ellos no ha sido resuelta todavía y justificaría futuros estudios al respecto (Sutterlin y cols., 2002; Lin y cols., 2003; Jiang y cols., 2014; Liazoghli y cols., 2014).

A. III El aparato de Golgi neuronal durante la hibernación del hámster Sirio

Dado que la hibernación del hámster Sirio es un modelo fisiológico de hiperfosforilación reversible de la proteína tau en la corteza cerebral, decidimos estudiar durante este proceso los posibles cambios del aparato de Golgi en las neuronas corticales.

Distribución de las proteínas del AG de neuronas corticales en el hámster Sirio en estado de eutermia

Para caracterizar las posibles alteraciones del aparato de Golgi (AG) de neuronas neocorticales e hipocampales en el hámster Sirio durante su hibernación, primero realizamos tinciones inmunocitoquímicas con anticuerpos frente a tres proteínas distintas del AG (GM130, MG160 y golgina84) para estudiar su distribución en animales control (estadio de eutermia).

Cada una de estas proteínas tiene una localización mayoritaria en cada uno de los tres compartimentos del AG: GM130 está principalmente localizada en el compartimento Cis del AG, MG160 en las cisternas mediales y golgina84 está presente a lo largo de toda la estructura del AG en un gradiente creciente hacia la cara trans del orgánulo. A pesar de estas diferencias respecto a su localización, nuestro estudio, utilizando tinciones dobles de inmunofluorescencia y microscopía confocal, reveló una apariencia morfológica similar del AG identificado mediante los distintos marcadores.

Mediante el uso del programa informático *Fiji (3D object counter tool)* estimamos el volumen y la superficie de los elementos inmunoreactivos del AG para cada uno de los tres distintos marcadores del AG de neuronas piramidales de las capas supra e infragranulares de la neocorteza y de las regiones hipocampales CA1 y CA3. Los resultados indican que en todas las regiones analizadas, la proteína MG160 muestra en general, una distribución más restringida en el AG que la golgina84 y GM130. Al

compararse los valores del AG obtenidos en las distintas poblaciones neuronales, se encontró una mayor superficie y volumen del AG en neuronas hipocampales, especialmente en las de CA3, que en las neocorticales. A continuación cuantificamos el grado de colocalización entre los distintos marcadores en secciones doblemente inmunoteñidas para dos combinaciones distintas de anticuerpos (MG160/GM130 y GM130/Golgina84). Dicha colocalización se analizó mediante la obtención del coeficiente de colocalización de Manders (Manders y cols., 1993), en el que el 0 representa falta total de colocalización y el 1 la colocalización completa. En todas las poblaciones neuronales, se encontró un valor menor en la combinación MG160/GM130 que en la combinación GM130/Golgina84, lo cual probablemente se deba a la distribución más amplia de GM130 respecto a la de MG160 en el AG. A pesar de que la apariencia del AG en las tinciones para tres marcadores es semejante la falta de una completa colocalización entre las distintas proteínas indica la existencia de microdominios en el AG donde los pares de proteínas testadas en cada combinación no se coexpresan.

Efectos diferenciales de la hibernación sobre la expresión de proteínas del AG

En este estudio describimos cómo el AG de neuronas hipocampales y neocorticales del hámster Sirio experimenta una compleja reorganización morfológica durante la hibernación. Se han analizado las variaciones en la expresión de golgina84, MG160 y GM130 durante el ciclo de hibernación mediante *Western blot* (WB) a partir de muestras obtenidas de animales sacrificados en los distintos estadios de la hibernación. El análisis reveló que durante el periodo de torpor (cuando el animal experimenta una caída dramática de su tasa metabólica) los niveles de expresión de las distintas proteínas del AG se modificaron de manera diferencial. Los niveles de expresión de MG160, normalizados con la expresión de β-actina, disminuyeron en las muestras provenientes de animales en estado de torpor en comparación con las muestras de animales eutérmicos, mientras que la expresión de la golgina84 permaneció inalterada y la de GM130 se incrementó. Los procesos que regulan el

descenso en la expresión de MG160 durante el torpor podrían participar en los mecanismos relacionados con la fragmentación del AG dado que en estudios previos se sugirió un papel importante de la proteína MG160 en la biogénesis y el funcionamiento del AG (Gonatas y cols., 1995, 1998).

Durante los cortos periodos de vigilia que se producen a lo largo de la fase de torpor, MG160 y GM130 mostraron niveles intermedios de expresión, es decir niveles intermedios entre los correspondientes a las fases de eutermia y torpor. Por el contrario, la expresión de la golgina84 se vio incrementada significativamente en las muestras provenientes de animales que han despertado del torpor respecto a la expresión propia de periodos de eutermia o de torpor. Se ha demostrado en células HEK293/tau que la interferencia en la expresión de la golgina84 afecta a la estructura del AG, induciendo su fragmentación (Jiang y col, 2014). A su vez se ha observado que la sobrexpresión de golgina84 corrige las alteraciones del AG inducidas por la brefeldina-A, lo que indica la implicación de esta proteína en el mantenimiento estructural del AG (Jiang y cols., 2014). Por tanto, es posible que la sobrexpresión de la golgina84 durante los periodos en los que el animal despierta del torpor pueda ser necesaria para la reorganización del AG que se produce en la transición entre los estados de torpor al de eutermia (véase más adelante).

A continuación estudiamos si los cambios en los niveles de expresión proteica observados mediante WB durante el ciclo de hibernación se reflejan en alteraciones de los patrones de inmunoreactividad o en la distribución de las distintas proteínas analizadas en el AG. La disminución durante la fase de torpor en los niveles de expresión de MG160 medidos por WB, fueron acompañados de la fragmentación de los elementos inmunoreactivos para MG160 y de una reducción en la intensidad de la inmunoreactividad. Esta reducción fue más evidente en neuronas neocorticales y en células piramidales de CA1 que en las de CA3, donde la inmunoreactividad para MG160 está preservada. Las alteraciones producidas en la expresión de la proteína MG160, se reflejaron además en una reducción significativa da la superficie y el volumen de los elementos inmunoreactivos para dicha proteína durante el estado de torpor, en todas las poblaciones neuronales analizadas, excepto en neuronas piramidales de CA3. Además, en la corteza somatosensorial, pero no en el hipocampo,

el coeficiente de colocalización de Manders de MG160/GM130 disminuyó en los animales del grupo torpor en comparación con los animales en eutermia o en los que han despertado del torpor. En el caso de la proteína GM130, no se encontraron cambios aparentes en la intensidad de su inmunoreactividad durante la hibernación. Sin embargo, al igual que en el caso de MG160, observamos profundas modificaciones morfológicas de los elementos inmunoreactivos para GM130 en todas las regiones analizadas, mostrando una apariencia fragmentada en el estadio de torpor que fue acompañado por un descenso en el volumen y la superficie de elementos del AG inmunoreactivos para GM130, especialmente en la región CA1 del hipocampo. En el caso de la golgina84, a pesar de la falta de cambios aparentes en la intensidad de su inmunoreactividad, observamos una fragmentación de los elementos inmunoreactivos del AG así como un descenso en su superficie y volumen. Estos cambios fueron acompañados por un incremento en el coeficiente de colocalización de Manders para GM130/Golgina84 durante el estado de torpor en prácticamente todas las áreas.

Dado que el tamaño del AG ha sido directamente relacionado con el nivel de actividad celular (Lucassen y cols., 1993; Salehi y cols., 1994), la fragmentación y reducción del tamaño del AG observado en este trabajo probablemente estén relacionadas con una reducción en la capacidad neuronal para el procesamiento y transporte de proteínas durante la fase de torpor. Esto estaría en concordancia con las reducciones descritas durante la hibernación en el tamaño del soma neuronal, en la complejidad de los árboles dendríticos o en la densidad de las espinas dendríticas (Popov y cols., 1992; Popov y Bocharova, 1992; von der Ohe y cols., 2006), así como la reducción de procesos costosos energéticamente como la transcripción o la síntesis proteica (Strumwasser, 1959; Walker y cols., 1977; Zhegunov, 1988; Rolfe y Brown, 1997; Frerichs y cols., 1998; Popov y cols., 1999; Buck y Barnes, 2000; van Breukelen y Martin, 2001, 2002). Sin embargo, los cambios en la expresión y en la localización de las proteínas del AG observados durante la hibernación parecen estar regulados de forma específica y compleja, dado que la expresión cerebral de las tres proteínas evaluadas mediante WB e inmunocitoquímica, varió de forma diferencial durante los diferentes estadios de la hibernación.

Cambios en el AG de neuronas con tau hiperfosforilado durante el estado de torpor

Estudios previos han descrito que durante el estado de torpor de la hibernación, la proteína asociada a microtúbulos tau se hiperfosforila en neuronas corticales, mientras que al volver a la fase de eutermia esta fosforilación desaparece (Arendt y cols., 2003; Härtig y cols., 2005, 2007; León-Espinosa y cols., 2013). En este trabajo hemos observado, en secciones teñidas inmunocitoquímicamente con anticuerpos AT8, que el tau hiperfosforilado se encuentra principalmente en una subpoblación de neuronas piramidales en la capa V de la neocorteza y en neuronas de CA3 y del hilus del hipocampo. Asimismo, en este trabajo se analizó si el AG de las neuronas con acúmulos de tau hiperfosforilado (AT8+) es más propenso a experimentar alteraciones morfológicas durante la fase de torpor que el de las neuronas AT8- .

En secciones de corteza somatosensorial del hámster en estado de torpor con dobles tinciones para AT8 y MG160 observamos que el volumen y la superficie de los elementos inmunoreactivos para MG160 fueron significativamente menores en neuronas con una intensa inmunoreactividad para AT8 que en neuronas AT8-, si bien no todas las neuronas AT8+ fueron afectadas igualmente. Estos resultados sugieren que la presencia en el soma de altos niveles de tau hiperfosforilado tendría un efecto perjudicial sobre la expresión de MG160 en el AG. De forma alternativa, el descenso en la expresión de MG160 durante el torpor podría favorecer la hiperfosforilación de tau. Esta hipótesis se basa en el hecho de que estudios previos han mostrado que MG160 puede unir diferentes factores de crecimiento de fibroblastos (FGFs), incluido el FGF-2, reduciendo la internalización de dichos factores e inhibiendo su acumulación intracelular (Burrus y cols., 1992; Zhou y cols., 1997; Zuber y cols., 1997; Yamaguchi y cols., 2003). Los niveles de FGF-2 parecen estar incrementados en la EA (Stopa y cols., 1990; Cummings y cols., 1993) y además, en células progenitoras neurales y en células PC12, se observó que la sobrexpresión de FGF-2 puede incrementar la actividad GSK3 e inducir la hiperfosforilación de tau en varios epítopos, incluido la serina 202, que es reconocido por los anticuerpos AT8 (Tatebayashi y cols., 1999, 2003). Por tanto, es posible que la reducción en la expresión de MG160 en células corticales

durante el estado de torpor, pueda inducir un incremento en los niveles intracelulares de FGF que podría llevar a la hiperfosforilación de tau observada con anticuerpos AT8.

Finalmente en este estudio hemos encontrado que durante el torpor no hubo diferencias en el tamaño de los elementos del AG positivos para la golgina84 entre neuronas piramidales de la capa V AT8+ y AT8-. Esto indica que no todas las proteínas del AG están afectadas de la misma forma por la acumulación de tau hiperfosforilado. Sin embargo, se sabe por estudios mediante WB, que el tau se puede hiperfosforilar en residuos distintos a los reconocidos por AT8 durante la hibernación (Stieler y cols., 2011). Por tanto, es necesario realizar nuevos estudios con el fin de explorar si las diversas alteraciones del AG podrían relacionarse con el grado de acumulación de tau hiperfosforilado en sitios distintos al de la serina 202 y la treonina 205, reconocidos por el anticuerpo AT8.

III- B Segmento inicial del axón

B. I Presencia de un orgánulo sacular gigante en el segmento inicial del axón de una subpoblación de neuronas piramidales de capa V

En un estudio previo realizado en nuestro laboratorio, se describió la presencia de una estructura que fue denominada como "orgánulo sacular gigante" (OSG) en el segmento inicial del axón (SIA) de neuronas de la capa V de la corteza cerebral (Sánchez-Ponce y cols., 2011). EL OSG se identificó mediante técnicas inmunocitoquímicas usando anticuerpos que reconocían tanto la sinaptopodina como la alfa-actina. En este trabajo hemos analizado la corteza cerebral de la rata para poder caracterizar la subpoblación de neuronas que contienen el OSG, así como su distribución en las distintas áreas corticales. Utilizando como referencia el atlas de Paxinos y Watson (Paxinos y Watson, 2007) observamos que las neuronas que contienen el OSG, representan una pequeña población de células piramidales en la parte superior de la capa V en todas las áreas corticales. Utilizando secciones coronales de 50 µm de grosor del cerebro de rata espaciadas a intervalos de 300 µm, inmunoteñidas con anticuerpos contra sinaptopodina observamos que el mayor porcentaje de células con el OSG se encuentra la corteza sensorimotora, aunque de forma ocasional también se encontraron estas neuronas en áreas como la orbitofrontal, cingular, insular, retroesplenial, peririnal, temporal asociativa y en las cortezas auditivas y visuales. Dado que el OSG se encontró de forma más frecuente en el SIA de neuronas piramidales de capa V de la corteza somatosensorial y motora, nos centramos en estas regiones para el resto de este estudio.

Atendiendo a criterios morfológicos, electrofisiológicos y de conectividad, existe una considerable heterogeneidad de poblaciones de neuronas piramidales en la neocorteza. De este modo, de manera general se distinguen dos tipos principales de neuronas piramidales: Las neuronas de tipo I son aquellas que poseen un penacho

dendrítico bien desarrollado o complejo, proyectan a dianas subcorticales como el estriado, el colículo superior, a núcleos del tronco encefálico y a la medula espinal, y tienen patrones de descargas de potenciales de acción en ráfagas cortas. Por el contrario, las células piramidales de tipo II poseen un penacho dendrítico menos extenso, proyectan a la corteza contralateral y al estriado ipsilateral o contralateral, y descargan potenciales de acción de forma no adaptativa (Molnar y Cheung 2006; Hattox y Nelson 2007; Molyneaux y cols., 2007). Además de esta clasificación general, se distinguen distintos tipos de neuronas en base a la expresión de distintas clases de combinaciones de marcadores neuronales, como factores de transcripción o distintos tipos de neurofilamentos (Angulo y cols., 2003; Tsiola y cols., 2003; Molnar y Cheung 2006). De acuerdo con estudios previos (Feng y cols., 2000; Porrero y cols., 2010) en ratones transgénicos Thy-1eYFP existe una alta densidad de neuronas que expresan la proteína amarilla fluorescente (siglas en inglés YFP) en la capa V de la neocorteza sensorimotora. El gen promotor Thy-1 se expresa además de forma diferencial en función del tipo de subpoblación cortical, según sea del tipo I (corticoespinal y corticocolicular) o del tipo II (corticotalámico y callosas) (Porrero y cols., 2010).

Para saber si existe alguna coincidencia entre subpoblaciones de neuronas piramidales que contienen el OSG y las que expresan el gen promotor Thy-1, realizamos una doble inmunotinción para la sinaptopodina y la anquirina-G (como marcador del SIA) en secciones cerebrales procedentes de dichos ratones transgénicos. Al estudiar la corteza somatosensorial y motora, encontramos que de un total de 129 neuronas piramidales con un OSG (identificados por la presencia de una estructura alargada inmunoreactiva para la sinaptopodina situada dentro del SIA), 43 (el 33,3%) fueron células que expresaban la proteína amarilla fluorescente (YFP+), mientras que el resto, 86 (66,7%), no la expresaban (YFP-). Además, el SIA de la mayoría (74,7%, n=359) de las neuronas que expresaban el transgén, carecían de OSG. Estos resultados indicaron que la expresión del promotor Thy-1 parece no estar asociado con la presencia del OSG en el SIA de las células piramidales de la capa V.

Posteriormente realizamos inmunotinciones dobles usando anticuerpos que reconocen la proteína SMI32 y sinaptopodina en tejido neocortical de rata y de ratón. De acuerdo con estudios previos (Molnar y Cheung, 2006), las neuronas

inmunoreactivas para SMI32 en la capa V corresponden a la población de neuronas piramidales de tipo I. Lo que observamos fue que la práctica totalidad de las neuronas que contenían un OSG en el SIA, son inmunoreactivas para SMI32 (ratones 100%, n=220; rata 97,6%, n=542). Esto fue corroborado en experimentos similares en tejido de ratones Thy-1eYFP, en los cuales observamos que todas las neuronas dotadas de OSG (identificados por la inmunoreactividad para sinaptopodina), sin tener en cuenta si expresaban o no el transgén de la proteína amarilla fluorescente, fueron también inmunoreactivas para SMI-32. Estos resultados muestran que el OSG está restringido al SIA de una subpoblación de neuronas piramidales de tipo I de la capa V. Las neuronas de tipo I de la capa V muestran patrones distintos de conectividad dependiendo del área cortical en el que se localice la neurona (O'Leary y Stanfield 1985, 1986; Koester y O'Leary 1993). Además, estudios recientes han clasificado además una amplia variedad de neuronas piramidales de proyección, especialmente aquellas de la capa V, basándose en la correlación entre la especificidad de su conectividad y el patrón de expresión génica, siendo posible llegar a definir molecularmente distintas clases funcionales de neuronas de proyección (Sorensen y cols., 2013). En la capa V corteza sensorimotora, donde hemos encontrado en este estudio la mayor proporción de neuronas con OSG, se ha descrito la expresión restringida de un pequeño número de genes específicos (Arlotta y cols., 2005). El hecho de que las neuronas de capa V que contengan el OSG en su SIA representen una subpoblación con unas proyecciones a áreas específicas o con un patrón de colateralización axonal concreto, pudiera correlacionar con un perfil de expresión génica específico, es un tema interesante que podría ser evaluado en futuros estudios.

Para identificar las áreas de proyección de las células piramidales que contienen un OSG en el SIA realizamos experimentos con microinyecciones del trazador retrógrado fluorescente *Fast Blue* (FB) en distintas regiones cerebrales combinados con inmunocitoquímica para sinaptopodina y anquirina-G con objeto de identificar los OSG y los SIA, respectivamente. En aquellos experimentos con inyecciones de FB en la corteza somatosensorial primaria observamos que las neuronas que contenían el OSG, pertenecían a una población distinta a la de aquellas con proyecciones callosas, marcadas retrógradamente. Además, el cuerpo celular de las neuronas de capa V con

proyecciones contralaterales fue significativamente más pequeño que aquellas con un OSG.

En experimentos con inyecciones de FB en el complejo ventrobasal del tálamo observamos muchas neuronas marcadas retrógradamente en la capa VI ipsilateral, y algunas de ellas en el borde de la capa V. Sin embargo, no observamos la presencia de ningún OSG en ninguna de las neuronas corticotalámicas. Por último, realizamos grandes inyecciones de FB en distintas regiones subcorticales no talámicas, como el estriado, el colículo superior/tegmento mesencefálico, núcleos pontinos y la medula espinal torácica. En todos estos casos, encontramos una subpoblación grande de neuronas marcadas retrógradamente que contenían un OSG en su SIA (53.3 %, n = 197; 65.4 %, n = 78; 67 %, n = 97; 70.6 %, n = 34, respectivamente). Todos estos resultados demuestran que el OSG representa una especialización dentro del SIA de una subpoblación de neuronas piramidales tipo I de la capa V que incluyen neuronas de proyección corticoestriatal, corticocolicular, corticopontino y corticoespinal.

Posteriormente se comparó el tamaño del soma de neuronas de proyección subcortical en relación con la presencia o ausencia del OSG en el SIA. Tomando en conjunto todos los datos procedentes de secciones de cuatro animales inyectados tanto en el estriado, como en el colículo superior, el núcleo pontino o la médula espinal, encontramos que el tamaño del soma de neuronas de capa V fue significativamente mayor en neuronas con el OSG que en aquellas sin él. Sin embargo, al analizar los datos tomados de forma independiente dentro de cada área de inyección, esta diferencia fue solo significativa en el caso de las poblaciones corticoestriatales y corticopontinas pero no en aquellas neuronas corticocoliculares y corticoespinales. Se encontraron además diferencias significativas entre el tamaño del soma de neuronas con el OSG que proyectan hacia el estriado (más pequeñas) con respecto a aquellas que proyectan al colículo superior, a núcleos pontinos o a la médula espinal. Por otro lado, teniendo en cuenta solo aquellas neuronas que no contenían el OSG, observamos que las subpoblaciones de neuronas corticocoliculares, corticopontinas y corticoespinales presentaron un mayor tamaño de soma comparado con las neuronas corticocorticales o corticotalámicas de capa V. Tomando todos los

resultados de forma conjunta, en la capa V el OSG se encontraría por tanto sólo en algunas neuronas de proyección descendente cuyo soma es de gran tamaño.

Con el objetivo de estudiar el origen y la funcionalidad del OSG, realizamos en secciones de neocorteza de rata, experimentos con tinciones inmunocitoquímicas dobles para sinaptopodina y GM130 o GRP78 como marcadores del aparato de Golgi (Nakamura y cols., 1995) y del retículo endoplásmico (Shim y cols., 2008; Pfaffenbach y Lee, 2011), respectivamente. En este material observamos que el OSG no presentó inmunoreactividad para el marcador del aparato de Golgi, mientras que sí se marcó con anticuerpos para GRP78, indicando que el OSG sería parte del retículo endoplásmico.

Por último, realizamos dobles marcajes para la ATPasa de calcio del retículo sarcoendoplásmico (SERCA) o el receptor 1 de inositol 1,4,5-trifosfato (IP_3R1), junto a la sinaptopodina. En estos experimentos observamos que los anticuerpos para SERCA e IP_3R1 marcaron estructuras alargadas que se extendían a lo largo de la longitud del SIA de una pequeña población de neuronas piramidales de la capa V, que fueron identificadas como OSG por su colocalización con la sinaptopodina. Por tanto, estos resultados demuestran que el OSG expresa IP3R1 y SERCA en la corteza cerebral de la rata.

Estudios previos han descrito que el calcio entra de forma transitoria en el SIA a través de canales de calcio sensibles a voltaje situados en la membrana plasmática tras la despolarización del soma en distintos tipos neuronales. Esta entrada de calcio participaría en la generación de potenciales de acción en el SIA (Yu y cols., 2008, 2010; Bender y Trussell 2009), y por tanto su regulación es fundamental, dado que diversos estudios han demostrado que los procesos de plasticidad del SIA, incluidos cambios en la longitud y posición dentro del axón (Grubb y Burrone 2010; Grubb y cols., 2011; Kuba y cols., 2010) son dependientes de calcio.

A su vez lesiones en el SIA provocan cambios estructurales en su citoesqueleto que afectan a la distribución de los canales de sodio dependientes de voltaje (Schafer y cols., 2009). La expresión en el OSG de IP_3R1 y SERCA (a través de los cuales se podría producir tanto la movilización como la recaptación de calcio respectivamente) sugiere

por tanto que el OSG podría tener un papel en la regulación espacio-temporal de los niveles de calcio. El OSG parece ser por tanto un almacén intracelular de calcio sensible a inositol trifosfato (IP_3), sin embargo las señales que promueven la liberación de calcio mediada por IP_3R1 en el SIA de esta población neuronal no se conocen todavía. Otras cuestiones pendientes de resolver serían por ejemplo saber cómo esta liberación puede coordinarse con otros posibles mecanismos de entrada y salida de calcio a través de la membrana plasmática, como se ha descrito en diferentes regiones cerebrales y tipos celulares (Bootman y cols., 2001; Blaustein y Golovina, 2001).

En el SIA de la mayoría de poblaciones de neuronas piramidales que carecen de OSG, existe en su lugar otra especialización del RE denominada como orgánulo de cisternas, que también expresa IP_3R1, SERCA y sinaptopodina. Se ha propuesto que estos orgánulos participarían también en la regulación de los niveles de calcio del SIA (Kosaka 1980; Benedeczky y cols., 1994; Bas Orth y cols., 2007; Jedlicka y cols., 2009; Sanchez-Ponce y cols., 2011). A pesar de estas similitudes a nivel funcional, hay diferencias importantes entre la organización del OSG y la de los orgánulos de cisterna. De acuerdo con estudios previos (Sánchez-Ponce y cols., 2011), el OSG está localizado en una posición central a lo largo de la longitud del SIA, con contactos sólo ocasionales a la membrana plasmática del SIA. El OSG está formado por túbulos largos y sacos aplanados que se alinean en paralelo con el eje longitudinal del axón. Son la continuación de estructuras tubulares similares situadas en la base del soma piramidal desde donde entran al cono del axón accediendo hasta el SIA. Por el contrario, el orgánulo de cisterna consiste en un apilamiento de cisternas membranosas aplanadas con un lumen estrecho, alternados con un material electrodenso, cuya cisterna más externa está asociada al lado interno de la membrana plasmática del axón. Además las cisternas se encuentran a lo largo del SIA asociadas a menudo con regiones del SIA que reciben contactos sinápticos (Palay y cols., 1968; Peters y cols., 1968; Jones y Powell 1969; Sloper y Powell 1979; Kosaka 1980; Somogyi y cols., 1983; Benedeczky y cols., 1994; Jedlicka y cols., 2009). En este trabajo no hemos observado, mediante microscopia confocal, la coexistencia de OSG y los orgánulos de cisternas en el SIA de la subpoblación de neuronas piramidales que contienen un OSG. Esto indica la existencia de diferentes tipos de estructuras dentro del SIA, que podrían participar en

la regulación de los niveles de calcio. Sin embargo, para confirmar esto resultaría necesario realizar experimentos con reconstrucciones en tres dimensiones del SIA a nivel ultraestructural para descartar la coexistencia de OSG y los orgánulos de cisternas.

Finalmente, hemos estudiado también el OSG en neuronas humanas a partir de secciones de regiones no epileptogénicas del área motora suplementaria (AMS) y de la neocorteza temporal lateral procedentes de biopsias obtenidas mediante el tratamiento quirúrgico de pacientes epilépticos. En este material hemos identificado el OSG en base a la expresión de sinaptopodina en el SIA (identificado mediante anticuerpos frente a espectrina-IVβ), de neuronas piramidales (26.6 %, n = 387 y 30.6 %, n = 346 en el área motora suplementaria y en la neocorteza temporal, respectivamente). A diferencia de lo observado en roedores, en los que el OSG sólo se encontró en el SIA de neuronas piramidales de capa V, en la corteza humana se observó que el OSG está también presente de forma ocasional en neuronas de capa III. Por último, observamos también la expresión de SERCA en el OSG de neuronas de la capa V tanto en el área suplementaria motora como en la neocorteza temporal. Esto sugiere que el OSG podría tener también en las neuronas de la neocorteza humana un papel importante en la regulación de los niveles de calcio en el SIA de algunas subpoblaciones de células piramidales, participando así en el correcto funcionamiento y mantenimiento del SIA en neuronas piramidales de proyección descendente.

B. II El segmento inicial del axón en neuronas corticales con acúmulos de tau hiperfosforilada en pacientes con la enfermedad de Alzheimer y en el modelo murino de taupatía P301S

Distintos estudios han destacado la importancia que podrían tener las alteraciones del segmento inicial del axón (SIA) en varias enfermedades psiquiátricas y neurológicas (por ejemplo, véase Buffington y Rasband, 2001). Desde hace unos años se ha atribuido al SIA una función de barrera de difusión de la proteína tau, promoviendo la restricción de las distintas isoformas de tau en dominios específicos de la neurona. También se ha descrito que esta función se altera en modelos murinos de la EA cuando tau se hiperfosforila y los microtúbulos se desorganizan, o en experimentos donde se disminuye la expresión de proteínas esenciales del SIA como la anquirina-G o EB1 (Li y cols., 2011; Sun y cols., 2014; Zempel y cols., 2017). En un estudio reciente en el modelo murino rTg4510 de taupatía, se ha descrito el desplazamiento distal del SIA en neuronas hipocampales (Hatch y cols., 2017), aunque en dicho estudio no se evaluó de forma directa la presencia de tau hiperfosforilado en dichas neuronas.

En este trabajo hemos evaluado si la presencia de tau hiperfosforilado en neuronas corticales podría estar asociada a alteraciones en la estructura o en la posición del SIA. Para ello hemos realizado experimentos inmunocitoquímicos en tejido cerebral procedente de tres fuentes distintas: 1) de autopsias de pacientes con EA, 2) de una autopsia realizada a un varón de 45 años de edad sin alteraciones neurológicas o psiquiátricas (sin diagnóstico de EA) pero cuya corteza cerebral presentaba una cantidad importante de ovillos neurofibrilares de tau hiperfosforilado, y 3) del modelo murino de taupatía P301S. En todos los casos se usaron simultáneamente anticuerpos para visualizar el SIA (espectrina-IVβ), la proteína tau hiperfosforilada (AT8) y el soma neuronal (NeuN). Para poder medir la distancia existente entre la base del soma de la célula piramidal y el punto de inicio y final del SIA, y poder obtener los valores de longitud y distancia al soma, se utilizó el software Imaris (herramienta *3D measurement point tool)*.

Alteraciones del SIA en neuronas de pacientes con la enfermedad de Alzheimer

Tomando conjuntamente los datos procedentes de todos los pacientes de Alzheimer analizados, hemos observado que la gran mayoría (82%) de las neuronas AT8+ tienen unos valores de longitud (n=50) y/o posición (punto de inicio) del SIA diferentes a las neuronas AT8- (n=87). No observamos diferencias en la longitud o en la posición del SIA del 17% restante de las neuronas AT8+ respecto a los valores de las neuronas negativas para AT8 (AT8-). Además, en el 56.5% de todas las neuronas AT8+ que presentaron cambios en la longitud del SIA, este presentó una mayor longitud (de 8.94 ±2.7 µm) que el de las neuronas AT8-, mientras que fue más corto (en 4.14 ±2.57 µm) en el 43.5% restante. También encontramos que en el 81.2% de las neuronas AT8+ analizadas, cuyo SIA presentó algún cambio de posición, su punto de inicio estuvo localizado más cerca del soma (desplazamiento proximal de 4.39 ± 2.36 µm) que en neuronas AT8-, mientras que se observó más distalmente (desplazamiento distal de 4.5 ±2.87 µm) en el restante 19.8%. Finalmente, algunas de las neuronas AT8+ (32.3%) mostraron diferencias tanto en la longitud como en la posición del SIA. Si bien las alteraciones observadas en el SIA de las neuronas con tau hiperfosforilado son variadas y heterogéneas, las alteraciones que se observaron con mayor frecuencia consistieron en el alargamiento y el desplazamiento proximal del SIA, aunque ambos fenómenos solo se dieron simultáneamente en la misma neurona de forma ocasional.

Alteraciones del SIA en neuronas con tau hiperfosforilado en un sujeto sin demencia y en el modelo murino P301S de taupatía.

Para tratar de evaluar en tejido humano el efecto debido solamente a la patología tau (en principio sin ningún otro factor patológico propio de la EA como las placas de β-amiloide), analizamos el SIA de neuronas en la corteza temporal de un paciente sin demencia, utilizado en estudios previos del laboratorio (Antón-Fernández y cols, 2017).

Dicho sujeto presentaba una cantidad considerable de neuronas con agregados de tau hiperfosforilado en distintas áreas corticales incluida la neocorteza temporal, en ausencia de placas de β-amiloide. En la neocorteza temporal de este caso, al igual que observamos en los pacientes, encontramos que en la gran mayoría (71.4%) de las neuronas AT8+, los valores de longitud y/o de posición (punto de inicio) del SIA presentaron diferencias al compararlos con los de las neuronas sin tau hiperfosforilado (AT8-). De todas aquellas neuronas AT8+ en las que se observaron diferencias en la longitud de su SIA, aproximadamente la mitad presentaron un SIA más largo que el de las neuronas AT8-. En cuanto a las neuronas AT8+ que mostraron diferencias en la posición de su SIA, al igual que en los pacientes, en la mayoría de los casos (75%) el SIA se localizó en una posición más proximal respecto a las neuronas AT8-. Además, de forma similar a lo que observamos en los pacientes, alrededor de un tercio de las neuronas con patología tau mostraron de forma simultánea cambios en el SIA tanto en longitud como en la posición dentro del axón.

Asimismo, para evaluar la posible relación entre la acumulación de tau hiperfosforilado y las alteraciones del SIA utilizamos también un modelo murino de taupatía (P301S), caracterizado por la presencia de neuronas AT8+ en la corteza sensorimotora en ausencia de patología amiloide. Estudiamos en la corteza somatosensorial de ratones transgénicos y control de 36 semanas de edad, el SIA de neuronas piramidales que desarrollaron agregados de fosfo-tau, comparándolo con el de aquellas neuronas adyacentes que no los desarrollaron. Al comparar la distribución general de la inmunoreactividad para la espectrina-IVβ, entre el grupo transgénico y el control, no se observaron cambios aparentes. Sin embargo, al analizar de forma más detallada las series de imágenes obtenidas por microscopía confocal, encontramos nuevamente alteraciones estructurales en el SIA de un número importante de neuronas que presentaban agregaciones de fosfo-tau. En algo más de la mitad de las neuronas AT8+ (52.2%), el AIS se encontró alterado en longitud y/o posición en comparación con el de las neuronas AT8-. En este caso el acortamiento del AIS en las neuronas AT8+ fue algo más común que el alargamiento (60/40%), mientras que desplazamiento proximal de este hacia el soma fue igual de frecuente que el desplazamiento distal.

Los resultados obtenidos apoyan por tanto lo observado en los pacientes con EA y sugieren la existencia de una relación entre la presencia intracelular de agregados de tau hiperfosforilado y las alteraciones en la longitud y posición del SIA.

Limitaciones del estudio

Una de las limitaciones del presente estudio consiste en la existencia de una importante variabilidad en la longitud del SIA entre neuronas de distintas capas corticales y entre diferentes poblaciones neuronales (Inda y cols, 2008; Höfflin y cols, 2017; León-Espinosa y cols, 2018). Con la metodología empleada en este trabajo no es posible conocer la longitud del SIA ni su posición en aquellas neuronas AT8+ antes de que estas desarrollaran los agregados de tau hiperfosforilado. Con objeto de minimizar dicha limitación y para evitar además la posible variabilidad interindividual en la longitud de los SIA, en este estudio hemos comparado en cada paciente por separado, la longitud del SIA y su posición en cada neurona AT8+, con respecto a la media y desviación estándar obtenida a partir de todas las neuronas AT8- de la misma capa cortical (neuronas vecinas). Para cada una de las medidas realizadas (longitud, posición del punto de inicio y punto de terminación del AIS), hemos considerado que los valores del SIA de cada neurona AT8+ era diferente de los valores medios del SIA de las neuronas AT8-, cuando las diferencias excedieron la desviación estándar.

Otra limitación consiste en que únicamente hemos utilizado anticuerpos AT8, que reconocen el tau fosforilado en la serina situada en la posición 202 y en la treonina 205. Por lo tanto, no podemos descartar que algunas de las neuronas negativas para AT8, tuvieran tau hiperfosforilado en otros residuos distintos a los reconocidos por los anticuerpos AT8. Sería interesante por tanto llevar a cabo nuevos estudios usando anticuerpos que reconocieran tau fosforilada en distintos residuos, en combinación con anticuerpos que visualizaran el SIA, para poder saber más acerca de la vulnerabilidad del SIA en relación a la progresión de la hiperfosforilación de tau a lo largo del desarrollo de la enfermedad.

Por otro lado, en este estudio el número de SIAs que ha sido posible analizar, fundamentalmente en tejido humano, ha sido relativamente pequeño. Distintos factores han contribuido a ello. Según nuestra experiencia, los anticuerpos contra la espectrina-IVβ (donados por Dr. Mathew Rasband, *University of Texas, USA*) representa la mejor opción para visualizar el SIA en tejido humano en combinación con los anticuerpos AT8, que detectan fosfo-tau. Sin embargo, de entre todos los casos de pacientes con EA de los que disponemos tejido cerebral en nuestro laboratorio, algunos de ellos ya utilizados en estudios anteriores, los anticuerpos frente a espectrina-IVβ solamente funcionaron en tejido procedente de tres pacientes (IF6, IF8 e IF13) con un estadio relativamente temprano de la enfermedad (estadio III de Braak). Por el contrario, no observamos inmunoreactividad para la espectrina-IVβ en el tejido proveniente de 8 pacientes fallecidos en estadios más avanzados de la enfermedad.

Estudios previos han descrito mediante *Western blot* que la expresión de anquirina-G y espectrina-IVβ, proteínas esenciales para el mantenimiento de la estructura del SIA (Jenkins y Bennet, 2001; Komada y Soriano, 2002; Hedstrom y cols., 2008), está muy reducida en pacientes en estadios avanzados de la enfermedad (estadios V-VI) en comparación con pacientes de estadios más tempranos (estadio I-II) (Sohn y colaboradores, 2016). Por lo tanto, esto podría explicar la falta de inmunoreactividad para espectrina-IVβ en los pacientes más avanzados que hemos empleado en nuestro estudio. Por otra parte, es conocido que el periodo *post mortem* del paciente previo a la fijación del su cerebro, así como los procedimientos de fijación, inclusión y tinción pueden afectar a la calidad de las tinciones inmunocitoquímicas (González Riano y cols., 2018). Sin embargo, en nuestras muestras el periodo *post mortem* previo a la fijación fue menor a 5 horas en la mayoría de los casos, y todas las muestras se procesaron mediante los mismos procedimientos, por lo que las diferencias observadas en la inmunoreactividad para la espectrina-IVβ del SIA, podrían estar más bien relacionadas con la evolución de la enfermedad. Por último, en dos de los tres pacientes utilizados (IF6 e IF8), la presencia de neuronas con tau hiperfosforilado (visualizados gracias a la inmunoreactividad producida por AT8) fue relativamente baja, lo que redujo aún más el número potencial de SIAs para el análisis.

Asimismo, se ha descrito previamente que el contacto o la proximidad del SIA a las placas de β-amiloide, cuya formación es de las principales características

histopatológicas de la EA, está asociado a la disminución en la longitud del SIA y en la expresión de espectrina-IVβ en neuronas del modelo murino de amiloidosis APP-PS1 (Marín y cols., 2016). Por lo tanto, la pérdida de la inmunoreactividad para espectrina-IVβ en algunos pacientes, podría ser también debida a la presencia de placas de amiloide. Sin embargo, nuestros resultados indican que en la EA la acumulación de placas no sería el único factor responsable de la alteración de la inmunoreactividad para espectrina-IVβ en el SIA, dado que la inmunoreactividad se conserva en pacientes con una cantidad relativamente alta de placas de amiloide (IF13). Además, para estudiar los posibles efectos sobre el SIA asociados solamente a la presencia intracelular de agregados de tau hiperfosforilado, y tratar de minimizar los efectos inducidos por su proximidad a las placas de amiloide, en este trabajo nos centramos únicamente en aquellos SIAs de neuronas no adyacentes a las placas de amiloide. Las placas se identificaron mediante la inmunoreactividad para AT8, con la que se pueden visualizar al menos una parte de las placas de amiloide, así como por la ausencia de somas neuronales en las placas (visualizados mediante NeuN).

Implicaciones funcionales de las alteraciones del SIA

Las alteraciones en longitud y/o posición del SIA encontradas en neuronas con agregados intracelulares de tau hiperfosforilado, probablemente estén alterando la excitabilidad neuronal, contribuyendo así a la disfunción de los circuitos en los que estas neuronas participan, lo que podría contribuir a la patofisiología de la EA. De hecho, recientemente se ha descrito que la alteración en la excitabilidad neuronal es un rasgo importante de la EA (Palop y Mucke, 2009), habiéndose sugerido que la proteína tau podría tener un papel importante y heterogéneo en la modulación de la excitabilidad neuronal. Por ejemplo, la disminución de los niveles de tau en modelos animales transgénicos o mediante terapia génica, induce una reducción en la excitabilidad de la corteza cerebral (Roberson y cols., 2007; DeVos y cols, 2013; Holth y cols., 2013;). Además la presencia de fosfo-tau en el dominio somatodendrítico *in vitro* parece disminuir la actividad neuronal (Thies y Mandelkow, 2007; Hoover y cols., 2010). Se han descrito también efectos muy diversos de la patología tau sobre la

actividad neuronal en ratones transgénicos P301L, según la región cortical afectada. Por ejemplo, en neuronas neocorticales de la corteza frontal se observó un incremento en la tasa de generación de potenciales de acción (Rocher y cols., 2010), en neuronas hipocampales se observó justo lo contrario, es decir, una reducción en la tasa de disparo (Hatch y col., 2017), mientras que en la corteza visual no se observaron cambios significativos en la actividad neuronal (Kuchibhotla y cols., 2014).

Por otro lado, se ha observado que los cambios en la actividad neuronal pueden afectar de manera diferencial al SIA de distintas poblaciones neuronales. Por ejemplo, la despolarización crónica de neuronas del giro dentado induce el acortamiento de su SIA (Evans y cols., 2015), mientras que en neuronas piramidales de CA1 produce un desplazamiento distal del mismo (Wefelmeyer y cols., 2015). Por lo tanto, teniendo en cuenta lo mencionado anteriormente, se podría especular que la heterogeneidad en los cambios de longitud y posición SIA encontrados en este trabajo, podrían estar relacionados con alteraciones diferenciales en la actividad neuronal inducidas por la presencia de tau hiperfosforilado en distintas poblaciones neuronales. Sin embargo, es necesario realizar estudios adicionales para confirmar o descartar esta posibilidad.

Asimismo, se ha descrito que la posición relativa del SIA, así como su longitud pueden modular la excitabilidad neuronal (Grubb y Burrone 2010; Kuba y cols., 2010) dándose una relación lineal negativa entre la tasa de disparo de potenciales de acción y la distancia del SIA al soma (Hatch y cols., 2017). De este modo, es probable que los cambios encontrados en este estudio en el SIA en neuronas con agregados de tau hiperfosforilado, tengan un impacto relevante sobre la excitabilidad de dichas células. Ya que dichos cambios son heterogéneos podrían ayudar a explicar los diferentes efectos que la presencia de la patología tau induce en diferentes poblaciones neuronales.

En resumen, el presente estudio demuestra que la mayor parte de las neuronas corticales con tau hiperfosforilado presenta alteraciones en el SIA. Las posibles relaciones causales que pueden establecerse entre la acumulación de tau fosforilado, los cambios en la actividad neuronal y las alteraciones estructurales del SIA parecen ser heterogéneas y complejas y podrían variar entre distintas poblaciones neuronales.

Por lo tanto, el esclarecimiento de la posible contribución de las alteraciones de los AIS a la fisiopatología de la enfermedad de Alzheimer requeriría futuros estudios para analizar distintas regiones del cerebro de estos pacientes (distintas áreas neocorticales, diferentes regiones del hipocampo, etc.) y la utilización de diversos anticuerpos que reconozcan tau hiperfosforilado en otros residuos distintos a los reconocidos por los anticuerpos AT8 en combinación con anticuerpos que permitan visualizar el SIA.

B. III Modificaciones del segmento inicial del axón en neuronas piramidales de la corteza cerebral durante la hibernación del hámster Sirio

Los principales resultados de este estudio se pueden resumir en tres puntos: primero hemos demostrado que la utilización de anticuerpos policlonales c-20, obtenidos en cabras y sintetizados originalmente frente un péptido de la proteína GRASP65 del aparato de Golgi (AG), es una excelente herramienta para visualizar el segmento inicial del axón (SIA) en neuronas de roedores. Esto permitió medir la longitud del SIA durante las distintas fases del ciclo de hibernación del hámster Sirio en combinación con la detección simultánea de tau fosforilada mediante anticuerpos monoclonales de ratón AT8. En segundo lugar, hemos comprobado que durante la fase de torpor del hámster la longitud del SIA se incrementa significativamente respecto a animales eutérmicos tanto en la corteza somatosensorial como en la región CA1 del hipocampo. En tercer lugar, observamos que el SIA de neuronas neocorticales de la capa V de animales en torpor, son significativamente más largos en neuronas que expresan fosfo-tau (AT8+) que en aquellas que carecieron de inmunoreactividad para AT8 (AT8-), sugiriendo que los cambios plásticos del SIA serían más pronunciados en aquellas neuronas que acumulan fosfo-tau.

Identificación del segmento inicial del axón (SIA) mediante anticuerpos policlonales c-20 (sc-19481)

Durante el desarrollo de los estudios descritos anteriormente acerca de la relación entre la hiperfosforilación de la proteína tau y las alteraciones estructurales del AG en la enfermedad de Alzheimer (EA) y en distintos modelos animales (Antón-Fernández y cols, 2015,2017a, 2017b) se usaron distintos anticuerpos para identificar el AG. Entre ellos, observamos que los anticuerpos policlonales c-20 obtenidos en cabra (Santa Cruz sc-19481) y sintetizados frente a un péptido correspondiente a la proteína humana GRASP65, reconocían el AG neuronal en tejido cerebral humano. En tejido procedente

de ratones y hámsteres este anticuerpo reconoce el AG con mucha menos intensidad, marcando, por el contrario, estructuras filiformes que se extendían desde la base del soma de las neuronas piramidales, reminiscentes del segmento inicial del axón (SIA). Para determinar si estas estructuras eran realmente SIAs, llevamos a cabo experimentos de doble marcaje, combinando anticuerpos c-20 con anticuerpos comerciales frente a anquirina-G (N*euromab*), que es uno de los principales componentes estructurales del SIA. Esta proteína, junto a la espectrina-IVβ, son elementos esenciales para el mantenimiento estructural y funcional del SIA, debido a su papel en la asociación de distintos tipos de canales iónicos dependientes de voltaje al citoesqueleto axonal (Rasband, 2010; Jenkins y cols, 2015; Leterrier, 2016), lo que determina las propiedades biofísicas del SIA, incluida la generación de potenciales de acción.

En neuronas procedentes de la capa II de la neocorteza de animales control (en eutermia), encontramos inmunoreactividad para el anticuerpo c-20 en 660 de 667 SIAs (99% de colocalización), identificados por la inmunoreactividad para anquirina-G (*neuromab*). Además, utilizando el software *Imaris* (mediante la herramienta "*measuremente point*") medimos la longitud del SIA (n=24) en experimentos de doble marcaje para c-20/anquirina-G, y encontramos que ambos tipos de inmunoreactividad tuvieron prácticamente la misma longitud (24.09 ± 3.36 µm con c-20 y 24.42 ± 3.08 µm con los anticuerpos de *Neuromab* frente a anquirina-G). Estos resultados indican que los anticuerpos c-20 representan un marcador fiable del SIA en tejido cerebral de ratón y hámster.

Caracterización de los anticuerpos c-20

Aunque la compañía productora de dichos anticuerpos no proporciona la secuencia completa ni la posición exacta del péptido inmunógeno empleado para inducir la producción de los anticuerpos, sí nos indicaron que fueron producidos contra un péptido de entre 15 y 25 aminoácidos situado en la región C-terminal (entre las posiciones 350 y 400) de la proteína GRASP65 de origen humano (NCBI AAH75854.1). Con objeto de determinar a qué componente del SIA se unen los anticuerpos c-20,

secuenciamos el péptido de bloqueo proporcionado por la compañía (Santa Cruz, sc-19481P) que se utilizó para obtener los anticuerpos c-20. Para ello se realizó una espectrometría de doble masa acoplada a cromatografía líquida (nLC MS/MS) en el Servicio de proteómica y genómica CIB (CSIC). Este análisis reveló que la secuencia de aminoácidos "EFEVSFLDSPGA", fue la secuencia peptídica más frecuentemente detectada por el espectrómetro (17 PSM), siendo por tanto el péptido inmunógeno más probable. A continuación realizamos una comparación de esta secuencia con la de las proteínas constituyentes del SIA mediante los programas *Blast* (*Basic Local Alignment Search Tool, NIH, U.S National Library of Medicine database*) y *Clustal Omega* (un programa de alineamiento de múltiples secuencias desarrollado por el Instituto Europeo de Bioinformática, EMBL-EBI). Este análisis reveló un 60% de homología con la secuencia situada entre la posición 3133 y la 3144 de la isoforma de 480-kDa de la anquirina-G, que es el componente principal del SIA y en donde se encuentra en mayor concentración (Kordeli y cols, 1995; Hedstrom y cols, 2008; Jenkins y cols, 2015).

Para intentar conocer las causas asociadas a las diferencias de los patrones de inmunoreactividad de los anticuerpos c-20 en distintas especies comparamos la secuencia del péptido inmunógeno con las secuencias de GRASP65 de roedores y humanos. Encontramos en roedores una prolina en la posición 374 que en humanos no está presente, habiendo en su lugar una leucina. Es probable que la presencia de esa prolina en roedores modifique la estructura secundaria de GRASP65, haciéndola distinta a la de humanos. De hecho, la simulación estructural de esta región proteica en ambas especies mediante el software Phyre2 (Kelley y cols, 2015) reveló la existencia de una estructura secundaria de tipo alfa hélice en humanos que sin embargo no está presente en roedores. Esto podría ayudar a explicar la baja eficiencia de unión de los anticuerpos c-20 a la proteína Grasp65 en roedores y en consecuencia la escasa visualización en estos animales del AG mediante el uso de los anticuerpos c-20. Es posible que como resultado de esta baja afinidad, se favorezca la unión de los anticuerpos c-20 a la proteína anquirina-G en roedores, generando una intensa inmunoreactividad del SIA. Finalmente, para saber si los anticuerpos c-20 se unen a la anquirina-G o a otra proteína conocida del SIA, realizamos experimentos de

inmunoprecipitación y de análisis por espectrometría de masas (Servicio de proteómica y genómica, CIB, CSIC). Para ello inmunoprecipitamos el homogeneizado de cerebro de ratón con anticuerpos c-20 y las proteínas precipitadas fueron separadas por electroforesis en gel de poliacrilamida con dodecilsulfato sódico (SDS-PAGE). Las bandas con el peso molecular esperado fueron cortadas del gel y posteriormente digeridas con tripsina y analizadas mediante cromatografía líquida combinada con espectrometría de masas (LC-MS). Los datos obtenidos por la espectroscopia de masas se contrastaron con la base de datos *Uniprot* del *Mus musculus* (que cuenta con 178667 entradas de secuencias proteicas) usando el motor de búsqueda SEQUEST. Este análisis mostró múltiples péptidos producidos por la digestión proteica que se correspondieron con 97 proteínas diferentes. De todas ellas, la anquirina-G fue el único componente conocido por estar presente en el SIA, que además mostró el tercer mejor índice de emparejamiento (*Score* o factor de fiabilidad) y el mayor porcentaje de cobertura (porcentaje de secuencia proteica reconocida). Además, uno de los péptidos de digestión fue detectado como péptido único de la anquirina-G. Todos estos resultados en su conjunto, nos indican que los anticuerpos c-20 reconocen de manera eficiente la anquirina-G en el cerebro de ratón, justificándose su uso como marcador fiable del SIA. Dada la escasa disponibilidad de reactivos diseñados para detectar el SIA en el hámster Sirio, la caracterización de este anticuerpo para su uso en estos animales tiene un interés particular ya que nos permitió realizar experimentos de doble marcaje mediante el uso simultáneo de anticuerpos monoclonales AT8 producidos en ratón para detectar tau hiperfosforilado.

Alargamiento del SIA durante la hibernación

Distintos estudios han demostrado que el SIA es una región esencial en la regulación de la actividad neuronal, mostrando además cambios plásticos en su estructura en respuesta a modificaciones en la actividad neuronal, lo que podría jugar un papel importante en la homeostasis de los circuitos neuronales y en las respuestas adaptativas del sistema nervioso (Grubb y Burrone, 2010; Kuba y cols, 2010;

Grundemann y Hausser 2010). Entre los diversos fenómenos de plasticidad del SIA descritos hasta ahora, se puede destacar la observada en el sistema auditivo del pollo, en el que la pérdida de actividad neuronal inducida por el bloqueo en la llegada de información sensorial presináptica condujo al incremento de la longitud del SIA de neuronas de los núcleos auditivos troncoencefálicos (Kuba y cols, 2010; Yamada y Kuba, 2016). También se ha observado que la deprivación de información visual durante el periodo crítico de la plasticidad de la corteza visual del ratón, evita el característico acortamiento del SIA, produciendo SIAs más largos de lo normal (Gutzmann y cols, 2014).

Para estudiar los posibles cambios en los SIAs que se podrían producir durante el ciclo de hibernación del hámster Sirio, así como su posible relación con la presencia de tau hiperfosforilado, realizamos experimentos usando tinciones de DAPI junto a dobles inmunotinciones combinando anticuerpos c-20, como marcador del SIA, y anticuerpos AT8 para visualizar la proteína tau hiperfosforilada. Primero medimos en series de imágenes en tres dimensiones obtenidas por microscopía confocal, la longitud de los SIAs de neuronas procedentes de capas II-III y V de la corteza somatosensorial, así como de la región CA1 del hipocampo, en animales control (en eutermia). En la neocorteza, la longitud del SIA en neuronas de las capas II-III y V de animales control fue de 22.23± 1.39 µm (n=154 SIAs, medidos en 9 animales distintos) y de 23.79 ±2.01 µm (n=141 SIAs, medidos en 9 animales distintos), respectivamente, mientras que en neuronas hipocampales de CA1, fueron significativamente más largos (31.76 ± 3.00 µm; test de ANOVA con la corrección de Bonferroni, n=192 SIAs, medidos en 9 animales distintos). A continuación analizamos las posibles variaciones de la longitud del SIA en animales en fase de torpor. En estos animales, la longitud del SIA en ambas regiones fue significativamente mayor que el observado en animales en eutermia. En neuronas de la capa II-III, esta longitud fue de 26.53 ±1.86 µm (n=210 SIAs, medidos en 12 animales distintos), mientras que en la capa V esta fue de 27.41 ± 2.19 µm (n=273 SIAs, medidos en 11 animales distintos). En neuronas hipocampales de CA1 la longitud del SIA fue de 37.93 ± 3.30 µm (n=113 SIAs medidos en 6 animales distintos). El análisis estadístico reveló que el AIS de neuronas neocorticales e hipocampales es significativamente más largo en neuronas de animales en torpor que en animales en

eutermia (p=0.0039, p=0.0273 y p=0.0313 en neuronas de capa II-III y capa V de la neocorteza, y en CA1, respectivamente) incrementándose la longitud del SIA un 19.48% (4.30 µm), un 13.20% (3.62 µm) y un 19.42% (6.17 µm) respectivamente.

Durante la fase de torpor se ha descrito un cese casi total de la actividad neuronal en áreas corticales y mesencefálicas (Strumwasser 1959; Igelmund, 1995; Igelmund y Heinemann 1995; South, 1972; Walker y cols, 1977). Por lo tanto es posible que el alargamiento del SIA observado en nuestros resultados pueda ser consecuencia de este cese de actividad neuronal durante el torpor. Se ha descrito que los cambios en la actividad neuronal afectan de forma diferencial al SIA de distintas poblaciones neuronales. Por ejemplo, la despolarización neuronal crónica induce el acortamiento del SIA en células granulares de giro dentado (Evans y cols, 2015) y un desplazamiento distal del SIA en neuronas piramidales hipocampales de CA1 (Wefelmeyer y cols, 2015). Dado que en nuestro trabajo hemos estudiado únicamente la corteza sensorial primaria y la región CA1 del hipocampo, es necesario realizar estudios adicionales en otras regiones para determinar si el alargamiento del SIA durante la fase de torpor es un proceso generalizado o es un fenómeno específico de las regiones estudiadas.

Aunque el alargamiento del SIA distal que se produce durante la fase de torpor es relativamente reducido (13-19%), este cambio podría inducir efectos relevantes para la excitabilidad neuronal ya que la región distal del SIA es donde se originan los potenciales de acción (Kole y cols, 2007; Baranauskas y cols, 2013). En el sistema auditivo del pollo, el alargamiento del SIA inducido por la deprivación de información sensorial conduce al incremento de los agrupamientos de canales de sodio dependientes de voltaje en el SIA, en paralelo a una reducción del umbral de excitabilidad neuronal (Kuba y cols, 2010). Aunque el conocimiento del significado biológico del alargamiento del SIA durante el torpor, así como los efectos directos que esta modificación pueda tener sobre la excitabilidad neuronal,— como por ejemplo cambios en las características del potencial de acción—requiere estudios adicionales, es probable que estén relacionados con el incremento en la duración de los potenciales de acción durante la fase de torpor de la hibernación (Krilowicz y cols, 1989), que se caracteriza por un descenso generalizado en la actividad eléctrica del cerebro (Strumwasser 1959; South et al. 1968; Mihailovic 1972). El alargamiento del SIA durante el torpor podría tener además consecuencias indirectas para la

excitabilidad de las neuronas piramidales, al modificar la relación espacial entre el SIA y las sinapsis axoaxónicas GABAérgicas procedentes de las células en candelabro (Muir y Kittler 2014; Wefelmeyer y cols, 2015). Todos los posibles efectos debidos a las alteraciones del SIA durante el torpor, podrían ser importantes a la hora de promover la entrada en los episodios de vigilia que se dan durante la hibernación (*arousal*), o la transición estacional definitiva desde el torpor a la fase de eutermia.

Para estudiar si el incremento de la longitud del SIA durante el torpor va acompañado con cambios en su posición, comparamos el punto de origen del SIA entre neuronas procedentes de animales en fases de eutermia o de torpor. En aquellas neuronas procedentes de animales eutérmicos encontramos que los SIAs se originan directamente desde la base del soma en la gran mayoría de las neuronas (173 de 189). En las restantes 16 neuronas (8.5%), el SIA fue localizado en una posición ligeramente más distal del axón, con un espacio entre la base del soma y el punto de inicio del SIA de 1.3 ±0.7 µm. De la misma forma, en neuronas de animales en estado de torpor, encontramos que en tan solo 10 de 121 neuronas (8.2%) el inicio del SIA fue localizado en una posición más distal (1.84 ± 0.55 µm), mientras que en la mayoría de las neuronas, el SIA emergía directamente desde la base del soma neuronal. Por tanto, estos resultados indican que el incremento en la longitud del SIA durante el torpor no está asociado al desplazamiento del punto de origen del SIA, sino probablemente al desplazamiento de su límite distal, caracterizado por la transición de la expresión de anquirina-G, propia del SIA, a la de la anquirina-B, presente en regiones más distales del axón (Galiano y cols, 2012). Por último, aunque se ha descrito que la sobreexpresión de la anquirina-G conduce al incremento de la longitud del SIA (Galiano y cols, 2012), los mecanismos moleculares que subyacen al incremento del longitud del SIA durante el torpor no se han explorado hasta el momento.

Por lo tanto, los resultados de este estudio avalan la utilización de la hibernación del hámster Sirio como modelo natural para estudiar los mecanismos adaptativos de plasticidad del SIA en condiciones no patológicas, así como las modificaciones compensatorias en respuesta a la disminución de la actividad neuronal.

Cambios del SIA durante el torpor en neuronas con tau hiperfosforilado

De acuerdo con estudios previos (Arendt y cols, 2003; Avila y cols, 2004; Hartig y cols, 2005; Hartig y cols, 2007; Stieler y cols, 2011; León-Espinosa y cols, 2013; Antón-Fernández y cols, 2015), durante la fase de torpor en la hibernación del hámster Sirio la proteína tau se hiperfosforila y se acumula en el compartimento somatodendrítico de algunas subpoblaciones neuronales de la corteza cerebral. Una vez que el animal vuelve al estado de eutermia, esta fosforilación disminuye a niveles normales (Arendt y cols, 2003; Hartig y cols, 2005; Hartig y cols, 2007; Stieler y cols, 2011; León-Espinosa y cols, 2013; Antón-Fernández y cols, 2015). De acuerdo con dichas observaciones, en nuestro material hemos observado niveles elevados de tau hiperfosforilado, en la serina 202 y la treonina 205 (identificados mediante anticuerpos AT8), en el cuerpo celular y dendritas apicales de una subpoblación de neuronas piramidales de la capa V de la neocorteza. No encontramos sin embargo inmunoreactividad para AT8 en el SIA de estas neuronas. A continuación estudiamos si las alteraciones del SIA son más frecuentes en las neuronas con tau hiperfosforilado que en las neuronas negativas para AT8. Realizamos dobles inmunotinciones con los anticuerpos AT8 y c-20en material procedente de animales en torpor y medimos la longitud del SIA de 133 neuronas piramidales positivas para AT8 y de 129 neuronas negativas para AT8. Observamos que durante la fase de torpor, la longitud del SIA en neuronas con inmunoreactividad para AT8 fue mayor (28.54 ± 2.29 µm) que el de aquellas que carecen de tau hiperfosforilada (27.47 ± 2.163 µm). Aunque la diferencia en las medias entre las AT8+ y AT8- fue solo de 1.07 µm (3.9%), esta diferencia fue significativa estadísticamente ($p=0.0488$). Una posible explicación de estos resultados sería que la plasticidad del SIA durante el torpor es algo más pronunciada en neuronas que presentan acumulaciones de tau hiperfosforilado. Se ha descrito que la presencia de tau fosforilado en el dominio somatodendrítico disminuye la actividad neuronal (Thies y Mandelkow 2007; Hoover y cols, 2010). Por lo tanto, esta reducción de la actividad neuronal podría ser más pronunciada en las neuronas AT8 positivas que en las AT8 negativas, lo que podría inducir un alargamiento mayor en el SIA de aquellas neuronas que acumulan tau hiperfosforilado.

Por otro lado, se sabe que las neuronas piramidales de la capa V son fisiológica y anatómicamente heterogéneas e incluyen distintas subpoblaciones en base a distintas características morfológicas y electrofisiológicas o a la expresión de distintas combinaciones de marcadores neuronales y patrones de expresión génica (Angulo y cols, 2003; Tsiola y cols, 2003; Molnar y Cheung 2006; Sorensen y cols, 2013). También se sabe que existe una variabilidad considerable en las propiedades morfológicas del SIA entre las distintas poblaciones de neuronas corticales (Hofflin y cols, 2017). Ya que hasta el momento desconocemos la identidad de la subpoblación de neuronas piramidales de capa V que acumulan fosfo-tau durante el torpor, una segunda posibilidad es que constituyan una subpoblación neuronal con un SIA particularmente grande en eutermia. Es por ello que sería necesario realizar nuevos estudios para distinguir entre ambas posibilidades.

A pesar de las similitudes existentes entre la acumulación somatodendrítica de tau hiperfosforilado que se produce en los mamíferos hibernantes durante la fase de torpor y la que se produce en las fases iniciales de la EA, hay diferencias evidentes que podrían estar relacionadas con la preservación de la integridad del SIA. El SIA actúa como una barrera de difusión que ayuda a mantener una distribución diferencial de las distintas isoformas de tau en dominios específicos de la neurona. Se ha descrito que la integridad de dicha barrera se altera en modelos de la EA en los que tau está hiperfosforilada, favoreciendo su acumulación en el dominio somatodendrítico (Li y cols, 2011). Estudios recientes han demostrado *in vitro* que la fosforilación de tau o la pérdida de expresión de la anquirina-G, altera la barrera de difusión del SIA induciendo la deslocalización de tau a lo largo de la neurona (Zempel y cols, 2017). Por el contrario, en nuestro estudio hemos observado que durante la fase de torpor, aquellas neuronas con tau hiperfosforilado, en las cuales la integridad del SIA está preservada (a juzgar por la inmunoreactividad para anquirina-G), el marcaje para AT8 se vio restringido exclusivamente al dominio somatodendrítico, no encontrándose nunca en los axones, incluido el SIA. Esto sugiere que la fosforilación de tau no es el único requerimiento necesario para la alteración de la barrera de difusión del SIA. La fosforilación de tau es consecuencia del equilibrio entre la actividad de varias quinasas y fosfatasas, algunas de las cuales están restringidas al dominio neuronal somatodendrítico o axonal (Bertrand y cols, 2010). Por lo tanto, además de las

diferencias entre la secuencia de la proteína tau del humano y del hámster Sirio, que podrían afectar a la fosforilación de tau (León-Espinosa y cols, 2013), nuestros resultados sugieren que la acumulación somatodendrítica de fosfo-tau en neuronas del hámster Sirio, a diferencia de la EA, podría estar relacionada con la activación de quinasas y/o inactivación de fosfatasas del dominio somatodendrítico, más que con la alteración de la barrera del SIA.

Desorganización del SIA tras el ictus isquémico durante la fase de normotermia

La hibernación en mamíferos incluye diversas respuestas adaptativas ante condiciones extremas. La fase de torpor está acompañada por una disminución de la actividad del sistema inmune, del metabolismo, de la temperatura corporal y del gasto cardiaco y flujo sanguíneo, lo que en condiciones normales resultaría en un cerebro isquémico (Frerichs y cols, 1994; Drew y cols, 2001; Zhou y cols, 2001; Bouma y cols, 2010a). Distintos estudios han observado que durante el torpor se producen procesos adaptativos neuroprotectores orientados a prevenir el daño neuronal. Entre dichos cambios se incluyen los que se producen en células de microglía, cambios estructurales en neuronas como la fragmentación y reducción del aparato de Golgi, o en la conectividad sináptica como por ejemplo la retracción de las espinas dendríticas (Popov y Bocharova 1992; von der Ohe y cols, 2006, 2007; Popov y cols, 2007; Bouma y cols, 2010a; Bouma y cols, 2010b; Antón-Fernandez y cols, 2015; Cogut y cols, 2017; Leon-Espinosa y cols, 2017). El presente estudio añade el SIA a la lista de estructuras neuronales que podrían beneficiarse de mecanismos de neuroprotección durante la hibernación. Estudios previos han mostrado que las condiciones isquémicas en cerebros de mamíferos no hibernantes, incluido el hombre, producen el desensamblaje del SIA (Schafer y cols, 2009; Hinman y cols, 2013; Del Puerto y cols, 2015; Coban y cols, 2017). Se ha observado que la isquemia inducida mediante la oclusión de la arteria cerebral media, es un modelo de ictus isquémico que conduce a la proteólisis mediada por calpaína de las proteínas esenciales para el mantenimiento estructural del SIA, como la anquirina-G y la espectrina-IVβ (Schafer y cols, 2009).

Asimismo, estudios recientes realizados con modelos de inflamación como la inyección periférica de lipopolisacárido o la que se produce en la esclerosis múltiple, han demostrado que el estrés oxidativo conduce a la activación de la calpaína, induciendo la pérdida de proteínas del SIA que alteran su estabilidad (Clark y cols, 2016,2017; Benusa y cols, 2017).

Los resultados de nuestro estudio demuestran que durante el torpor, a juzgar por la inmunoreactividad para la anquirina-G, no se produce la degradación de los SIAs de neuronas corticales, lo que sugiere la existencia de mecanismos neuroprotectores que preservarían durante la hibernación la expresión de la anquirina-G en el SIA.

Para comprobar si esos mecanismos neuroprotectores evitan la degradación de los SIAs en condiciones de hipoxia/isquemia en la fase de normotermia, estudiamos triples inmunotinciones de anquirina-G/Iba-1/NeuN en secciones cerebrales procedentes de animales en los cuales se indujeron isquemias focales a través de la oclusión permanente de la rama frontal de la arteria cerebral media. Como se esperaba, la inmunoreactividad para iba-1 reveló la región infartada en la neocorteza ipsilateral que afectó principalmente a la corteza somatosensorial primaria. En esta región infartada, la inmunoreactividad para iba-1 en las células microgliales fue muy intensa. Además, estas células mostraron frecuentemente un fenotipo hipertrófico no ramificado en comparación con la morfología de las células microgliales en reposo, situadas en la corteza somatosensorial y motora contralateral. Al contrario que en las regiones contralaterales que no fueron afectadas por la oclusión arterial, donde se observaron patrones normales de inmunoreactividad para el SIA, en la región infartada se observó una importante pérdida en la inmunoreactividad para anquirina-G en los SIAs (visualizados tanto con c-20 como con anticuerpos de *Neuromab*). En general no se observaron SIAs positivos para la anquirina-G en la región infartada o al menos éstos mostraron un tamaño muy reducido. Estos resultados indican que en el hámster Sirio, la acumulación de anquirina-G en el SIA se pierde y por tanto la integridad del SIA se altera tras la exposición a condiciones de isquemia e hipoxia durante las fases de normotermia. Esto contrasta con la preservación de la expresión de la anquirina-G en el SIA durante condiciones de isquemia/hipoxia asociadas con la fase de torpor de la hibernación.

Es sabido que la fase de torpor está asociada a un estado de tolerancia frente a la hipoxia y a la aglicemia propias de este periodo (Frerichs y cols, 1998), gracias al incremento en la actividad de sistemas de defensa antioxidante, que permiten una mayor tolerancia al daño cerebral en comparación con el que produciría un fenómeno similar en animales no hibernantes (Buzadzic y cols, 1990; Buzadzic y cols, 1997; Drew y cols, 2001; Zhou y cols, 2001; Carey y cols, 2003; Ross y Drew 2006; Osborne y Hashimoto 2006; Drew y cols, 2007; Dave y cols, 2012; Vucetic y cols, 2013; Yin y cols, 2016). La preservación de la integridad del SIA en el hámster Sirio durante el torpor descrita en este trabajo, sugiere la existencia de mecanismos neuroprotectores durante esta fase de la hibernación que podrían participar en la atenuación del estrés oxidativo que, en condiciones de normotermia, conduce a la pérdida de proteínas estructurales del SIA mediante la activación de proteínas proteolíticas como la calpaína. Dado que la fase de torpor va acompañada por un estado de hipotermia, se podría especular con la posibilidad de que algunos de estos mecanismos pudieran también contribuir a la neuroprotección frente a situaciones de isquemia de la hipotermia terapéutica, en la cual la disminución de la tasa metabólica va acompañada de una reducción en la formación de especies reactivas de oxígeno (Karibe y cols, 1994; Katz y cols, 2004; Yenari y Hemmen 2010; Dietrich y Bramlett 2010; Yenari y Han 2012; Piironen y cols, 2014; Wu y cols, 2017). No obstante, la confirmación de esta hipótesis requeriría más investigación en este sentido. Los animales en hibernación representan por tanto un modelo viable para estudiar los mecanismos que confieren neuroprotección frente a la isquemia y que podrían impedir la degeneración de los SIAs tras un daño cerebral severo, incluido el ictus isquémico.

IV – CONCLUSIONES

Aparato de Golgi

I. El Aparato de Golgi (AG) de numerosas neuronas piramidales del hipocampo y la neocorteza temporal de pacientes con la enfermedad de Alzheimer (EA), se encuentra alterado respecto al de neuronas procedentes de sujetos control, siendo las alteraciones más frecuentes la fragmentación y la disminución de superficie y volumen del AG.

II. Las alteraciones del AG en la EA son más pronunciadas en neuronas piramidales que acumulan la proteína tau hiperfosforilada, siendo más moderadas en neuronas con un patrón de tau en estadio de pre-ovillo que en aquellas donde se han formado ovillos neurofibrilares.

III. En el modelo murino de taupatía P301S, la presencia de tau no altera la morfología y el tamaño del AG de las neuronas piramidales de la corteza cerebral. Sin embargo, la hiperfosforilación de tau y la presencia de ovillos neurofibrilares, sí que alteran la morfología y reducen el tamaño del AG.

IV. El AG de neuronas corticales en el hámster Sirio, muestra durante la fase de torpor de la hibernación una pronunciada fragmentación. Estos cambios ocurren en paralelo al descenso de la expresión de la proteína MG160 y al aumento en la expresión de GM130. Dicha fragmentación es reversible una vez que el animal se despierta en las fases de *arousal* en las cuales se incrementan los niveles de expresión de golgina84

V. La presencia de acúmulos de tau hiperfosforilado en una subpoblación de neuronas piramidales de capa V, está asociada con alteraciones más pronunciadas en el AG durante la fase de torpor de la hibernación.

VI. Todos estos resultados apuntan a la existencia de una relación entre la hiperfosforilación de tau y las alteraciones morfométricas del AG de las neuronas piramidales. Dichas alteraciones podrían afectar al procesamiento y distribución de proteínas y contribuir a la patofisiología de la EA.

Segmento inicial del axón

I. El orgánulo sacular gigante es una especialización del retículo endoplásmico presente en el segmento inicial del axón de una subpoblación en capa V de neuronas piramidales de la corteza cerebral de roedores y del cerebro humano. La expresión de las proteínas SERCA e IP_3R1 en el orgánulo sacular, sugiere su participación en la regulación de los niveles de calcio dentro del segmento inicial del axón.

II. La integridad del segmento inicial del axón de neuronas corticales del hámster sirio, evaluada mediante la immunoreactividad para anquirina G, se pierde en condiciones de hipoxia e isquemia inducidas por la oclusión de la arteria cerebral media. Sin embargo, dicha integridad se mantiene durante la fase de torpor de la hibernación.

III. Durante la fase de torpor se produce un incremento de longitud del segmento inicial de axón de neuronas piramidales de CA1 y de las capas supra e infragranulares de la corteza somatosensorial, que es más pronunciado en neuronas de capa V que presentan acúmulos de tau hiperfosforilada.

IV. En pacientes con la enfermedad de Alzheimer, el segmento inicial del axón de las neuronas con agregados de tau hiperfosforilada experimenta cambios heterogéneos en su longitud y posición. Los cambos más frecuentes fueron el alargamiento y el desplazamiento proximal. Puesto que las alteraciones del segmento inicial del axón afectan a la excitabilidad neuronal, estos cambios podrían tener consecuencias relevantes en la patofisiología de la enfermedad.

V. Las observaciones realizadas en ratones transgénicos P301S, respaldan la asociación entre entre la acumulación de tau hiperfosforilado y las alteraciones del segmento inicial del axón.

IV–BIBLIOGRAFÍA

Alonso-Nanclares L, Gonzalez-Soriano J, Rodriguez JR, DeFelipe J (2008) Gender differences in human cortical synaptic density. Proceedings of the National Academy of Sciences of the United States of America 105:14615-14619.
Alonso AD, Beharry C, Corbo CP, Cohen LS (2016) Molecular mechanism of prion-like tau-induced neurodegeneration. Alzheimer's & dementia 12:1090-1097.
Alzheimer A (1907) Über eine eigenartige Erkrankung der Hirnrinde. AIlgemeine Zeitschrift für Psychiatrie und Psychisch-Gerichtliche Medizin 64: 146-148.
Alzheimer A (1911) Über eigenartige krankheitsfälle des späteren alters. Zeitschrift für die gesamte Neurologie und Psychiatrie 4: 356-85 (123,205).
Angulo MC, Staiger JF, Rossier J, Audinat E (2003) Distinct local circuits between neocortical pyramidal cells and fast-spiking interneurons in young adult rats. Journal of neurophysiology 89:943-953.
Anton-Fernandez A, Leon-Espinosa G, DeFelipe J, Munoz A (2015) Changes in the Golgi Apparatus of Neocortical and Hippocampal Neurons in the Hibernating Hamster. Frontiers in neuroanatomy 9:157.
Anton-Fernandez A, Rubio-Garrido P, DeFelipe J, Munoz A (2015) Selective presence of a giant saccular organelle in the axon initial segment of a subpopulation of layer V pyramidal neurons. Brain Structure and Function 220 (2):869-884.
Anton-Fernandez A, Merchan-Rubira J, Avila J, Hernandez F, DeFelipe J, Munoz A (2017) Phospho-Tau Accumulation and Structural Alterations of the Golgi Apparatus of Cortical Pyramidal Neurons in the P301S Tauopathy Mouse Model. Journal of Alzheimers Disease 60 (2):651-661.
Anton-Fernandez A, Aparicio-Torres G, Tapia S, DeFelipe J, Munoz A (2017) Morphometric alterations of Golgi apparatus in Alzheimer's disease are related to tau hyperphosphorylation. Neurobiology of disease 97:11-23.
Arendt T, Bruckner MK, Gertz HJ, Marcova L (1998) Cortical distribution of neurofibrillary tangles in Alzheimer's disease matches the pattern of neurons that retain their capacity of plastic remodelling in the adult brain. Neuroscience 83:991-1002.
Arendt T, Stieler J, Strijkstra AM, Hut RA, Rudiger J, Van der Zee EA, Harkany T, Holzer M, Hartig W (2003) Reversible paired helical filament-like phosphorylation of tau is an adaptive process associated with neuronal plasticity in hibernating animals. The Journal of neuroscience 23:6972-6981.
Arendt T (2004) Neurodegeneration and plasticity. International journal of developmental neuroscience 22:507-514.
Arendt T, Stieler JT, Holzer M (2016) Tau and tauopathies. Brain research bulletin 126:238-292.
Arlotta P, Molyneaux BJ, Chen J, Inoue J, Kominami R, Macklis JD (2005) Neuronal subtype-specific genes that control corticospinal motor neuron development in vivo. Neuron 45:207-221.
Arnold SE, Hyman BT, Flory J, Damasio AR, Van Hoesen GW (1991) The topographical and neuroanatomical distribution of neurofibrillary tangles and neuritic plaques in the cerebral cortex of patients with Alzheimer's disease. Cerebral cortex 1:103-116.
Aronov S, Aranda G, Behar L, Ginzburg I (2002) Visualization of translated tau protein in the axons of neuronal P19 cells and characterization of tau RNP granules. Journal of cell science 115:3817-3827.
Arrasate M, Perez M, Avila J (2000) Tau dephosphorylation at tau-1 site correlates with its association to cell membrane. Neurochemical research 25:43-50.
Aslan JE, Thomas G (2009) Death by committee: organellar trafficking and communication in apoptosis. Traffic 10:1390-1404.
Avila J, Lucas JJ, Perez M, Hernandez F (2004) Role of tau protein in both physiological and pathological conditions. Physiology Reviews 84 (2):361-384.
Avila J (2006) Tau phosphorylation and aggregation in Alzheimer's disease pathology. FEBS letters 580:2922-2927.

Baalman KL, Cotton RJ, Rasband SN, Rasband MN (2013) Blast wave exposure impairs memory and decreases axon initial segment length. Journal of neurotrauma 30:741-751.
Baloyannis SJ (2014) Golgi apparatus and protein trafficking in Alzheimer's disease. Journal of Alzheimer's disease 42 Suppl 3:S153-162.
Ballatore C, Lee VM, Trojanowski JQ (2007) Tau-mediated neurodegeneration in Alzheimer's disease and related disorders. Nature reviews Neuroscience 8:663-672.
Baranauskas G, David Y, Fleidervish IA (2013) Spatial mismatch between the Na+ flux and spike initiation in axon initial segment. Proceedings of the National Academy of Sciences of the United States of America (10):4051-4056.
Barnes BM (1989) Freeze avoidance in a mammal: body temperatures below 0 degree C in an Arctic hibernator. Science 244:1593-1595.
Barr FA, Puype M, Vandekerckhove J, Warren G (1997) GRASP65, a protein involved in the stacking of Golgi cisternae. Cell 91:253-262.
Barr FA, Nakamura N, Warren G (1998) Mapping the interaction between GRASP65 and GM130, components of a protein complex involved in the stacking of Golgi cisternae. The EMBO journal 17:3258-3268.
Bas Orth C, Schultz C, Muller CM, Frotscher M, Deller T (2007) Loss of the cisternal organelle in the axon initial segment of cortical neurons in synaptopodin-deficient mice. The Journal of comparative neurology 504:441-449.
Bascom RA, Srinivasan S, Nussbaum RL (1999) Identification and characterization of golgin-84, a novel Golgi integral membrane protein with a cytoplasmic coiled-coil domain. The Journal of biological chemistry 274:2953-2962.
Baumann K, Mandelkow EM, Biernat J, Piwnica-Worms H, Mandelkow E (1993) Abnormal Alzheimer-like phosphorylation of tau-protein by cyclin-dependent kinases cdk2 and cdk5. FEBS letters 336:417-424.
Bellouze S, Schafer MK, Buttigieg D, Baillat G, Rabouille C, Haase G (2014) Golgi fragmentation in pmn mice is due to a defective ARF1/TBCE cross-talk that coordinates COPI vesicle formation and tubulin polymerization. Human molecular genetics 23:5961-5975.
Bender KJ, Trussell LO (2009) Axon initial segment Ca2+ channels influence action potential generation and timing. Neuron 61:259-271.
Benedeczky I, Molnar E, Somogyi P (1994) The cisternal organelle as a Ca(2+)-storing compartment associated with GABAergic synapses in the axon initial segment of hippocampal pyramidal neurones. Experimental brain research 101:216-230.
Benusa SD, George NM, Sword BA, DeVries GH, Dupree JL (2017) Acute neuroinflammation induces AIS structural plasticity in a NOX2-dependent manner. Journal of Neuroinflammation 14 (1):116.
Bertrand J, Plouffe V, Senechal P, Leclerc N (2010) The pattern of human tau phosphorylation is the result of priming and feedback events in primary hippocampal neurons. Neuroscience 168:323-334.
Bertrand J, Senechal P, Zummo-Soucy M, Plouffe V, Leclerc N (2010b) The formation of tau pathological phospho-epitopes in the axon is prevented by the dephosphorylation of selective sites in primary hippocampal neurons over-expressing human tau. Journal of Neurochemistry 114 (5):1353-1367.
Bexiga MG, Simpson JC (2013) Human diseases associated with form and function of the Golgi complex. International journal of molecular sciences 14:18670-18681.
Biernat J, Gustke N, Drewes G, Mandelkow EM, Mandelkow E (1993) Phosphorylation of Ser262 strongly reduces binding of tau to microtubules: distinction between PHF-like immunoreactivity and microtubule binding. Neuron 11:153-163.
Binder LI, Frankfurter A, Rebhun LI (1985) The distribution of tau in the mammalian central nervous system. The Journal of Cell Biology 101 (4):1371-1378.
Blaustein MP, Golovina VA (2001) Structural complexity and functional diversity of endoplasmic reticulum Ca(2+) stores. Trends in neurosciences 24:602-608.

Blennow K, de Leon MJ, Zetterberg H (2006) Alzheimer's disease. Lancet 368:387-403.
Bocharova LS, Gordon R, Rogachevskii VV, Ignatev DA, Khutsian SS (2011) Cyclic structural changes in endoplasmic reticulum and Golgi apparatus in the hippocampal neurons of ground squirrels during hibernation. Tsitologiia 53:259-269.
Boiko T, Van Wart A, Caldwell JH, Levinson SR, Trimmer JS, Matthews G (2003) Functional specialization of the axon initial segment by isoform-specific sodium channel targeting. Journal of Neuroscience 23 (6):2306-2313.
Bootman MD, Lipp P, Berridge MJ (2001) The organisation and functions of local Ca(2+) signals. Journal of cell science 114:2213-2222.
Bossard C, Bresson D, Polishchuk RS, Malhotra V (2007) Dimeric PKD regulates membrane fission to form transport carriers at the TGN. The journal of cell biology 179: 1123–1131.
Bouma HR, Strijkstra AM, Boerema AS, Deelman LE, Epema AH, Hut RA, Kroese FG, Henning RH (2010) Blood cell dynamics during hibernation in the European Ground Squirrel. Veterinary Immunology and Immunopathology 136 (3-4):319-323.
Braak H, Braak E (1985) On areas of transition between entorhinal allocortex and temporal isocortex in the human brain. Normal morphology and lamina-specific pathology in Alzheimer's disease. Acta neuropathologica 68:325-332.
Braak H, Braak E (1986) Ratio of pyramidal cell versus nonpyramidal cells in the human frontal cortex and changes in ratio with ageing and Alzheimer's disease. In: D.F. Swaab, E. Fliers, M. Mirmiran, W.A. Vangool and F. Van Hauren (Eds.), Aging of the Brain and Alzheimer's Disease, Progress in Brain Research, 70, Elsevier, Amsterdam, pp. 185-212.
Braak H, Braak E, Kalus P (1989) Alzheimer's disease: areal and laminar pathology in the occipital isocortex. Acta neuropathologica 77:494-506.
Braak H, Braak E (1991) Neuropathological stageing of Alzheimer-related changes. Acta neuropathologica 82:239-259.
Braak H, Braak E (1995) Staging of Alzheimer's disease-related neurofibrillary changes. Neurobiology of aging 16:271-278; discussion 278-284.
Braak H, Alafuzoff I, Arzberger T, Kretzschmar H, Del Tredici K (2006) Staging of Alzheimer disease-associated neurofibrillary pathology using paraffin sections and immunocytochemistry. Acta neuropathologica 112:389-404.
Bramblett GT, Goedert M, Jakes R, Merrick SE, Trojanowski JQ, Lee VM (1993) Abnormal tau phosphorylation at Ser396 in Alzheimer's disease recapitulates development and contributes to reduced microtubule binding. Neuron 10:1089-1099.
Brandt R, Leger J, Lee G (1995) Interaction of tau with the neural plasma membrane mediated by tau's amino-terminal projection domain. The Journal of cell biology 131:1327-1340.
Brion JP, Smith C, Couck AM, Gallo JM, Anderton BH (1993) Developmental changes in tau phosphorylation: fetal tau is transiently phosphorylated in a manner similar to paired helical filament-tau characteristic of Alzheimer's disease. Journal of neurochemistry 61:2071-2080.
Brodmann K (1909) Vergleichende Lokalisationslehre der Grosshirnrinde. Leipzig: Edit. Barth.
Buck CL, Barnes BM (2000) Effects of ambient temperature on metabolic rate, respiratory quotient, and torpor in an arctic hibernator. American journal of physiology-regulatory, integrative and comparative physiology 279:R255-262.
Buee L, Bussiere T, Buee-Scherrer V, Delacourte A, Hof PR (2000) Tau protein isoforms, phosphorylation and role in neurodegenerative disorders. Brain research reviews 33:95-130.
Buffington SA, Rasband MN (2011) The axon initial segment in nervous system disease and injury. European Journal of Neuroscience 34 (10):1609-1619.

Bullmann T, Seeger G, Stieler J, Hanics J, Reimann K, Kretzschmann TP, Hilbrich I, Holzer M, Alpar A, Arendt T (2016) Tau phosphorylation-associated spine regression does not impair hippocampal-dependent memory in hibernating golden hamsters. Hippocampus 26 (3):301-318.

Burgos PV, Mardones GA, Rojas AL, daSilva LL, Prabhu Y, Hurley JH, Bonifacino JS (2010) Sorting of the Alzheimer's disease amyloid precursor protein mediated by the AP-4 complex. Developmental cell 18:425-436.

Burrus LW, Zuber ME, Lueddecke BA, Olwin BB (1992) Identification of a cysteine-rich receptor for fibroblast growth factors. Molecular and cellular biology 12:5600-5609.

Buzadzic B, Blagojevic D, Korac B, Saicic ZS, Spasic MB, Petrovic VM (1997) Seasonal variation in the antioxidant defense system of the brain of the ground squirrel (Citellus citellus) and response to low temperature compared with rat. Comparative Biochemistry and Physiology- Part C: Pharmacology, Toxicology and Endocrinology 117 (2):141-149.

Buzadzic B, Spasic M, Saicic ZS, Radojicic R, Petrovic VM, Halliwell B (1990) Antioxidant defenses in the ground squirrel Citellus citellus. 2. The effect of hibernation. Free Radical Biology and Medicine 9 (5):407-413.

Caceres A, Kosik KS (1990) Inhibition of neurite polarity by tau antisense oligonucleotides in primary cerebellar neurons. Nature 343:461-463.

Carey HV, Rhoads CA, Aw TY (2003) Hibernation induces glutathione redox imbalance in ground squirrel intestine. Journal of Comparative Physiology B 173 (4):269-276.

Chand AN, Galliano E, Chesters RA, Grubb MS (2015) A distinct subtype of dopaminergic interneuron displays inverted structural plasticity at the axon initial segment. The Journal of neuroscience 35:1573-1590.

Chandra SE, Kable P, Morrison GH, Webb W (1991) Calcium sequestration in the Golgi apparatus of cultured mammalian cells revealed by laser scanning confocal microscopy and ion microscopy. Journal of Cell Science 100: 747–752.

Chapin SJ, Bulinski JC (1991) Non-neuronal 210 x 10(3) Mr microtubule-associated protein (MAP4) contains a domain homologous to the microtubule-binding domains of neuronal MAP2 and tau. Journal of cell science 98 (Pt 1):27-36.

Chin SS, Goldman JE (1996) Glial inclusions in CNS degenerative diseases. Journal of neuropathology and experimental neurology 55:499-508.

Choy RW, Cheng Z, Schekman R (2012) Amyloid precursor protein (APP) traffics from the cell surface via endosomes for amyloid beta (Abeta) production in the trans-Golgi network. Proceedings of the National Academy of Sciences of the United States of America 109:E2077-2082.

Cifuentes F, Gonzalez CE, Fiordelisio T, Guerrero G, Lai FA, Hernandez-Cruz A (2001) A ryanodine fluorescent derivative reveals the presence of high-affinity ryanodine binding sites in the Golgi complex of rat sympathetic neurons, with possible functional roles in intracellular Ca(2+) signaling. Cellular signalling 13:353-362.

Clark K, Sword BA, Dupree JL (2017) Oxidative Stress Induces Disruption of the Axon Initial Segment. ASN Neuro 9 (6):1759091417745426.

Clark KC, Josephson A, Benusa SD, Hartley RK, Baer M, Thummala S, Joslyn M, Sword BA, Elford H, Oh U, Dilsizoglu-Senol A, Lubetzki C, Davenne M, DeVries GH, Dupree JL (2016) Compromised axon initial segment integrity in EAE is preceded by microglial reactivity and contact. Glia 64 (7):1190-1209.

Clermont Y, Xia L, Rambourg A, Turner JD, Hermo L (1993) Structure of the Golgi apparatus in stimulated and nonstimulated acinar cells of mammary glands of the rat. The Anatomical record 237:308-317.

Cluett EB, Brown WJ (1992) Adhesion of Golgi cisternae by proteinaceous interactions: intercisternal bridges as putative adhesive structures. Journal of cell science 103 (Pt 3):773-784.

Coban H, Tung S, Yoo B, Vinters HV, Hinman JD (2017) Molecular Disorganization of Axons Adjacent to Human Cortical Microinfarcts. Frontiers in Neurology 8:405.
Cogut V, Bruintjes JJ, Eggen BJL, van der Zee EA, Henning RH (2017) Brain inflammatory cytokines and microglia morphology changes throughout hibernation phases in Syrian hamster. Brain Behavior and Immunity 68:17-22.
Cole NB, Sciaky N, Marotta A, Song J, Lippincott-Schwartz J (1996) Golgi dispersal during microtubule disruption: regeneration of Golgi stacks at peripheral endoplasmic reticulum exit sites. Molecular biology of the cell 7:631-650.
Cook C, Carlomagno Y, Gendron TF, Dunmore J, Scheffel K, Stetler C, Davis M, Dickson D, Jarpe M, DeTure M, Petrucelli L (2014) Acetylation of the KXGS motifs in tau is a critical determinant in modulation of tau aggregation and clearance. Human Molecular Genetics 1;23(1):104-16.
Cruz DA, Lovallo EM, Stockton S, Rasband M, Lewis DA (2009) Postnatal development of synaptic structure proteins in pyramidal neuron axon initial segments in monkey prefrontal cortex. The Journal of comparative neurology 514:353-367.
Cummings BJ, Su JH, Cotman CW (1993) Neuritic involvement within bFGF immunopositive plaques of Alzheimer's disease. Experimental neurology 124:315-325.
Dai CL, Chen X, Kazim SF, Liu F, Gong CX, Grundke-Iqbal I, Iqbal K (2015) Passive immunization targeting the N-terminal projection domain of tau decreases tau pathology and improves cognition in a transgenic mouse model of Alzheimer disease and tauopathies. Journal of neural transmission 122:607-617.
Dai CL, Tung YC, Liu F, Gong CX, Iqbal K (2017) Tau passive immunization inhibits not only tau but also Abeta pathology. Alzheimer's research & therapy 9:1.
Dalton AJ y Felix M (1954) Cylologic and cytochemical characteristics of the Golgi substances of epitelial cells of the epididymis in situ in homogenates and after isolation. The American Journal of Anatomy 94:171-207.
Dave KR, Christian SL, Perez-Pinzon MA, Drew KL (2012) Neuroprotection: lessons from hibernators. Comparative Biochemistry and Physiology- Part B: Biochemistry and Molecular Biology 162 (1-3):1-9.
De Matteis MA, Luini A (2008) Exiting the Golgi complex. Nature reviews Molecular cell biology 9:273-284.
DeVos SL, Goncharoff DK, Chen G, Kebodeaux CS, Yamada K, Stewart FR, Schuler DR, Maloney SE, Wozniak DF, Rigo F, Bennett CF, Cirrito JR, Holtzman DM, Miller TM (2013) Antisense reduction of tau in adult mice protects against seizures. Journal of Neuroscience 33 (31):12887-12897.
Del Puerto A, Fronzaroli-Molinieres L, Perez-Alvarez MJ, Giraud P, Carlier E, Wandosell F, Debanne D, Garrido JJ (2015) ATP-P2X7 Receptor Modulates Axon Initial Segment Composition and Function in Physiological Conditions and Brain Injury. Cerebral Cortex 25 (8):2282-2294.
Debanne D, Campanac E, Bialowas A, Carlier E, Alcaraz G (2011) Axon physiology. Physiological reviews 91:555-602.
DeFelipe J, Jones EG (1991) Cajal's Degeneration and Regeneration of the Nervous System. New York: Oxford University Press.
DeFelipe J, Farinas I (1992) The pyramidal neuron of the cerebral cortex: morphological and chemical characteristics of the synaptic inputs. Progress in neurobiology 39:563-607.
DeFelipe J, Alonso-Nanclares L, Blatow M, Caputi A, Monyer H (2005) Anatomical and molecular heterogeneity of cortical GABAergic interneurons. Microcircuits: The Interface between Neurons and Global Brain Function. Cambridge: The MIT Press.
Delobel P, Flament S, Hamdane M, Mailliot C, Sambo AV, Begard S, Sergeant N, Delacourte A, Vilain JP, Buee L (2002) Abnormal Tau phosphorylation of the Alzheimer-type also occurs during mitosis. Journal of neurochemistry 83:412-420.

Diao A, Rahman D, Pappin DJ, Lucocq J, Lowe M (2003) The coiled-coil membrane protein golgin-84 is a novel rab effector required for Golgi ribbon formation. The Journal of cell biology 160:201-212.

Dickey CA, Kamal A, Lundgren K, Klosak N, Bailey RM, Dunmore J, Ash P, Shoraka S, Zlatkovic J, Eckman CB, Patterson C, Dickson DW, Nahman NS, Jr., Hutton M, Burrows F, Petrucelli L (2007) The high-affinity HSP90-CHIP complex recognizes and selectively degrades phosphorylated tau client proteins. The Journal of clinical investigation 117:648-658.

Dietrich WD, Bramlett HM (2010) The evidence for hypothermia as a neuroprotectant in traumatic brain injury. Neurotherapeutics 7 (1):43-50.

Dixit R, Ross JL, Goldman YE, Holzbaur EL (2008) Differential regulation of dynein and kinesin motor proteins by tau. Science 319:1086-1089.

Dotti CG, Simons K (1990) Polarized sorting of viral glycoproteins to the axon and dendrites of hippocampal neurons in culture. Cell 62:63-72.

Drechsel DN, Hyman AA, Cobb MH, Kirschner MW (1992) Modulation of the dynamic instability of tubulin assembly by the microtubule-associated protein tau. Molecular biology of the cell 3:1141-1154.

Drew KL, Rice ME, Kuhn TB, Smith MA (2001) Neuroprotective adaptations in hibernation: therapeutic implications for ischemia-reperfusion, traumatic brain injury and neurodegenerative diseases. Free Radical Biology and Medicine 31 (5):563-573.

Drew KL, Buck CL, Barnes BM, Christian SL, Rasley BT, Harris MB (2007) Central nervous system regulation of mammalian hibernation: implications for metabolic suppression and ischemia tolerance. Journal of Neurochemistry 102 (6):1713-1726.

Drewes G, Trinczek B, Illenberger S, Biernat J, Schmitt-Ulms G, Meyer HE, Mandelkow EM, Mandelkow E (1995) Microtubule-associated protein/microtubule affinity-regulating kinase (p110mark). A novel protein kinase that regulates tau-microtubule interactions and dynamic instability by phosphorylation at the Alzheimer-specific site serine 262. The Journal of biological chemistry 270:7679-7688.

Drewes G, Ebneth A, Mandelkow EM (1998) MAPs, MARKs and microtubule dynamics. Trends in biochemical sciences 23:307-311.

Droscher A (1998) The history of the Golgi apparatus in neurones from its discovery in 1898 to electron microscopy. Brain research bulletin 47:199-203.

Drubin DG, Kirschner MW (1986) Tau protein function in living cells. The Journal of cell biology 103:2739-2746.

Durr G, Strayle J, Plemper R, Elbs S, Klee SK, Catty P, Wolf DH, Rudolph HK (1998) The medial-Golgi ion pump Pmr1 supplies the yeast secretory pathway with Ca2+ and Mn2+ required for glycosylation, sorting, and endoplasmic reticulum-associated protein degradation. Molecular biology of the cell 9:1149-1162.

Duyckaerts C y Dickson D (2003) Neuropathology of Alzheimer's disease. Neurodegeneration: The Molecular Pathology of Dementia and Movement Disorders. Basel: Neuropath Press 47–65.

Ebneth A, Godemann R, Stamer K, Illenberger S, Trinczek B, Mandelkow E (1998) Overexpression of tau protein inhibits kinesin-dependent trafficking of vesicles, mitochondria, and endoplasmic reticulum: implications for Alzheimer's disease. The Journal of cell biology 143:777-794.

Egea G, Lazaro-Dieguez F, Vilella M (2006) Actin dynamics at the Golgi complex in mammalian cells. Current opinion in cell biology 18:168-178.

Elyaman W, Yardin C, Hugon J (2002) Involvement of glycogen synthase kinase-3beta and tau phosphorylation in neuronal Golgi disassembly. Journal of neurochemistry 81:870-880.

Evans MD, Dumitrescu AS, Kruijssen DL, Taylor SE, Grubb MS (2015) Rapid Modulation of Axon Initial Segment Length Influences Repetitive Spike Firing. Cell Reports 13 (6):1233-1245.

Evans MD, Sammons RP, Lebron S, Dumitrescu AS, Watkins TB, Uebele VN, Renger JJ, Grubb MS (2013) Calcineurin signaling mediates activity-dependent relocation of the axon initial segment. The Journal of neuroscience 33:6950-6963.
Fabri M, Manzoni T (1996) Glutamate decarboxylase immunoreactivity in corticocortical projecting neurons of rat somatic sensory cortex. Neuroscience 72:435-448.
Fan J, Hu Z, Zeng L, Lu W, Tang X, Zhang J, Li T (2008) Golgi apparatus and neurodegenerative diseases. International journal of developmental neuroscience 26:523-534.
Farah CA, Perreault S, Liazoghli D, Desjardins M, Anton A, Lauzon M, Paiement J, Leclerc N (2006) Tau interacts with Golgi membranes and mediates their association with microtubules. Cell motility and the cytoskeleton 63:710-724.
Feijoo C, Campbell DG, Jakes R, Goedert M, Cuenda A (2005) Evidence that phosphorylation of the microtubule-associated protein Tau by SAPK4/p38delta at Thr50 promotes microtubule assembly. Journal of cell science 118:397-408.
Feldman ML (1984) Morphology of the neocortical pyramidal neuron. In: Cerebral Cortex, Vol. 1. Cellular Components of the Cerebral Cortex. New York: Plenum Press 123-200.
Feng G, Mellor RH, Bernstein M, Keller-Peck C, Nguyen QT, Wallace M, Nerbonne JM, Lichtman JW, Sanes JR (2000) Imaging neuronal subsets in transgenic mice expressing multiple spectral variants of GFP. Neuron 28:41-51.
Ferrer I, Lopez-Gonzalez I, Carmona M, Arregui L, Dalfo E, Torrejon-Escribano B, Diehl R, Kovacs GG (2014) Glial and neuronal tau pathology in tauopathies: characterization of disease-specific phenotypes and tau pathology progression. Journal of neuropathology and experimental neurology 73:81-97.
Finlay BL, Darlington RB (1995) Linked regularities in the development and evolution of mammalian brains. Science 268:1578-1584.
Franke WW, Kartenbeck J, Krien S, VanderWoude WJ, Scheer U, Morre DJ (1972) Inter- and intracisternal elements of the Golgi apparatus. A system of membrane-to-membrane cross-links. Zeitschrift fur Zellforschung und mikroskopische Anatomie 132:365-380.
Frerichs KU, Smith CB, Brenner M, DeGracia DJ, Krause GS, Marrone L, Dever TE, Hallenbeck JM (1998) Suppression of protein synthesis in brain during hibernation involves inhibition of protein initiation and elongation. Proceedings of the National Academy of Sciences of the United States of America 95:14511-14516.
Frerichs KU, Kennedy C, Sokoloff L, Hallenbeck JM (1994) Local cerebral blood flow during hibernation, a model of natural tolerance to "cerebral ischemia". Journal of Cerebral Blood Flow and Metabolism 14 (2):193-205.
Fujita Y, Okamoto K, Sakurai A, Gonatas NK, Hirano A (2000) Fragmentation of the Golgi apparatus of the anterior horn cells in patients with familial amyotrophic lateral sclerosis with SOD1 mutations and posterior column involvement. Journal of the neurological sciences 174:137-140.
Fujita Y, Ohama E, Takatama M, Al-Sarraj S, Okamoto K (2006) Fragmentation of Golgi apparatus of nigral neurons with alpha-synuclein-positive inclusions in patients with Parkinson's disease. Acta neuropathologica 112:261-265.
Fuller SC (1911) A study of the miliary plaques found in brains of the aged. American Journal of Insanity 58:147–219.
Garner CC, Tucker RP, Matus A (1988) Selective localization of messenger RNA for cytoskeletal protein MAP2 in dendrites. Nature 336:674-677.
Galiano MR, Jha S, Ho TS, Zhang C, Ogawa Y, Chang KJ, Stankewich MC, Mohler PJ, Rasband MN (2012) A distal axonal cytoskeleton forms an intra-axonal boundary that controls axon initial segment assembly. Cell 149 (5):1125-1139.
Geiser F (2004) Metabolic rate and body temperature reduction during hibernation and daily torpor. Annual review of physiology 66:239-274.

Geiser F, Martin GM (2013) Torpor in the Patagonian opossum (Lestodelphys halli): implications for the evolution of daily torpor and hibernation. Die Naturwissenschaften 100:975-981.
Gendreau KL, Hall GF (2013) Tangles, Toxicity, and Tau Secretion in AD - New Approaches to a Vexing Problem. Frontiers in neurology 4:160.
Geschwind DH, Rakic P (2013) Cortical evolution: judge the brain by its cover. Neuron 80:633-647.
Glick BS (2002) Can the Golgi form de novo? Nature reviews Molecular cell biology 3:615-619.
Goedert M, Spillantini MG, Jakes R, Rutherford D, Crowther RA (1989) Multiple isoforms of human microtubule-associated protein tau: sequences and localization in neurofibrillary tangles of Alzheimer's disease. Neuron 3:519-526.
Goedert M, Spillantini MG, Potier MC, Ulrich J, Crowther RA (1989b) Cloning and sequencing of the cDNA encoding an isoform of microtubule-associated protein tau containing four tandem repeats: differential expression of tau protein mRNAs in human brain. The EMBO journal 8:393-399.
Goedert M, Jakes R, Crowther RA, Six J, Lubke U, Vandermeeren M, Cras P, Trojanowski JQ, Lee VM (1993) The abnormal phosphorylation of tau protein at Ser-202 in Alzheimer disease recapitulates phosphorylation during development. Proceedings of the National Academy of Sciences of the United States of America 90:5066-5070.
Goedert M, Jakes R, Crowther RA, Cohen P, Vanmechelen E, Vandermeeren M, Cras P (1994) Epitope mapping of monoclonal antibodies to the paired helical filaments of Alzheimer's disease: identification of phosphorylation sites in tau protein. The Biochemical journal 301 (Pt 3):871-877.
Gomez-Ramos A, Diaz-Hernandez M, Rubio A, Miras-Portugal MT, Avila J (2008) Extracellular tau promotes intracellular calcium increase through M1 and M3 muscarinic receptors in neuronal cells. Molecular and cellular neurosciences 37:673-681.
Gonatas JO, Mezitis SG, Stieber A, Fleischer B, Gonatas NK (1989) MG-160. A novel sialoglycoprotein of the medial cisternae of the Golgi apparatus [published eeratum appears in J Biol Chem 1989 Mar 5;264(7):4264]. The Journal of biological chemistry 264:646-653.
Gonatas JO, Mourelatos Z, Stieber A, Lane WS, Brosius J, Gonatas NK (1995) MG-160, a membrane sialoglycoprotein of the medial cisternae of the rat Golgi apparatus, binds basic fibroblast growth factor and exhibits a high level of sequence identity to a chicken fibroblast growth factor receptor. Journal of cell science 108 (Pt 2):457-467.
Gonchar YA, Johnson PB, Weinberg RJ (1995) GABA-immunopositive neurons in rat neocortex with contralateral projections to S-I. Brain research 697:27-34.
Gong CX, Singh TJ, Grundke-Iqbal I, Iqbal K (1993) Phosphoprotein phosphatase activities in Alzheimer disease brain. Journal of neurochemistry 61:921-927.
Gonzalez-Riano C, Tapia-Gonzalez S, Garcia A, Munoz A, DeFelipe J, Barbas C (2017) Metabolomics and neuroanatomical evaluation of post-mortem changes in the hippocampus. Brain Structure and Function 222 (6):2831-2853.
Greenfield JP, Tsai J, Gouras GK, Hai B, Thinakaran G, Checler F, Sisodia SS, Greengard P, Xu H (1999) Endoplasmic reticulum and trans-Golgi network generate distinct populations of Alzheimer beta-amyloid peptides. Proceedings of the National Academy of Sciences of the United States of America 96:742-747.
Griffith LM, Pollard TD (1982) The interaction of actin filaments with microtubules and microtubule-associated proteins. The Journal of biological chemistry 257:9143-9151.
Grubb MS, Burrone J (2010a) Activity-dependent relocation of the axon initial segment fine-tunes neuronal excitability. Nature 465:1070-1074.
Grubb MS, Burrone J (2010b) Building and maintaining the axon initial segment. Current opinion in neurobiology 20:481-488.

Grubb MS, Shu Y, Kuba H, Rasband MN, Wimmer VC, Bender KJ (2011) Short- and long-term plasticity at the axon initial segment. The Journal of neuroscience 31:16049-16055.
Grundemann J, Hausser M (2010) Neuroscience: A plastic axonal hotspot. Nature 465 (7301):1022-1023.
Guo T, Noble W, Hanger DP (2017) Roles of tau protein in health and disease. Acta neuropathologica 133:665-704.
Gutzmann A, Ergul N, Grossmann R, Schultz C, Wahle P, Engelhardt M (2014) A period of structural plasticity at the axon initial segment in developing visual cortex. Frontiers in neuroanatomy 8:11.
Haase G, Rabouille C (2015) Golgi Fragmentation in ALS Motor Neurons. New Mechanisms Targeting Microtubules, Tethers, and Transport Vesicles. Frontiers in neuroscience 9:448.
Hamada MS, Kole MH (2015) Myelin loss and axonal ion channel adaptations associated with gray matter neuronal hyperexcitability. The Journal of neuroscience 35:7272-7286.
Hammerschlag R, Stone GC, Bolen FA, Lindsey JD, Ellisman MH (1982) Evidence that all newly synthesized proteins destined for fast axonal transport pass through the Golgi apparatus. The Journal of cell biology 93:568-575.
Hanger DP, Seereeram A, Noble W (2009) Mediators of tau phosphorylation in the pathogenesis of Alzheimer's disease. Expert review of neurotherapeutics 9:1647-1666.
Hartig W, Oklejewicz M, Strijkstra AM, Boerema AS, Stieler J, Arendt T (2005) Phosphorylation of the tau protein sequence 199-205 in the hippocampal CA3 region of Syrian hamsters in adulthood and during aging. Brain research 1056:100-104.
Hartig W, Stieler J, Boerema AS, Wolf J, Schmidt U, Weissfuss J, Bullmann T, Strijkstra AM, Arendt T (2007) Hibernation model of tau phosphorylation in hamsters: selective vulnerability of cholinergic basal forebrain neurons - implications for Alzheimer's disease. The European journal of neuroscience 25:69-80.
Harty RC, Kim TH, Thomas EA, Cardamone L, Jones NC, Petrou S, Wimmer VC (2013) Axon initial segment structural plasticity in animal models of genetic and acquired epilepsy. Epilepsy research 105:272-279.
Hatch RJ, Wei Y, Xia D, Gotz J (2017) Hyperphosphorylated tau causes reduced hippocampal CA1 excitability by relocating the axon initial segment. Acta neuropathologica 133:717-730.
Hattox AM, Nelson SB (2007) Layer V neurons in mouse cortex projecting to different targets have distinct physiological properties. Journal of neurophysiology 98:3330-3340.
Hedstrom KL, Xu X, Ogawa Y, Frischknecht R, Seidenbecher CI, Shrager P, Rasband MN (2007) Neurofascin assembles a specialized extracellular matrix at the axon initial segment. The Journal of cell biology 178:875-886.
Hedstrom KL, Ogawa Y, Rasband MN (2008) AnkyrinG is required for maintenance of the axon initial segment and neuronal polarity. The Journal of cell biology 183:635-640.
Himmler A (1989) Structure of the bovine tau gene: alternatively spliced transcripts generate a protein family. Molecular and cellular biology 9:1389-1396.
Hinman JD, Rasband MN, Carmichael ST (2013) Remodeling of the axon initial segment after focal cortical and white matter stroke. Stroke 44 (1):182-189.
Hirano A, Zimmerman HM (1962) Alzheimer's neurofibrillary changes. A topographic study. Archives of neurology 7:227-242.
Hirokawa N, Funakoshi T, Sato-Harada R, Kanai Y (1996) Selective stabilization of tau in axons and microtubule-associated protein 2C in cell bodies and dendrites contributes to polarized localization of cytoskeletal proteins in mature neurons. The Journal of cell biology 132:667-679.
Hofflin F, Jack A, Riedel C, Mack-Bucher J, Roos J, Corcelli C, Schultz C, Wahle P, Engelhardt M (2017) Heterogeneity of the Axon Initial Segment in Interneurons and Pyramidal Cells of Rodent Visual Cortex. Frontiers in Cellular Neuroscience 11:332.

Holth JK, Bomben VC, Reed JG, Inoue T, Younkin L, Younkin SG, Pautler RG, Botas J, Noebels JL (2013) Tau loss attenuates neuronal network hyperexcitability in mouse and Drosophila genetic models of epilepsy. Journal of Neuroscience 23;33(4):1651-9..

Hong M, Chen DC, Klein PS, Lee VM (1997) Lithium reduces tau phosphorylation by inhibition of glycogen synthase kinase-3. The Journal of biological chemistry 272:25326-25332.

Hoover BR, Reed MN, Su J, Penrod RD, Kotilinek LA, Grant MK, Pitstick R, Carlson GA, Lanier LM, Yuan LL, Ashe KH, Liao D (2010) Tau mislocalization to dendritic spines mediates synaptic dysfunction independently of neurodegeneration. Neuron 68 (6):1067-1081.

Houser CR, Barber RP, Vaughn JE (1984) Immunocytochemical localization of glutamic acid decarboxylase in the dorsal lateral vestibular nucleus: evidence for an intrinsic and extrinsic GABAergic innervation. Neuroscience letters 47:213-220.

Hu L, Chen C (2007) Pathological changes of ultrastructures of oligodendrocytes following ischemic brain injury in 3-day-old premature rats. Chinese journal of contemporary pediatrics 9:225-228.

Hu W, Tian C, Li T, Yang M, Hou H, Shu Y (2009) Distinct contributions of Na(v)1.6 and Na(v)1.2 in action potential initiation and backpropagation. Nature neuroscience 12:996-1002.

Hübner AH (1908) Zur Histopathologie der senilen Hirnrinde. Archives of Psychiatry and Neurology 46:598–609.

Huse JT, Liu K, Pijak DS, Carlin D, Lee VM, Doms RW (2002) Beta-secretase processing in the trans-Golgi network preferentially generates truncated amyloid species that accumulate in Alzheimer's disease brain. The Journal of biological chemistry 277:16278-16284.

Huynh DP, Yang HT, Vakharia H, Nguyen D, Pulst SM (2003) Expansion of the polyQ repeat in ataxin-2 alters its Golgi localization, disrupts the Golgi complex and causes cell death. Human molecular genetics 12:1485-1496.

Hyman BT, Van Hoesen GW, Damasio AR, Barnes CL (1984) Alzheimer's disease: cell-specific pathology isolates the hippocampal formation. Science 225:1168-1170.

Hyman BT, Van Hoesen GW, Kromer LJ, Damasio AR (1986) Perforant pathway changes and the memory impairment of Alzheimer's disease. Annals of neurology 20:472-481.

Igelmund P (1995) Modulation of synaptic transmission at low temperatures by hibernationrelated changes in ionic microenvironment in hippocampal slices of golden hamsters. Cryobiology 32 (4):334-343.

Igelmund P, Heinemann U (1995) Synaptic transmission and paired-pulse behaviour of CA1 pyramidal cells in hippocampal slices from a hibernator at low temperature: importance of ionic environment. Brain Research 689 (1):9-20.

Igelmund P (1996) Hibernation and hippocampal synaptic transmission, in Adaptation to Cold: Tenth International Hibernation Symposium. Armidale: University of New England Press 159–166.

Illenberger S, Zheng-Fischhofer Q, Preuss U, Stamer K, Baumann K, Trinczek B, Biernat J, Godemann R, Mandelkow EM, Mandelkow E (1998) The endogenous and cell cycle-dependent phosphorylation of tau protein in living cells: implications for Alzheimer's disease. Molecular biology of the cell 9:1495-1512.

Inda MC, DeFelipe J, Munoz A (2009) Morphology and distribution of chandelier cell axon terminals in the mouse cerebral cortex and claustroamygdaloid complex. Cerebral Cortex 19 (1):41-54.

Iqbal K, Liu F, Gong CX, Alonso Adel C, Grundke-Iqbal I (2009) Mechanisms of tau-induced neurodegeneration. Acta neuropathologica 118:53-69.

Irwin DJ, Abrams JY, Schonberger LB, Leschek EW, Mills JL, Lee VM, Trojanowski JQ (2013) Evaluation of potential infectivity of Alzheimer and Parkinson disease proteins in recipients of cadaver-derived human growth hormone. JAMA neurology 70:462-468.

Ittner LM, Ke YD, Delerue F, Bi M, Gladbach A, van Eersel J, Wolfing H, Chieng BC, Christie MJ, Napier IA, Eckert A, Staufenbiel M, Hardeman E, Gotz J (2010) Dendritic function of tau

mediates amyloid-beta toxicity in Alzheimer's disease mouse models. Cell 142:387-397.
Iwamoto N, Emson PC (1991) Demonstration of neurofibrillary tangles in parvalbumin-immunoreactive interneurones in the cerebral cortex of Alzheimer-type dementia brain. Neuroscience letters 128:81-84.
Jeckel D, Karrenbauer A, Birk R, Schmidt RR, Wieland F (1990) Sphingomyelin is synthesized in the cis Golgi. FEBS letters 261:155-157.
Jedlicka P, Schwarzacher SW, Winkels R, Kienzler F, Frotscher M, Bramham CR, Schultz C, Bas Orth C, Deller T (2009) Impairment of in vivo theta-burst long-term potentiation and network excitability in the dentate gyrus of synaptopodin-deficient mice lacking the spine apparatus and the cisternal organelle. Hippocampus 19:130-140.
Jenkins SM, Bennett V (2001) Ankyrin-G coordinates assembly of the spectrin-based membrane skeleton, voltage-gated sodium channels, and L1 CAMs at Purkinje neuron initial segments. The Journal of cell biology 155:739-746.
Jenkins TW, Truex RC (1963) Dissection of the Human Brain as a Method for Its Fractionation by Weight. The Anatomical record 147:359-366.
Jenkins PM, Kim N, Jones SL, Tseng WC, Svitkina TM, Yin HH, Bennett V (2015) Giant ankyrin-G: a critical innovation in vertebrate evolution of fast and integrated neuronal signaling. Proceedings of the National Academy of Sciences of the United States of America 112 (4):957-964.
Jiang Q, Wang L, Guan Y, Xu H, Niu Y, Han L, Wei YP, Lin L, Chu J, Wang Q, Yang Y, Pei L, Wang JZ, Tian Q (2014) Golgin-84-associated Golgi fragmentation triggers tau hyperphosphorylation by activation of cyclin-dependent kinase-5 and extracellular signal-regulated kinase. Neurobiology of aging 35:1352-1363.
Jones EG, Powell TP (1969) Synapses on the axon hillocks and initial segments of pyramidal cell axons in the cerebral cortex. Journal of cell science 5:495-507.
Jones EG (1984) History of Cortical Cytology. Cerebral Cortex. New York: Plenum Press 1-28.
Jones SL, Korobova F, Svitkina T (2014) Axon initial segment cytoskeleton comprises a multiprotein submembranous coat containing sparse actin filaments. The Journal of cell biology 205:67-81.
Jones SL, Svitkina TM (2016) Axon Initial Segment Cytoskeleton: Architecture, Development, and Role in Neuron Polarity. Neural plasticity 2016:6808293.
Joshi G, Bekier ME, Wang Y (2015) Golgi fragmentation in Alzheimer's disease. Frontiers in neuroscience 9:340.
Joshi G, Wang Y (2015) Golgi defects enhance APP amyloidogenic processing in Alzheimer's disease. BioEssays: news and reviews in molecular, cellular and developmental biology 37:240-247.
Jucker M, Beyreuther K, Haass C, Nitsch R, Christen Y (2006) Alzheimer: 100 Years and Beyond. Heidelberg: Springer.
Jung D, Filliol D, Miehe M, Rendon A (1993) Interaction of brain mitochondria with microtubules reconstituted from brain tubulin and MAP2 or TAU. Cell motility and the cytoskeleton 24:245-255.
Kaphzan H, Buffington SA, Jung JI, Rasband MN, Klann E (2011) Alterations in intrinsic membrane properties and the axon initial segment in a mouse model of Angelman syndrome. The Journal of neuroscience 31:17637-17648.
Karch CM, Jeng AT, Goate AM (2012) Extracellular Tau levels are influenced by variability in Tau that is associated with tauopathies. The Journal of biological chemistry 287:42751-42762.
Karecla PI, Kreis TE (1992) Interaction of membranes of the Golgi complex with microtubules in vitro. European journal of cell biology 57:139-146.

Karibe H, Chen SF, Zarow GJ, Gafni J, Graham SH, Chan PH, Weinstein PR (1994) Mild intraischemic hypothermia suppresses consumption of endogenous antioxidants after temporary focal ischemia in rats. Brain Research 649 (1-2):12-18.
Katz LM, Young AS, Frank JE, Wang Y, Park K (2004) Regulated hypothermia reduces brain oxidative stress after hypoxic-ischemia. Brain Research 1017 (1-2):85-91.
Kelley LA, Mezulis S, Yates CM, Wass MN, Sternberg MJE (2015) The Phyre2 web portal for protein modeling, prediction and analysis. Nature Protocols 10:845.
Kepes F, Rambourg A, Satiat-Jeunemaitre B (2005) Morphodynamics of the secretory pathway. International review of cytology 242:55-120.
Klumperman J (2011) Architecture of the mammalian Golgi. Cold Spring Harbor perspectives in biology 3(7).
Kobayashi S, Ishiguro K, Omori A, Takamatsu M, Arioka M, Imahori K, Uchida T (1993) A cdc2-related kinase PSSALRE/cdk5 is homologous with the 30 kDa subunit of tau protein kinase II, a proline-directed protein kinase associated with microtubule. FEBS letters 335:171-175.
Kobayashi T, Storrie B, Simons K, Dotti CG (1992) A functional barrier to movement of lipids in polarized neurons. Nature 359:647-650.
Koester SE, O'Leary DD (1993) Connectional distinction between callosal and subcortically projecting cortical neurons is determined prior to axon extension. Developmental biology 160:1-14.
Kole MH, Letzkus JJ, Stuart GJ (2007) Axon initial segment Kv1 channels control axonal action potential waveform and synaptic efficacy. Neuron 55 (4):633-647.
Kole MH, Ilschner SU, Kampa BM, Williams SR, Ruben PC, Stuart GJ (2008) Action potential generation requires a high sodium channel density in the axon initial segment. Nature neuroscience 11:178-186.
Komada M, Soriano P (2002) [Beta]IV-spectrin regulates sodium channel clustering through ankyrin-G at axon initial segments and nodes of Ranvier. Journal of Cell Biology 156 (2):337-348.
Kondylis V, van Nispen tot Pannerden HE, Herpers B, Friggi-Grelin F, Rabouille C (2007) The golgi comprises a paired stack that is separated at G2 by modulation of the actin cytoskeleton through Abi and Scar/WAVE. Developmental cell 12:901-915.
Konishi Y, Setou M (2009) Tubulin tyrosination navigates the kinesin-1 motor domain to axons. Nature neuroscience 12:559-567.
Kopke E, Tung YC, Shaikh S, Alonso AC, Iqbal K, Grundke-Iqbal I (1993) Microtubule-associated protein tau. Abnormal phosphorylation of a non-paired helical filament pool in Alzheimer disease. The Journal of biological chemistry 268:24374-24384.
Kordeli E, Lambert S, Bennett V (1995) AnkyrinG. A new ankyrin gene with neural-specific isoforms localized at the axonal initial segment and node of Ranvier. The Journal of Biological Chemistry 270 (5):2352-2359.
Kosaka T (1980) The axon initial segment as a synaptic site: ultrastructure and synaptology of the initial segment of the pyramidal cell in the rat hippocampus (CA3 region). Journal of neurocytology 9:861-882.
Kosik KS, Finch EA (1987) MAP2 and tau segregate into dendritic and axonal domains after the elaboration of morphologically distinct neurites: an immunocytochemical study of cultured rat cerebrum. Journal of Neuroscience 7 (10):3142-3153.

Kovacech B, Novak M (2010) Tau truncation is a productive posttranslational modification of neurofibrillary degeneration in Alzheimer's disease. Current Alzheimer research 7:708-716.
Kovacs GG, Budka H (2010) Current concepts of neuropathological diagnostics in practice: neurodegenerative diseases. Clinical neuropathology 29:271-288.

Kovacs GG, Kwong LK, Grossman M, Irwin DJ, Lee EB, Robinson JL, Suh E, Van Deerlin VM, Lee VM, Trojanowski JQ (2016) Tauopathy with hippocampal 4-repeat tau immunoreactive spherical inclusions: a report of three cases. Brain pathology.

Kremerskothen J, Plaas C, Kindler S, Frotscher M, Barnekow A (2005) Synaptopodin, a molecule involved in the formation of the dendritic spine apparatus, is a dual actin/alpha-actinin binding protein. Journal of neurochemistry 92:597-606.

Krilowicz BL, Edgar DM, Heller HC (1989) Action potential duration increases as body temperature decreases during hibernation. Brain Research 498 (1):73-80.

Ksiezak-Reding H, Pyo HK, Feinstein B, Pasinetti GM (2003) Akt/PKB kinase phosphorylates separately Thr212 and Ser214 of tau protein in vitro. Biochimica et biophysica acta 1639:159-168.

Kuba H, Ishii TM, Ohmori H (2006) Axonal site of spike initiation enhances auditory coincidence detection. Nature 444:1069-1072.

Kuba H, Oichi Y, Ohmori H (2010) Presynaptic activity regulates Na(+) channel distribution at the axon initial segment. Nature 465 (7301):1075-1078.

Kuba H, Adachi R, Ohmori H (2014) Activity-dependent and activity-independent development of the axon initial segment. The Journal of neuroscience 34:3443-3453.

Kuba H, Oichi Y, Ohmori H (2010) Presynaptic activity regulates Na(+) channel distribution at the axon initial segment. Nature 465:1075-1078.

Kuchibhotla KV, Wegmann S, Kopeikina KJ, Hawkes J, Rudinskiy N, Andermann ML, Spires-Jones TL, Bacskai BJ, Hyman BT (2014) Neurofibrillary tangle-bearing neurons are functionally integrated in cortical circuits in vivo. Proceedings of the National Academy of Sciences of the United States of America 111 (1):510-514.

LaPointe NE, Morfini G, Pigino G, Gaisina IN, Kozikowski AP, Binder LI, Brady ST (2009) The amino terminus of tau inhibits kinesin-dependent axonal transport: implications for filament toxicity. Journal of neuroscience research 87:440-451.

Leon-Espinosa G, DeFelipe J, Munoz A (2012) Effects of amyloid-beta plaque proximity on the axon initial segment of pyramidal cells. Journal of Alzheimers Disease 29 (4):841-852.

Leon-Espinosa G, Garcia E, Garcia-Escudero V, Hernandez F, Defelipe J, Avila J (2013) Changes in tau phosphorylation in hibernating rodents. Journal of neuroscience research 91:954-962.

Leon-Espinosa G, Regalado-Reyes M, DeFelipe J, Munoz A (2017) Changes in neocortical and hippocampal microglial cells during hibernation. Brain Structure and Function.

Leterrier C, Dargent B (2014) No Pasaran! Role of the axon initial segment in the regulation of protein transport and the maintenance of axonal identity. Seminars in cell and developmental biology 27:44-51.

Leterrier C (2016) The Axon Initial Segment, 50Years Later: A Nexus for Neuronal Organization and Function. Current Topic in Membranes 77:185-233.

Levine TP, Misteli T, Rabouille C, Warren G (1995) Mitotic disassembly and reassembly of the Golgi apparatus. Cold Spring Harbor symposia on quantitative biology 60:549-557.

Li X, Kumar Y, Zempel H, Mandelkow EM, Biernat J, Mandelkow E (2011) Novel diffusion barrier for axonal retention of Tau in neurons and its failure in neurodegeneration. The EMBO journal 30:4825-4837.

Liazoghli D, Perreault S, Micheva KD, Desjardins M, Leclerc N (2005) Fragmentation of the Golgi apparatus induced by the overexpression of wild-type and mutant human tau forms in neurons. The American journal of pathology 166:1499-1514.

Lin WL, Lewis J, Yen SH, Hutton M, Dickson DW (2003) Ultrastructural neuronal pathology in transgenic mice expressing mutant (P301L) human tau. Journal of neurocytology 32:1091-1105.

Lindwall G, Cole RD (1984) Phosphorylation affects the ability of tau protein to promote microtubule assembly. The Journal of biological chemistry 259:5301-5305.

Liu F, Grundke-Iqbal I, Iqbal K, Gong CX (2005) Contributions of protein phosphatases PP1, PP2A, PP2B and PP5 to the regulation of tau phosphorylation. The European journal of neuroscience 22:1942-1950.
Liu F, Iqbal K, Grundke-Iqbal I, Hart GW, Gong CX (2004) O-GlcNAcylation regulates phosphorylation of tau: a mechanism involved in Alzheimer's disease. Proceedings of the National Academy of Sciences of the United States of America 101:10804-10809.
Liu F, Zaidi T, Iqbal K, Grundke-Iqbal I, Gong CX (2002) Aberrant glycosylation modulates phosphorylation of tau by protein kinase A and dephosphorylation of tau by protein phosphatase 2A and 5. Neuroscience 115:829-837.
Lorente de Nó R (1949) Cerebral cortex: architecture, intracortical connections, motor projections. In Fulton's Physiology of the Nervous System. London: Oxford University Press 288-300.
Lorincz A, Nusser Z (2010) Molecular identity of dendritic voltage-gated sodium channels. Science 328 (5980):906-909.
Lowe M (2002) Golgi complex: biogenesis de novo?. Current biology CB 12:R166-167.
Lucas JJ, Hernandez F, Gomez-Ramos P, Moran MA, Hen R, Avila J (2001) Decreased nuclear beta-catenin, tau hyperphosphorylation and neurodegeneration in GSK-3beta conditional transgenic mice. The EMBO journal 20:27-39.
Lucassen PJ, Ravid R, Gonatas NK, Swaab DF (1993) Activation of the human supraoptic and paraventricular nucleus neurons with aging and in Alzheimer's disease as judged from increasing size of the Golgi apparatus. Brain research 632:105-113.
Maas T, Eidenmüller J, Brandt R (2000) Interaction of tau with the neural membrane cortex is regulated by phosphorylation at sites that are modified in paired helical filaments. The Journal of Biological Chemistry 275(21):15733-40.
Mandell JW, Banker GA (1996) A spatial gradient of tau protein phosphorylation in nascent axons. Journal of Neuroscience 16 (18):5727-5740
Mandelkow EM, Drewes G, Biernat J, Gustke N, Van Lint J, Vandenheede JR, Mandelkow E (1992) Glycogen synthase kinase-3 and the Alzheimer-like state of microtubule-associated protein tau. FEBS letters 314:315-321.
Mander EMM, Verbeek FJ, Aten JA (1993) Measurement of co-localization of objects in dual-colour confocal images. Journal of microscopy 169:3:375–382.
Marin MA, Ziburkus J, Jankowsky J, Rasband MN (2016) Amyloid-beta plaques disrupt axon initial segments. Experimental Neurology 281:93-98.
Martin L, Latypova X, Wilson CM, Magnaudeix A, Perrin ML, Terro F (2013) Tau protein phosphatases in Alzheimer's disease: the leading role of PP2A. Ageing Research Reviews 12(1):39-49.
Mescher A (2013) Junqueira's Basic Histology: Text and Atlas. McGraw-Hill Education.
Mellman I, Simons K (1992) The Golgi complex: in vitro veritas? Cell 68:829-840.
Merino-Serrais P, Benavides-Piccione R, Blazquez-Llorca L, Kastanauskaite A, Rabano A, Avila J, DeFelipe J (2013) The influence of phospho-tau on dendritic spines of cortical pyramidal neurons in patients with Alzheimer's disease. Brain 136:1913-1928.
Migheli A, Butler M, Brown K, Shelanski ML (1988) Light and electron microscope localization of the microtubule-associated tau protein in rat brain. Journal of Neuroscience 8 (6):1846-1851.
Mihailovic LJT (1972) Cortical and subcortical electrical activity in hibernation and hypothermia. In: South FE, Hannon JP, J.R. W, E.T. P, N.R. A (eds) Hibernation and Hypothermia, Perspectives and Challenges. Elsevier, Amsterdam, pp 487-534.
Mirra SS, Heyman A, McKeel D, Sumi SM, Crain BJ, Brownlee LM, Vogel FS, Hughes JP, van Belle G, Berg L (1991) The Consortium to Establish a Registry for Alzheimer's Disease (CERAD). Part II. Standardization of the neuropathologic assessment of Alzheimer's disease. Neurology 41 (4):479-486.

Molnar Z, Cheung AF (2006) Towards the classification of subpopulations of layer V pyramidal projection neurons. Neuroscience research 55:105-115.
Molyneaux BJ, Arlotta P, Menezes JR, Macklis JD (2007) Neuronal subtype specification in the cerebral cortex. Nature reviews Neuroscience 8:427-437.
Mondragon-Rodriguez S, Perry G, Luna-Munoz J, Acevedo-Aquino MC, Williams S (2014) Phosphorylation of tau protein at sites Ser(396-404) is one of the earliest events in Alzheimer's disease and Down syndrome. Neuropathology and applied neurobiology 40:121-135.
Morishima-Kawashima M, Ihara Y (2002) Alzheimer's disease: beta-Amyloid protein and tau. Journal of neuroscience research 70:392-401.
Morris M, Knudsen GM, Maeda S, Trinidad JC, Ioanoviciu A, Burlingame AL, Mucke L (2015) Tau post-translational modifications in wild-type and human amyloid precursor protein transgenic mice. Nature neuroscience 18:1183-1189.
Mountjoy CQ, Roth M, Evans NJ, Evans HM (1983) Cortical neuronal counts in normal elderly controls and demented patients. Neurobiology of aging 4:1-11.
Mourelatos Z, Gonatas JO, Cinato E, Gonatas NK (1996) Cloning and sequence analysis of the human MG160, a fibroblast growth factor and E-selectin binding membrane sialoglycoprotein of the Golgi apparatus. DNA and cell biology 15:1121-1128.
Muir J, Kittler JT (2014) Plasticity of GABAA receptor diffusion dynamics at the axon initial segment. Frontiers in Cell Neuroscience 8:151.
Mukrasch MD, Biernat J, von Bergen M, Griesinger C, Mandelkow E, Zweckstetter M (2005) Sites of tau important for aggregation populate {beta}-structure and bind to microtubules and polyanions. The Journal of biological chemistry 280:24978-24986.
Munro S (2011) The golgin coiled-coil proteins of the Golgi apparatus. Cold Spring Harbor perspectives in biology 3.
Nakamura N (2010) Emerging new roles of GM130, a cis-Golgi matrix protein, in higher order cell functions. Journal of pharmacological sciences 112:255-264.
Nakamura N, Rabouille C, Watson R, Nilsson T, Hui N, Slusarewicz P, Kreis TE, Warren G (1995) Characterization of a cis-Golgi matrix protein, GM130. The Journal of cell biology 131:1715-1726.
Nakata T, Hirokawa N (2003) Microtubules provide directional cues for polarized axonal transport through interaction with kinesin motor head. Journal of Cell Biology 162:1045–1055.
Nelson AD, Jenkins PM (2017) Axonal Membranes and their domains: Assembly and Function of the Axon Initial Segment and Node of Ranvier. Frontiers in Cellular Neuroscience 11:136.
Neve RL, Harris P, Kosik KS, Kurnit DM, Donlon TA (1986) Identification of cDNA clones for the human microtubule-associated protein tau and chromosomal localization of the genes for tau and microtubule-associated protein 2. Brain research 387:271-280.
O'Leary DD, Stanfield BB (1985) Occipital cortical neurons with transient pyramidal tract axons extend and maintain collaterals to subcortical but not intracortical targets. Brain research 336:326-333.
O'Leary DD, Stanfield BB (1986) A transient pyramidal tract projection from the visual cortex in the hamster and its removal by selective collateral elimination. Brain research 392:87-99.
Oddo S, Billings L, Kesslak JP, Cribbs DH, LaFerla FM (2004) Abeta immunotherapy leads to clearance of early, but not late, hyperphosphorylated tau aggregates via the proteasome. Neuron 43:321-332.
Osborne PG, Hashimoto M (2006) Brain antioxidant levels in hamsters during hibernation, arousal and cenothermia. Behavioural Brain Research 168 (2):208-214.
Palade, G. E. 1952 A study of fixation for electron microscopy. The journal of experimental medicine 95 ; 285- 298.

Palay SL, Sotelo C, Peters A, Orkand PM (1968) The axon hillock and the initial segment. The Journal of cell biology 38:193-201.
Palop JJ, Mucke L (2009) Epilepsy and cognitive impairments in Alzheimer disease. Archives of Neurology 66 (4):435-440.
Panda D, Miller HP, Wilson L (1999) Rapid treadmilling of brain microtubules free of microtubule-associated proteins in vitro and its suppression by tau. Proceedings of the National Academy of Sciences of the United States of America 96:12459-12464.
Papasozomenos SC, Binder LI (1987) Phosphorylation determines two distinct species of Tau in the central nervous system. Cell motility and the cytoskeleton 8:210-226.
Papasozomenos SC (1997) The heat shock-induced hyperphosphorylation of tau is estrogen-independent and prevented by androgens: implications for Alzheimer disease. Proceedings of the National Academy of Sciences of the United States of America 94:6612-6617.
Paxinos G, Watson C (2007) The Rat Brain in Stereotaxic Coordinates. Academic Press.
Pearson RC, Esiri MM, Hiorns RW, Wilcock GK, Powell TP (1985) Anatomical correlates of the distribution of the pathological changes in the neocortex in Alzheimer disease. Proceedings of the National Academy of Sciences of the United States of America 82:4531-4534.
Pelletier L, Stern CA, Pypaert M, Sheff D, Ngo HM, Roper N, He CY, Hu K, Toomre D, Coppens I, Roos DS, Joiner KA, Warren G (2002) Golgi biogenesis in Toxoplasma gondii. Nature 418:548-552.
Perea G, Araque A (2010) GLIA modulates synaptic transmission. Brain research reviews 63:93-102.
Peters A, Proskauer CC, Kaiserman-Abramof IR (1968) The small pyramidal neuron of the rat cerebral cortex. The axon hillock and initial segment. The Journal of cell biology 39:604-619.
Peters A, Sethares C, Harriman KM (1990) Different kinds of axon terminals forming symmetric synapses with the cell bodies and initial axon segments of layer II/III pyramidal cells. II. Synaptic junctions. Journal of neurocytology 19:584-600.
Peters A, Palay SL, Webster H (1991) The fine structure of the nervous system. New York: Oxford University Press.
Pezzati R, Bossi M, Podini P, Meldolesi J, Grohovaz F (1997) High-resolution calcium mapping of the endoplasmic reticulum-Golgi-exocytic membrane system. Electron energy loss imaging analysis of quick frozen-freeze dried PC12 cells. Molecular biology of the cell 8:1501-1512.
Pfaffenbach KT, Lee AS (2011) The critical role of GRP78 in physiologic and pathologic stress. Current opinion in cell biology 23:150-156.
Piironen K, Tiainen M, Mustanoja S, Kaukonen KM, Meretoja A, Tatlisumak T, Kaste M (2014) Mild hypothermia after intravenous thrombolysis in patients with acute stroke: a randomized controlled trial. Stroke 45 (2):486-491.
Pollock NJ, Mirra SS, Binder LI, Hansen LA, Wood JG (1986) Filamentous aggregates in Pick's disease, progressive supranuclear palsy, and Alzheimer's disease share antigenic determinants with microtubule-associated protein, tau. Lancet 2:1211.
Pooler AM, Phillips EC, Lau DH, Noble W, Hanger DP (2013) Physiological release of endogenous tau is stimulated by neuronal activity. EMBO reports 14:389-394.
Pooler AM, Usardi A, Evans CJ, Philpott KL, Noble W, Hanger DP (2012) Dynamic association of tau with neuronal membranes is regulated by phosphorylation. Neurobiology of aging 33:431 e427-438.
Pope WB, Lambert MP, Leypold B, Seupaul R, Sletten L, Krafft G, Klein WL (1994) Microtubule-associated protein tau is hyperphosphorylated during mitosis in the human neuroblastoma cell line SH-SY5Y. Experimental neurology 126:185-194.

Popov VI, Bocharova LS (1992) Hibernation-induced structural changes in synaptic contacts between mossy fibres and hippocampal pyramidal neurons. Neuroscience 48:53-62.
Popov VI, Bocharova LS, Bragin AG (1992) Repeated changes of dendritic morphology in the hippocampus of ground squirrels in the course of hibernation. Neuroscience 48:45-51.
Popov VI, Ignat'ev DA, Lindemann B (1999) Ultrastructure of taste receptor cells in active and hibernating ground squirrels. Journal of electron microscopy 48:957-969.
Popov VI, Medvedev NI, Patrushev IV, Ignatev DA, Morenkov ED, Stewart MG (2007) Reversible reduction in dendritic spines in CA1 of rat and ground squirrel subjected to hypothermia-normothermia in vivo: A three-dimensional electron microscope study. Neuroscience 149 (3):549-560.
Popovic MA, Foust AJ, McCormick DA, Zecevic D (2011) The spatio-temporal characteristics of action potential initiation in layer 5 pyramidal neurons: a voltage imaging study. The Journal of physiology 589:4167-4187.
Porat A, Elazar Z (2000) Regulation of intra-Golgi membrane transport by calcium. The Journal of biological chemistry 275:29233-29237.
Porrero C, Rubio-Garrido P, Avendano C, Clasca F (2010) Mapping of fluorescent protein-expressing neurons and axon pathways in adult and developing Thy1-eYFP-H transgenic mice. Brain research 1345:59-72.
Preuss U, Doring F, Illenberger S, Mandelkow EM (1995) Cell cycle-dependent phosphorylation and microtubule binding of tau protein stably transfected into Chinese hamster ovary cells. Molecular biology of the cell 6:1397-1410.
Preuss U, Mandelkow EM (1998) Mitotic phosphorylation of tau protein in neuronal cell lines resembles phosphorylation in Alzheimer's disease. European journal of cell biology 76:176-184.
Puelles L (2011) Pallio-pallial tangential migrations and growth signaling: new scenario for cortical evolution? Brain, behavior and evolution 78:108-127.
Purves D, George J Augustine, David Fitzpatrick, Lawrence C Katz, Anthony-Samuel LaMantia, James O McNamara, and S Mark Williams (2001) Neuroscience. Sunderland (MA): Sinauer Associates.
Puthenveedu MA, Linstedt AD (2001) In search of an essential step during mitotic Golgi disassembly and inheritance. Experimental cell research 271:22-27.
Puthenveedu MA, Bachert C, Puri S, Lanni F, Linstedt AD (2006) GM130 and GRASP65-dependent lateral cisternal fusion allows uniform Golgi-enzyme distribution. Nature cell biology 8:238-248.
Rabouille C, Misteli T, Watson R, Warren G (1995) Reassembly of Golgi stacks from mitotic Golgi fragments in a cell-free system. The Journal of cell biology 129:605-618.
Rakic P (1988) Specification of cerebral cortical areas. Science 241:170-176.
Ramón y Cajal R (1892) El nuevo concepto de la histología de los centros nerviosos. Revista de Ciencias Médicas 18: 457-476.
Ramón y Cajal R (1917) Recuerdos de mi vida, Vol.2. Historia de mi labor científica. Madrid: Moya.
Rasband MN (2010) The axon initial segment and the maintenance of neuronal polarity. Nature Reviews Neuroscience 11 (8):552-562.
Reynolds CH, Garwood CJ, Wray S, Price C, Kellie S, Perera T, Zvelebil M, Yang A, Sheppard PW, Varndell IM, Hanger DP, Anderton BH (2008) Phosphorylation regulates tau interactions with Src homology 3 domains of phosphatidylinositol 3-kinase, phospholipase Cgamma1, Grb2, and Src family kinases. The Journal of biological chemistry 283:18177-18186.
Roberson ED, Scearce-Levie K, Palop JJ, Yan F, Cheng IH, Wu T, Gerstein H, Yu GQ, Mucke L (2007) Reducing endogenous tau ameliorates amyloid beta-induced deficits in an Alzheimer's disease mouse model. Science 316 (5825):750-754.

Rocher AB, Crimins JL, Amatrudo JM, Kinson MS, Todd-Brown MA, Lewis J, Luebke JI (2010) Structural and functional changes in tau mutant mice neurons are not linked to the presence of NFTs. Experimental Neurology 223 (2):385-393.

Rodriguez OC, Schaefer AW, Mandato CA, Forscher P, Bement WM, Waterman-Storer CM (2003) Conserved microtubule-actin interactions in cell movement and morphogenesis. Nature cell biology 5:599-609.

Rothschild D y Kasanin J (1936) Clinicopathologic study of Alzheimer's disease. Archives of Neurology and Psychiatry 36:293-321.

Rolfe DF, Brown GC (1997) Cellular energy utilization and molecular origin of standard metabolic rate in mammals. Physiological reviews 77:731-758.

Ross AP, Drew KL (2006) Potential for discovery of neuroprotective factors in serum and tissue from hibernating species. Mini Reviews in Medicinal Chemistry 6 (8):875-884.

Ruf T, Geiser F (2015) Daily torpor and hibernation in birds and mammals. Biological Reviews of the Cambridge Philosophical Society 90 (3):891-926.

Sakurai A, Okamoto K, Fujita Y, Nakazato Y, Wakabayashi K, Takahashi H, Gonatas NK (2000) Fragmentation of the Golgi apparatus of the ballooned neurons in patients with corticobasal degeneration and Creutzfeldt-Jakob disease. Acta neuropathologica 100:270-274.

Salehi A, Lucassen PJ, Pool CW, Gonatas NK, Ravid R, Swaab DF (1994) Decreased neuronal activity in the nucleus basalis of Meynert in Alzheimer's disease as suggested by the size of the Golgi apparatus. Neuroscience 59:871-880.

Salehi A, Heyn S, Gonatas NK, Swaab DF (1995a) Decreased protein synthetic activity of the hypothalamic tuberomamillary nucleus in Alzheimer's disease as suggested by smaller Golgi apparatus. Neuroscience letters 193:29-32.

Salehi A, Ravid R, Gonatas NK, Swaab DF (1995b) Decreased activity of hippocampal neurons in Alzheimer's disease is not related to the presence of neurofibrillary tangles. Journal of neuropathology and experimental neurology 54:704-709.

Saman S, Kim W, Raya M, Visnick Y, Miro S, Saman S, Jackson B, McKee AC, Alvarez VE, Lee NC, Hall GF (2012) Exosome-associated tau is secreted in tauopathy models and is selectively phosphorylated in cerebrospinal fluid in early Alzheimer disease. The Journal of Biological Chemistry 3;287(6):3842-9.

Sanchez-Ponce D, DeFelipe J, Garrido JJ, Munoz A (2011) In vitro maturation of the cisternal organelle in the hippocampal neuron's axon initial segment. Molecular and cellular neurosciences 48:104-116.

Satoh A, Wang Y, Malsam J, Beard MB, Warren G (2003) Golgin-84 is a rab1 binding partner involved in Golgi structure. Traffic 4:153-161.

Schafer DP, Jha S, Liu F, Akella T, McCullough LD, Rasband MN (2009) Disruption of the axon initial segment cytoskeleton is a new mechanism for neuronal injury. The Journal of neuroscience 29:13242-13254.

Schluter A, Del Turco D, Deller T, Gutzmann A, Schultz C, Engelhardt M (2017) Structural Plasticity of Synaptopodin in the Axon Initial Segment during Visual Cortex Development. Cerebral cortex 27:4662-4675.

Schnitzler JG (1911) Zur Abgrenzung der sogenannten Alzheimerschen Erkrankung. Zeitschrift für die gesamte Neurologie und Psychiatrie 7:34–57.

Sengupta A, Kabat J, Novak M, Wu Q, Grundke-Iqbal I, Iqbal K (1998) Phosphorylation of tau at both Thr 231 and Ser 262 is required for maximal inhibition of its binding to microtubules. Archives of biochemistry and biophysics 357:299-309.

Sheetz MP, Pfister KK, Bulinski JC, Cotman CW (1998) Mechanisms of trafficking in axons and dendrites: implications for development and neurodegeneration. Progress in neurobiology 55:577-594.

Shim SY, Wang J, Asada N, Neumayer G, Tran HC, Ishiguro K, Sanada K, Nakatani Y, Nguyen MD (2008) Protein 600 is a microtubule/endoplasmic reticulum-associated protein in CNS neurons. The Journal of neuroscience 28:3604-3614.

Shorter J, Warren G (1999) A role for the vesicle tethering protein, p115, in the post-mitotic stacking of reassembling Golgi cisternae in a cell-free system. The Journal of cell biology 146:57-70.

Simchowicz T (1911) Histologische Studien über die senile Demenz. Nissl-Alzheimers Histology and Histopathology. Arbeit Hirn 4:267–444.

Simic G, Babic Leko M, Wray S, Harrington C, Delalle I, Jovanov-Milosevic N, Bazadona D, Buee L, de Silva R, Di Giovanni G, Wischik C, Hof PR (2016) Tau Protein Hyperphosphorylation and Aggregation in Alzheimer's Disease and Other Tauopathies, and Possible Neuroprotective Strategies. Biomolecules 6:6.

Singh TJ, Zaidi T, Grundke-Iqbal I, Iqbal K (1995) Modulation of GSK-3-catalyzed phosphorylation of microtubule-associated protein tau by non-proline-dependent protein kinases. FEBS letters 358:4-8.

Sinka R, Gillingham AK, Kondylis V, Munro S (2008) Golgi coiled-coil proteins contain multiple binding sites for Rab family G proteins. The Journal of cell biology 183:607-615.

Sloper JJ, Powell TP (1979) A study of the axon initial segment and proximal axon of neurons in the primate motor and somatic sensory cortices. Philosophical transactions of the Royal Society of London Series B, Biological sciences 285:173-197.

Slusarewicz P, Nilsson T, Hui N, Watson R, Warren G (1994) Isolation of a matrix that binds medial Golgi enzymes. The Journal of cell biology 124:405-413.

Sohda M, Misumi Y, Yamamoto A, Nakamura N, Ogata S, Sakisaka S, Hirose S, Ikehara Y, Oda K (2010) Interaction of Golgin-84 with the COG complex mediates the intra-Golgi retrograde transport. Traffic 11:1552-1566.

Sohn PD, Tracy TE, Son HI, Zhou Y, Leite RE, Miller BL, Seeley WW, Grinberg LT, Gan L (2016) Acetylated tau destabilizes the cytoskeleton in the axon initial segment and is mislocalized to the somatodendritic compartment. Molecular Neurodegeneration 11 (1):47.

Somogyi P, Nunzi MG, Gorio A, Smith AD (1983) A new type of specific interneuron in the monkey hippocampus forming synapses exclusively with the axon initial segments of pyramidal cells. Brain research 259:137-142.

Song AH, Wang D, Chen G, Li Y, Luo J, Duan S, Poo MM (2009) A selective filter for cytoplasmic transport at the axon initial segment. Cell 136:1148-1160.

Sontag JM, Sontag E (2014) Protein phosphatase 2A dysfunction in Alzheimer's disease. Frontiers in molecular neuroscience 7:16.

Sorensen SA, Bernard A, Menon V, Royall JJ, Glattfelder KJ, Hirokawa K, Mortrud M, Miller JA, Zeng H, Hohmann JG, Jones AR, Lein ES (2013) Correlated Gene Expression and Target Specificity Demonstrate Excitatory Projection Neuron Diversity. Cerebral Cortex 25(2):433-49.

Sorensen SA, Bernard A, Menon V, Royall JJ, Glattfelder KJ, Desta T, Hirokawa K, Mortrud M, Miller JA, Zeng H, Hohmann JG, Jones AR, Lein ES (2015) Correlated gene expression and target specificity demonstrate excitatory projection neuron diversity. Cerebral cortex 25:433-449.

South FE (1972) Hibernation and hypothermia, perspectives and challenges. Symposium held at Snow-mass-at-Aspen, Colorado, January 3-8, 1971. Elsevier Pub. Co., Amsterdam, New York, South FE, J.E. B, H.D. D, A.D. E (1968) Sleep, hibernation, and hypothermia in the yellow-bellied marmot (M.flaviventris). In: Musacchia XJ, J.F.Saunders (eds) Depressed Metabolism. Elsevier, New york, pp 277-312.

Spacek J (1985) Three-dimensional analysis of dendritic spines. II. Spine apparatus and other cytoplasmic components. Anatomy and embryology 171:235-243.

Spillantini MG, Goedert M, Crowther RA, Murrell JR, Farlow MR, Ghetti B (1997) Familial multiple system tauopathy with presenile dementia: a disease with abundant neuronal and glial tau filaments. Proceedings of the National Academy of Sciences of the United States of America 94:4113-4118.

Spillantini MG, Goedert M (1998) Tau protein pathology in neurodegenerative diseases. Trends in neurosciences 21:428-433.

Stamer K, Vogel R, Thies E, Mandelkow E, Mandelkow EM (2002) Tau blocks traffic of organelles, neurofilaments, and APP vesicles in neurons and enhances oxidative stress. The Journal of cell biology 156:1051-1063.

Stanley P (2011) Golgi glycosylation. Cold Spring Harbor perspectives in biology 3.

Steegmaier M, Levinovitz A, Isenmann S, Borges E, Lenter M, Kocher HP, Kleuser B, Vestweber D (1995) The E-selectin-ligand ESL-1 is a variant of a receptor for fibroblast growth factor. Nature 373:615-620.

Stieber A, Mourelatos Z, Gonatas NK (1996) In Alzheimer's disease the Golgi apparatus of a population of neurons without neurofibrillary tangles is fragmented and atrophic. The American journal of pathology 148:415-426.

Stieler JT, Bullmann T, Kohl F, Barnes BM, Arendt T (2009) PHF-like tau phosphorylation in mammalian hibernation is not associated with p25-formation. Journal of neural transmission 116:345-350.

Stieler JT, Bullmann T, Kohl F, Toien O, Bruckner MK, Hartig W, Barnes BM, Arendt T (2011) The physiological link between metabolic rate depression and tau phosphorylation in mammalian hibernation. PloS one 6:e14530.

Stoler O, Fleidervish IA (2016) Functional implications of axon initial segment cytoskeletal disruption in stroke. Acta Pharmacologica Sinica 37 (1):75-81.

Stopa EG, Gonzalez AM, Chorsky R, Corona RJ, Alvarez J, Bird ED, Baird A (1990) Basic fibroblast growth factor in Alzheimer's disease. Biochemical and biophysical research communications 171:690-696.

Storrie B, White J, Rottger S, Stelzer EH, Suganuma T, Nilsson T (1998) Recycling of golgi-resident glycosyltransferases through the ER reveals a novel pathway and provides an explanation for nocodazole-induced Golgi scattering. The Journal of cell biology 143:1505-1521.

Storrie B, Yang W (1998) Dynamics of the interphase mammalian Golgi complex as revealed through drugs producing reversible Golgi disassembly. Biochimica et biophysica acta 1404:127-137.

Strumwasser F (1959) Regulatory mechanisms, brain activity and behavior during deep hibernation in the squirrel, Citellus beecheyi. American Journal of Physiology 196 (1):23-30.

Strumwasser F (1959b) Thermoregulatory, brain and behavioral mechanisms during entrance into hibernation in the squirrel, Citellus beecheyi. American Journal of Physiology 196, 15–22.

Su B, Wang X, Drew KL, Perry G, Smith MA, Zhu X (2008) Physiological regulation of tau phosphorylation during hibernation. Journal of neurochemistry 105:2098-2108.

Sun X, Wu Y, Gu M, Liu Z, Ma Y, Li J, Zhang Y (2014) Selective filtering defect at the axon initial segment in Alzheimer's disease mouse models. Proceedings of the National Academy of Sciences of the United States of America 111 (39):14271-14276.

Sultan A, Nesslany F, Violet M, Begard S, Loyens A, Talahari S, Mansuroglu Z, Marzin D, Sergeant N, Humez S, Colin M, Bonnefoy E, Buee L, Galas MC (2011) Nuclear tau, a key player in neuronal DNA protection. The Journal of biological chemistry 286:4566-4575.

Sutterlin C, Hsu P, Mallabiabarrena A, Malhotra V (2002) Fragmentation and dispersal of the pericentriolar Golgi complex is required for entry into mitosis in mammalian cells. Cell 109:359-369.

Takamine K, Okamoto K, Fujita Y, Sakurai A, Takatama M, Gonatas NK (2000) The involvement of the neuronal Golgi apparatus and trans-Golgi network in the human olivary hypertrophy. Journal of the neurological sciences 182:45-50.

Takeuchi H, Iba M, Inoue H, Higuchi M, Takao K, Tsukita K, Karatsu Y, Iwamoto Y, Miyakawa T, Suhara T, Trojanowski JQ, Lee VM, Takahashi R (2011) P301S mutant human tau transgenic mice manifest early symptoms of human tauopathies with dementia and altered sensorimotor gating. PloS one 6:e21050.

Tatebayashi Y, Iqbal K, Grundke-Iqbal I (1999) Dynamic regulation of expression and phosphorylation of tau by fibroblast growth factor-2 in neural progenitor cells from adult rat hippocampus. The Journal of neuroscience 19:5245-5254.

Tatebayashi Y, Lee MH, Li L, Iqbal K, Grundke-Iqbal I (2003) The dentate gyrus neurogenesis: a therapeutic target for Alzheimer's disease. Acta neuropathologica 105:225-232.

Thies E, Mandelkow EM (2007) Missorting of tau in neurons causes degeneration of synapses that can be rescued by the kinase MARK2/Par-1. The Journal of Neuroscience 27 (11):2896-2907.

Thyberg J, Moskalewski S (1985) Microtubules and the organization of the Golgi complex. Experimental cell research 159:1-16.

Thyberg J, Moskalewski S (1999) Role of microtubules in the organization of the Golgi complex. Experimental cell research 246:263-279.

Tolnay M, Probst A (1999) REVIEW: tau protein pathology in Alzheimer's disease and related disorders. Neuropathology and applied neurobiology 25:171-187.

Tsiola A, Hamzei-Sichani F, Peterlin Z, Yuste R (2003) Quantitative morphologic classification of layer 5 neurons from mouse primary visual cortex. The Journal of comparative neurology 461:415-428.

Usardi A, Pooler AM, Seereeram A, Reynolds CH, Derkinderen P, Anderton B, Hanger DP, Noble W, Williamson R (2011) Tyrosine phosphorylation of tau regulates its interactions with Fyn SH2 domains, but not SH3 domains, altering the cellular localization of tau. The FEBS journal 278:2927-2937.

van Breukelen F, Martin SL (2002) Reversible depression of transcription during hibernation. Journal of comparative physiology B, Biochemical, systemic, and environmental physiology 172:355-361.

Vanoevelen J, Raeymaekers L, Dode L, Parys JB, De Smedt H, Callewaert G, Wuytack F, Missiaen L (2005) Cytosolic Ca2+ signals depending on the functional state of the Golgi in HeLa cells. Cell calcium 38:489-495.

Vincent I, Rosado M, Davies P (1996) Mitotic mechanisms in Alzheimer's disease? The Journal of cell biology 132:413-425.

Voeltz GK, Prinz WA (2007) Sheets, ribbons and tubules - how organelles get their shape. Nature reviews Molecular cell biology 8:258-264.

Vogelsberg-Ragaglia V, Schuck T, Trojanowski JQ, Lee VM (2001) PP2A mRNA expression is quantitatively decreased in Alzheimer's disease hippocampus. Experimental neurology 168:402-412.

Vogt C y Vogt O (1919) Allgemeinere Ergebnisse unserer Hirnforschung. Journal of Psychology and Neurology 25: 279-462.

Von der Ohe CG, Darian-Smith C, Garner CC, Heller HC (2006) Ubiquitous and temperature-dependent neural plasticity in hibernators. The Journal of Neuroscience 26:10590-10598.

von der Ohe CG, Garner CC, Darian-Smith C, Heller HC (2007) Synaptic protein dynamics in hibernation. The Journal of Neuroscience 27 (1):84-92.

Vucetic M, Stancic A, Otasevic V, Jankovic A, Korac A, Markelic M, Velickovic K, Golic I, Buzadzic B, Storey KB, Korac B (2013) The impact of cold acclimation and hibernation on antioxidant defenses in the ground squirrel (Spermophilus citellus): an update. Free Radical Biology and Medicine 65:916-924.

Walker JM, Glotzbach SF, Berger RJ, Heller HC (1977) Sleep and hibernation in ground squirrels (Citellus spp): electrophysiological observations. American Journal of Physiology 233, R213–R221.
Wandinger-Ness A, Bennett MK, Antony C, Simons K (1990) Distinct transport vesicles mediate the delivery of plasma membrane proteins to the apical and basolateral domains of MDCK cells. The Journal of cell biology 111:987-1000.
Wang Y, Mandelkow E (2016) Tau in physiology and pathology. Nature reviews Neuroscience 17:5-21.
Waters MG, Hughson FM (2000) Membrane tethering and fusion in the secretory and endocytic pathways. Traffic 1:588-597.
Wefelmeyer W, Cattaert D, Burrone J (2015) Activity-dependent mismatch between axo-axonic synapses and the axon initial segment controls neuronal output. Proceedings of the National Academy of Sciences of the United States of America 112 (31):9757-9762.
Weidman P, Roth R, Heuser J (1993) Golgi membrane dynamics imaged by freeze-etch electron microscopy: views of different membrane coatings involved in tubulation versus vesiculation. Cell 75:123-133.
Weingarten MD, Lockwood AH, Hwo SY, Kirschner MW (1975) A protein factor essential for microtubule assembly. Proceedings of the National Academy of Sciences of the United States of America 72:1858-1862.
Whyte JR, Munro S (2002) Vesicle tethering complexes in membrane traffic. Journal of cell science 115:2627-2637.
Williams DR (2006) Tauopathies: classification and clinical update on neurodegenerative diseases associated with microtubule-associated protein tau. Internal medicine journal 36:652-660.
Winckler B, Forscher P, Mellman I (1999) A diffusion barrier maintains distribution of membrane proteins in polarized neurons. Nature 397:698-701.
Wu D, Shi J, Elmadhoun O, Duan Y, An H, Zhang J, He X, Meng R, Liu X, Ji X, Ding Y (2017) Dihydrocapsaicin (DHC) enhances the hypothermia-induced neuroprotection following ischemic stroke via PI3K/Akt regulation in rat. Brain Research 1671:18-25.
Xia D, Li C, Gotz J (2015) Pseudophosphorylation of Tau at distinct epitopes or the presence of the P301L mutation targets the microtubule-associated protein Tau to dendritic spines. Biochimica et biophysica acta 1852:913-924.
Xu K, Zhong G, Zhuang X (2013) Actin, spectrin, and associated proteins form a periodic cytoskeletal structure in axons. Science 339:452-456.
Xue SB, Nicoud MR, Cui J, Jovin (1994) High concentration of calcium ions in Golgi apparatus. Cell Research 4: 97–108.
Yadav S, Linstedt AD (2011) Golgi positioning. Cold Spring Harbor perspectives in biology 3(5): a005322.
Yamada R, Kuba H (2016) Structural and Functional Plasticity at the Axon Initial Segment. Frontiers in cellular neuroscience 10:250.
Yamaguchi F, Morrison RS, Gonatas NK, Takahashi H, Sugisaki Y, Teramoto A (2003) Identification of MG-160, a FGF binding medial Golgi sialoglycoprotein, in brain tumors: an index of malignancy in astrocytomas. International journal of oncology 22:1045-1049.
Yenari MA, Hemmen TM (2010) Therapeutic hypothermia for brain ischemia: where have we come and where do we go?. Stroke 41 (10 Suppl):S72-74.
Yenari MA, Han HS (2012) Neuroprotective mechanisms of hypothermia in brain ischaemia. Nature Reviews Neuroscience 13 (4):267-278.
Yin Q, Ge H, Liao CC, Liu D, Zhang S, Pan YH (2016) Antioxidant Defenses in the Brains of Bats during Hibernation. PLoS One 11 (3):e0152135.

Yoshida H, Ihara Y (1993) Tau in paired helical filaments is functionally distinct from fetal tau: assembly incompetence of paired helical filament-tau. Journal of neurochemistry 61:1183-1186.

Yoshiyama Y, Higuchi M, Zhang B, Huang SM, Iwata N, Saido TC, Maeda J, Suhara T, Trojanowski JQ, Lee VM (2007) Synapse loss and microglial activation precede tangles in a P301S tauopathy mouse model. Neuron 53:337-351.

Yu Y, Shu Y, McCormick DA (2008) Cortical action potential backpropagation explains spike threshold variability and rapid-onset kinetics. The Journal of neuroscience 28:7260-7272.

Yu Y, Maureira C, Liu X, McCormick D (2010) P/Q and N channels control baseline and spike-triggered calcium levels in neocortical axons and synaptic boutons. The Journal of neuroscience 30:11858-11869.

Zempel H, Dennissen FJA, Kumar Y, Luedtke J, Biernat J, Mandelkow EM, Mandelkow E (2017) Axodendritic sorting and pathological missorting of Tau are isoform-specific and determined by axon initial segment architecture. The Journal of biological chemistry 292:12192-12207.

Zhegunov GF (1988) Protein synthesis in cardiac cells and the ultrastructural dynamics of cardiomyocytes of hibernating animals during the hibernation cycle. Tsitologiia 30:157-162.

Zhong G, He J, Zhou R, Lorenzo D, Babcock HP, Bennett V, Zhuang X (2014) Developmental mechanism of the periodic membrane skeleton in axons. eLife 3:e04581.

Zhou Z, Zuber ME, Burrus LW, Olwin BB (1997) Identification and characterization of a fibroblast growth factor (FGF) binding domain in the cysteine-rich FGF receptor. The Journal of biological chemistry 272:5167-5174.

Zhou F, Zhu X, Castellani RJ, Stimmelmayr R, Perry G, Smith MA, Drew KL (2001) Hibernation, a model of neuroprotection. The American journal of pathology 158:2145-2151.

Zilkova M, Zilka N, Kovac A, Kovacech B, Skrabana R, Skrabanova M, Novak M (2011) Hyperphosphorylated truncated protein tau induces caspase-3 independent apoptosis-like pathway in the Alzheimer's disease cellular model. Journal of Alzheimer's disease 23:161-169.

Zuber ME, Zhou Z, Burrus LW, Olwin BB (1997) Cysteine-rich FGF receptor regulates intracellular FGF-1 and FGF-2 levels. Journal of cellular physiology 170:217-227.

V - COMPENDIO DE ARTÍCULOS PUBLICADOS

A.I Antón-Fernández A, Aparicio Torres G, Tapia S, DeFelipe J and Muñoz A "Morphometric alterations of Golgi apparatus in Alzheimer's disease are related to tau hyperphosphorylation". *Neurobiology of disease*, 2017, 97A;11-23.

A.II Antón-Fernández A, Merchán J, Avila J, Hernandez F, DeFelipe J, and Muñoz A. "Phospho-Tau Accumulation and Structural Alterations of the Golgi Apparatus of Cortical Pyramidal Neurons in the P301S Tauopathy Mouse Model". *Journal of Alzheimer's disease,* 2017, 60(2): 651–661.

A.III Antón-Fernández A*, León Espinosa G*, DeFelipe J, Muñoz A "Changes in the Golgi apparatus of neocortical and hippocampal neurons in the hibernating hámster". *Frontiers in Neuroanatomy,* 2015, 9: 157.

B.I Antón-Fernández A, Rubio-Garrido JP, DeFelipe J and Muñoz A. "Selective presence of a giant saccular organelle in the axon initial segment of a subpopulation of layer V pyramidal neurons", *Brain structure and function*, 2015, 220(2):869-84.

B.II Antón-Fernández A, León Espinosa G, DeFelipe J, Muñoz A. Phospho-tau accumulation and the structural alterations of the pyramidal cell axon initial segment in Alzheimer´s disease. In preparation.

B.III León-Espinosa G*, Antón-Fernández A*, Tapia S, Defelipe J, Muñoz A. "Changes of the axon initial segment of pyramidal cells during hibernation". Enviado a *Brain, Structure and function;* en revisión. *Co-autoría por igual contribución.

Neurobiology of Disease 97 (2017) 11–23

Contents lists available at ScienceDirect

Neurobiology of Disease

journal homepage: www.elsevier.com/locate/ynbdi

Morphometric alterations of Golgi apparatus in Alzheimer's disease are related to tau hyperphosphorylation

Alejandro Antón-Fernández [a,b], Guillermo Aparicio-Torres [a,b], Silvia Tapia [a,b], Javier DeFelipe [a,b,c], Alberto Muñoz [a,b,d,*]

[a] Instituto Cajal, CSIC, Madrid, Spain
[b] Laboratorio Cajal de Circuitos Corticales (CTB), Universidad Politécnica de Madrid, Madrid, Spain
[c] CIBERNED, Centro de Investigación Biomédica en Red de Enfermedades Neurodegenerativas, Spain
[d] Department of Cell Biology, Complutense University, Madrid, Spain

ARTICLE INFO

Article history:
Received 4 May 2016
Revised 3 October 2016
Accepted 23 October 2016
Available online 26 October 2016

Keywords:
Taupathy
Dementia
Human hippocampus
Human neocortex
Microtubules
Neurofibrillary tangles

ABSTRACT

The Golgi apparatus (GA) is a highly dynamic organelle, which is mainly involved in the post-translational processing and targeting of cellular proteins and which undergoes significant morphological changes in response to different physiological and pathological conditions. In the present study, we have analyzed the possible alterations of GA in neurons from the temporal neocortex and hippocampus of Alzheimer's disease (AD) patients, using double immunofluorescence techniques, confocal microscopy and 3D quantification techniques. We found that in AD patients, the percentage of temporal neocortical and CA1 hippocampal pyramidal neurons with a highly altered GA is much higher (approximately 65%) in neurons with neurofibrillary tangles (NFT) than in NFT-free neurons (approximately 6%). Quantitative analysis of the surface area and volume of GA elements in neurons revealed that, compared with NFT-free neurons, NFT-bearing neurons had a reduction of approximately one half in neocortical neurons and one third in CA1 neurons. In both regions, neurons with a pre-tangle stage of phospho-tau accumulation had surface area and GA volume values that were intermediate, that is, between those of NFT-free and NFT-bearing neurons. These findings support the idea that the progressive accumulation of phospho-tau is associated with structural alterations of the GA including fragmentation and a decrease in the surface area and volume of GA elements. These alterations likely impact the processing and trafficking of proteins, which might contribute to neuronal dysfunction in AD.

1. Introduction

The Golgi apparatus (GA) is an essential organelle in the processing and targeting of cellular proteins, and its disruption is related to neuronal dysfunctions and human diseases (Gonatas et al., 2006; Hu et al., 2007). It has been shown that the GA undergoes morphological plasticity processes that affect the GA shape and protein content under different physiological and pathological conditions (Anton-Fernandez et al., 2015; Fan et al., 2008; Glick, 2002; Levine et al., 1995). In different neurological diseases, including Alzheimer's disease (AD), the GA of certain populations of neurons becomes fragmented (Baloyannis, 2014; Dal Canto, 1996; Fan et al., 2008; Fujita et al., 2006; Fujita and Okamoto, 2005; Fujita et al., 2002; Gonatas et al., 1998b; Gonatas et al., 2006; Gonatas et al., 1992; Hu et al., 2007; Huse et al., 2002; Liazoghli et al., 2005; Mizuno et al., 2001; Rabouille and Haase, 2015; Sakurai et al., 2000; Stieber et al., 1996). Several studies carried out in animal models of AD have related this fragmentation to the accumulation of either amyloid β (Aβ) or hyperphosphorylated microtubule-associated protein tau—the two main pathological hallmarks of AD (see Jiang et al., 2014; Joshi and Wang, 2015; Liazoghli et al., 2005). However, the precise temporal sequence and the possible relationships between GA fragmentation and the accumulation of Aβ plaques or neurofibrillary tangles of hyperphosphorylated tau during the evolution of AD have not been fully characterized.

Proper functioning of the GA is necessary for Aβ production and for trafficking and maturation of amyloid precursor protein APP and its processing enzymes (Burgos et al., 2010; Choy et al., 2012; Greenfield et al., 1999; Huse et al., 2002; Joshi et al., 2015). In addition, studies using the APPswe/PS1ΔE9 animal model of the disease have reported that the accumulation of Aβ peptides leads to Golgi fragmentation, mediated by cdk5-dependent phosphorylation of Grasp 65, which in turn accelerates APP trafficking and Aβ production (Joshi et al., 2015; Joshi and Wang, 2015). Furthermore, the integrity of the microtubule (Burkhardt, 1998; Cole et al., 1996) and actin (Egea et al., 2006) cytoskeleton is necessary for the maintenance of the structural characteristics and the positioning of the GA. Various studies have suggested the existence of

* Corresponding author at: Laboratorio Cajal de circuitos corticales, Centro de Tecnología Biomédica, Universidad Politécnica, Madrid, Pozuelo de Alarcón, Madrid, 28223, Spain.
E-mail address: amunozc@bio.ucm.es (A. Muñoz).
Available online on ScienceDirect (www.sciencedirect.com).

http://dx.doi.org/10.1016/j.nbd.2016.10.005

feedback mechanisms between tau hyperphosphorylation, microtubule organization and GA fragmentation. For instance, it has been proposed that the microtubule-interacting protein tau, which is localized on GA membranes along with many of the tau phosphorylation-related kinases participates in the association between Golgi membranes and microtubules (Farah et al., 2006). It has been suggested that tau pathology precedes GA fragmentation since, in animal models of AD, the overexpression of tau induced GA fragmentation (Liazoghli et al., 2005; Lin et al., 2003). However, other studies showing tau hyperphosphorylation after brefeldin A or nocodazole treatments of HEK293/tau cells led to the suggestion that tau hyperphosphorylation is a downstream event that is a consequence of the disorganization of the GA (Sutterlin et al., 2002; Jiang et al., 2014).

Pioneering studies in AD patients reported that the alterations (including fragmentation and decreases in size) of the GA of hippocampal neurons are unrelated to the content of intracellular NFT in CA1 hippocampal field (Salehi et al., 1995) or preferentially associated with neurons devoid of NTF in the subiculum and entorhinal cortex (Stieber et al., 1996). However, during the course of our research into the possible alterations of the GA in the hippocampus and neocortex of AD patients using different methodological approaches to those used by Salehi et al. (1995) and Stieber et al. (1996), we found that the progressive accumulation of phospho-tau may be associated with the fragmentation of the GA. Thus, in the present study, we have reexamined this issue using double immunofluorescence techniques, high-resolution confocal microscopy and 3D reconstruction and quantification methods to measure the volume and surface area of the GA in neurons from control cases and from AD patients with pre-tangle and tangle stages of hyperphosphorylated tau accumulation. To label the GA, we used antibodies that recognize MG160, an integral membrane Golgi protein commonly used as a GA marker (Anton-Fernandez et al., 2015; Burrus et al., 1992; Gonatas et al., 1998a; Gonatas et al., 1995; Stieber et al., 1995; Stieber et al., 1996; Yamaguchi et al., 2003; Zhou et al., 1997; Zuber et al., 1997).

Importantly, differences in age (Jiang et al., 2014), fixation procedure and postmortem period prior to fixation might affect the structural characteristics of the GA. These factors vary between the control and the AD patient groups used in previous reports (Ellisman et al., 1987; Salehi et al., 1995; Stieber et al., 1996) and might also affect the morphology of the GA, as evaluated in the present study by the expression of MG160. Therefore, in order to evaluate the possible influence of normal aging and the postmortem delay period on the analysis of MG160 expression in the GA and discriminate the interference between these potential changes and those associated with the course of AD, we have analyzed the GA in brain sections from C57BL/6J mice with different ages and from mice with different postmortem times before brain fixation.

The results of the present study indicate that, in AD patients, the GA of numerous cortical and hippocampal neurons undergo specific and profound alterations including fragmentation and a decrease in the volume and surface area of the elements that are immunoreactive for MG160. These changes are likely to affect the protein processing, glycosylation and sorting (Wang et al., 2008; Xiang et al., 2013) and are more pronounced and more frequently found in neurons with a progressive accumulation of hyperphosphorylated tau. Therefore, the perturbation of the microtubule network by tau hyperphosphorylation could alter GA structure and the secretory pathway, impairing the highly regulated processes of protein sorting in neuronal compartments.

2. Materials and methods

Human brain tissue was obtained at autopsy from two sources: from seven patients with AD (aged 64–89) and from control human brain tissue from five individuals (aged 40–66) who died due to an accident or other cause and were free of any known neurological or psychiatric illness (Table 1). The AD brain and some control brain tissues were obtained from the *Instituto de Neuropatología* (Dr. I. Ferrer, *Servicio de Anatomía Patológica*, IDIBELL-*Hospital Universitario de Bellvitge*, Barcelona, Spain; IF4, IF10, IF12, IF13 and M16 cases), from the *Banco de Tejidos Fundación* CIEN (Dr. A. Rábano, *Área de Neuropatología*, *Centro Alzheimer*, *Fundación Reina Sofia*, *Madrid*, Spain; Vk11 case) and from the Neurological Tissue Bank (*Biobanc-Hospital Clínic-IDIBAPS*, Universidad de Barcelona, Spain; Bcn 5, Bcn7, Bcn8, Bcn13 cases). Control human brains were also obtained from Dr. Ricardo Insausti, *Facultad de Medicina*, *Universidad UCLM* (Albacete, Spain; AB1, AB2). Following neuropathological examination, the AD stages were defined according to the CERAD (Consortium to Establish a Registry for Alzheimer's Disease; (Mirra et al., 1991) and the Braak and Braak criteria (Braak and Braak, 1995); Table 1). Information regarding TDP43 inclusions was available for four of the seven patients used (Bcn5, Bcn7, Bcn8 and Bcn13). None of them showed TDP43 inclusions in CA1 or temporal neocortex, and only Bcn7 had TDP43 inclusions in neurons of the amigdala.

The postmortem delay between death and tissue processing ranged between 1.5 and 5.5 h (Table 1), and the brain samples were obtained following the guidelines of the Institutional Ethical Committees, which also granted approval. Tissue from some of these human brains has been used in previous studies (Blazquez-Llorca et al., 2010; Blazquez-Llorca et al., 2011).

Upon removal, the brains were immediately fixed in cold 4% paraformaldehyde in phosphate buffer (PB: 0.1 M, pH 7.4), and after 2 h, the tissue was cut into small blocks and post-fixed in the same fixative for 24–48 h at 4 °C. However, one human patient (AB1) was intraarterially perfused through the internal carotid arthery <1 h after death with a saline solution followed by 4% paraformaldehyde in PB. The brain was then removed and post-fixed as mentioned above. After fixation, all the specimens were immersed in graded sucrose solutions and stored in a cryoprotectant solution at −20 °C. Serial sections (50 μm) of the cortical tissue were obtained using a vibratome (St. Louis, MO, USA), and the sections from each region and case were batch-processed for immunohistochemical staining. The sections immediately adjacent to those stained immunohistochemically were Nissl-stained in order to identify the cortical areas and the laminar boundaries.

2.1. Immunofluorescence

For immunofluorescence experiments, free floating serial sections (50-μm thick) were first rinsed in PB and then pre-treated in 1.66% H_2O_2 for 30 min to inactivate the endogenous peroxidase activity and were then preincubated for 1 h in PB with 0.25% Triton-X100 and 3% normal serum of the species in which the secondary antibodies were raised (Vector Laboratories, Burlingame, CA, USA). The sections were then incubated for 48 h at 4 °C in the same stock solution containing the following primary antibodies in the combinations indicated: rabbit anti-MG160 (Abcam, 1:100), mouse anti-NeuN (Chemicon, 1:2000), mouse phospho-PHF-tau pSer202 + Thr205 antibody (AT8, 1:2000, Pierce Endogen).

After rinsing in PB, the sections were incubated for 2 h at room temperature in the appropriate combinations of Alexa 488- or Alexa 594-conjugated goat anti-mouse or goat anti-rabbit antibodies (1:2000; Molecular Probes, Eugene, OR, USA). Sections were also stained with a nuclear stain DAPI (4,6-diamidino-2-phenylindole; Sigma, St. Louis, MO, U.S.A.). After rinsing in PB, the sections were treated with Autofluorescence Eliminator Reagent (Chemicon) to reduce autofluorescence, mounted in antifade mounting medium (ProlongGold, Invitrogen) and studied by confocal microscopy (Zeiss, 710).

From the temporal neocortex and the CA1 region of the hippocampus, we obtained image stacks recorded at 0.35 μm intervals through separate channels with a 63x oil-immersion lens (NA, 1.40, refraction index, 1.45). The number of optical planes in the confocal stacks ranged from 40 to 142 (mean = 84.5) in the neocortex and 69 to 183 (mean = 108.3) in the hippocampus. ZEN 2012 software (Zeiss) was used to construct composite images from each optical series by combining the

Table 1
Summary of clinical and surgical data. Neurological diagnosis defined according to Braak and Braak criteria (Braak and Braak, 1995), defined by different stages (from I to VI) and also according to CERAD criteria (Consortium to Establish a Registry for Alzheimer's Disease; Mirra et al., 1991), which use a semi-quantitative score of the density of neuritic plaques in the most severely affected region of the isocortex (A = mild presence of plaques, B = moderate presence of plaques, C = severe presence of plaques).

AD patients	Cortical area	Age (years)	Gender	Postmortem delay	Neurological diagnosis	Cause of death
Bcn5	Area 21	83	Female	4 h	AD V/VI – C	Respiratory infection
Bcn7	Area 21	89	Female	4/4.5 h	AD VI – C	–
Bcn8	Area 21	85	Female	5/6 h	AD VI – C	–
P3 (IF4)	Area 22	80	Female	3 h	AD III – B	Pneumonia
P11 (IF13)	Area 20/21	75	Male	2 h	AD III – B	Lymphoproliferative disorder
P13 (Bcn13)	–	83	Male	2.5 h	AD	–
P14 (Vk11)	Area 20/21	87	Female	1.5 h	AD III/IV – A	Respiratory infection
Non-demented cases						
AB1	Area 21	45	Male	<1 h	–	Pleural *mesothelioma*
AB2	Area 21, 38	50	Female	4 h	–	Septic shock of pulmonary origin
M16	Area 20	40	Male	–	–	Traffic accident
C7 (IF10)	Area 20	66	Male	2 h	–	Bilateral pneumonia plus cardiac post-transplant
P10 (IF12)	Area 20/21	52	Male	2 h	–	Carcinoma – bronchopneumonia

images recorded through the different channels, and the same software was used to obtain Z projection images (image resolution: 1024 × 1024 pixels; pixel size: 0.11 μm). Adobe Photoshop (CS4) software was used to compose figures.

2.2. Image analysis and statistics

Fiji software (3D object counter tool) was used to analyze the volume and surface area of the elements immunostained for the different GA markers in image stacks according to a previous study (Anton-Fernandez et al., 2015). A limitation of the present study is that unfortunately the combinations of antibodies used, known to work satisfactorily in human brain tissue, did not allow the simultaneous visualization of the GA (MG160), the neuronal somata (NeuN) and phospho-PHF-tau (AT8). Despite this, we cropped 3D substacks from the original confocal stacks taken from AT8-MG160 double-stained sections counterstained with DAPI, trying to limit the analysis to the complete GA corresponding to the somata of single neurons. These cells included neurons without hyperphosphorylated tau (AT8−) and neurons with hyperphosphorylated tau (AT8+) at different stages (non-tangle-bearing neurons and tangle-bearing neurons; see Table 2 for the number of neurons of each type analyzed for all of the brain regions and cases studied). To make sure that we analyzed complete cell bodies, the substacks were centered on the location of those single DAPI-stained neuronal nuclei that were separated in all dimensions from the edges of the stack by at least 10 μm. From these positions, we analyzed the whole thickness of the confocal stacks and we defined the limits of every image substack according to the 'reach' of the MG160-ir elements surrounding the selected neuronal nuclei. The number of optical planes in the cropped confocal substacks ranged from 10 to 62 (mean = 52) in the neocortex and 15 to 89 (mean = 40) in the hippocampus. We selected isolated neurons that were separated from other neurons by neuropil, in order to avoid the inclusion of MG160-ir elements belonging to neighboring neurons. For this purpose, in AT8+ neurons, the presence of AT8 immunostaining helped to identify the limits of the neuronal somata. In AT8− neurons, background MG160 staining also helped to distinguish neuronal somata from neuropil. To determine differences between values obtained in AT8− neurons and AT8+ non-tangle-bearing and tangle-bearing neurons, paired Friedman analysis of variance tests were performed using SPSS software (version 22). When the Friedman test was significant, a Wilcoxon matched pair test was performed between groups.

2.3. Aging and postmortem autolysis effects on Golgi apparatus

The human tissue used in the present study came from patients who died at different ages and with different postmortem delay periods until brain fixation—up to 6 h in some cases (Table 1). Thus, in order to test the possible involvement of aging and postmortem autolysis effects on the structure of the neuronal GA, and to discriminate between these effects and those related to AD, in the present study we analyzed GA immunostaining in two groups of mice. These experiments were performed in accordance with the guidelines established by the European Union regarding the use and care of laboratory animals (86/609/EEC) and the experimental procedures were approved by our institutional animal use and care committee. Special care was taken to minimize animal suffering and to reduce the number of animals used to the minimum required for statistical accuracy.

In order to test possible effects of aging on the GA of pyramidal neurons, we analyzed C57BL/6J mice (Charles River Laboratories, Wilmington, MA) at different ages: 8, 32, 60 and 80 weeks (three animals per age group). Animals were sacrificed by a lethal intraperitoneal injection of sodium pentobarbital (200 mg/kg b.w.) and were then perfused intracardially with a saline solution followed by 4% paraformaldehyde in PB. The brain of each animal was removed, post-fixed by immersion in the same fixative for 24 h at 4 °C, cryoprotected in 30% sucrose and serial coronal sections (50-μm thick) were obtained with a freezing sliding microtome (Microm HM 450, Microm International, Germany).

To assess post-mortem time-induced effects on the structure of the GA, two-month-old male C57BL/6J mice (n = 3, per group) (Charles River Laboratories) were used. Mice were deeply anaesthetized with a pentobarbital lethal injection (200 mg/kg b.w, Vetoquinol, Madrid,

Table 2
Table showing the percentages and total number (in parenthesis) of pyramidal neurons analyzed, from the CA1 and temporal neocortex of control cases and Alzheimer disease patients, showing the relationship between the appearance of Golgi apparatus (GA) (NF, *non-fragmented*; F, *fragmented*; HA, *highly altered*) with the different patterns of immunostaining for PHF-tauAT8 (AT8−, type I and II).

			Ctx			CA1		
			NF	F	HA	NF	F	HA
Control			91.6 (296)	7.4 (24)	1 (3)	75.78 (144)	22.6 (43)	1.6 (3)
Patients	All cell types		58.7 (430)	24 (176)	17.3 (127)	33.09 (236)	43.19 (308)	23.7 (169)
	AT8−		71.8 (412)	21.9 (126)	6.3 (36)	47.9 (201)	45.7 (192)	6.4 (27)
	AT8+	Type I	25.4 (14)	40 (22)	34.5 (19)	16.6 (28)	46.7 (79)	36.7 (62)
		Type II	3.9 (4)	26.9 (28)	69.2 (72)	5.7 (7)	29.8 (37)	64.5 (80)

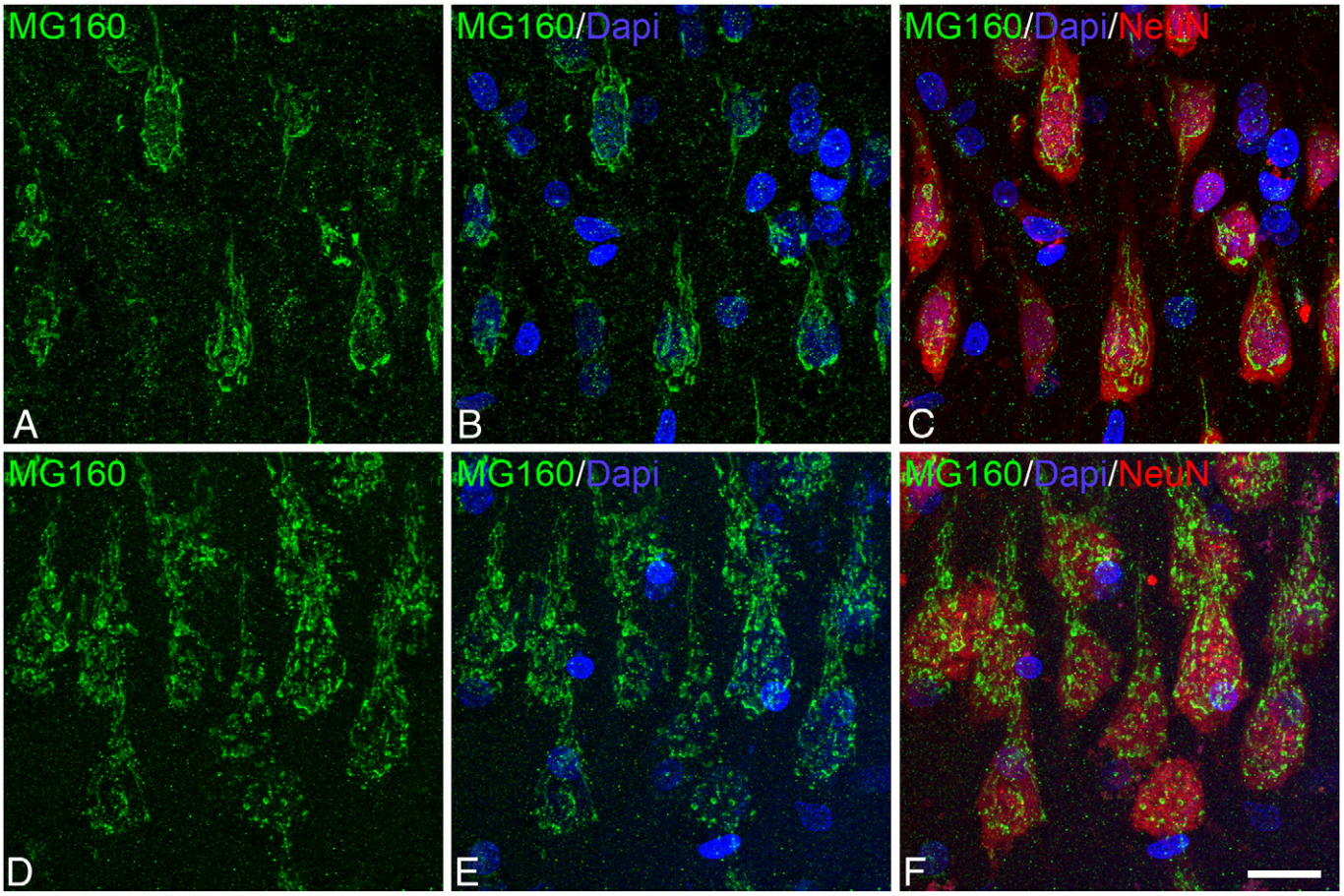

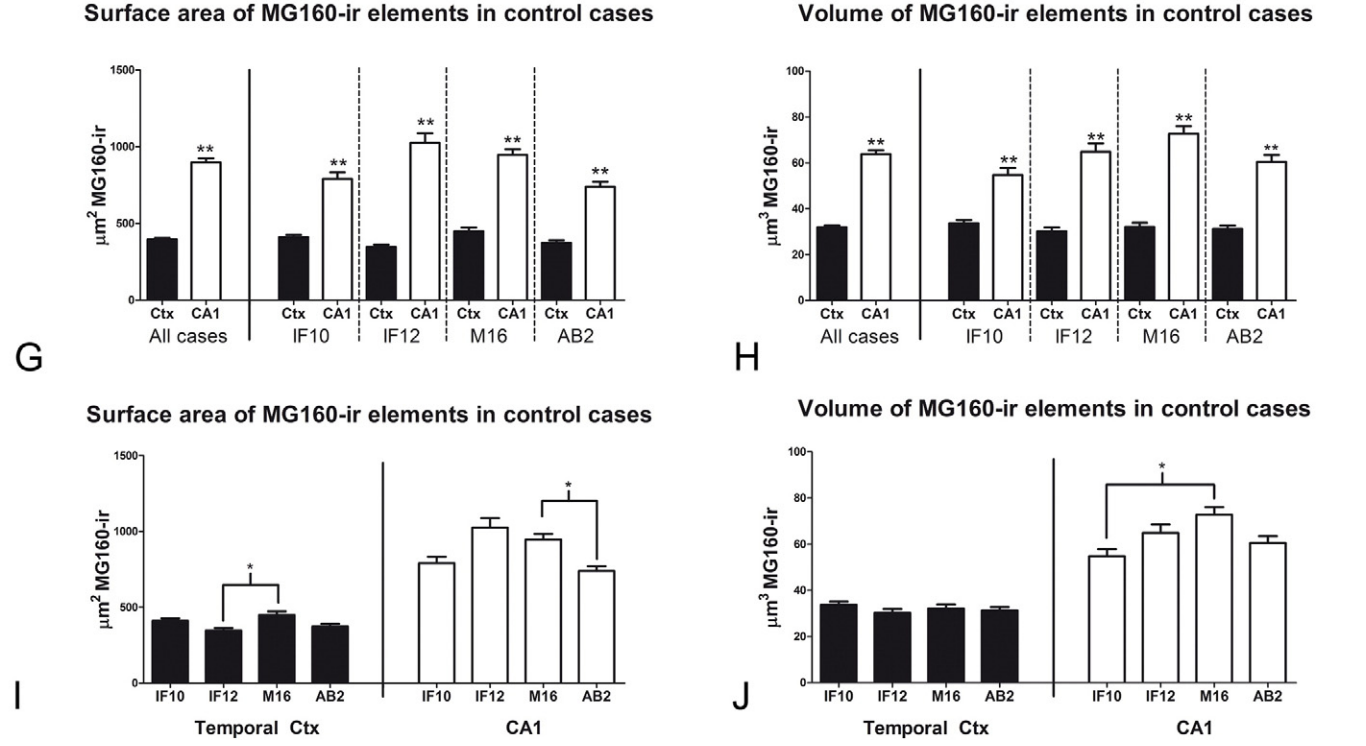

Fig. 1. Distribution of MG160 in the GA of human pyramidal neurons A–F: Trios of confocal stack projection images taken from the temporal neocortex (A–C) and the CA1 hippocampal region (D–F) of sections double-immunostained for MG160/NeuN and counterstained with DAPI showing the distribution of MG160 in the GA. Scale bar in F indicates 18 µm in A–C and 16 µm in D–F. G–J: Histograms showing surface area (G, I) and volume (H, J) values (mean ± SE) of GA elements immunoreactive for MG160, obtained from cropped confocal image stacks including complete single pyramidal neurons from temporal neocortex (black bars; total n = 323) and CA1 (white bars; total n = 189). G and H show the statistical comparisons of mean values (surface area and volume, respectively) between neocortical and hippocampal neurons. I and J show the comparisons of the values obtained across the different cases in each region (Friedman test, $^{*}p \leq 0.01$; $^{**}p \leq 0.001$). Note that in all cases the surface area and volume values of MG160-ir elements in CA1 are higher than in neocortical pyramidal cells (G, H) despite the inter-individual differences (I, J).

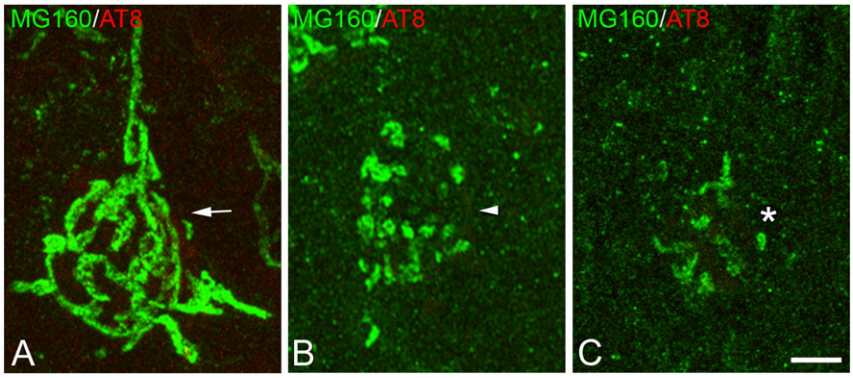

Fig. 2. Morphological types of Golgi apparatus Confocal stack projection mages taken from the temporal neocortex of sections from control cases, double-immunostained for MG160/AT8 showing examples of neurons with a *non-fragmented* (A), *fragmented* (B) or *highly altered* (C) GA. Scale bar indicates 4,8 μm.

Spain). The cadavers were subjected to different post-mortem times and temperature conditions. Two groups of mice were maintained at room temperature for 0.5 and 2 h, respectively. A third group was kept at room temperature for 2 h followed by 3 h at 4 °C in a fridge. The brains were then removed from the skull and fixed by immersion with 4% paraformaldehyde for 20 h at 4 °C. After fixation, brains were cryoprotected in 30% sucrose and then flash-frozen in isopentane (2-methylbutane, Merck, Billerica, MA), cooled in a 70% ethanol dry ice bath, and stored at −80° until cutting. Coronal sections (30 μm) were cut with a freezing sliding microtome (Microm HM450). Sections from all animal groups were immunocytochemically stained as described above using anti-MG160 antibodies. Confocal image stacks were taken from the temporal neocortex and the hippocampal formation and were analyzed in the same way as described for the human tissue (see above). To determine differences between values obtained in animals with different postmortem delay times as well as in mice groups with different ages, Kruskal-Wallis one-way analysis of variance was performed followed by Bonferroni-corrected Mann-Whitney *U* test, using SPSS software.

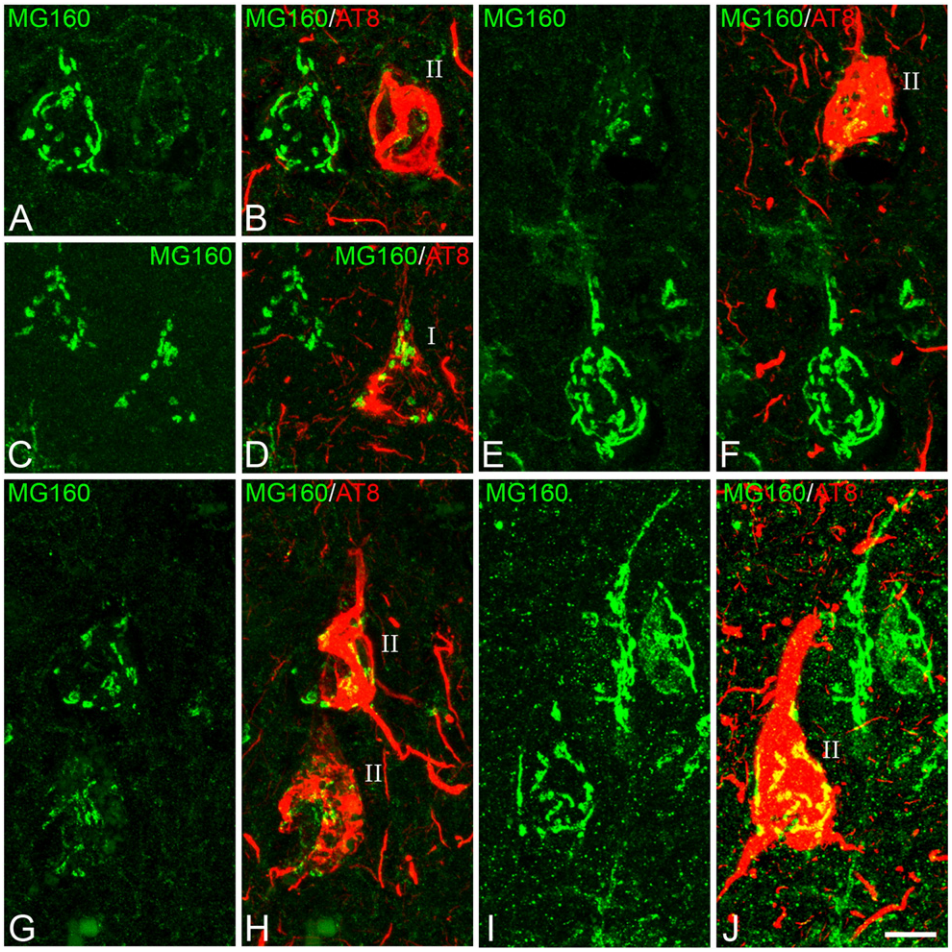

Fig. 3. Distribution of MG160 in the GA of AT8 − and AT8 + human neocortical pyramidal neurons A, B; C, D; E, F; G, H; I, J: pairs of confocal stack projection images taken from the temporal neocortex of sections double-immunostained for MG160/AT8 showing the distribution of MG160 in the GA of AT8 −, and AT8 + (type I and type II) pyramidal neurons. Scale bar shown in J indicates 6.4 μm in A and B, 9.1 μm in C and D, 8.1 μm in E and F, 9.6 μm in G and H and 8.8 μm in I and J.

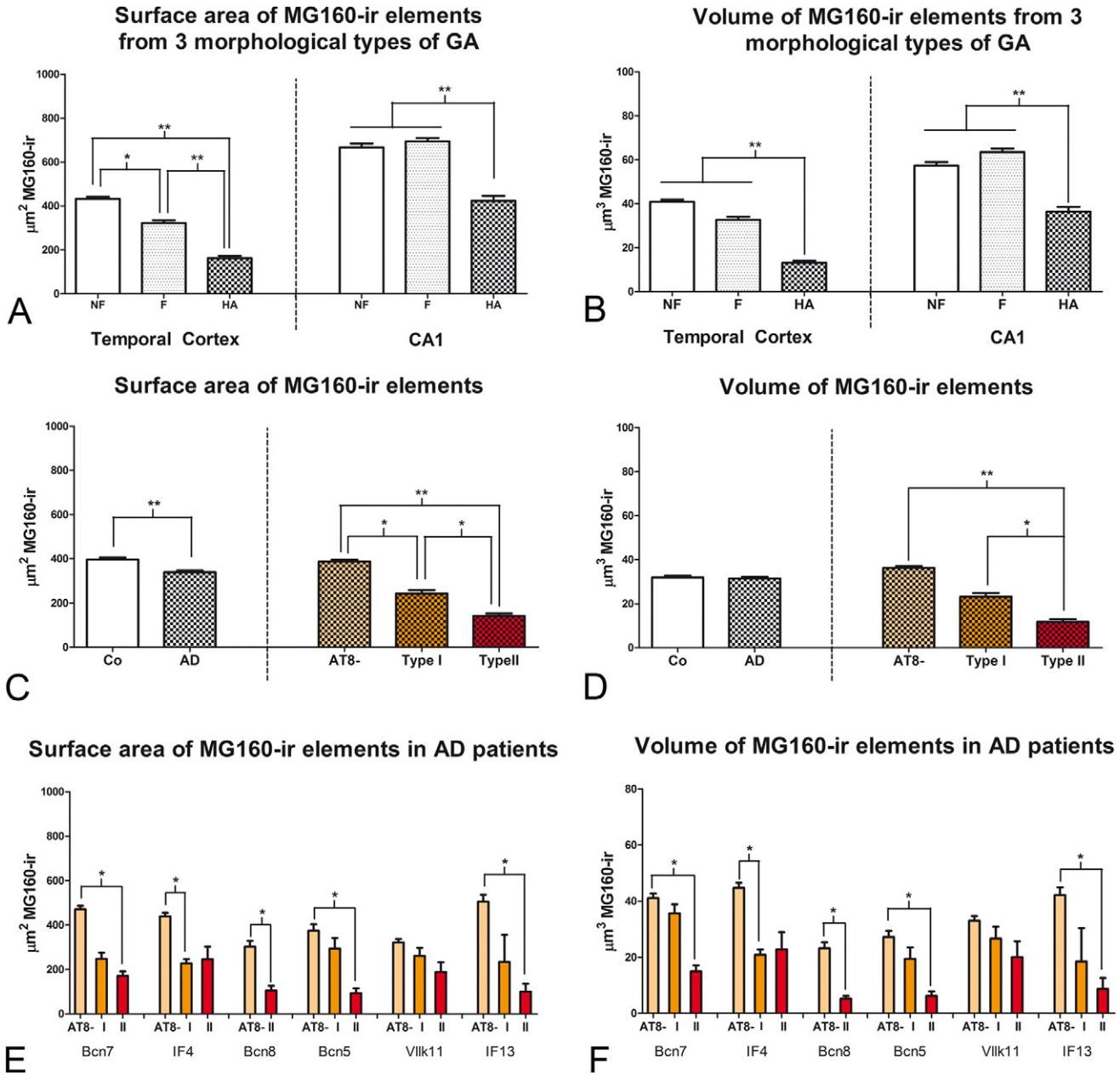

Fig. 4. Measurements of the GA in neocortical pyramidal neurons from AD patients A and B: histograms show comparisons in surface area (A) and volume (B) values of MG160-ir elements between neurons with *non-fragmented*, *fragmented* or *highly altered* GA in AD cases (Friedman test, *p ≤ 0.01; **p ≤ 0.001). C–D: histograms showing, on the left side, surface area (C) and volume (D) values (mean ± SE) of MG160-ir GA elements, in control (white bars, n = 323) and AD (patterned bars, n = 733) pyramidal neurons from temporal neocortex. Note that Golgi elements had a higher surface area (but not volume) in control than in neurons from AD patients. Also note (in the histograms on the right) that for AD neurons (taking all cases together) both surface area and volume values were reduced in AT8 + (especially in type II) neurons, compared to AT8 − neurons. Note that in E and F there was a tendency for this reduction in all AD patients analyzed, with statistically significant differences between the different cell types of each patient in five out of the six cases analyzed (Friedman test, *p ≤ 0.01; **p ≤ 0.001).

3. Results

3.1. Distribution of MG160 in the GA of control human cortical neurons

To characterize alterations in the Golgi apparatus (GA) of AD patients, we first studied its normal morphological characteristics in neocortical and hippocampal pyramidal neurons from human control autopsy cases. We studied sections stained with DAPI and double-immunostained with antibodies that recognize the neuronal marker NeuN and MG160, a sialoglycoprotein that is frequently used as a GA marker and is mainly localized in the medial cisternae of the GA (Fig. 1). The identification of pyramidal neurons relied on the presence of an apical dendrite. MG160-ir GA elements were located in the neuronal cytoplasm, as defined by the NeuN immunostaining, usually in a perinuclear position. We found a significant variability in the morphological characteristics of GA elements that were immunoreactive (ir) for MG160, which we qualitatively subdivided into three different morphological types (Fig. 2, Table 2):

1) neurons with a GA that showed a normal non-fragmented (NF in Table 2, arrows in Fig. 2A) appearance, consisting of a network of twisted and convoluted cisternae and tubular structures with a ribbon-like appearance that was distributed throughout the cell body and partially extended to the apical dendrite.

2) neurons with a fragmented (F in Table 2, arrowheads in Fig. 2B) GA—without ribbon-like appearance and often showing a variable number of independent elements with globular appearance dispersed throughout the soma—that were more abundant in CA1 than in the neocortex.

3) neurons in which the GA, as identified by MG160 immunostaining, was very scarce or had a *highly altered* (HA) morphology (HA in Table 2, asterisks in Fig. 2C).

The percentage of neurons with a *non-fragmented* GA was higher in the temporal neocortex than in the CA1 hippocampal field (Table 2). In addition, GA of neocortical neurons (Fig. 1A–C) showed a less complex appearance, that is, with a lower degree of cisternae extension and convolution than in the case of hippocampal neurons (Fig. 1D–F).

To further characterize the GA in control neocortical and hippocampal CA1 pyramidal neurons, we used the 3D object counter tool in the Fiji software package to quantify the volume and surface area of MG160-ir GA elements of the different control human brains (Figs. 1G–J). We found a significantly larger volume and surface area of MG160-ir elements in CA1 hippocampal neurons than in neurons from temporal neocortex (Fig. 1G, H). We found the same trend when data from different control cases were analyzed separately (Fig. 1G, H). We also compared the mean values for the surface and volume of the MG160-ir GA elements between the different cases. Both in neocortical and CA1 pyramidal cells, these values were very homogeneous across cases with only few inter-individual comparisons yielding statistically significant differences (Fig. 1I, J).

3.2. Alterations in MG-160 distribution in the GA of neurons from Alzheimer disease patients

According to previous studies (Salehi et al., 1995; Stieber et al., 1996), the GA in neurons from AD patients is altered, usually showing a fragmented appearance in some cortical neurons. In the present study we found that the fragmentation of the GA in some neurons, both in neocortex and CA1 pyramidal neurons, was apparently associated with a reduction in the size of the GA (Fig. 4A, B). The surface area and volume of the GA was reduced in *fragmented* neurons (only in temporal neocortex), and especially in *highly altered* neurons, as compared with *non-fragmented* neurons (Fig. 4A, B).

The possible relationship between GA fragmentation and the progressive neuronal accumulation of hyperphosphorylated tau protein has not been explored thoroughly in previous studies. Here, we have analyzed this relationship both in pyramidal neurons from temporal neocortex and CA1 of AD patients, in confocal stacks taken from sections with double immunofluorescence staining using antibodies directed to MG160, and AT8 antibodies which recognize phospho Ser202 and phospho Thr205 sites in microtubule-associated tau protein (Figs. 3–5), and counterstained with Dapi. According to one of our previous studies (Blazquez-Llorca et al., 2010), it is possible to distinguish between AT8-negative neurons and two types of tau AT8-ir neurons showing different patterns of immunostaining for paired helical filaments (PHF): pattern I, which have diffuse cytoplasmic staining with no fibrillar aggregates (pre-tangle stage) and pattern II, which typically form NTF. Regarding GA fragmentation—considering all cell types analyzed in AD patients—we found that, as in control cases, the percentage of neurons with a *fragmented* and *highly altered* GA was higher in CA1 than in temporal neocortex (Table 2). Considering neurons with different patterns of PHF-tauAT8 immunostaining separately, we found that the percentage of neurons with a normal, *non-fragmented* GA appearance decreased in AD patients, even in AT8-negative neurons, as compared to controls, indicating a generalized alteration of GA in AD (Table 2). In addition, we observed that, compared to AT8-negative neurons, the percentage of neocortical and hippocampal neurons showing a *highly altered* GA was higher in those neurons with hyperphosphorylated tau (both in type I and more markedly in type II neurons) (Table 2, Figs. 3, 5).

We also found a general drop in surface area and volume of MG160-ir GA elements in neocortical and hippocampal neurons from AD patients compared to neurons from control cases (Figs. 4C–D, 5G–H). In order to determine if there was a specific deleterious effect of the accumulation of hyperphosphorylated tau on the GA in AD patients, we analyzed these data distinguishing between cells in pre-tangle stage (type I, Figs. 3, 5D) and in tangle stage (type II, Figs 3, 5). According to the above qualitative analysis, the results showed a progressive decline in the mean surface area and mean volume of MG160-ir GA elements from AT8− to type I and, more markedly, type II AT8-positive neurons—both in the temporal neocortex (Fig. 4C,D) and in CA1 (Fig. 5G,H). To evaluate the possible influences of inter-individual variability on these results, we analyzed separately data obtained from the different AD patients. The results showed a similar trend in all patients, with the decrease in surface area and volume of GA reaching statistical significance in most (but not all) of the patients (Figs. 4E–F, 5I–J).

3.3. Alterations of the Golgi apparatus in neurons with hyperphosphorylated tau in a non-demented case

To test in human tissue the effects induced by the sole presence of the aggregation of hyperphosphorylated tau (presumably without any other possible pathologic factors present in the AD such as the presence of β-amyloid plaques), we studied the morphological features of neuronal GA in a human brain from a 45-year-old male adult who was free of any neurological or psychiatric disease (not diagnosed with AD) and had died from a lung tumor (AB1, see Table 1). In the brain of this patient, we found a relatively large number of neurons with intracellular aggregation of hyperphosphorylated tau protein in temporal (Brodmann areas 20, 21, 22 and 38), prefrontal (9, 10 12) and frontal (areas 44, 45, 46 and 47) cortical areas while they were not detected in other cortical regions such as the primary motor (area 4), primary somatosensory (area 3b), primary visual (area 17) cortical areas. No β-amyloid plaques were found in any of these regions. In confocal stacks taken from sections double-immunostained for MG160 and hyperphosphorylated tau (AT8 antibodies), we obtained surface area and volume values of MG160-ir GA elements (Fig. 6J–K) in neurons with phospho-tau (in pre-tangle (I) and tangle (II) stages) and without phospho-tau, in CA1 (Fig. 6A–C). Values were also obtained in the temporal neocortex, in area 22 (Fig. 6D–F) and in area 38 (Fig. 6G–I), where tau-ir neurons were more abundant. The results in the three regions analyzed showed a general reduction in surface area and volume measurements of MG160-ir in AT8+ neurons, which reached statistical significance only in the type II pattern of AT8 immunostaining, that is, in neurofibrillary tangle-bearing neurons (Fig. 5J–K).

Consequently, these results further support the idea that the aggregation of hyperphosphorylated tau may exert a specific deleterious effect on the morphological features of the GA in cortical neurons, which might contribute to neuronal dysfunction and degeneration in AD.

3.4. Effects of aging and postmortem delay on the morphological features of the neuronal GA

The differences in the size and fragmentation of the GA found between control and AD cases, and even the inter-individual differences found within each group, could be partially due to the differences in age of the patients and/or postmortem delay before fixation procedures. Fixation by immersion might also contribute to the differences in the GA between neocortical and CA1 hippocampal neurons (Table 2) as a consequence of the deeper localization of CA1 compared to the neocortex. Therefore, to evaluate the potential contribution of these factors to the observed differences and to help elucidate those alterations that were due to the course of the disease, we next used C57BL/6J mice with different ages (2, 8, 15 and 20 months, Fig. 7A, B, E, F) and young adult mice brains, which were extracted and fixed by immersion after different postmortem delays (Fig. 7C, D, G, H). We measured the surface area and volume of the MG160-ir GA elements in CA1 and CA3 hippocampal neurons and supra- and infra-granular pyramidal neurons from somatosensory cortex in confocal stacks taken from sections

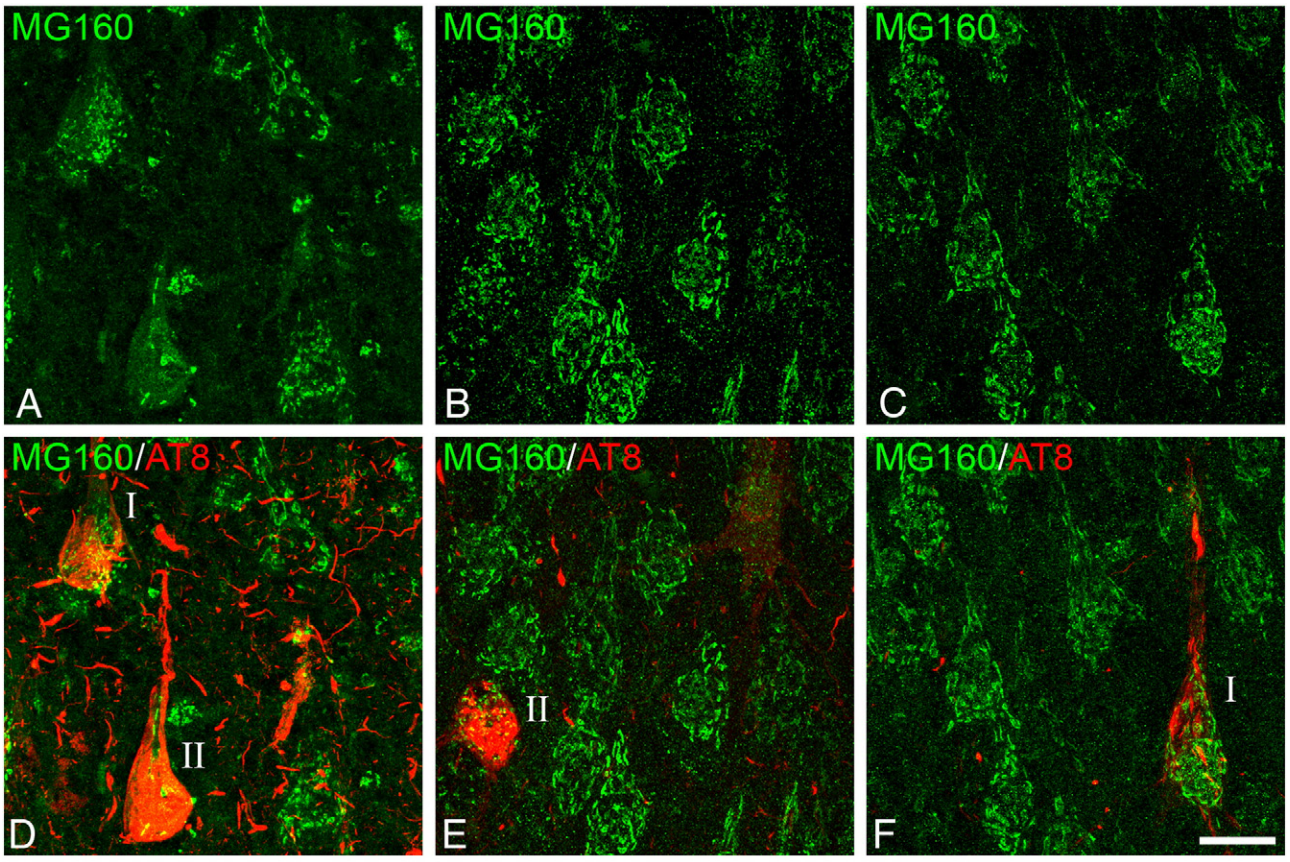
MG160
A
MG160
B
MG160
C
MG160/AT8
I
II
D
MG160/AT8
II
E
MG160/AT8
I
F

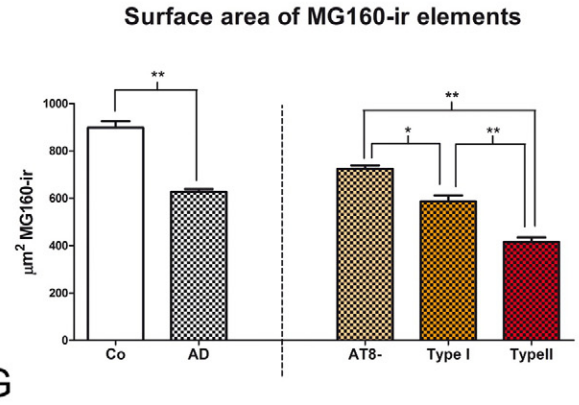
Surface area of MG160-ir elements
µm2 MG160-ir
Co
AD
AT8-
Type I
TypeII
G

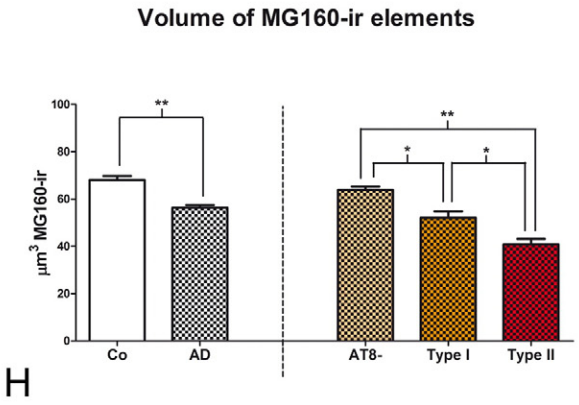
Volume of MG160-ir elements
µm3 MG160-ir
Co
AD
AT8-
Type I
Type II
H

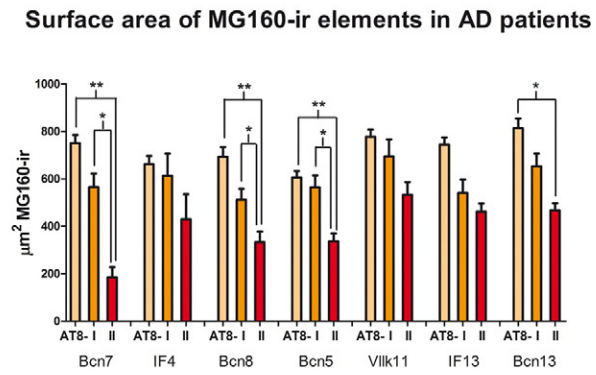
Surface area of MG160-ir elements in AD patients
µm2 MG160-ir
AT8- I II
Bcn7
IF4
Bcn8
Bcn5
VIIk11
IF13
Bcn13
I

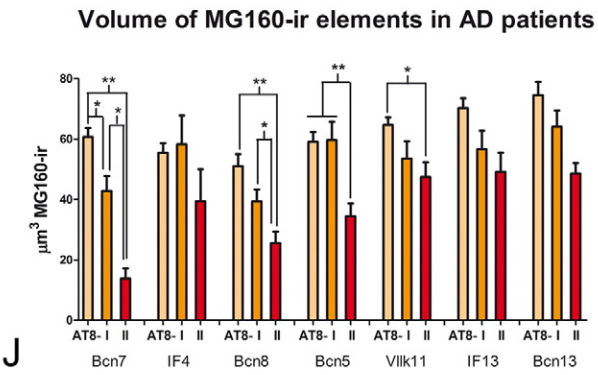
Volume of MG160-ir elements in AD patients
µm3 MG160-ir
AT8- I II
Bcn7
IF4
Bcn8
Bcn5
VIIk11
IF13
Bcn13
J

double-immunostained for MG160 and hyperphosphorylated tau (AT8 antibody).

As expected, in all regions and ages analyzed we found no AT8 immunostaining above background levels. That is, all neurons analyzed were AT8 negative. In addition, the GA of neurons in all regions and age groups had a normal, non-fragmented appearance (Fig. 7A, B). The quantitative analysis revealed no differences between the different age groups in terms of the surface area and volume of MG160-ir elements of supragranular pyramidal neurons (Fig. 7E, F). However, a tendency for a reduction with age in the size of the GA, as judged by MG160 immunostaining, was found in pyramidal neurons from infragranular neocortical layers and the CA3 region. This reduction was more marked in pyramidal neurons from CA1 (Fig. 7E, F). Finally, we found that the surface area and volume of MG160-ir GA elements of pyramidal neurons were sensitive to the post-mortem delay period, as they were significantly reduced, in all regions examined, in animals with postmortem periods of 2 h and 5 h as compared with those with a delay of 30 min before fixation (Fig. 7G, H).

4. Discussion

The present results show that MG160 is widely expressed in the GA of human and mouse neocortical and hippocampal neurons. Using this protein as a GA marker, we showed by immunofluorescence, confocal microscopy and 3D quantification that, in both species, both the volume and surface area of the GA in CA1 hippocampal neurons are larger than in neocortical neurons, which is in line with previous studies in the cerebral cortex of Syrian hamsters (Anton-Fernandez et al., 2015). The present study also shows that the GA in mouse neocortical neurons is sensitive to aging and delay time prior to fixation—a sensitivity which is even more marked in the case of hippocampal neurons. These factors should therefore be taken in consideration when analyzing the differences in the size of the GA between human control neurons and those from AD patients (see below) or when comparing animal models of AD with patients, as the brain from animal models is commonly fixed by perfusion with no postmortem period.

In human control cases we also found that the GA of <10% of the neocortical neurons analyzed displayed a *fragmented* or *highly altered* appearance with a concomitant reduction in volume and surface area of the MG160-ir elements with respect to neurons with a *non-fragmented* GA. We consider that these alterations of the GA could be a consequence of the postmortem delay time before fixation. In the case of CA1 hippocampal neurons, the percentage of neurons with an altered GA was almost 25%—markedly higher than in the neocortical neurons. This observation could be related to the deeper position of CA1 compared to the more superficial location of the neocortex and the consequent longer period prior to fixation of the hippocampus by immersion or it may be that the hippocampal neurons are more sensitive to postmortem factors than the neocortex.

Our results also show that, in both temporal neocortex and hippocampus, the percentage of neurons with a *fragmented* GA was higher in brain samples from AD patients than in human control tissue. This is in general agreement with previous studies showing GA fragmentation in neurons from AD patients, which suggested an important role of GA fragmentation in the neuropathology and pathogenesis of AD (Baloyannis, 2014; Salehi et al., 1995; Stieber et al., 1996). GA fragmentation in our material was associated with important reductions in the volume and surface area of the MG160-expressing elements of the GA. Considering that (1) there was a significant difference in age between the control group and the AD patients used both in previous reports (Stieber et al., 1995) and in the present study (control, mean ± SD: 50.6 ± 9.8 years; AD, mean ± SD 83.1 ± 4.6 years) and (2) a decrease in volume and surface area of MG160-ir GA elements was observed in aged mice in CA1 in the present work, we cannot rule out the possibility that the decreases observed in AD patients—especially those in the CA1 region—could be in part due to aging of AD patients and not a consequence of the disease itself. However, this is unlikely since fragmentation of the neuronal GA from AD patients was also reported in a study using groups of control subjects and AD patients with no differences in age (Salehi et al., 1995). Postmortem time prior to fixation also affect the morphological features of the GA (present results). However, in the present study, there were no differences in this parameter between the control and AD cases and they is therefore not considered to be a factor contributing to the observed differences in GA volume and surface area.

4.1. GA fragmentation and immunostaining for AT8

The present work also showed that GA fragmentation and significant reductions in the volume and surface area of the MG160-expressing elements of the GA were more pronounced in neurons with a progressive accumulation of phospho-tau (that is, pretangle and tangle states, as revealed by AT8 antibodies that detect phosphorylations in Ser202/Thr205) than in AT8-negative neurons. This observation supports the idea that the aggregation of hyperphosphorylated tau may exert a specific deleterious effect on the morphological features of the GA. This is in partial disagreement with pioneering studies in AD patients reporting that the alterations (including fragmentation and decreases in size) of the GA of hippocampal neurons are unrelated to the content of intracellular NFT in the CA1 hippocampal field (Salehi et al., 1995) and preferentially associated with neurons devoid of NTF in the subiculum and entorhinal cortex (Stieber et al., 1996). Methodological differences might contribute to the discrepancies between the present work and these two studies as they were carried out in paraffin-embedded brain tissue blocks from AD patients with heterogeneous postmortem periods and fixed in formaldehyde for over 1 month. Furthermore, the size of the GA was estimated in 2D in 5-6 μm-thick sections, and therefore the cell body of the pyramidal cells examined was likely incomplete as the diameter of the soma of the majority of pyramidal cells is larger than 5 μm, whereas we made full 3D reconstructions using confocal microscopy. In addition, the identification of the GA with conventional light microscopy relied on its immunocytochemical staining using light opaque chromogens as well as the subsequent (Salehi et al., 1995) or simultaneous (Stieber et al., 1996) staining of intracellular NFTs using, respectively, the silver Bodian technique or histochemical methods with a different colored chromogen. The fixation procedures used in these studies might have affected the preservation of the GA and the sectioning and staining methods used may have interfered with the measurement of the size of the GA or the assessment of the level of tau hyperphosphorylation.

In the present study, the 3D segmentation of the GA elements was based on the observed threshold selection of fluorescent labeling. The threshold selection was adjusted slightly for each case, although the quality of immunostaining was similar in all cases. In addition, the threshold that was set for each confocal stack of images equally affected

Fig. 5. Distribution of MG160 in the GA of AT8− and AT8+ human CA1 pyramidal neurons A, D; B, E; C, F; Pairs of confocal stack projection images taken from sections from the hippocampal CA1 region double-immunostained for MG160/AT8 showing the distribution of MG160 in the GA of AT8−, and AT8+ (type I and type II) pyramidal neurons. Scale bar in F indicates 20 μm in A–D and C–F, and 19 μm in B–E. Histograms showing, on the left side, higher surface area (G) and volume (H) values (mean ± SE) of MG160-ir GA elements, in control (white bars, n = 189) compared with AD (patterned bars, n = 713) CA1 pyramidal neurons. Note on the right side that for AD neurons (taking all cases together) both surface area and volume values were reduced in AT8+ (especially in type II) neurons, compared to AT8− neurons. Note that in I and J there was a tendency for this reduction in all AD patients analyzed, with statistically significant differences between the different cell types of each patient in four out of the seven cases analyzed.

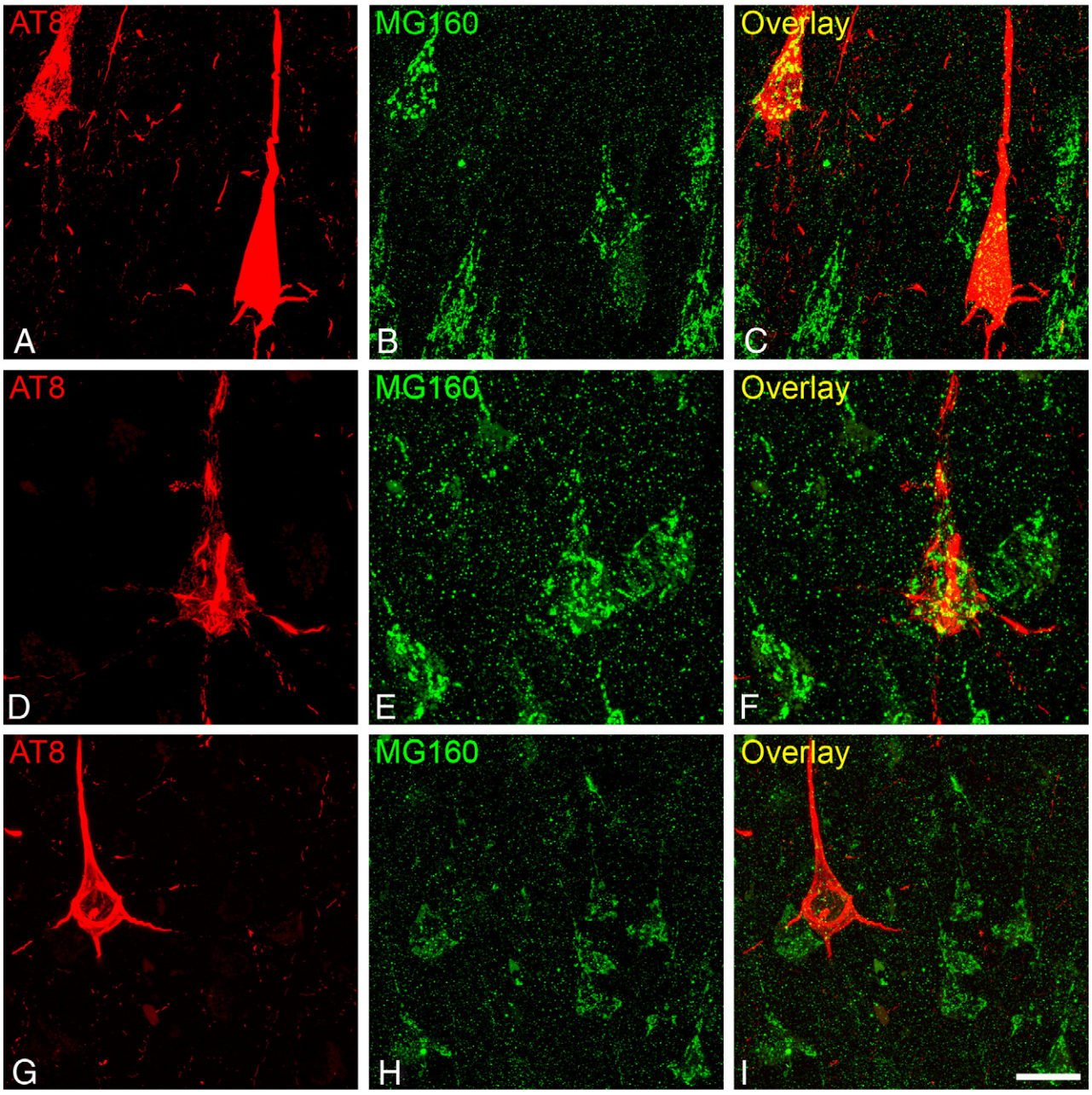
AT8
MG160
Overlay
A
B
C
D
E
F
G
H
I

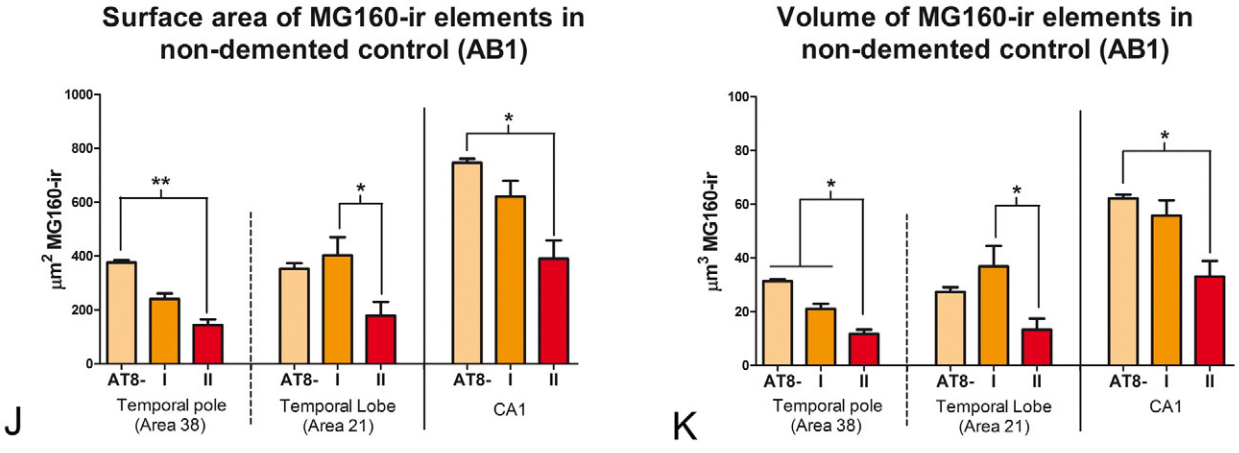
Surface area of MG160-ir elements in non-demented control (AB1)
µm2 MG160-ir
1000
800
600
400
200
0
**
*
*
AT8-
I
II
Temporal pole (Area 38)
Temporal Lobe (Area 21)
CA1
J
Volume of MG160-ir elements in non-demented control (AB1)
µm3 MG160-ir
100
80
60
40
20
0
*
*
*
K

the AT8 − and AT8 + neurons contained in each microscopic field. Since labeling intensities influence the perceived size, the present methodology might induce some bias in the measurement of absolute values of GA surface area and volume. However, the main observation of the present study—showing a progressive reduction of the GA size associated with the increase in the accumulation of phospho-tau (from pretangle to neurofibrillary tangle-bearing neurons)—was consistently observed in all cases (see Fig. 5).

This suggests that the presence of phospho-tau aggregates might exert a progressive damage on the GA of human neurons. This is supported by the fact that GA alterations in AD patients were more pronounced in pyramidal neurons from CA1 than from the temporal neocortex (present work) and according to Braak and Braak studies (Braak and Braak, 1995) during the stereotypical spatiotemporal progression of AD, NFTs appear at earlier stages and progresses earlier in CA1 than in neocortex. In addition, the specific structural alterations in the GA observed in AT8 + NFT-bearing neocortical and hippocampal neurons from the brain of a non-demented patient who had not been diagnosed with AD and in the absence of β-amyloid plaques (present work) also support the idea that the presence of NFT is by itself enough to induce alterations on the structure of the GA. Interestingly, the relationship between tau hyperphosphorylation and GA alterations is in agreement with different lines of evidence and has also been established in previous studies using animal models of AD (Liazoghli et al., 2005). For example, the transitory GA fragmentation that mitotic dividing cells undergo is concomitant to an increase in tau phosphorylation, as revealed by antibodies that also recognize neurofibrillary tangles in AD such as AT8 (Delobel et al., 2002; Illenberger et al., 1998; Pope et al., 1994; Preuss et al., 1995; Preuss and Mandelkow, 1998; Vincent et al., 1996). In addition, the reversible alterations in volume and surface area of MG160-ir elements of the GA during the torpor phase of hibernation has also been related to the phospho-tau content, revealed with AT8 antibodies (Anton-Fernandez et al., 2015).

4.2. Temporal relationship between GA fragmentation and tau hyperphosphorylation

Regarding the temporal relationship between GA fragmentation and tau hyperphosphorylation, it is known that, among other factors, the integrity of the microtubule cytoskeleton determines the position and morphological properties of the GA (Burkhardt, 1998; Cole et al., 1996). It was suggested that tau binds Golgi membranes and microtubules (Farah et al., 2006). Therefore, morphological features of the GA might be potentially altered by the microtubule alterations induced by tau hyperphosphorylation. It has been proposed that in AD, tau pathology is an upstream event that precedes GA fragmentation since tau overexpression led to the fragmentation of the neuronal GA (Liazoghli et al., 2005; Lin et al., 2003). Nevertheless, tau hyperphosphorylation has been reported in HEK293/tau cells—after treatments with the microtubule-depolymerizing agent, nocodazole or the Golgi-disturbing agent, brefeldin A—which would indicate that fragmentation of GA is an upstream event required to trigger tau hyperphosphorylation (Jiang et al., 2014; Sutterlin et al., 2002).

Therefore, further studies should be carried out to unravel the time-relation of tau-phosphorylation and GA alterations, due to its crucial relevance for understanding pathology progression in AD.

4.3. Alterations in the GA AT8 − neurons

The present results have revealed alterations in the GA of AT8 − neurons. This is in line with the reported GA fragmentation in neurons without NFT, identified using silver staining techniques (Baloyannis, 2014; Salehi et al., 1995) or immunostaining for bFGF (Stieber et al., 1996). It is possible that some AT8 − neurons with a fragmented or altered GA might have tau that is hyperphosphorylated at residues other than Ser202/Thr205 (which are recognized by AT8 antibodies). Whether or not the degree of accumulation of phospho-tau that is hyperphosphorylated at different sites is correlated with the extent of GA alterations should be explored in further studies using PHF1 or AT180 antibodies which recognize tau that is hyperphosphorylated at other sites (Goedert et al., 1994).

However, other factors such as the presence of β-amyloid plaques could be responsible for the GA fragmentation reported here in pyramidal neurons that were not immunoreactive for AT8. Indeed, trafficking and maturation of APP, its processing enzymes and Aβ production have been shown to be dependent on the integrity of the GA (Burgos et al., 2010; Choy et al., 2012; Greenfield et al., 1999; Huse et al., 2002; Joshi et al., 2015; Joshi and Wang, 2015). In addition, in the APPswe/PS1ΔE9 animal model of AD, it has been reported that the accumulation Aβ peptide in neurons might induce GA fragmentation, thereby accelerating the traffic of APP and the production of Aβ (Joshi et al., 2015; Joshi and Wang, 2015).

It has also been reported that approximately 50% of AD patients may also develop TDP-43 pathology in certain brain regions (see Wilson et al., 2011). This pathology has been found to correlate with GA fragmentation in spinal cord neurons in patients with Amyotrophic lateral sclerosis (Fujita and Okamoto, 2005). Therefore, although TDP-43 pathology might potentially contribute to GA alterations in neurons from AD patients, this was not the case in the four out of seven patients used in this study for which information regarding TDP43 inclusions was available.

Regardless of additional possible factors that might induce GA alterations, the present study revealed that, in neocortical and hippocampal neurons from AD patients, the changes in the microtubule network related to tau hyperphosphorylation was associated with the fragmentation and reduction in volume and surface area of the GA.

Since the level of cell activity has been directly related to the size of the GA (Lucassen et al., 1993; Salehi et al., 1995), the alterations of the GA observed in the present study would likely result in a deregulation of neuronal calcium levels (Li et al., 2013) and alterations in protein synthesis, modification, and sorting (Salehi et al., 1995; Wang et al., 2008; Xiang et al., 2013). This suggests that the defects in the GA are likely to contribute to the neurotoxicity associated with AD.

Acknowledgements

The authors declare no conflict of interest. This work was supported by grants from the following entities: SAF 2015-66603-P from the Ministerio de Economía y Competitividad; Centro de Investigación en Red sobre Enfermedades Neurodegenerativas (CIBERNED, CB06/05/0066, Spain); and a grant from the Alzheimer's Association (ZEN-15-321663).

Fig. 6. Distribution of MG160 in the GA of AT8 − and AT8 + human CA1 and neocortical pyramidal neurons in a non-demented control case Pairs of confocal stack projection images taken from CA1 (A–C) and areas 21 (D–F) and 38 (G–I) of the temporal neocortex from sections double-immunostained for MG160/AT8 showing the distribution of MG160 in the GA of AT8 −, and AT8 + (type I and type II) pyramidal neurons from a human in a non-demented control case. Scale bar in I indicates 24 μm in A–C, 14 μm in D–F and 22,65 in G–I. Histograms show surface area (J) and volume (K) values (mean ± SE) of MG160-ir GA elements, in AT8 − neurons (area 38 n = 397; area 21 n = 133; CA1 n = 185) and AT8 + neurons (patterns I and II; area 38, n = 49; area 21, n = 12; CA1, n = 47). Note that both surface area and volume values were significantly reduced in type II AT8 + neurons, compared to AT8 − neurons (Friedman test, *p ≤ 0.01; **p ≤ 0.001).

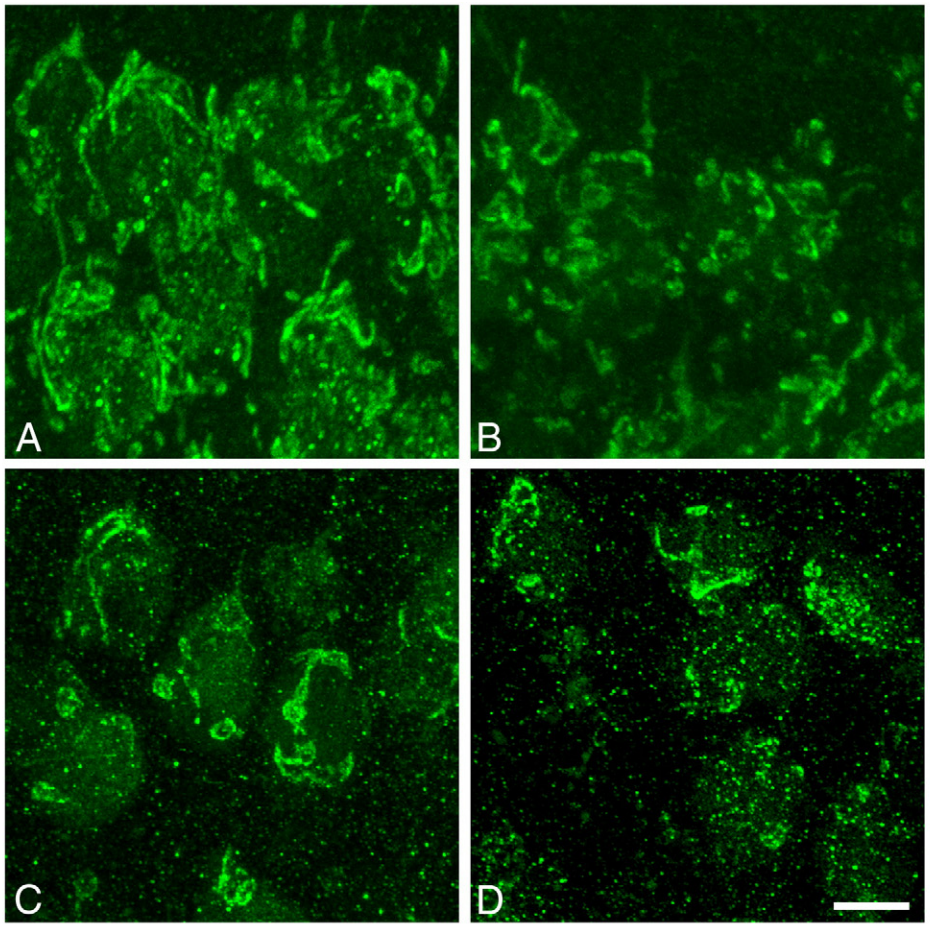
A
B
C
D

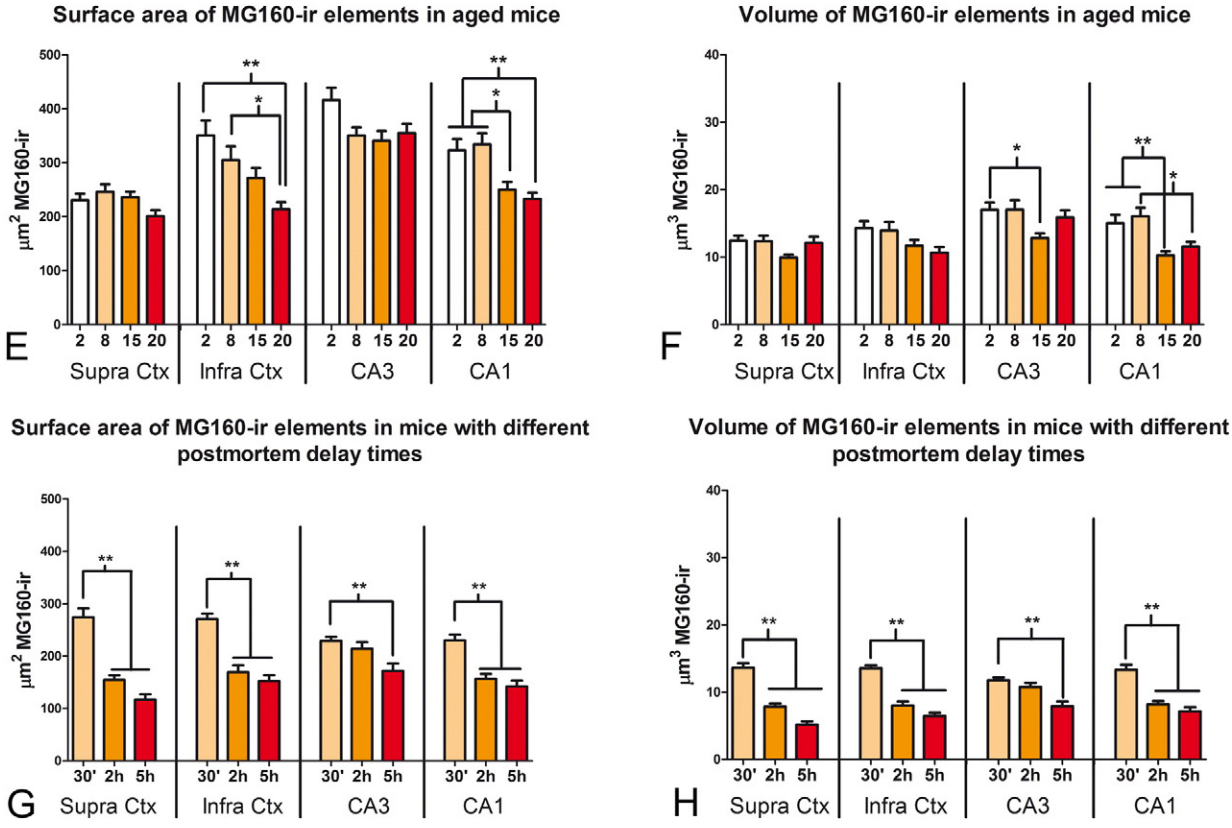
Surface area of MG160-ir elements in aged mice
µm² MG160-ir
E
Supra Ctx
Infra Ctx
CA3
CA1
Volume of MG160-ir elements in aged mice
µm³ MG160-ir
F
Surface area of MG160-ir elements in mice with different postmortem delay times
G
Volume of MG160-ir elements in mice with different postmortem delay times
H
30' 2h 5h
2 8 15 20

This project received funding from the European Union's Horizon 2020 research and innovation programme under grant agreement No. 720270 (Human Brain Project).

References

Anton-Fernandez, A., et al., 2015. Changes in the Golgi apparatus of neocortical and hippocampal neurons in the hibernating hamster. Front. Neuroanat. 9, 157.

Baloyannis, S.J., 2014. Golgi apparatus and protein trafficking in Alzheimer's disease. J. Alzheimers Dis. 42 (Suppl. 3), S153–S162.

Blazquez-Llorca, L., et al., 2010. Pericellular innervation of neurons expressing abnormally hyperphosphorylated tau in the hippocampal formation of Alzheimer's disease patients. Front. Neuroanat. 4, 20.

Blazquez-Llorca, L., et al., 2011. Abnormal tau phosphorylation in the thorny excrescences of CA3 hippocampal neurons in patients with Alzheimer's disease. J. Alzheimers Dis. 26, 683–698.

Braak, H., Braak, E., 1995. Staging of Alzheimer's disease-related neurofibrillary changes. Neurobiol. Aging 16, 271–278 (discussion 278-84).

Burgos, P.V., et al., 2010. Sorting of the Alzheimer's disease amyloid precursor protein mediated by the AP-4 complex. Dev. Cell 18, 425–436.

Burkhardt, J.K., 1998. The role of microtubule-based motor proteins in maintaining the structure and function of the Golgi complex. Biochim. Biophys. Acta 1404, 113–126.

Burrus, L.W., et al., 1992. Identification of a cysteine-rich receptor for fibroblast growth factors. Mol. Cell. Biol. 12, 5600–5609.

Choy, R.W., et al., 2012. Amyloid precursor protein (APP) traffics from the cell surface via endosomes for amyloid beta (Abeta) production in the trans-Golgi network. Proc. Natl. Acad. Sci. U. S. A. 109, E2077–E2082.

Cole, N.B., et al., 1996. Golgi dispersal during microtubule disruption: regeneration of Golgi stacks at peripheral endoplasmic reticulum exit sites. Mol. Biol. Cell 7, 631–650.

Dal Canto, M.C., 1996. The Golgi apparatus and the pathogenesis of Alzheimer's disease. Am. J. Pathol. 148, 355–360.

Delobel, P., et al., 2002. Abnormal Tau phosphorylation of the Alzheimer-type also occurs during mitosis. J. Neurochem. 83, 412–420.

Egea, G., et al., 2006. Actin dynamics at the Golgi complex in mammalian cells. Curr. Opin. Cell Biol. 18, 168–178.

Ellisman, M.H., et al., 1987. Diagnostic levels of ultrasound may disrupt myelination. Exp. Neurol. 98, 78–92.

Fan, J., et al., 2008. Golgi apparatus and neurodegenerative diseases. Int. J. Dev. Neurosci. 26, 523–534.

Farah, C.A., et al., 2006. Tau interacts with Golgi membranes and mediates their association with microtubules. Cell Motil. Cytoskeleton 63, 710–724.

Fujita, Y., Okamoto, K., 2005. Golgi apparatus of the motor neurons in patients with amyotrophic lateral sclerosis and in mice models of amyotrophic lateral sclerosis. Neuropathology 25, 388–394.

Fujita, Y., et al., 2002. The Golgi apparatus is fragmented in spinal cord motor neurons of amyotrophic lateral sclerosis with basophilic inclusions. Acta Neuropathol. 103, 243–247.

Fujita, Y., et al., 2006. Fragmentation of Golgi apparatus of nigral neurons with alpha-synuclein-positive inclusions in patients with Parkinson's disease. Acta Neuropathol. 112, 261–265.

Glick, B.S., 2002. Can the Golgi form de novo? Nat. Rev. Mol. Cell Biol. 3, 615–619.

Goedert, M., et al., 1994. Epitope mapping of monoclonal antibodies to the paired helical filaments of Alzheimer's disease: identification of phosphorylation sites in tau protein. Biochem. J. 301 (Pt 3), 871–877.

Gonatas, N.K., et al., 1992. Fragmentation of the Golgi apparatus of motor neurons in amyotrophic lateral sclerosis. Am. J. Pathol. 140, 731–737.

Gonatas, J.O., et al., 1995. MG-160, a membrane sialoglycoprotein of the medial cisternae of the rat Golgi apparatus, binds basic fibroblast growth factor and exhibits a high level of sequence identity to a chicken fibroblast growth factor receptor. J. Cell Sci. 108 (Pt 2), 457–467.

Gonatas, J.O., et al., 1998a. Truncations of the C-terminal cytoplasmic domain of MG160, a medial Golgi sialoglycoprotein, result in its partial transport to the plasma membrane and filopodia. J. Cell Sci. 111 (Pt 2), 249–260.

Gonatas, N.K., et al., 1998b. The involvement of the Golgi apparatus in the pathogenesis of amyotrophic lateral sclerosis, Alzheimer's disease, and ricin intoxication. Histochem. Cell Biol. 109, 591–600.

Gonatas, N.K., et al., 2006. Fragmentation of the Golgi apparatus in neurodegenerative diseases and cell death. J. Neurol. Sci. 246, 21–30.

Greenfield, J.P., et al., 1999. Endoplasmic reticulum and trans-Golgi network generate distinct populations of Alzheimer beta-amyloid peptides. Proc. Natl. Acad. Sci. U. S. A. 96, 742–747.

Hu, Z., et al., 2007. The study of Golgi apparatus in Alzheimer's disease. Neurochem. Res. 32, 1265–1277.

Huse, J.T., et al., 2002. Beta-secretase processing in the trans-Golgi network preferentially generates truncated amyloid species that accumulate in Alzheimer's disease brain. J. Biol. Chem. 277, 16278–16284.

Illenberger, S., et al., 1998. The endogenous and cell cycle-dependent phosphorylation of tau protein in living cells: implications for Alzheimer's disease. Mol. Biol. Cell 9, 1495–1512.

Jiang, Q., et al., 2014. Golgin-84-associated Golgi fragmentation triggers tau hyperphosphorylation by activation of cyclin-dependent kinase-5 and extracellular signal-regulated kinase. Neurobiol. Aging 35, 1352–1363.

Joshi, G., Wang, Y., 2015. Golgi defects enhance APP amyloidogenic processing in Alzheimer's disease. BioEssays 37, 240–247.

Joshi, G., et al., 2015. Golgi fragmentation in Alzheimer's disease. Front. Neurosci. 9, 340.

Levine, T.P., et al., 1995. Mitotic disassembly and reassembly of the Golgi apparatus. Cold Spring Harb. Symp. Quant. Biol. 60, 549–557.

Li, L.H., et al., 2013. The Golgi apparatus: panel point of cytosolic Ca2 + regulation. Neurosignals 2013, 272–284.

Liazoghli, D., et al., 2005. Fragmentation of the Golgi apparatus induced by the overexpression of wild-type and mutant human tau forms in neurons. Am. J. Pathol. 166, 1499–1514.

Lin, W.L., et al., 2003. Ultrastructural neuronal pathology in transgenic mice expressing mutant (P301L) human tau. J. Neurocytol. 32, 1091–1105.

Lucassen, P.J., et al., 1993. Activation of the human supraoptic and paraventricular nucleus neurons with aging and in Alzheimer's disease as judged from increasing size of the Golgi apparatus. Brain Res. 632, 105–113.

Mirra, S.S., et al., 1991. The Consortium to Establish a Registry for Alzheimer's Disease (CERAD). Part II. Standardization of the neuropathologic assessment of Alzheimer's disease. Neurology 41, 479–486.

Mizuno, Y., et al., 2001. Familial Parkinson's disease. Alpha-synuclein and parkin. Adv. Neurol. 86, 13–21.

Pope, W.B., et al., 1994. Microtubule-associated protein tau is hyperphosphorylated during mitosis in the human neuroblastoma cell line SH-SY5Y. Exp. Neurol. 126, 185–194.

Preuss, U., Mandelkow, E.M., 1998. Mitotic phosphorylation of tau protein in neuronal cell lines resembles phosphorylation in Alzheimer's disease. Eur. J. Cell Biol. 76, 176–184.

Preuss, U., et al., 1995. Cell cycle-dependent phosphorylation and microtubule binding of tau protein stably transfected into Chinese hamster ovary cells. Mol. Biol. Cell 6, 1397–1410.

Rabouille, C., Haase, G., 2015. Editorial: Golgi pathology in neurodegenerative diseases. Front. Neurosci. 9, 489.

Sakurai, A., et al., 2000. Fragmentation of the Golgi apparatus of the ballooned neurons in patients with corticobasal degeneration and Creutzfeldt-Jakob disease. Acta Neuropathol. 100, 270–274.

Salehi, A., et al., 1995. Decreased activity of hippocampal neurons in Alzheimer's disease is not related to the presence of neurofibrillary tangles. J. Neuropathol. Exp. Neurol. 54, 704–709.

Stieber, A., et al., 1995. MG160, a membrane protein of the Golgi apparatus which is homologous to a fibroblast growth factor receptor and to a ligand for E-selectin, is found only in the Golgi apparatus and appears early in chicken embryo development. Exp. Cell Res. 219, 562–570.

Stieber, A., et al., 1996. In Alzheimer's disease the Golgi apparatus of a population of neurons without neurofibrillary tangles is fragmented and atrophic. Am. J. Pathol. 148, 415–426.

Sutterlin, C., et al., 2002. Fragmentation and dispersal of the pericentriolar Golgi complex is required for entry into mitosis in mammalian cells. Cell 109, 359–369.

Vincent, I., et al., 1996. Mitotic mechanisms in Alzheimer's disease? J. Cell Biol. 132, 413–425.

Wang, Y., et al., 2008. Golgi cisternal unstacking stimulates COPI vesicle budding and protein transport. PLoS One 3, e1647.

Wilson, A.C., et al., 2011. TDP-43 in aging and Alzheimer's disease - a review. Int. J. Clin. Exp. Pathol. 4, 147–155.

Xiang, Y., et al., 2013. Regulation of protein glycosylation and sorting by the Golgi matrix proteins GRASP55/65. Nat. Commun. 4, 1659.

Yamaguchi, F., et al., 2003. Identification of MG-160, a FGF binding medial Golgi sialoglycoprotein, in brain tumors: an index of malignancy in astrocytomas. Int. J. Oncol. 22, 1045–1049.

Zhou, Z., et al., 1997. Identification and characterization of a fibroblast growth factor (FGF) binding domain in the cysteine-rich FGF receptor. J. Biol. Chem. 272, 5167–5174.

Zuber, M.E., et al., 1997. Cysteine-rich FGF receptor regulates intracellular FGF-1 and FGF-2 levels. J. Cell. Physiol. 170, 217–227.

Fig. 7. Effects of aging and the postmortem delay period on the distribution of MG160 in the GA of pyramidal neurons A and B: confocal stack projection mages showing examples of MG160 immunostaining of the GA of CA1 pyramidal neurons from mice aged 2 (A) and 20 (B) months. C and D show the MG160 immunostaining of the GA of layer II neocortical pyramidal neurons from mice fixed after postmortem periods of 30 min (C) or 5 h (D). Scale bar in D indicates 5,3 μm. Histograms show the reductions in surface area (E and G) and volume (F and H) values (mean ± SE) of MG160-ir GA elements, in pyramidal neurons from different areas in mice with different ages (E and F) or mice fixed after different postmortem times G and H). (Kruskal Wallis test, *p ≤ 0.01; **p ≤ 0.001).

Journal of Alzheimer's Disease 60 (2017) 651–661
DOI 10.3233/JAD-170332
IOS Press

Phospho-Tau Accumulation and Structural Alterations of the Golgi Apparatus of Cortical Pyramidal Neurons in the P301S Tauopathy Mouse Model

Alejandro Antón-Fernández[a,b], Jesús Merchán-Rubira[c], Jesús Avila[c,d], Félix Hernández[c,d], Javier DeFelipe[a,b,d] and Alberto Muñoz[a,b,d,e,*]
[a]*Instituto Cajal, CSIC, Madrid, Spain*
[b]*Laboratorio Cajal de Circuitos Corticales (CTB), Universidad Politécnica de Madrid, Madrid, Spain*
[c]*Centro de Biología Molecular Severo Ochoa (CSIC-UAM), Madrid, Spain*
[d]*CIBERNED, Centro de Investigación Biomédica en Red de Enfermedades Neurodegenerativas, Spain*
[e]*Department of Cell Biology, Complutense University, Madrid, Spain*

Accepted 17 July 2017

Abstract. The Golgi apparatus (GA) is a highly dynamic organelle involved in the processing and sorting of cellular proteins. In Alzheimer's disease (AD), it has been shown to decrease in size and become fragmented in neocortical and hippocampal neuronal subpopulations. This fragmentation and decrease in size of the GA in AD has been related to the accumulation of hyperphosphorylated tau. However, the involvement of other pathological factors associated with the course of the disease, such as the extracellular accumulation of amyloid-β (Aβ) aggregates, cannot be ruled out, since both pathologies are present in AD patients. Here we use the P301S tauopathy mouse model to examine possible alterations of the GA in neurons that overexpress human tau (P301S mutated gene) in neocortical and hippocampal neurons, using double immunofluorescence techniques and confocal microscopy. Quantitative analysis revealed that neurofibrillary tangle (NFT)-bearing neurons had important morphological alterations and reductions in the surface area and volume of the GA compared with NFT-free neurons. Since in this mouse model there are no Aβ aggregates typical of AD, the present findings support the idea that the progressive accumulation of phospho-tau is associated with structural alterations of the GA, and that these changes may occur in the absence of Aβ pathology.

Keywords: Golgi apparatus, hippocampus, neocortex, neurofibrillary tangles, tauopathies

INTRODUCTION

The Golgi apparatus (GA) plays a critical role in processing and targeting cellular proteins, and its alterations give rise to neuronal dysfunctions and a variety of human diseases [1, 2]. The GA adapts to different physiological and pathological conditions by plastic changes in shape and protein content [3–6]. In Alzheimer's disease (AD), the GA of certain populations of neurons becomes fragmented and there is experimental evidence for the link between GA fragmentation and the two main pathological hallmarks of the disease, namely the accumulation of amyloid-β (Aβ) peptides and the presence of neurofibrillary tangles (NFT) made of hyperphosphorylated microtubule-associated protein tau [7–16].

*Correspondence to: Alberto Muñoz, PhD, Laboratorio Cajal de Circuitos Corticales, Centro de Tecnología Biomédica, Universidad Politécnica, Madrid, Pozuelo de Alarcón, Madrid 28223, Spain. Tel.: +34 4524900/Ext. 1943; E-mail: amunozc@bio.ucm.es.

ISSN 1387-2877/17/$35.00

In pioneering studies in the cerebral cortex from AD patients, it was reported that the GA of certain neuronal populations of neurons becomes fragmented and decreases in size [17, 18]. However, there is some controversy regarding the possible link between fragmentation of the GA in cortical neurons and the intracellular content of NFT. The first studies on the possible alterations of GA in the cerebral cortex from AD patients were controversial. For example, Salehi et al. [17] reported that there was fragmentation and a decrease in size of the GA and that these alterations were unrelated to the intracellular content of NFT, whereas Stieber et al. [18] reported that these alterations were preferentially associated with neurons devoid of NTF. However, recent studies in the neocortex and hippocampus of AD patients using different experimental approaches to those employed by Stieber et al. [18] and Salehi et al. [17] have shown that the progressive accumulation of hyperphosphorylated tau is associated with the reduction and the morphometric alterations of GA [19]. Nevertheless, there are factors that might affect the structural characteristics of the GA, such as the age of the patients, tissue fixation procedure, and postmortem period prior to fixation [19]. In addition to NFTs, AD patient tissue is characterized by other pathologic hallmarks, namely, the accumulation of extracellular fibrillar Aβ in amyloid plaques and elevated levels of soluble Aβ oligomers in the brain. This Aβ pathology occurs to variable degrees in different patients and may also affect the structure of the GA. All of these considerations might help account for the different results reported by different laboratories. Here we have studied the possible relationship between alterations of the GA with NFT in neocortical and hippocampal neurons of the P301S tauopathy mouse model. This mouse model is characterized by the absence of Aβ plaques and carries a P301S human microtubule-associated protein tau (MAPT) gene mutation. This P301S (PS19) mouse overexpresses this gene at a level fivefold higher than the expression of the endogenous tau mouse protein, triggering —from 6 months of age onwards— the formation of NFT (similar to those observed in AD) in relatively few neurons, labeled with PHF1 as well as with Gallyas staining in both cortical and hippocampal regions [20]. In addition, between 3 and 6 months of age, P301 mice undergo a progressive accumulation of insoluble and highly phosphorylated tau species that can be detected by AT8 (phospho-Ser202 and phosho-Thr205), PHF1 (phospho-Ser396 and phospho-Ser404), and AT270 (phospho-Thr181) phosphorylation-dependent antibodies, like abnormal tau in purified AD paired helical filaments [20, 21].

The present results indicate that the overexpression of this mutated human tau gene does not seem to induce general alterations in the GA of pyramidal neurons from neocortex and hippocampus. However, the presence of hyperphosphorylated tau and NFT seems to be deleterious for the structural integrity of GA as alterations in morphology and important reductions in the size were found in the GA of NFT-bearing neurons.

MATERIALS AND METHODS

In the present study, we have used transgenic mice P301S for the human tau gene and wild-type control littermates. The P301S mouse model, obtained from Jackson laboratory (B6;C3-Tg(Prnp-MAPT*P301S)PS19Vle/J), carries a mutant (P301S) human MAPT gene encoding T34-tau isoform (1N4R) driven by the mouse prion-protein promoter (Prnp) on a B6C3H/F1 genetic background. A group was analyzed at the age of 2 weeks, and a second group was analyzed at 36 weeks when these animals show learning and motor deficits [20]. A total of 5 mice aged 2 weeks ($n = 2$ for WT, $n = 3$ for P301S) and 12 mice aged 36 weeks ($n = 5$ for WT, $n = 7$ for P301S) were analyzed. All mice were housed at the "Centro de Biología Molecular Severo Ochoa" animal facility. Mice were housed four per cage with food and water available *ad libitum* and maintained in a temperature-controlled environment on a 12/12 h light-dark cycle with light onset at 07 : 00 h. Animal housing and maintenance protocols followed the guidelines of Council of Europe Convention ETS123, recently revised as indicated in Directive 86/609/EEC. Animal experiments were performed under protocols (P15/P16/P18/P22) approved by the Institutional Animal Care and Utilization Committee (Comité de Ética de Experimentación Animal del CBM, CEEA-CBM, Madrid, Spain). Animals were sacrificed by a lethal intraperitoneal injection of sodium pentobarbital (200 mg/kg b.w.) and were then perfused intracardially with a saline solution followed by 4% paraformaldehyde in PB. The brain of each animal was removed and post-fixed by immersion in the same fixative for 24 h at 4°C. After rinsing in PB, brains were cut in the sagital plane using a vibratome (Leica VT2100S). Serial parasagital sections (50 μm thick) were cryoprotected in 30% sucrose solution in PB and stored

in ethyleneglicol/glycerol at –20°C until they were used.

For immunofluorescence experiments, free-floating serial sections were first rinsed in PB and then preincubated for 1 h in PB with 0.25% Triton-X100 and 3% normal serum of the species in which the secondary antibodies were raised (Vector Laboratories, Burlingame, CA, USA). The sections were then incubated for 48 h at 4°C in the same stock solution containing the following primary antibodies in the combinations indicated: rabbit anti-MG160 (Abcam, 1 : 100), rabbit anti-Grasp65 (Abcam, 1 : 500), mouse anti human tau (Abcam, T13, 1 : 5000), rabbit anti-NeuN (Millipore, 1 : 2000) and mouse anti-phospho-PHF-tau pSer202+ Thr205 antibody (AT8, 1 : 2000, Pierce Endogen). After rinsing in PB, the sections were first incubated for 2 h at room temperature in biotinylated goat anti-rabbit antibody (1 : 200) to amplify the GA immunoreactivity signal. Sections were then rinsed in PB and incubated for 2 h at room temperature in Alexa 594-conjugated goat anti-mouse and streptavidin-coupled Alexa 488 (1 : 1000; Molecular Probes, Eugene, OR, USA). Sections were also stained with a nuclear stain — DAPI (4,6-diamidino-2-phenylindole; Sigma, St. Louis, MO, USA). After rinsing in PB, the sections were mounted in antifade mounting medium (ProlongGold, Invitrogen) and studied by conventional fluorescence and confocal microscopy (Zeiss, 710). Confocal image stacks, from the somatosensory neocortex and CA1 hippocampal region of control and P301 S mice, were recorded at 0.35 μm intervals through separate channels with a 63x oil-immersion lens (NA, 1.40, refraction index, 1.45). ZEN 2012 software (Zeiss) was used to construct composite images from each optical series by combining the images recorded through the different channels, and the same software was used to obtain Z projection images (image resolution: 1024×1024 pixels; pixel size: 0.11 μm). Adobe Photoshop (CS4) software was used to compose figures. Fiji software (3D object counter tool) was used to analyze the volume and surface area of the elements immunostained for the different GA markers in image stacks. Based on methods used in previous studies (see [19] for a detailed description), we cropped 3D substacks from the original confocal stacks taken from AT8−MG160 or AT8−Grasp65 double-stained sections counterstained with DAPI, trying to limit the analysis to the complete GA corresponding to the somata of single neurons. In P301S animals, these cells included pyramidal neurons with (AT8+) or without (AT8 –) hyperphosphorylated tau, which were selected such that they were similar in size and from neighboring zones with similar Z depths within the stacks, in order to minimize possible sources of bias due to neuronal population heterogeneity or antibody penetration within the tissue. We measured the volume and surface area of GA elements and calculated the percentages of variation of these parameters between AT8+ and AT8− in P301 mice, and between AT8− neurons in P301 and wild-type animals. To determine differences between values obtained in wild-type and mutant P301 mice in the different age groups (2 and 36 weeks), Kruskal-Wallis one-way analysis of variance was performed followed by a Bonferroni-corrected Mann-Whitney U-test for pairwise comparisons, using SPSS software (version 22). The Wilcoxon pair test was used to compare mean values obtained in AT8+ and AT8− neurons from mutant P301 mice, whereas a Mann-Whitney U-test was used to check differences between AT8+ neurons from mutant mice and neurons from wild-type mice.

RESULTS

In the present work, we have studied the morphological features of the Golgi apparatus (GA) of pyramidal neurons from the somatosensory cortex and CA1 hippocampal region, in relation to the accumulation of hyperphosphorylated tau, in P301S transgenic and control animals aged 2 and 36 weeks. In line with previous descriptions of this mouse model [20], in the hippocampus and neocortex of 2-week-old P301S mice, we found no phospho-tau positive (AT8+) neurons despite the fact that all neurons in these regions overexpress MAPT P301S mutated tau gene, as revealed by immunostaining using anti-human tau (T13) antibodies (Fig. 1). We have studied sections counterstained with DAPI and immunostained with antibodies that recognize MG160, a sialoglycoprotein that is mainly localized in the medial cisternae of the GA, or GRASP65, a peripheral protein localized primarily in the cis-Golgi both in combination with AT8 antibodies recognizing phospho Ser202 and phospho Thr205 sites in microtubule-associated tau protein [22] (Figs. 2 and 3). In both wild-type and P301S animals at 2 weeks of age, the GA of hippocampal and neocortical pyramidal neurons (as revealed by Grasp65 and MG160 immunostaining) consisted of a network of twisted cisternae with a ribbon-like appearance distributed throughout the cell body and frequently

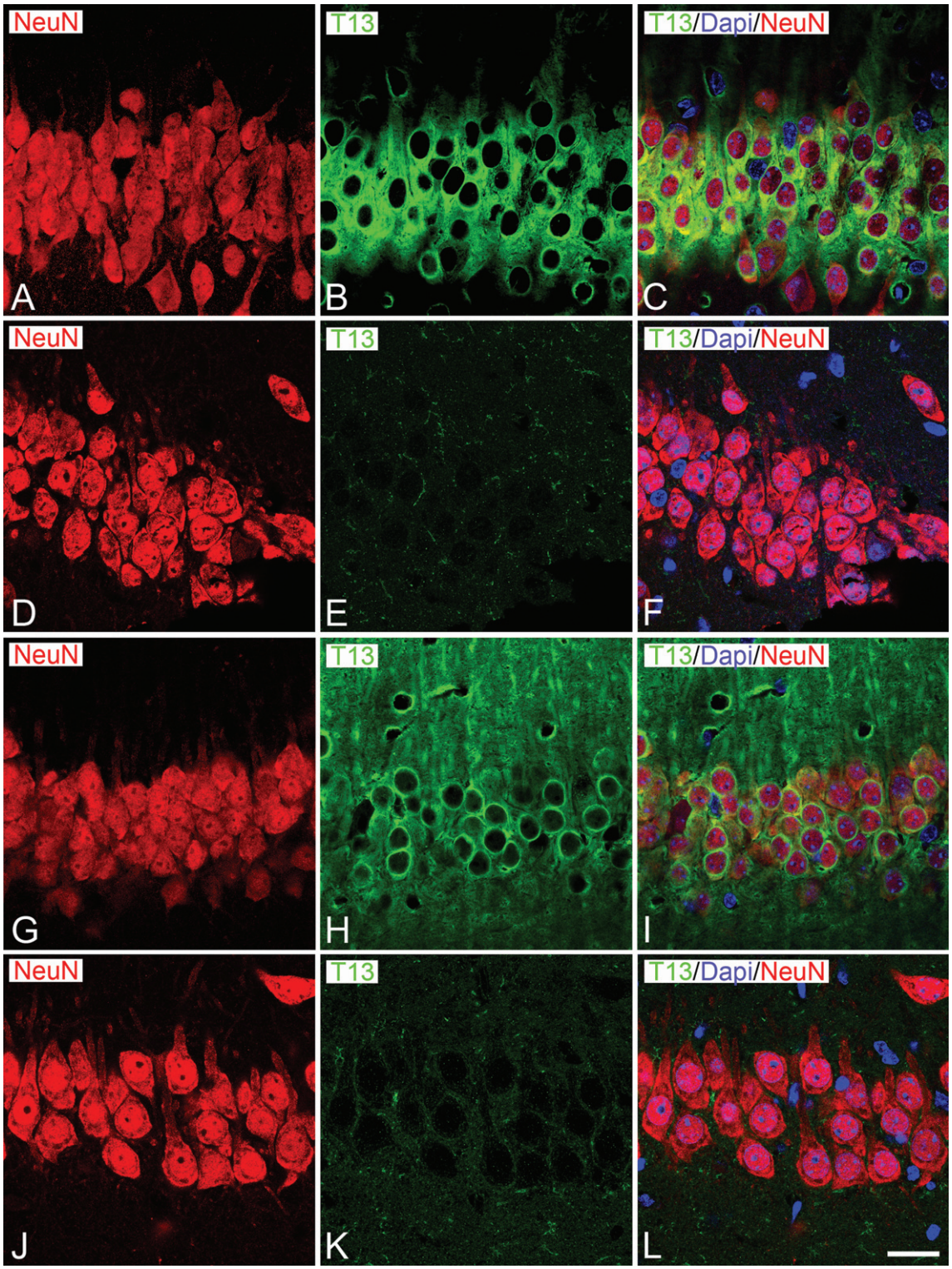

Fig. 1. Expression of human tau in hippocampal CA1 neurons from P301S and wild-type mice. Trios of confocal stack projection images taken from T13/NeuN double immunostained- and DAPI counterstained-sections from the CA of P301S (A-C, G-I) and wild-type (D-F, J-L) mice aged 2 (A-F) or 36 weeks (G-L). Images show at both ages the expression of human tau (T13 immunoreactivity, green) in CA1 neurons, as revealed by NeuN immuniostaining (red), in P301 mice in contrast to wild-type mice. Scale bar shown in L indicates 22 μm.

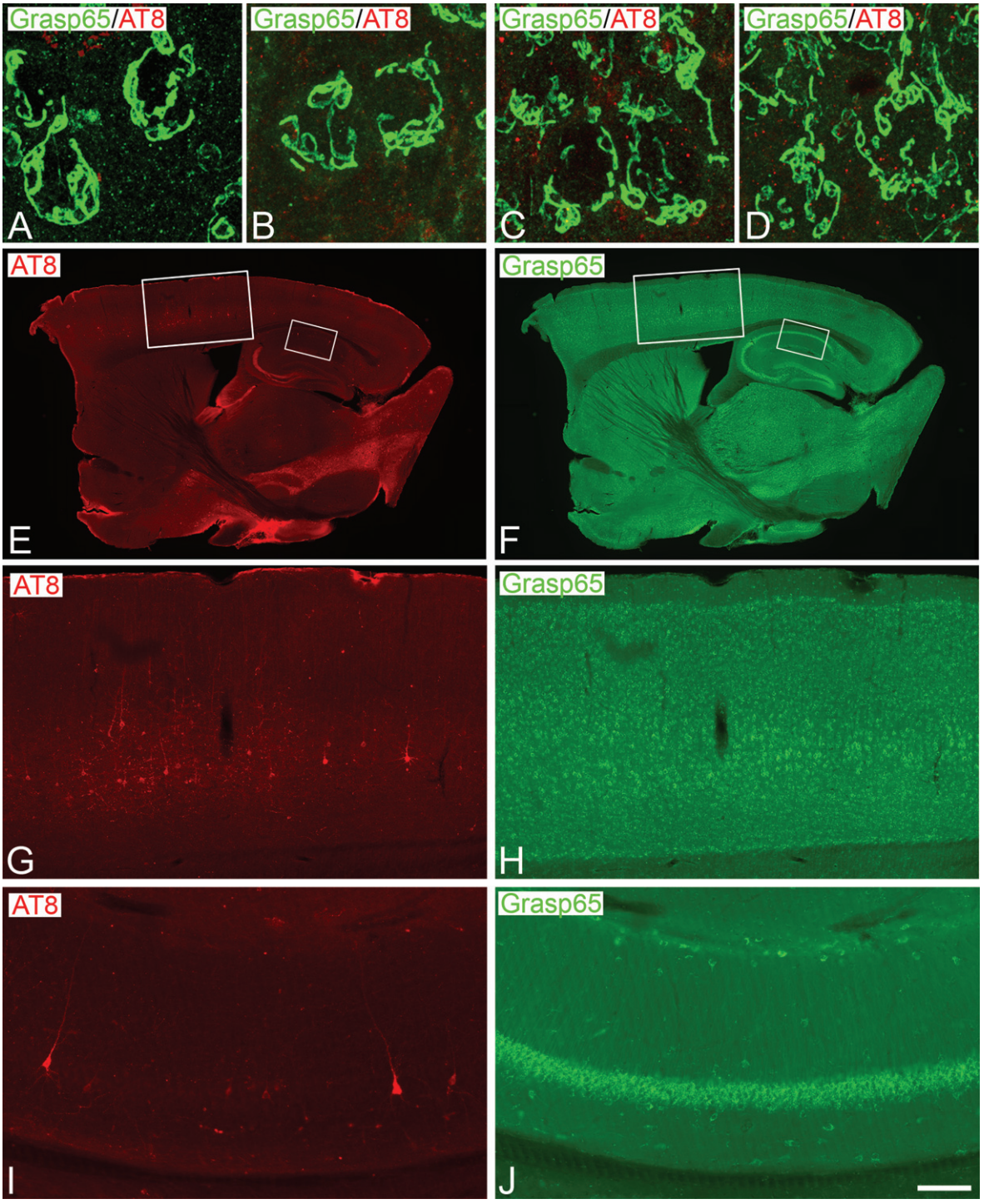

Fig. 2. Distribution of Grasp65 in the GA of neurons from P301S and wild-type mice. A–D) Confocal stack projection images taken from Grasp 65/AT8 double-immunostained sections from the hindlimb region of the somatosensory neocortex (A, B) and the CA1 hippocampal region (C, D) of wild-type (A, C) and P301 (B, D) animals aged 2 weeks. Note the absence of AT8+ neurons in both regions at this age and the similar appearance of the Grasp65-ir GA elements between wild-type and P301S animals. E−J show pairs of conventional fluorescence images taken from a Grasp 65/AT8 double-immunostained parasagital section from the brain of 36-week-old P301 mice showing the distribution of AT8+ neurons in the somatosensory cortex (G, H) and the CA1 hippocampal region (I, J). Squared zones in E and F are shown at higher magnification in G−J. Scale bar shown in J indicates 7 μm in A−D, 1035 μm in E−F, 210 μm in G−H and 100 μm in I−J.

extending partially to the apical dendrite (Fig. 2A–D). This observation was in line with previous descriptions in other mammalian species, including humans [6, 19]. Using confocal microscopy and 3D quantitative techniques, we found no differences between wild-type and P301S animals at 2 weeks of age in terms of the surface area and volume of GA elements of neocortical and CA1 hippocampal neurons (as revealed both by Grasp65 and MG160 immunostaining) (Fig. 4). In line with previous reports [20], in 36-week-old P301S animals, we found a subpopulation of phospho-tau accumulating, AT8+ neurons throughout the neocortex and hippocampal formation. AT8+ neurons were found in CA hippocampal fields; dentate gyrus and subiculum; insular cortex; primary and secondary motor cortex; primary and secondary visual cortex; retrosplenial granular cortex; and different areas of somatosensory cortex (barrel field, hindlimb, shoulder, trunk, and upper lip regions). We focused on the CA1 hippocampal region and the hindlimb region of the somatosensory cortex in which AT8+ neurons in 36-week-old P301S mice were found to be more abundant (Fig. 2E, G, I). Most of the AT8+ neurons in these regions showed either a pre-tangle pattern or an intermediate pattern (pattern IIa according to [23]) of NFTs, whereas the presence of AT8+ neurons with an advanced (IIb) pattern of NFT was scarce.

No apparent general changes in the overall distribution of MG160 or Grasp65 (Fig. 2F, H, J) immunostaining was found between wild-type and P301S 36-week-old mice. However, the analysis of confocal image stacks at higher magnification revealed that some hippocampal and neocortical neurons displayed an altered morphology of the GA elements, as revealed by both markers, consisting of an apparent retraction and a loss of tubular structures of the GA that often showed a lobular appearance and was polarized to an extreme of the cell body (Fig. 3). We also found that the percent of neurons with an altered GA morphology was much higher in neurons with intracellular hyperphosphorylated tau aggregates (AT8+) than in adjacent AT8− neurons (Fig. 3K) (MG160 : 73.2% of AT8+ neurons versus 19.1% of AT8− neurons; Grasp 65 : 69.5% of AT8+ neurons versus 22.1% of AT8− neurons).

To quantify the possible retraction of the GA and to study whether this retraction might be related to the intracellular content of hyperphosphorylated tau aggregates, we selected —in confocal stacks from CA1 and neocortex— AT8+ and adjacent AT8− pyramidal neurons located at the same z position range within the stacks. In stacks taken from 36-week-old animals, we measured the volume and surface area of Grasp65-ir or MG160-ir GA elements and compared between the mean values in AT8+ and AT8− neurons, as well as comparing them with values obtained from age-matched wild-type animals (AT8−).

In the two regions analyzed, no significant differences were found between wild-type neurons and AT8− neurons from P301S mice in terms of the surface area and volume of the GA elements, as revealed by both markers (Fig. 4). However, in both regions, pyramidal neurons with intracellular hyperphosphorylated tau aggregates (AT8+) showed a reduction in the surface area and volume of the GA elements as compared with AT8− neurons from P301S or wild-type animals (Fig. 4). However, this reduction did not reach statistical significance in the case of the GA surface area of CA1 neurons immunostained with Grasp65 (Fig. 4G, H) probably due to the relatively low number of AT8+ NFT-bearing neurons found in this tissue (Fig. 2 I, J). Finally, we calculated the mean percentage of GA decrease in AT8+ neurons as compared with AT8− neurons in 36-week-old P301S mice, taking together data from the CA1 and neocortical stacks. The mean percentage reduction in surface area and volume of GA elements was higher when analyzed with MG160 immunostaining (26.4% and 28.3%, respectively) than when estimated using Grasp65 immunostaining (14.8% and 13.2%, respectively).

DISCUSSION

The main results of the present study demonstrate that although the accumulation of tau protein of human origin in P301S mouse model is not sufficient to induce structural alterations of the GA, the hyperphosphorylation of this mutated tau and its aggregation forming NFT-like structures induce profound alterations in the GA structure as evaluated by MG160 and Grasp65 GA markers.

We have shown that at 2 weeks of age, tau was not hyperphosphorylated, as revealed by AT8 antibodies that detect phosphorylations in Ser202/Thr205. At this age, when P301S mice already overexpress MAPT P301S mutated tau gene, as revealed by T13 immunostaining (see Fig. 1) and according to previous studies [20], we found no differences between P301S mutant and wild-type animals in the general morphology of the GA of neocortical and hippocampal neurons, or in the surface area and volume of

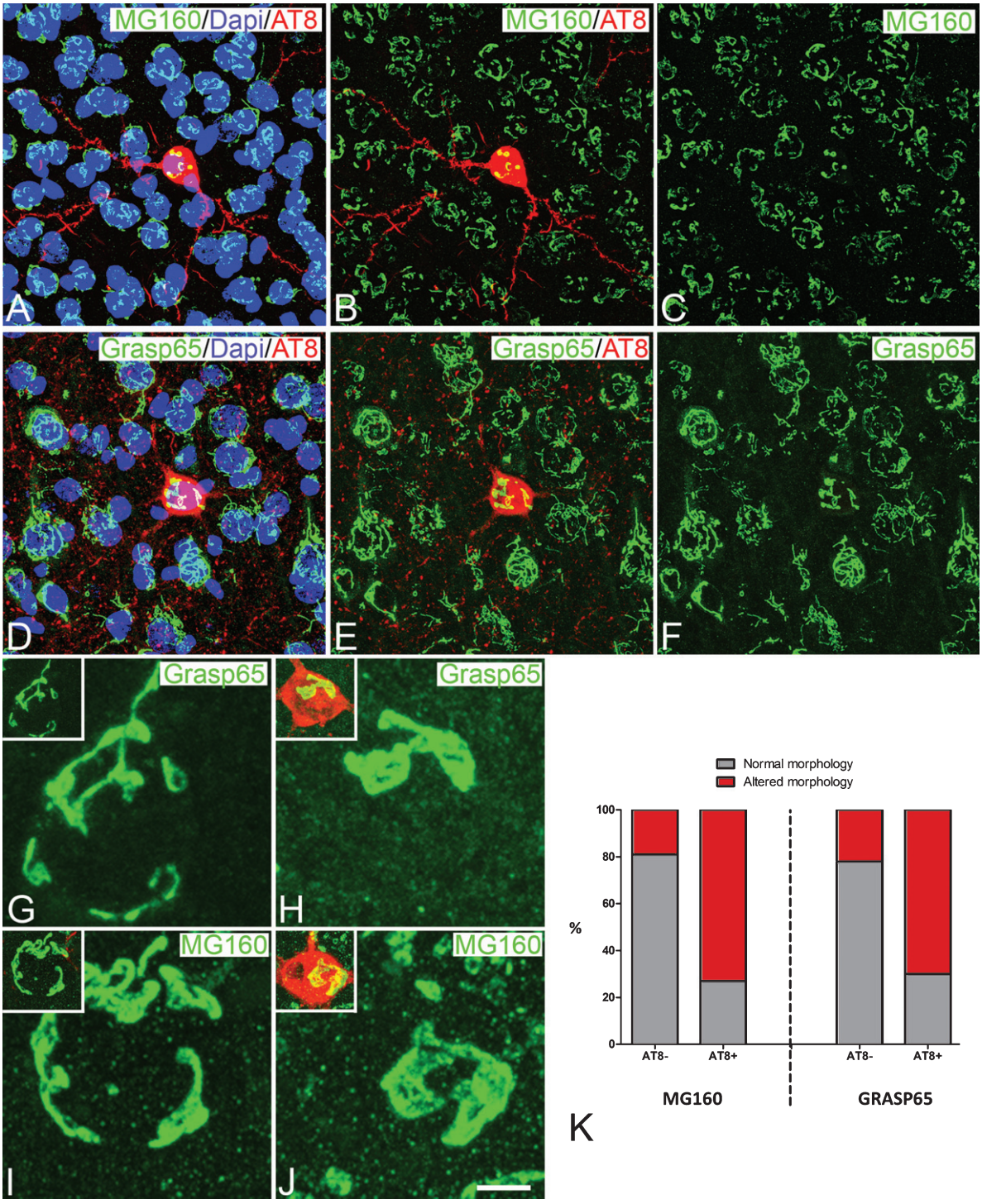

Fig. 3. A–C, D–E) Trios of confocal stack projection images taken from MG160/AT8 or Grasp 65/AT8 double immunostained- and DAPI counterstained-sections from the hindlimb somatosensory cortex of P301S mice aged 36 weeks. Images show the distribution of MG160-ir (A–C) and Grasp65-ir (D–F) GA elements of AT8– and AT8+ neurons. G–J) Higher-magnification confocal projection images showing the alterations of the GA in AT8+ neurons (H, J) as compared with AT8− neurons (G, I) with each of the GA markers used. Insets show inmunofluorescence for AT8 in red. Scale bar in J indicates 21 μm in A–F and 3.6 μm in G–J. K) Bar histograms showing the percentages of AT8− and AT8+ neurons with an altered Golgi apparatus as identified by MG160 or Grasp65 immunostaining ($n = 1099$).

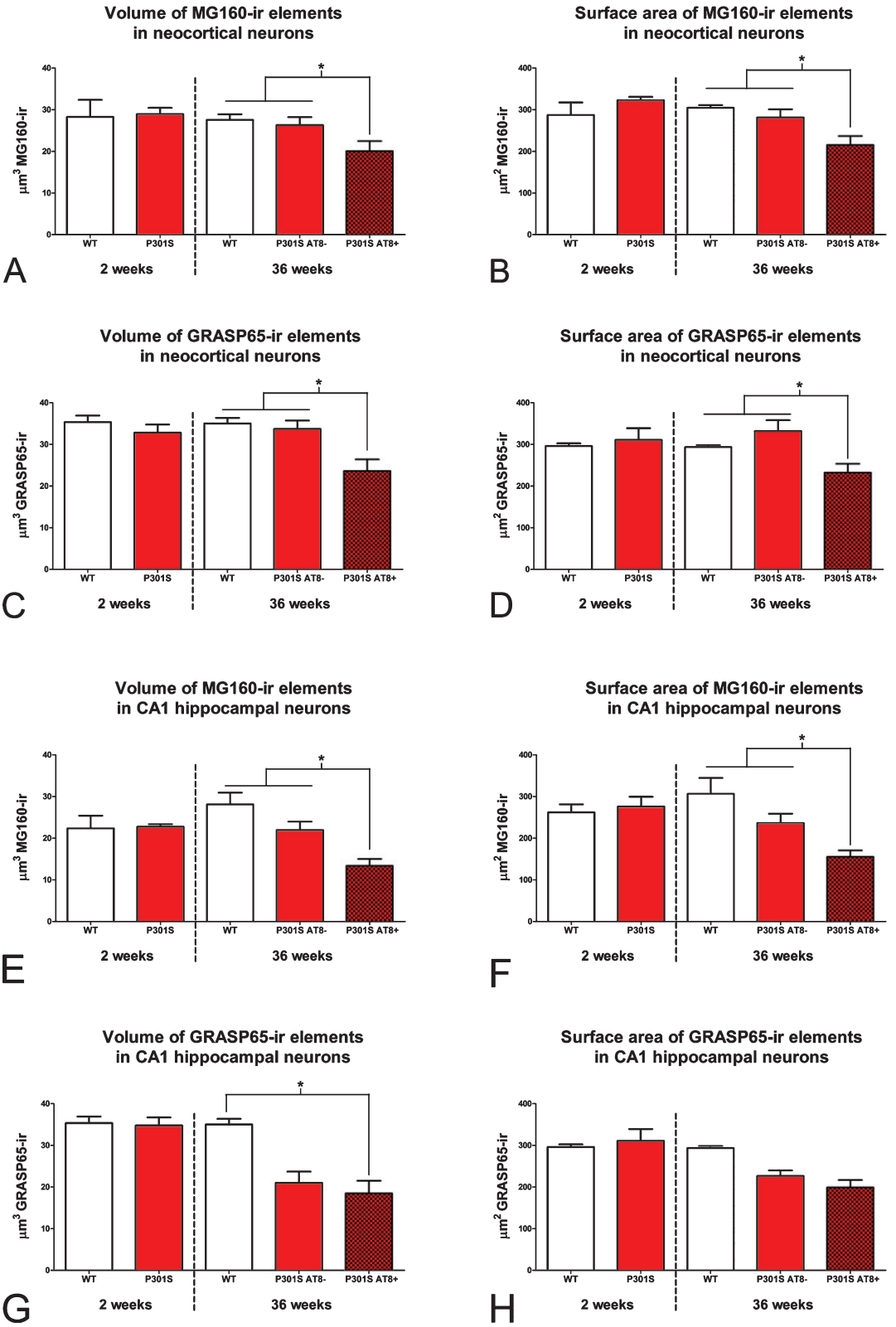
Volume of MG160-ir elements in neocortical neurons
µm3 MG160-ir
Surface area of MG160-ir elements in neocortical neurons
µm2 MG160-ir
Volume of GRASP65-ir elements in neocortical neurons
µm3 GRASP65-ir
Surface area of GRASP65-ir elements in neocortical neurons
µm2 GRASP65-ir
Volume of MG160-ir elements in CA1 hippocampal neurons
µm3 MG160-ir
Surface area of MG160-ir elements in CA1 hippocampal neurons
µm2 MG160-ir
Volume of GRASP65-ir elements in CA1 hippocampal neurons
µm3 GRASP65-ir
Surface area of GRASP65-ir elements in CA1 hippocampal neurons
µm2 GRASP65-ir
WT
P301S
WT
P301S AT8-
P301S AT8+
2 weeks
36 weeks
A
B
C
D
E
F
G
H

GA as evaluated with quantitative techniques. Similarly, we found no differences in the same parameters between wild-type neurons and AT8− neurons from P301 36-week-old mice, that is, an age when neurons would hypothetically accumulate more mutated tau. Therefore, we can conclude that in this model the overexpression of P301S mutated tau alone is not enough to induce GA alterations in cortical neurons. Although it is possible that tau in P301S animals at these ages might be hyperphosphorylated at residues other than Ser202/Thr205, our results demonstrate that these putative tau hyperphosphorylations (which are not detectable by the AT8 antibodies used in the present study) would not be sufficient to induce morphological alterations of neuronal GA.

Previous *in vitro* studies showed on one hand that the overexpression of either wild-type human Tau4R or its mutant forms like P301L in transfected rat cultured hippocampal neurons, induced GA fragmentation [16], and on the other hand, that this overexpression leads to tau hyperphosphorylation [24, 25]. However, the direct relationship between tau hyperphosphorylation and GA alteration in cortical neurons was not addressed. In the present study, we found that the accumulation of phospho-tau in P301S is associated with structural alterations of the GA since the percent of neurons with an altered morphology of the GA was much higher in AT8+ neurons than in adjacent AT8− neurons. In the hyperphosphorylated tau aggregate-bearing neurons, these alterations included a change from the typical ribbon-like appearance with multiple tubular structures to a lobulated appearance and a change from a homogeneous to a polarized distribution in the body. However, it should be noted that, in our material, we did not find evidence for GA fragmentation in AT8+ neurons, which contrasts with the fragmentation reported in CP-13+ spinal cord motor neurons (in which tau phosphorylated at serine 202 is labeled), in a study using 10–12-month-old JNPL3 mutant mice, which overexpress P301L mutated tau gene [16]. Several factors might have contributed the differences between the two studies regarding the fragmentation of the GA, namely differences in 1) the age of the animals studied [19]; 2) the type of tau mutation and the consequent type of hyperphosphorylation and aggregation; 3) the antibodies used to detect phospho-tau; and 4) the neuronal population studied. The present observations also contrast with the fragmentation of the GA described in AT8+ cortical pyramidal cells from AD patients [19], indicating that GA alterations in P301 mouse only partially reproduce those occurring during the development of the disease.

In previous studies from our laboratory using the same methodology as that used in the present work, we showed important reductions in the surface area and volume of the GA elements in AT8+ neurons in neocortical and hippocampal neurons from AD patients [19]. We suggested that the progressive accumulation of phospho-tau was associated with structural alterations of the GA. However, we could not rule out the possible involvement of different factors present in AD patients which could be deleterious for the GA integrity, such as amyloid oligomers [13–15, 26] which are bi-directionally related to tau pathology [27–29], aging, and post-mortem delay period before tissue processing [19], as well as other unknown factors associated with the progression of the disease. The present results obtained from a tauopathy mouse model —in which the unique pathologic factor is the presence of human mutant tau and the development of NFT-like hyperphosphorylated tau aggregates, similar to those seen in human tissue [20]— further support the idea that the accumulation of phospho-tau is associated with structural alterations of the GA [19]. Although both processes seem to appear concomitantly, the causal relationship between them has not yet been resolved and warrants further research [8, 13, 16, 30].

The size of the GA has been correlated with cell activity levels, and the integrity of the GA is required for the proper control of the processing, sorting and transport of many important proteins that are essential for neuronal physiology [14, 15, 17, 31–34], including amyloid- β protein precursor and its processing enzymes [7, 9, 11, 12, 14]. Therefore, the retraction of the GA in cortical neurons is likely to induce functional impairment in the normal activity of those

Fig. 4. Histograms showing volume (A, C, E, and G) and surface area (B, D, F, and H) values (mean ± SE) of MG160-ir (A, B, E, and F) and Grasp65-ir (C, D, G, and H) GA elements, in neurons from the neocortex (top) and hippocampus (bottom) of wild-type (white bars) and P301 transgenic (red bars) mice. Note that at 2 weeks of age (left side of each histogram), the surface area and volume of GA of neocortical and hippocampal neurons are similar in wild-type and P301S animals. In contrast, at 36 weeks of age (right side of each histogram), note the reduction of surface area and volume values in P301S AT8+ neurons (dark red) as compared to AT8– neurons (light red) both from P301S and wild-type mice (Kruskal Wallis and Wilcoxon tests, $^{*}p \leq 0.05$). AT8– neurons (somatosensory cortex, $n = 298$ for Grasp65 and $n = 269$ for MG160; CA1, $n = 76$ for Grasp65 and $n = 188$ for MG160) and AT8+ neurons (somatosensory cortex, $n = 82$ for Grasp65 and $n = 85$ for MG160; CA1, $n = 26$ for Grasp65 and $n = 75$ for MG160).

neurons affected by the hyperphosphorylated tau, and such functional impairment is likely to participate in the pathophysiology of AD.

ACKNOWLEDGMENTS

This work was supported by grants from the following entities: SAF 2015-66603-P and BFU-2016-77885-P from the Ministerio de Economía y Competitividad; Centro de Investigación en Red sobre Enfermedades Neurodegenerativas (CIBERNED, CB06/05/0066, Spain); and a grant from the Alzheimer's Association (ZEN-15-321663). J. M-R was supported by a predoctoral fellowship from La Caixa foundation. This project received funding from the European Union's Horizon 2020 research and innovation program under grant agreement No. 720270.

Authors' disclosures available online (http://j-alz.com/manuscript-disclosures/17-0332r1).

REFERENCES

[1] Gonatas NK, Stieber A, Gonatas JO (2006) Fragmentation of the Golgi apparatus in neurodegenerative diseases and cell death. *J Neurol Sci* **246**, 21-30.

[2] Hu Z, Zeng L, Huang Z, Zhang J, Li T (2007) The study of Golgi apparatus in Alzheimer's disease. *Neurochem Res* **32**, 1265-1277.

[3] Levine TP, Misteli T, Rabouille C, Warren G (1995) Mitotic disassembly and reassembly of the Golgi apparatus. *Cold Spring Harb Symp Quant Biol* **60**, 549-557.

[4] Glick BS (2002) Can the Golgi form de novo? *Nat Rev Mol Cell Biol* **3**, 615-619.

[5] Fan J, Hu Z, Zeng L, Lu W, Tang X, Zhang J, Li T (2008) Golgi apparatus and neurodegenerative diseases. *Int J Dev Neurosci* **26**, 523-534.

[6] Anton-Fernandez A, Leon-Espinosa G, DeFelipe J, Munoz A (2015) Changes in the Golgi apparatus of neocortical and hippocampal neurons in the hibernating hamster. *Front Neuroanat* **9**, 157.

[7] Greenfield JP, Tsai J, Gouras GK, Hai B, Thinakaran G, Checler F, Sisodia SS, Greengard P, Xu H (1999) Endoplasmic reticulum and trans-Golgi network generate distinct populations of Alzheimer beta-amyloid peptides. *Proc Natl Acad Sci U S A* **96**, 742-747.

[8] Sutterlin C, Hsu P, Mallabiabarrena A, Malhotra V (2002) Fragmentation and dispersal of the pericentriolar Golgi complex is required for entry into mitosis in mammalian cells. *Cell* **109**, 359-369.

[9] Huse JT, Liu K, Pijak DS, Carlin D, Lee VM, Doms RW (2002) Beta-secretase processing in the trans-Golgi network preferentially generates truncated amyloid species that accumulate in Alzheimer's disease brain. *J Biol Chem* **277**, 16278-16284.

[10] Farah CA, Perreault S, Liazoghli D, Desjardins M, Anton A, Lauzon M, Paiement J, Leclerc N (2006) Tau interacts with Golgi membranes and mediates their association with microtubules. *Cell Motil Cytoskeleton* **63**, 710-724.

[11] Burgos PV, Mardones GA, Rojas AL, daSilva LL, Prabhu Y, Hurley JH, Bonifacino JS (2010) Sorting of the Alzheimer's disease amyloid precursor protein mediated by the AP-4 complex. *Dev Cell* **18**, 425-436.

[12] Choy RW, Cheng Z, Schekman R (2012) Amyloid precursor protein (APP) traffics from the cell surface via endosomes for amyloid beta (Abeta) production in the trans-Golgi network. *Proc Natl Acad Sci U S A* **109**, E2077-2082.

[13] Jiang Q, Wang L, Guan Y, Xu H, Niu Y, Han L, Wei YP, Lin L, Chu J, Wang Q, Yang Y, Pei L, Wang JZ, Tian Q (2014) Golgin-84-associated Golgi fragmentation triggers tau hyperphosphorylation by activation of cyclin-dependent kinase-5 and extracellular signal-regulated kinase. *Neurobiol Aging* **35**, 1352-1363.

[14] Joshi G, Bekier ME 2nd, Wang Y (2015) Golgi fragmentation in Alzheimer's disease. *Front Neurosci* **9**, 340.

[15] Joshi G, Wang Y (2015) Golgi defects enhance APP amyloidogenic processing in Alzheimer's disease. *Bioessays* **37**, 240-247.

[16] Liazoghli D, Perreault S, Micheva KD, Desjardins M, Leclerc N (2005) Fragmentation of the Golgi apparatus induced by the overexpression of wild-type and mutant human tau forms in neurons. *Am J Pathol* **166**, 1499-1514.

[17] Salehi A, Ravid R, Gonatas NK, Swaab DF (1995) Decreased activity of hippocampal neurons in Alzheimer's disease is not related to the presence of neurofibrillary tangles. *J Neuropathol Exp Neurol* **54**, 704-709.

[18] Stieber A, Mourelatos Z, Gonatas NK (1996) In Alzheimer's disease the Golgi apparatus of a population of neurons without neurofibrillary tangles is fragmented and atrophic. *Am J Pathol* **148**, 415-426.

[19] Anton-Fernandez A, Aparicio-Torres G, Tapia S, DeFelipe J, Munoz A (2017) Morphometric alterations of Golgi apparatus in Alzheimer's disease are related to tau hyperphosphorylation. *Neurobiol Dis* **97**, 11-23.

[20] Yoshiyama Y, Higuchi M, Zhang B, Huang SM, Iwata N, Saido TC, Maeda J, Suhara T, Trojanowski JQ, Lee VM (2007) Synapse loss and microglial activation precede tangles in a P301S tauopathy mouse model. *Neuron* **53**, 337-351.

[21] Fernandez-Nogales M, Santos-Galindo M, Merchan-Rubira J, Hoozemans JJM, Rabano A, Ferrer I, Avila J, Hernandez F, Lucas JJ (2017) Tau-positive nuclear indentations in P301S tauopathy mice. *Brain Pathol* **27**, 314-322.

[22] Goedert M, Jakes R, Vanmechelen E (1995) Monoclonal antibody AT8 recognises tau protein phosphorylated at both serine 202 and threonine 205. *Neurosci Lett* **189**, 167-169.

[23] Merino-Serrais P, Benavides-Piccione R, Blazquez-Llorca L, Kastanauskaite A, Rabano A, Avila J, DeFelipe J (2013) The influence of phospho-tau on dendritic spines of cortical pyramidal neurons in patients with Alzheimer's disease. *Brain* **136**, 1913-1928.

[24] Bertrand J, Plouffe V, Senechal P, Leclerc N (2010) The pattern of human tau phosphorylation is the result of priming and feedback events in primary hippocampal neurons. *Neuroscience* **168**, 323-334.

[25] Bertrand J, Senechal P, Zummo-Soucy M, Plouffe V, Leclerc N (2010) The formation of tau pathological phosphoepitopes in the axon is prevented by the dephosphorylation of selective sites in primary hippocampal neurons overexpressing human tau. *J Neurochem* **114**, 1353-1367.

[26] Joshi G, Chi Y, Huang Z, Wang Y (2014) Abeta-induced Golgi fragmentation in Alzheimer's disease enhances Abeta production. *Proc Natl Acad Sci U S A* **111**, E1230-1239.

[27] Oddo S, Billings L, Kesslak JP, Cribbs DH, LaFerla FM (2004) Abeta immunotherapy leads to clearance of early, but not late, hyperphosphorylated tau aggregates via the proteasome. *Neuron* **43**, 321-332.

[28] Dai B, Li D, Xi W, Luo F, Zhang X, Zou M, Cao M, Hu J, Wang W, Wei G, Zhang Y, Liu C (2015) Tunable assembly of amyloid-forming peptides into nanosheets as a retrovirus carrier. *Proc Natl Acad Sci U S A* **112**, 2996-3001.

[29] Dai CL, Tung YC, Liu F, Gong CX, Iqbal K (2017) Tau passive immunization inhibits not only tau but also Abeta pathology. *Alzheimers Res Ther* **9**, 1.

[30] Lin WL, Lewis J, Yen SH, Hutton M, Dickson DW (2003) Ultrastructural neuronal pathology in transgenic mice expressing mutant (P301L) human tau. *J Neurocytol* **32**, 1091-1105.

[31] Lucassen PJ, Ravid R, Gonatas NK, Swaab DF (1993) Activation of the human supraoptic and paraventricular nucleus neurons with aging and in Alzheimer's disease as judged from increasing size of the Golgi apparatus. *Brain Res* **632**, 105-113.

[32] Dries DR, Yu G (2008) Assembly, maturation, and trafficking of the gamma-secretase complex in Alzheimer's disease. *Curr Alzheimer Res* **5**, 132-146.

[33] Wang Y, Wei JH, Bisel B, Tang D, Seemann J (2008) Golgi cisternal unstacking stimulates COPI vesicle budding and protein transport. *PLoS One* **3**, e1647.

[34] Xiang Y, Zhang X, Nix DB, Katoh T, Aoki K, Tiemeyer M, Wang Y (2013) Regulation of protein glycosylation and sorting by the Golgi matrix proteins GRASP55/65. *Nat Commun* **4**, 1659.

frontiers in Neuroanatomy

ORIGINAL RESEARCH
published: 15 December 2015
doi: 10.3389/fnana.2015.00157

Changes in the Golgi Apparatus of Neocortical and Hippocampal Neurons in the Hibernating Hamster

Alejandro Antón-Fernández[1,2†], *Gonzalo León-Espinosa*[1,2,3†], *Javier DeFelipe*[1,2,4] *and Alberto Muñoz*[1,2,5*]

[1] Departamento de Neurobiología Funcional y de Sistemas, Instituto Cajal, CSIC, Madrid, Spain, [2] Laboratorio Cajal de Circuitos Corticales, Centro de Tecnología Biomédica, Universidad Politécnica de Madrid, Madrid, Spain, [3] Facultad de Farmacia, Universidad San Pablo CEU, Madrid, Spain, [4] Centro de Investigación Biomédica en Red de Enfermedades Neurodegenerativas, Madrid, Spain, [5] Departamento de Biología Celular, Facultad de Biología, Universidad Complutense, Madrid, Spain

Hibernating animals have been used as models to study several aspects of the plastic changes that occur in the metabolism and physiology of neurons. These models are also of interest in the study of Alzheimer's disease because the microtubule-associated protein tau is hyperphosphorylated during the hibernation state known as torpor, similar to the pretangle stage of Alzheimer's disease. Hibernating animals undergo torpor periods with drops in body temperature and metabolic rate, and a virtual cessation of neural activity. These processes are accompanied by morphological and neurochemical changes in neurons, which reverse a few hours after coming out of the torpor state. Since tau has been implicated in the structural regulation of the neuronal Golgi apparatus (GA) we have used Western Blot and immunocytochemistry to analyze whether the GA is modified in cortical neurons of the Syrian hamster at different hibernation stages. The results show that, during the hibernation cycle, the GA undergo important structural changes along with differential modifications in expression levels and distribution patterns of Golgi structural proteins. These changes were accompanied by significant transitory reductions in the volume and surface area of the GA elements during torpor and arousal stages as compared with euthermic animals.

Keywords: hibernation, GM130, Golgin84, MG160, pyramidal neuron

OPEN ACCESS

Edited by:
Agustín González, Universidad Complutense de Madrid, Spain

Reviewed by:
Giorgio Innocenti, Karolinska Institutet, Sweden
Stavros J. Baloyannis, Aristotelian University of Thessaloniki, Greece

***Correspondence:**
Alberto Muñoz
amunozc@bio.ucm.es

† *These authors have contributed equally to this work.*

Received: *15 September 2015*
Accepted: *16 November 2015*
Published: *15 December 2015*

Citation:
Antón-Fernández A, León-Espinosa G, DeFelipe J and Muñoz A (2015) Changes in the Golgi Apparatus of Neocortical and Hippocampal Neurons in the Hibernating Hamster. Front. Neuroanat. 9:157. doi: 10.3389/fnana.2015.00157

INTRODUCTION

The Golgi complex is a cellular organelle involved in the processing, modification, transport and targeting of cellular proteins. It is composed of stacks comprising closely apposed flattened cisternae and vesicles usually localized in the juxtanuclear area (Képès et al., 2005; Egea et al., 2006; Yadav and Linstedt, 2011) and held in position due to microtubule (MT)-dependent mechanisms. In mammalian cells, these stacks are laterally linked to form a membrane network, termed the Golgi ribbon, that allows an increase in the efficiency of glycosylation by creating enzymatic subcompartments in the order required for processing (Storrie et al., 1998; Storrie and Yang, 1998). Despite the degree of organization of the Golgi apparatus (GA), it has been shown that this organelle is highly dynamic and, under a variety of physiological processes, such as mitotic cell division (Levine et al., 1995), and pathological conditions, it can combine enormous rates of membrane flux with the ability to rapidly change its shape, redistribute different Golgi resident proteins (Glick, 2002) and even to disassemble and reassemble (Fan et al., 2008).

Hibernation is a physiological condition that allows hibernating mammalian species to survive in cold climates during times of reduced food availability. Hibernating animals have been used as models to study several aspects of plastic changes that occur in the metabolism and physiology of neurons in the normal brain under these conditions. In small mammals, hibernation is characterized by periods of reduced body temperature and metabolic rate, called torpor, that can last several days, interspersed with short arousal periods of activity and normothermia (Geiser, 2004, 2013; Geiser and Martin, 2013). Hibernation results in a decrease in metabolic rate (Zhou et al., 2001) and requires drastic physiological changes to maintain the energy savings (Geiser, 2004, 2013; Geiser and Martin, 2013). During torpor bouts, transcription and protein synthesis are severely depressed to keep energetically demanding cellular processes like transcription and translation to a minimum, with such processes recovering fully during the interbout arousal (Zhegunov, 1988; Rolfe and Brown, 1997; van Breukelen and Martin, 2001). With regard to the reduced protein synthesis, previous electron microscopy observations in taste bud cells (Popov et al., 1999) and in CA3 pyramidal neurons (Bocharova et al., 2011) revealed a transitory reduction in the number of polyribosomes and in rough endoplasmic reticulum profiles during torpor stages. Regarding the GA, a transitory fragmentation or disassembly along with a loss of flattened cisternae during torpor have been reported in studies using conventional electron microscopy (Popov et al., 1999; Bocharova et al., 2011). The structural maintenance of the Golgi ribbon has been shown to depend on protein complexes made by the 65kD Golgi reassembly stacking protein (GRASP65) and the 130 kD *cis*-Golgi matrix protein (GM130), both of which are mainly localized in the *cis*-Golgi compartment and are responsible for tethering lateral cisternae together, thereby promoting their fusion (Nakamura et al., 1995; Barr et al., 1997, 1998; Puthenveedu et al., 2006). The architecture of the GA has also been shown to depend on Golgin84, a rab protein present throughout the Golgi stacks with an increasing gradient toward the *trans*-side (Diao et al., 2003; Satoh et al., 2003; Sohda et al., 2010). Interference with Golgin84 expression has been shown to disrupt the Golgi ribbon and induce the appearance of Golgi fragments dispersed throughout the cell (Jiang et al., 2014). The distribution of these proteins in the neuronal GA of cortical neurons in hibernating animals is not known, and it is also not clear whether their expression and/or distribution change during the different phases of the hibernation cycle. In the present study we have used Western blot, immunocytochemistry and confocal microscopy to analyze the expression levels and distribution patterns of GM130 and Golgin84 in the Syrian hamster *Mesocricetus auratus* in torpor, arousal and euthermic states. Similarly we have analyzed the expression of MG160, a 160 kDa membrane sialoglycoprotein residing in the medial cisternae of the GA that is involved in the traffic, processing and probably in the regulation of endogenous or autocrine FGFs and that has been suggested to play important roles in the biogenesis and function of the GA (Gonatas et al., 1995, 1998a). The results indicate that the GA undergoes a profound and reversible morphological and neurochemical reorganization during the hibernation cycle that likely affects the ability to process and sort proteins.

In addition, mammalian hibernation has been proposed as a model to study certain physiological aspects of microtubule-associated protein tau phosphorylation *in vivo*. Indeed, this model may be useful to study the neuroprotection mechanisms in the first stages of neurodegenerative disorders such as Alzheimer's disease (AD), since neurons from hibernating animals show a transitory PHF (Paired Helical Filaments)-like tau phosphorylation with some similarities to that of patients at early stages of the disease (Zhou et al., 2001; Arendt et al., 2003; Avila et al., 2004; Härtig et al., 2005, 2007; Su et al., 2008; Stieler et al., 2011; León-Espinosa et al., 2013). Since tau has been localized in association with Golgi membranes, where it could serve as a link between these structures and microtubules (Farah et al., 2006), and the GA undergo widespread structural alterations in neurons of patients and animal models of AD (Gonatas et al., 1998b; Liazoghli et al., 2005; Hu et al., 2007), in the present study we analyze whether the alterations of the GA in cortical neurons of hibernating hamsters during torpor might be correlated with the accumulation of hyperphosphorylated tau.

MATERIALS AND METHODS

All experimental procedures were carried out at the animal facility of the San Pablo CEU University of Madrid (SVA-CEU.USP, registration number ES 28022 0000015) and were approved by the institutional Animal Experiment Ethics Committee. A total of 21 male 4-month-old Syrian hamsters (*Mesocricetus auratus*) were purchased from Janvier Labs. The animals had free access to food and water and were kept at 23°C with a 8:16 h light/dark cycle for a 4–6-week acclimatization period in our animal facility. Subsequently, in order to obtain arousal and torpor experimental groups, some animals were transferred to a special chamber that allowed the control of the temperature and photoperiod—two essential factors that affect hibernation. We designed this chamber (developed by Tiselius s.l.) with 6 individual cages to induce hibernation based on previous studies (Arendt et al., 2003). The chamber makes it possible to gradually reduce the temperature (LM35 sensors), control the illumination (adjustable LED RGB that controls intensity and color) and monitor the hamsters by measuring the general locomotor activity with a PIR (passive infrared) sensor mounted on top of each cage. Furthermore, we recorded all data obtained in a notebook computer to distinguish between the torpor and arousal phases during the hibernation cycle using the software package Fastwinter1.9 (developed by Tiselius s.l.). Hibernating animals showed torpor phases with a period of inactivity of 24 h whereas non-hibernating euthermic animals did not. The status of the animals was confirmed by body temperature measurements (infra-red thermometer) since the body temperature of a hibernating hamster falls to almost 5°C, whereas it is about 33°C in euthermic animals. As hibernation initiation proceeds with non-regular torpor bouts, we considered animals to be torpid only when they had completed three full bouts of torpor before they were sacrificed. Arousal from torpor

was initiated by rising the temperature of animals artificially with a thermal blanket. Arousal animals were sacrificed 90 min later once they had been taken out of the hibernation cage. In this study, animals were compared at three stages: control or euthermic ($n = 7$), torpor ($n = 9$), and arousal ($n = 5$).

For immunocytochemical experiments, control animals and animals from different hibernation states (torpor and arousal) were sacrificed by a lethal intraperitoneal injection of sodium pentobarbital (40 mg/kg) and were then perfused intracardially with a saline solution (together with heparin) followed by 4% paraformaldehyde in 0.1 M phosphate buffer (PB, pH 7.4). The brain of each animal was removed and postfixed by immersion in the same fixative for 24 h at 4°C. Serial coronal sections (50-μm thick) were obtained with a Vibratome (St Louis, MO, USA).

Immunofluorescence

Sections were first rinsed in PB and preincubated for 1 h at room temperature in a stock solution containing 3% normal serum of the species in which the secondary antibodies were raised (Vector Laboratories, Burlingame, CA, USA) diluted in PB with Triton X-100 (0.25%). Thereafter, the sections were incubated for 48 h at 4°C in the same stock solution containing the following primary antibodies, either alone or in the combinations indicated: mouse anti-AT8 (Pierce Endogen, 1:2000), mouse anti-GM130 (BD, 1:50), rabbit anti-MG160 (Abcam, 1:100), and rabbit anti-Golgin84 (Santa Cruz, 1:500). After rinsing in PB, the sections were incubated for 2 h at room temperature in the appropriate combinations of Alexa 488- or Alexa 594-conjugated goat anti-mouse or goat anti-rabbit antibodies (1:2000; Molecular Probes, Eugene, OR, USA). Sections were also stained with the nuclear stain DAPI (4,6 diamino-2-fenilindol; Sigma, St. Louis, MO, EEUU). Finally, the sections were washed in PB, mounted in antifade mounting medium (ProlongGold, Invitrogen) and studied by confocal microscopy (Zeiss, 710). Z sections were recorded at 0.35 μm intervals through separate channels, and ZEN 2012 software (Zeiss) was then used to construct composite images from each optical series by combining the images recorded through the different channels (image resolution: 1024 × 1024 pixels; pixel size: 0.11 μm). Colocalization of different pairs of Golgi markers was studied in double-stained sections with the aid of ZEN-lite 2012 software (Zeiss) estimating the Manders coefficient in cropped confocal stacks including complete single neurons (15 neurons per region and animal). Fiji software (3D Object counter) was used to analyze the volume and surface area of the puncta immunostained for the different GA markers in image stacks.

To determine differences between values obtained in control, torpor, and arousal groups, Kruskal-Wallis one-way analysis of variance was performed followed by Bonferroni-corrected Mann-Whitney *U*-test for pairwise comparisons, using SPSS software (version 22). To study possible differences between different regions and Golgi markers in the control group, Friedman test was performed. Wilcoxon test was used to compare mean values obtained in AT8-positive and -negative neurons. Adobe Photoshop (CS4) software was used to compose figures.

DAB Immunostaining

Free-floating sections were pretreated with 1.66% H_2O_2 for 30 min to quench the endogenous peroxidase activity, and then for 1 h in PB with 0.25% Triton-X and 3% normal goat serum (Vector Laboratories). The sections were then incubated overnight at 4°C with the mouse anti-AT8 antibody (Pierce Endogen, 1:2000) and the following day they were rinsed and incubated for 1 h in biotinylated goat anti-mouse IgG (1:200; Vector Laboratories). Antibody binding was detected with a Vectastain ABC immunoperoxidase kit (Vector Laboratories) and visualized with the chromogen 3,3′ diaminobenzidine tetrahydrochloride (DAB; Sigma- Aldrich, St. Louis, MO). After staining, the sections were dehydrated, cleared with xylene, and coverslips were applied.

Western-blotting

Animals were sacrified by cervical dislocation followed by decapitation. Brains were extracted and protein samples were prepared from thick brain slices, extending from -1 to -4 with respect to Bregma (Morin and Wood, 2001). Tissue was homogenized with the aid of a potter and a syringe needle in a buffer containing 20 mM HEPES, pH 7.4; 100 mM NaCl; 50 mM NaF; 1% Triton X-100; 5 mM EDTA; 1 mM sodium orthovanadate; 5 mM Okadaic acid, 30 mM β-Glycerophosphate, 5 mM Sodium pyrophosphate tetrabasic and the complete protease inhibitor cocktail (Roche Diagnostics). Protein concentration was quantified by a Bradford assay and 30 μg of total protein were subjected to electrophoresis in 10% SDS-polyacrylamide gel and transferred to a nitrocellulose membrane (Schleinder & Schuell, Keene, NH). Membranes were incubated overnight at 4°C with the following primary antibodies: mouse anti-GM130 (BD, 1:500), rabbit anti-MG160 (Abcam, 1:250), rabbit anti-Golgin84 (SC, 1:500), or mouse anti beta-actin (Sigma, 1:5000). After washing, the membranes were incubated with the corresponding peroxidase conjugated secondary antibody (1:1000; Dako, Glostrup, Denmark) for 2 h at room temperature. The antibodies were visualized using ECL (Amersham, 1:1000; Dako, Glostrup, Denmark), densitometric analysis was carried out with Image J software and the differences between the mean values obtained in control, arousal, and torpor animal groups were compared by one way Kruskall Wallis (Dunn's *post-hoc* test) (GraphPad Prism, version 5).

RESULTS

Distribution of Golgi Proteins in Cortical Neurons of Euthermic Hamsters

To characterize possible alterations during the hibernation cycle in the Golgi apparatus (GA) of neocortical and hippocampal neurons of Syrian hamsters, we first performed experiments with immunocytochemical staining using antibodies directed against GM130, MG160, and Golgin84 to study their distribution in euthermic hamsters (**Figure 1**).

It has been previously established that GM130 is mainly localized in the *cis*-Golgi compartment, MG160 is localized

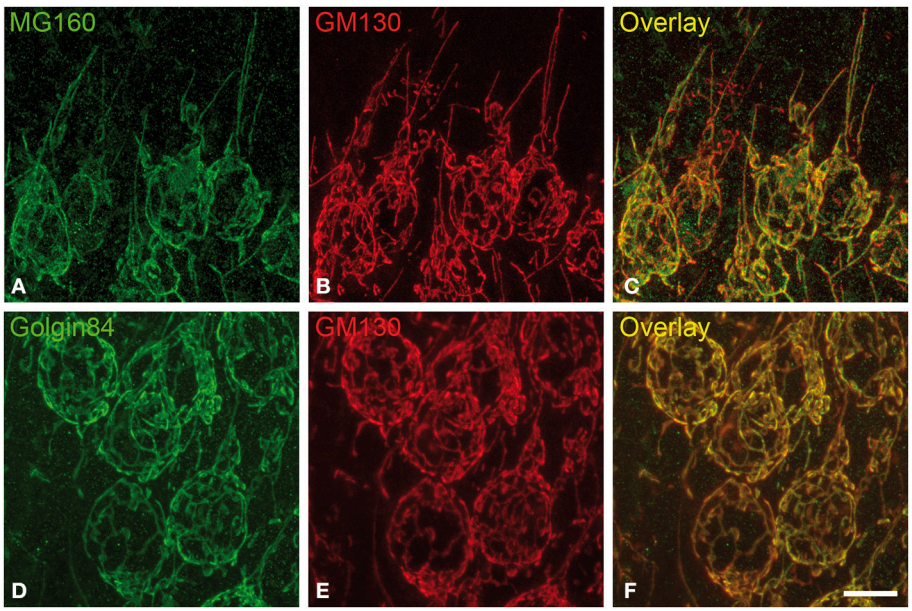

FIGURE 1 | Distribution of GA proteins in cortical neurons from euthermic hamsters. (A–F) Pairs of images taken from hippocampal sections double-immunostained for MG160/GM130 **(A–C)** and Golgin84/GM130 **(D–F)** showing their distribution in the GA of CA1 pyramidal neurons from euthermic hamsters. Note the similar distribution patterns and the high degree of colocalization. Scale bar in **(F)** indicates 9.5 μm.

in the medial cisternae and golgin-84 is present throughout the Golgi stacks with an increasing gradient toward the trans-side (see Introduction for references). In spite of this, the light microscopy observations in the present study revealed a similar morphological appearance of the GA in sections immunostained for each of the three GA markers (**Figure 1**). The GA in hippocampal neurons consisted of a network of twisted and convoluted cisternae and tubular structures with a ribbon-like appearance, and was distributed throughout the cell body around the nucleus and partially extended to the apical dendrite (**Figure 1**). In neocortical neurons, the GA, as revealed with the three markers, also showed a ribbon-like appearance although it had a less complex appearance, that is, it had a lower degree of cisternae extension and convolution than in the case of hippocampal neurons (Figures S1, S2).

Using the 3D object counter tool in the Fiji software package, we quantified the volume and the surface area of GA elements immunoreactive for the three markers in pyramidal neurons (identified by the pyramidal shape of the soma and presence of an apical dendrite) from supra- and infra-granular layers of the neocortex, and from CA1 and CA3 hippocampal regions. The results indicate that in all regions analyzed MG160 shows, in general, a more restricted distribution in the GA than Golgin84 and GM130 (**Figures 2A,B**). In addition, when values from the different neuronal populations were compared, the GA in hippocampal neurons, especially in CA3 neurons, stained with the three different markers, showed a significantly larger surface area and volume than in neocortical pyramidal neurons from supragranular and infragranular layers (**Figures 2C,D**).

To gain a deeper insight into the distribution patterns of the different GA markers in euthermic hamsters, we then quantified their degree of colocalization in pyramidal neurons from neocortex and CA1 and CA3 hippocampal regions in MG160/GM130 and GM130-Golgin84 double-immunostained sections (**Figures 1**, **2E,F**). In all neuronal populations analyzed, a lower Manders coefficient of colocalization (Manders et al., 1993) was found for MG160/GM130 than for GM130/Golgin84 (with "0" representing a lack of colocalization and "1" representing complete colocalization). This was probably due to the wide distribution of GM130 in the GA and the more restricted distribution of MG160. Despite the similar morphological appearance of the GA, revealed by immunostaining with the three different antibodies in the present study, the lack of complete colocalization in the MG160/GM130 and GM130/Golgin84 double-stained sections indicate the existence of microdomains in the GA where the two proteins tested in each combination are not co-expressed (**Figures 1C,F**).

Differential Effects of Hibernation on the Expression of Golgi Proteins

We then analyzed the possible variations of Golgin84, MG160, and GM130 expression during the hibernation cycle by examining Western blots of protein samples obtained from animals sacrificed in the different hibernation stages (**Figure 3**). The analysis revealed that torpor bouts differentially affected expression levels of Golgi markers normalized to the expression of b-actin (**Figure 3**). Levels of MG160 decreased in samples from animals in torpor state compared to control expression levels, whereas expression of Golgin84 remained unaltered and GM130 expression increased (**Figure 3**). During arousal, MG160 and GM130 showed intermediate levels of expression, that is, between control and torpor levels. By contrast, in two

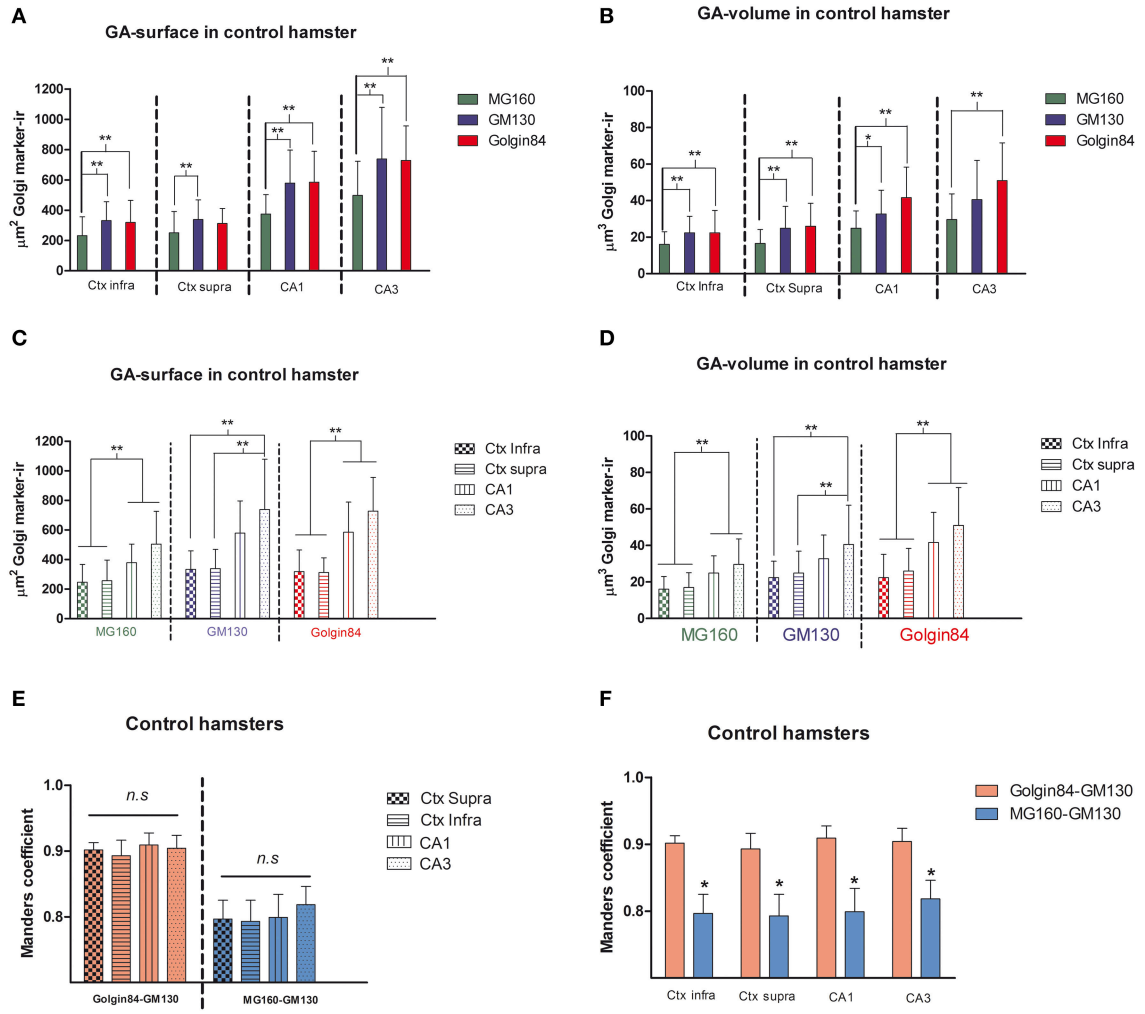

FIGURE 2 | (A–D) Histograms showing surface area **(A,C)** and volume **(B,D)** values (mean ± SD) of GA elements immunoreactive for MG160, GM130, and Golgin84, obtained from cropped confocal image stacks ($n > 15$ in all cases) including complete single pyramidal neurons from supra and infragranular neocortical layers and CA1 and CA3 hippocampal regions. **(A,B)** Show the statistical comparisons between mean values (surface area and volume respectively) obtained with the different Golgi markers within each brain region. **(C,D)** Show the comparisons of the values obtained with each marker across the different brain regions. (Kruskall-Wallis, $^{*}p \leq 0.01$; $^{**}p \leq 0.001$). **(E,F)** Show comparisons across the different brain regions and within each brain region, respectively, of the mean values of Manders colocalization coefficient obtained for MG160/GM130 and Golgin84/GM130. Values for each marker combination and region were obtained from every image confocal plane of cropped image stacks corresponding to 15 fully reconstructed neurons. Kruskall-Wallis test found significant differences in the comparisons of every possible combination of mean values ($p \leq 0.001$).

cases, the expression of Golgin84 was more intense in samples from arousal animals than during euthermia or torpor states (**Figure 3**).

We then analyzed, in immunocytochemically stained material, whether the hibernation-related changes in protein expression levels observed by Western blot were reflected in alterations in intensity or distribution patterns of Golgi markers in neocortical and hippocampal neurons (**Figures 4–6**, Figures S1, S2). As the levels of MG160 expression decreased in arousal and especially in torpor, observed by Western Blot, there was a corresponding reduction in the intensity of MG160 immunostaining (**Figure 4**, Figure S1). This reduction was more evident in neocortical neurons and CA1 pyramidal cells than in CA3 pyramidal neurons in which MG160 immunostaining was well preserved although MG160-ir elements did display a fragmented appearance (**Figure 4**, Figure S1). Alterations in MG160 expression were evidenced by a significant reduction in the surface area and volume of immunoreactive elements of MG160-ir elements in all neuronal populations analyzed, except CA3 pyramidal neurons, in which these parameters were slightly increased in torpid animals (**Figure 5**). Accordingly, in somatosensory cortex, but not in the hippocampus, decreases in the MG160/GM130 Manders colocalization coefficient were found in torpor as compared to control and arousal states (**Figure 6**).

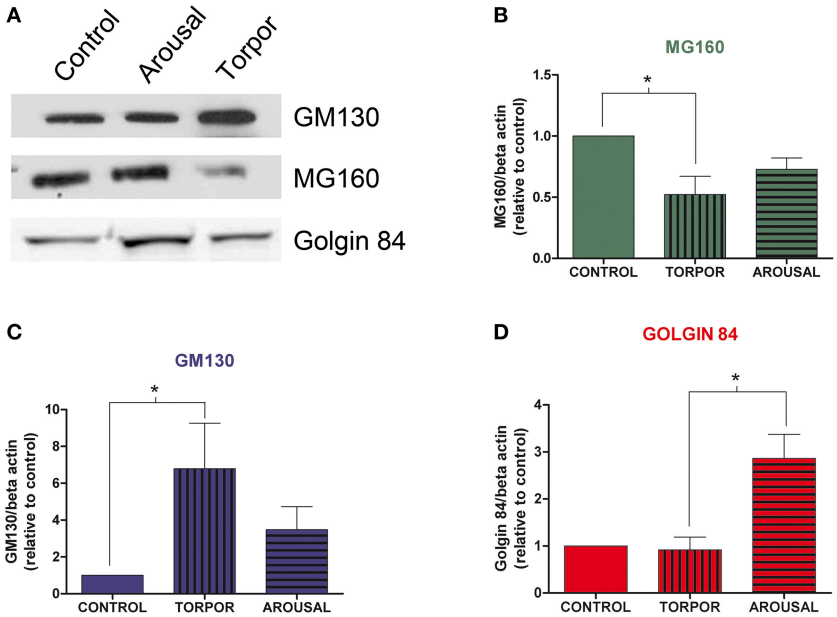

FIGURE 3 | Alterations in Golgi protein expression during the hibernation of Syrian hamsters. (A) Western blot of GM130, MG160, and Golgin84 in protein samples extracted from euthermic (control) and hibernating (arousal and torpor phase) hamsters. Histograms show GM160 **(B)**, MG130 **(C)**, and Golgin84 **(D)** expression normalized to β-actin. The data represent the mean ± SD of three independent experiments. Note the increase of GM130 and the decrease of MG160 expression in arousal and more markedly in torpor as compared to control animals. Also note the high Golgin84 expression levels during arousal (Kruskall-Wallis, $^{*}p \leq 0.05$).

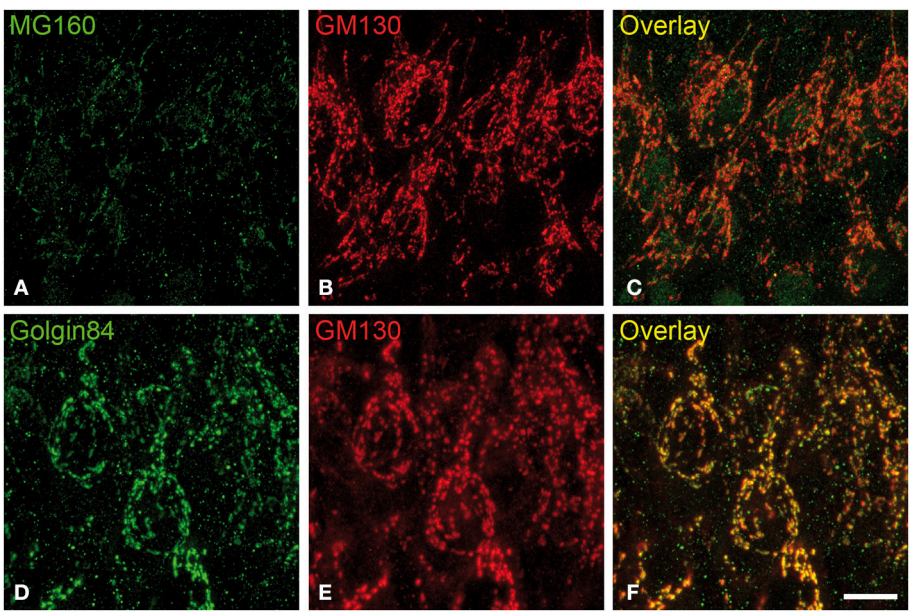

FIGURE 4 | Distribution of GA proteins in cortical neurons from torpid hamsters. (A–F) Pairs of images taken from hippocampal sections double-immunostained for MG160/GM130 **(A–C)** and Golgin84/GM130 **(D–F)** showing their distribution in the GA of CA1 pyramidal neurons from hamsters at torpor. Note the reduction of MG160 immunostaining and the strong fragmentation of the GA as revealed with the different Golgi markers. Scale bar in **(F)** indicates 9.5 μm.

No changes were found in the apparent intensity of GM130 immunostaining in hibernating hamsters. However, profound morphological modifications of GM130-ir elements of the GA were found; in all regions analyzed, they showed a fragmented appearance in arousal and particularly in torpor animals as compared with controls (Figures S1, S2). This fragmentation was accompanied by a decrease in the volume and surface area of GM130-ir elements during hibernation,

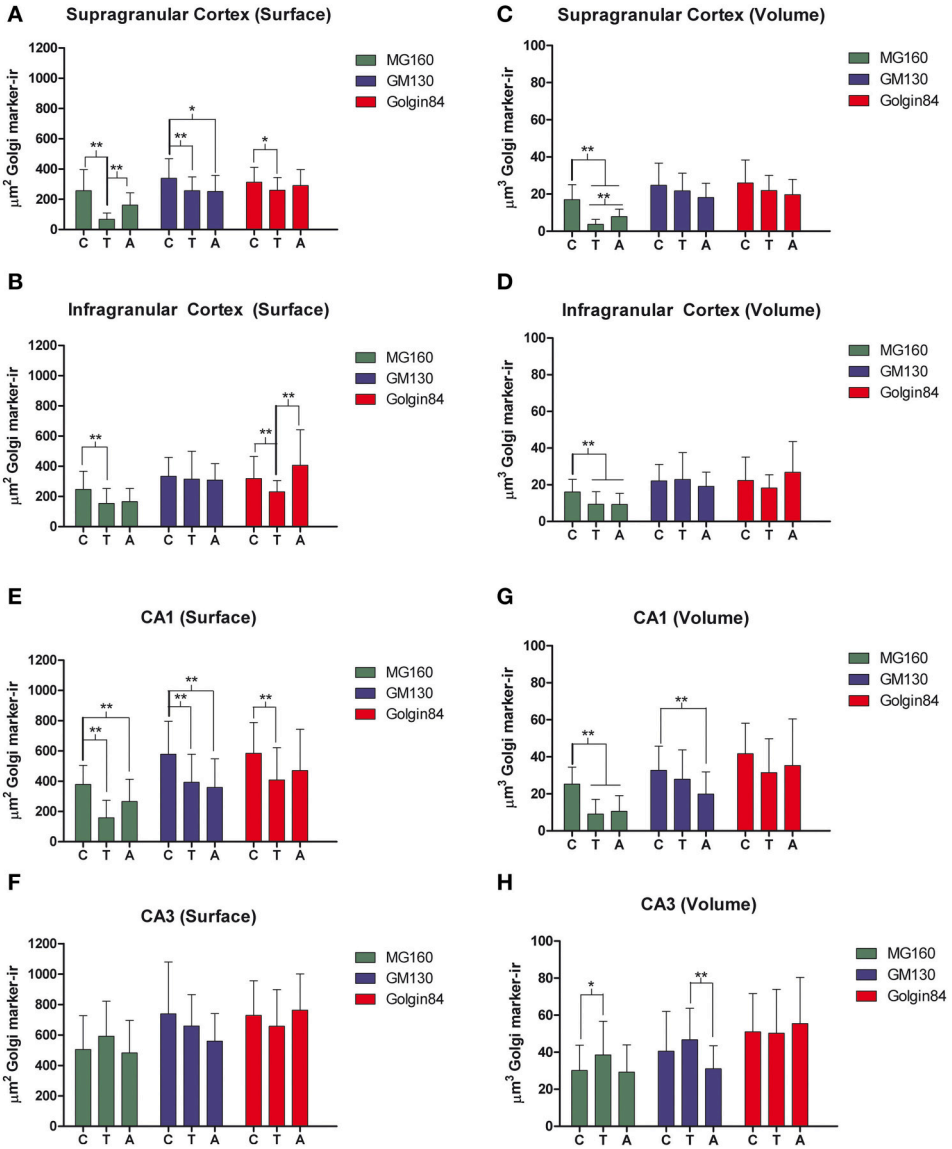

FIGURE 5 | Histograms showing volume and surface area values (mean ± SD) of GA elements immunoreactive for MG160, GM130, and Golgin84, obtained from cropped confocal image stacks ($n > 15$ in all cases) including complete single pyramidal neurons from supra (A,C) and infragranular (B,D) neocortical layers and CA1 (E,G) and CA3 (F,H) hippocampal regions from euthermic (control) animals and animals during arousal and torpor. Kruskall-Wallis, $^{*}p \leq 0.01$; $^{**}p \leq 0.002$; c, control; t, torpor; a, arousal.

which reached statistical significance especially in the CA1 region of the hippocampus (**Figure 5**). Similar alterations to those found with GM130 were observed for Golgin84 immunostaining in torpid animals. These included—without apparent changes in intensity of Golgin84 immunostaining—an intense fragmentation (**Figure 4**, Figures S1, S2) and a decrease in surface area, but not volume, of Golgin84-ir elements, which reached statistical significance in infragranular neocortical and CA1 neurons (**Figure 5**). These changes were accompanied by an increase in the GM130/Golgin84 colocalization Manders coefficient during torpor in all areas except in CA1 (**Figure 6**).

Golgi Apparatus Changes in Neurons with Hyperphosphorylated Tau During Torpor

Previous studies have described that during the torpor phase of hibernation tau protein is highly phosphorylated in cortical neurons, whereas after arousal this high phosphorylation decreases to normal levels (Arendt et al., 2003; Härtig et al., 2005, 2007; León-Espinosa et al., 2013). In accordance with these studies, the present results (from brain sections immunocytochemically stained with AT8 antibody which recognizes phospho Ser202 and phospho Thr205 sites in Tau protein) indicate that, in the Syrian hamster, tau hyperphosphorylation is particularly evident in a subpopulation

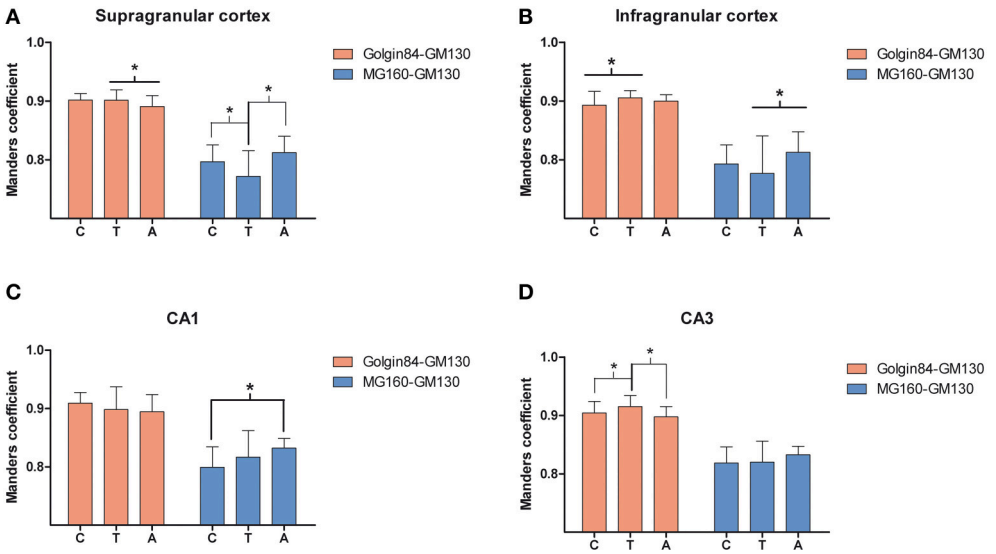

FIGURE 6 | Comparisons in supra (A) and infragranular (B) neocortical layers and in the CA1 (C) and CA3 (D) region of the hippocampus between mean values of Manders colocalization coefficient obtained for MG160/GM130 and Golgin84/GM130 in control, arousal and torpor animals. Values for each marker combination, region and animal were obtained from every image confocal plane of cropped image stacks corresponding to 15 fully reconstructed neurons. Kruskall-wallis test found significant differences in the comparisons of every possible combination of mean values (*$p \leq 0.05$). c, control; t, torpor; a, arousal.

of pyramidal neurons in layer V of the neocortex and in neurons of the CA3 and hilar regions of the hippocampus (**Figure 7**). Next we studied whether neurons with hyperphosphorylated tau were more or less prone to undergo morphological alterations in the GA during the hibernation cycle. For this purpose, in the somatosensory cortex of hamsters at torpor, we analyzed confocal image stacks from layer V neurons double immunostained for AT8 and MG160 to examine whether alterations in MG160 expression in the GA were more pronounced in neurons with tau hyperphosphorylation (AT8-positive) than in AT8-negative neurons. We found that the mean volume and surface area of MG160-ir elements were significantly lower in AT8+ neurons than in the surrounding AT8− neurons, although not all AT8+ neurons were equally affected (**Figure 8**). However, this does not seem to be the case in the hippocampus, where the reduction in GA MG160 immunostaining was more pronounced in CA1 than in CA3 neurons (**Figure 5**) even though AT8 immunostaining was more intense in CA3 than in CA1 (**Figure 7**).

Finally, in AT8/Golgin84 double-immunostained sections from torpor animals, we observed that the surface area and volume of Golgin84-ir GA elements were similar in AT8+ neurons and AT8- neurons (**Figure 8**). These results indicate that the accumulation of hyperphosphorylated tau at Ser202 and Thr205 during the torpor stage of hibernation seems to be independent of the concomitant reversible shrinkage and fragmentation of the GA.

DISCUSSION

The main results of the present study, schematically summarized in **Figure 9**, show that MG160 and, to a wider extent, GM130 and Golgin84 are expressed in the GA of neocortical and hippocampal neurons in euthermic Syrian hamsters. We also showed quantitatively that during the hibernation cycle, the GA undergoes significant and protein-specific changes in expression levels and distribution patterns of these Golgi protein components. Furthermore, these changes were accompanied by a transitory Golgi fragmentation with reductions in the volume and surface area of the GA during torpor and arousal stages that varied between different regions. We also found selective changes in the GA in neurons expressing high levels of hyperphosphorylated tau.

Fragmentation of the Golgi Apparatus During Hibernation

The GA in nerve tissue becomes fragmented in a variety of pathological conditions as already noted since the times of Cajal in cells at the edges of mechanical lesions (DeFelipe and Jones, 1991). Later numerous studies have reported Golgi fragmentation in apoptotic cells (Aslan and Thomas, 2009) and in a variety of pathological conditions including Alzheimer's disease, amyotrophic lateral sclerosis, Creutzfeldt-Jacob disease, multiple system atrophy, Parkinson's disease, spinocerebellar ataxia type 2 and Niemann-Pick type C (Gonatas et al., 1992; Dal Canto, 1996; Stieber et al., 1996; Sakurai et al., 2000, 2002; Walkley and Suzuki, 2004; Fujita et al., 2006; Eschbach and Dupuis, 2011). It is well known that GA in different cell types undergoes a transitory fragmentation during mitotic cell division along with some of the mechanisms that regulate this fragmentation. During mitosis, the GA is disassembled in early prophase with a splitting of GA into small, round, disconnected and dispersed elements, and is reassembled in telophase (Levine et al., 1995; Corda et al., 2012). Previous

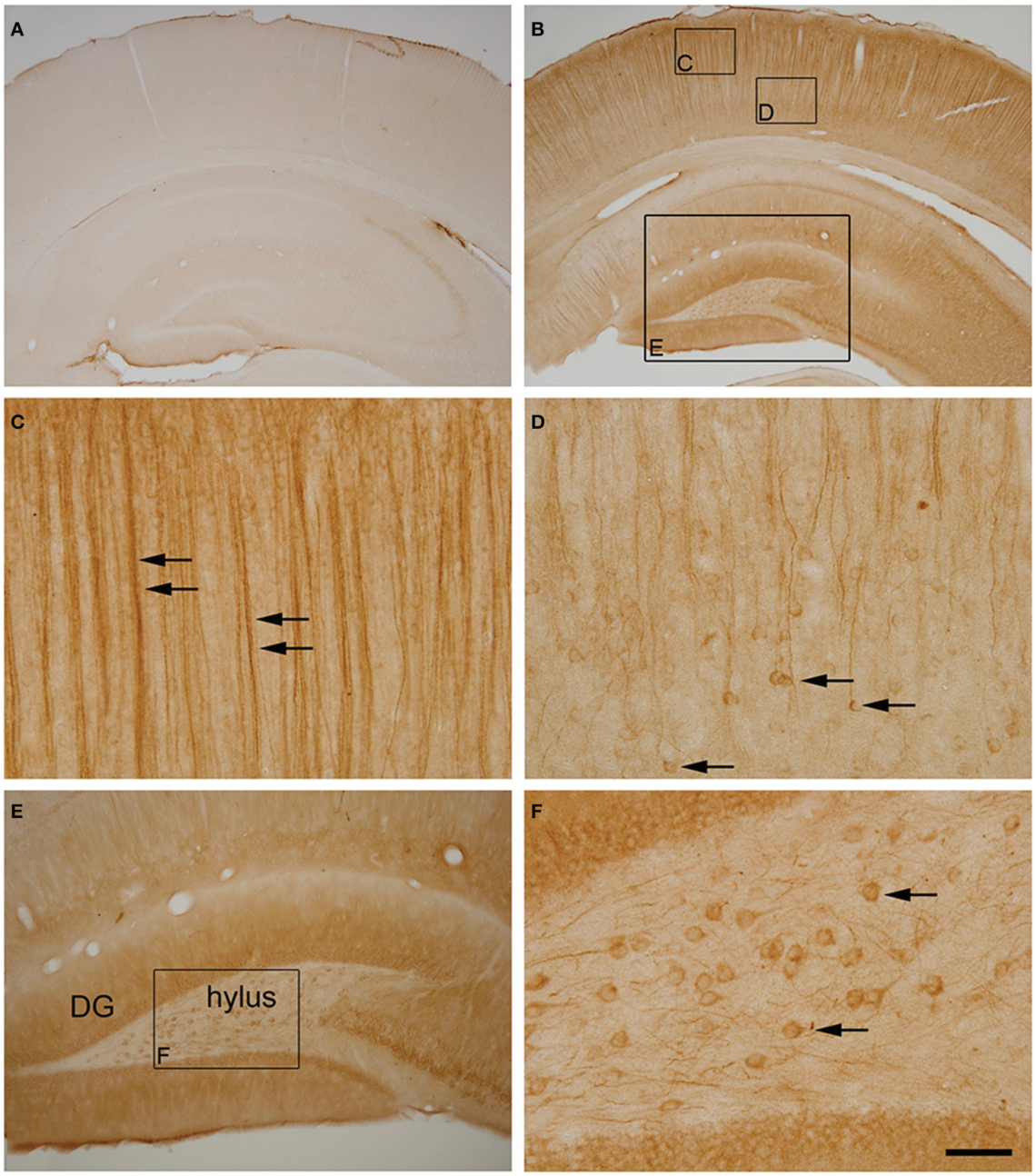

FIGURE 7 | (A,B) Photomicrographs showing the patterns of hyperphosphorylated tau immunostaining (AT8 antibody) in the neocortex and hippocampus of control **(A)** and torpid **(B)** Syrian hamsters. Small squared zones in **(B)** are shown at higher magnification in **(C,D)**. Note the AT8 immunostaining of layer V neuronal cell bodies (arrows in **D**) and their apical dendrites in layer III (arrows in **C**). The large squared zone in **(B)** and squared zone in **(E)** are shown at higher magnification in **(E,F)**, respectively. Note the intense AT8 immunostaining in hylar neurons (arrows in **F**). Scale bar in F indicates 570 μm in **(A,B)**, 57 μm in **(C,D,F)** and 115 μm in **(E)**.

studies have demonstrated the involvement of the Golgi protein tether complex, including GM130, GRASP65, p115, giantin, and Rab GTPases, in the stacking and lateral tethering of Golgi cisternae that allow ribbon formation and the regulation of the Golgi disassembly and reassembly during mitosis (Nakamura et al., 1995; Barr et al., 1997, 1998; Shorter and Warren, 1999; Puthenveedu and Linstedt, 2001, 2005; Puthenveedu et al., 2006; Nakamura, 2010). Along with the tether complex, Golgin84 was also suggested to play a key role in the assembly and maintenance of Golgi ribbon in mammalian cells (Diao et al., 2003). The cisternal unstacking and the disassembly of the GA at the onset of mitosis have been related to the inhibition of p115 binding to GM130 by GM130 phosphorylation and to the phosphorylation of Grasp65 (Nakamura et al., 1997; Lowe et al., 1998, 2000; Puthenveedu and Linstedt, 2001; Wang et al., 2003, 2005; Nakamura, 2010).

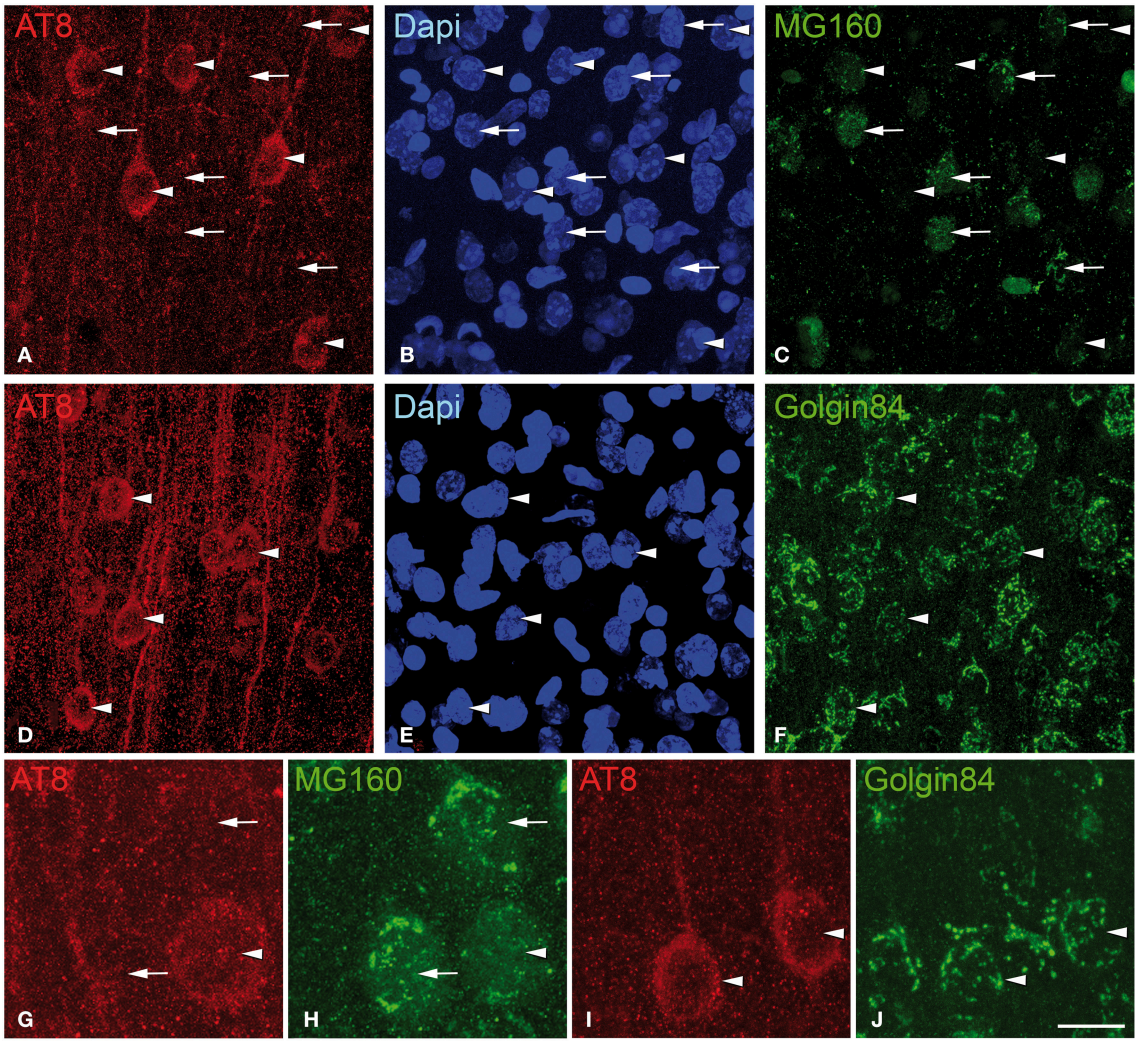

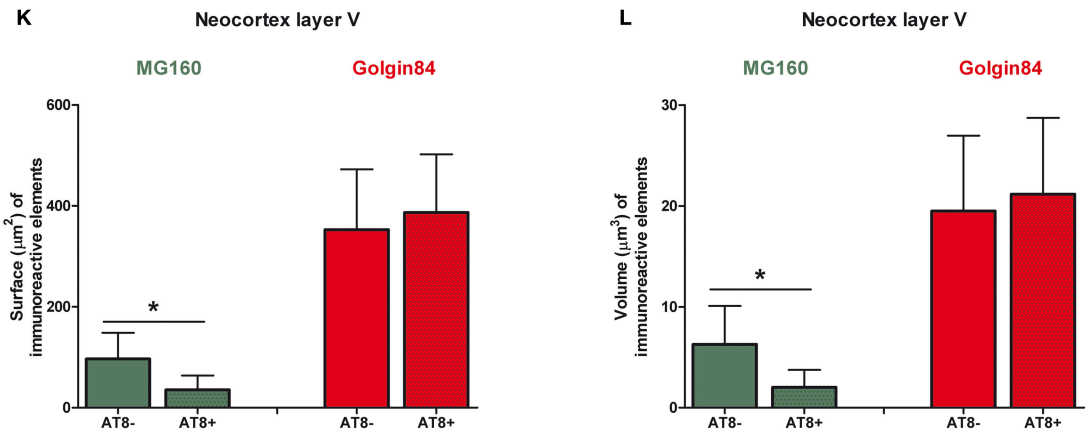

FIGURE 8 | Microphotographs taken from layer V of the somatosensory cortex from Syrian hamsters in torpor state. Sections were double stained with antibodies directed against AT8 and MG160 **(A–C,G,H)**, and against AT8 and Golgin84 **(D–F,I,J)**, counterstained with Dapi. Arrowheads indicate AT8 positive neurons whereas arrows indicate adjacent AT8 negative neurons. Note the marked reduction in MG160 immunostaining of the GA in AT8+ neurons and the similar pattern of Golgin84 immunostaining between AT8+ and AT8− neurons. Histograms show surface area **(K)** and volume **(L)** values (mean ± SD) of GA elements immunoreactive for MG160 and Golgin84 in AT8+ cells and in AT8− cells. Wilcoxon test found significant differences in the comparisons between AT8+ and AT8− cells in both volume and surface area values of MG160-ir (*$p \leq 0.001$) but not Golgin84-ir elements. Scale bar in **(J)** indicates 20 μm in **(A–F)**, 7 μm in **(G,H)** and 10.5 μm in **(I,J)**.

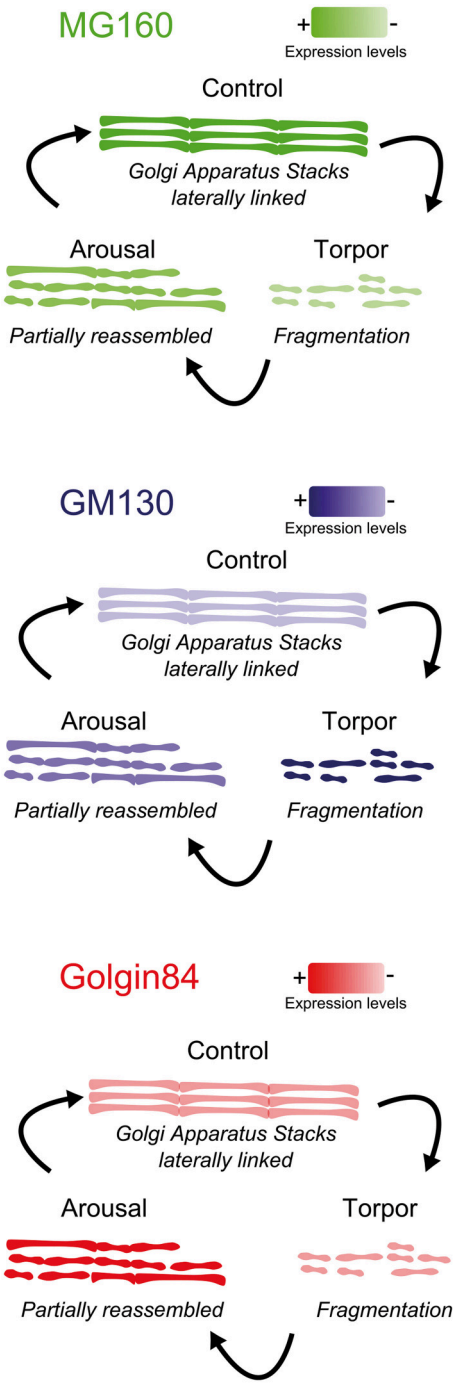

FIGURE 9 | Summarizing diagram showing the structural alterations of the GA during the hibernation cycle along with changes in the expression levels of the GM130, MG160, and Golgin84 GA proteins.

In the present study, we demonstrate that during hibernation, the GA of hippocampal and neocortical neurons undergoes a pronounced morphological reorganization in Syrian hamsters. A strong fragmentation along with a volume decrease of the GA in torpid animals was found by immunostaining for GM130, MG160, and Golgin84. Future electron microscopic observations would be necessary to determine the extent of the Golgi ribbon fragmentation during hibernation and establish whether it affects the integrity of the Golgi stacks. However, previous electron microscopy observations in taste bud cells of hibernating ground squirrels noted a transitory fragmentation or disassembly of the GA during the torpor phase in which dictyosomes were rarely seen and instead clusters of small vesicles appeared (Popov et al., 1999; Bocharova et al., 2011). Although, the mechanisms underlying neuronal Golgi fragmentation during torpor remain to be explored, the present Western Blot observations revealed a drop in whole brain MG160 brain expression levels along with an increase in those for GM130 in torpid animals as compared with euthermic animals. This was accompanied by an important reduction in the levels of MG160 immunostaining of the GA in hippocampal and neocortical neurons. The down-regulation of MG160 expression during torpor could participate in the mechanisms involved in the fragmentation of the GA since MG160 has been proposed to play important roles in the biogenesis and functioning of the GA (Gonatas et al., 1995, 1998a).

The present Western blot data also showed that brain expression levels of Golgin84 are transiently increased during arousal. The interference with Golgin84 expression has been shown to disrupt the Golgi ribbon and induce the appearance of Golgi fragments in HEK293/tau cells (Jiang et al., 2014). In addition, overexpressing of Golgin84 rescued brefelding-A-induced Golgi alterations, indicating the important role of Golgin84 in the structural maintenance of the GA (Jiang et al., 2014). Therefore, it is tempting to speculate that the up-regulation of Golgin84 expression during arousal (present results) is required for the rapid rebuilding or reorganization of the Golgi ribbon apparatus during arousal leading the animals from torpor to euthermia. Although, the biological relevance of these arousals is still not known, previous reports indicate that they could be related to a neuroprotective role (Daan et al., 1991; Arendt et al., 2003). Our results may suggest that a rapid GA structure recovery takes place during arousal, as a GA reorganization is needed for the adaptation of neurons to arousal-torpor bouts.

Hibernation is a state of low energy availability (Humphries et al., 2003) with a virtual cessation of neuronal activity in cortical and midbrain areas (Strumwasser, 1959; South, 1972; Walker et al., 1977; Igelmund, 1996). Given that the size of the GA has been directly related to the level of cell activity (Lucassen et al., 1993; Salehi et al., 1994), the fragmentation and reduction of the GA observed in the present study is probably related to a reduced neuronal capacity for protein processing, modification and targeting during torpor. This is in line with the hibernation-related reductions in cell body area, dendritic arbor complexity and spine density previously reported (Popov et al., 1992; Popov and Bocharova, 1992; von der Ohe et al., 2006) and the general decrease in energetically expensive processes such as transcription and protein synthesis (Strumwasser, 1959; Walker et al., 1977; Zhegunov, 1988; Rolfe and Brown, 1997; Frerichs et al., 1998; Popov et al., 1999; Buck and Barnes, 2000; van Breukelen and

Martin, 2001, 2002). However, changes in protein expression and localization during hibernation seem to be complex, highly regulated, protein-specific processes. For instance, brain expression patterns of the three GA proteins evaluated in the present study by Western Blot and immunocytochemistry are differentially regulated during torpor and arousal in Syrian hamsters. In addition, in hibernating ground squirrels a rapid and transitory dissociation of pre- and post-synaptic proteins from synapses have been reported during torpor in parallel with dendritic retractions and loss of synaptic connectivity (von der Ohe et al., 2006, 2007). Whether, these processes are related to the alterations of the GA found in the present study warrants further research.

Golgi Apparatus Fragmentation and Tau Hyperphosphorylation

It is known that the structure of the Golgi complex also depends on the integrity of the cytoskeleton. For instance, actin depolymerization causes Golgi stacks to fragment and results in swelling of cisternae (Egea et al., 2006). The disruption of the microtubules or the dynein/dynactin complex, that bind the Golgi complex to the microtubules, also causes marked changes in Golgi shape and localization (Cole et al., 1996; Burkhardt et al., 1997). It has been proposed that, among other functions, the microtubule interacting protein tau—which is localized on GA membranes—could serve as a link between the Golgi membranes and microtubules, along with many of the tau phosphorylation-related kinases which are also located in the GA (Farah et al., 2006). Therefore, the perturbation of the microtubule network by tau hyperphosphorylation could alter GA structure and the secretory pathway, and impair the highly regulated processes of protein sorting in neuronal compartments. Different studies have shown that, during the mitotic division of different cell types, GA fragmentation is concomitant with a general phosphorylation of tau which is recognized by phosphorylation-dependent antibodies used to label neurofibrillary tangles in Alzheimer's disease (AD), such as PHF1, AT8, AT100, or AT180 (Pope et al., 1994; Preuss et al., 1995; Vincent et al., 1996; Illenberger et al., 1998; Preuss and Mandelkow, 1998; Delobel et al., 2002). In AD patients, the GA of cortical neurons undergo widespread structural alterations before the formation of neurofibrillary tangles (Stieber et al., 1996). In animal models of AD, the overexpression of tau induces Golgi fragmentation in neurons leading to the suggestion that in AD brains the tau pathology precedes Golgi fragmentation (Lin et al., 2003; Liazoghli et al., 2005). However, studies in HEK293/tau cells showed that Golgi-disturbing agents, brefeldin A and nocodazole, induced tau hyperphosphorylation suggesting that Golgi fragmentation could be an upstream event triggering tau hyperphosphorylation through activation of kinases (Jiang et al., 2014). Previous studies have proposed that, in terms of tau phosphorylation, hibernating animals show some similarities to AD patients at the early stages of the disease, as neurons from torpid animals show a marked increase of hyperphosphorylated tau in contrast to euthermic animals (Zhou et al., 2001; Arendt et al., 2003; Arendt, 2004; Avila et al., 2004; Härtig et al., 2005, 2007; Su et al., 2008; Stieler et al., 2011). Our results shows that, in torpor state, the reduction in the volume and surface area of the MG160-ir elements of the GA in layer V neocortical neurons is more pronounced in AT8+ than in AT8− neurons, suggesting that hyperphosphorylated tau has a significant deleterious effect on the MG160 expression at the GA. Alternatively, the decrease in MG160 expression during torpor might have an effect on tau hyperphosphorylation at Ser202/Thr205 sites. This is supported by the fact that MG160 can bind to different FGFs, including FGF-2, reducing FGF internalization and inhibiting the intracellular accumulation of this growth factor (Burrus et al., 1992; Zhou et al., 1997; Zuber et al., 1997; Yamaguchi et al., 2003). FGF-2 levels are increased in AD (Stopa et al., 1990; Cummings et al., 1993) and it has been shown, in neural progenitor cells and in PC12 cells, that FGF-2 upregulation can increase GSK3 activity and induce the hyperphosphorylation of tau protein in various epitopes including S202, recognized by AT8 (Tatebayashi et al., 1999, 2003). Therefore, it is possible that the reduction in the MG160 expression in neocortical cells during torpor results in increased intracellular FGF levels that lead to the tau hyperphosphorylation observed with AT8 antibody. Further studies are needed to test this hypothesis both in hibernating animals, in tissue from AD patients and in cellular models of the disease.

Finally, we have shown in the present study that, during torpor, there are no differences between AT8+ and AT8− layer V pyramidal neurons immunostained with Golgin84 in terms of the reduction in volume and surface area of the GA. This indicated that not all GA proteins are affected by hyperphosphorylated tau accumulation. However, it is known from Western Blot studies that tau is hyperphosphorylated at different residues besides AT8 recognition sites during hibernation (Stieler et al., 2011). Therefore, further studies should explore whether the extent of GA alterations is correlated with degree of accumulation of tau hyperphosphorylated at sites other than Ser202/Thr205.

AUTHOR CONTRIBUTIONS

AA and GL equal contribution. AA, GL, and AM designed research; AA and GL performed research and analyzed data; JD and AM wrote the paper.

ACKNOWLEDGMENTS

This work was supported by grants from the following entities: the Spanish Ministry of Economy and Competitiveness (grants SAF2010-18218 to AM and BFU2012-34963 to JD) and the Centre for Networked Biomedical Research into Neurodegenerative Diseases (CIBERNED, CB06/05/0066 to JD).

SUPPLEMENTARY MATERIAL

The Supplementary Material for this article can be found online at: http://journal.frontiersin.org/article/10.3389/fnana.2015.00157

REFERENCES

Arendt, T. (2004). Neurodegeneration and plasticity. *Int. J. Dev. Neurosci.* 22, 507–514. doi: 10.1016/j.ijdevneu.2004.07.007

Arendt, T., Stieler, J., Strijkstra, A. M., Hut, R. A., Rudiger, J., Van der Zee, E. A., et al. (2003). Reversible paired helical filament-like phosphorylation of tau is an adaptive process associated with neuronal plasticity in hibernating animals. *J. Neurosci.* 23, 6972–6981.

Aslan, J. E., and Thomas, G. (2009). Death by committee: organellar trafficking and communication in apoptosis. *Traffic* 10, 1390–1404. doi: 10.1111/j.1600-0854.2009.00951.x

Avila, J., Lucas, J. J., Perez, M., and Hernandez, F. (2004). Role of tau protein in both physiological and pathological conditions. *Physiol. Rev.* 84, 361–384. doi: 10.1152/physrev.00024.2003

Barr, F. A., Nakamura, N., and Warren, G. (1998). Mapping the interaction between GRASP65 and GM130, components of a protein complex involved in the stacking of Golgi cisternae. *EMBO J.* 17, 3258–3268. doi: 10.1093/emboj/17.12.3258

Barr, F. A., Puype, M., Vandekerckhove, J., and Warren, G. (1997). GRASP65, a protein involved in the stacking of Golgi cisternae. *Cell* 91, 253–262. doi: 10.1016/S0092-8674(00)80407-9

Bocharova, L. S., Gordon, R. Ya., Rogachevskii, V. V., Ignat'ev, D. A., and Khutsian, S. S. (2011). Cyclic structural changes in endoplasmic reticulum and Golgi apparatus in the hippocampal neurons of ground squirrels during hibernation. *Tsitologiia* 53, 259–269. doi: 10.1134/S1990519X11030023

Buck, C. L., and Barnes, B. M. (2000). Effects of ambient temperature on metabolic rate, respiratory quotient, and torpor in an arctic hibernator. *Am. J. Physiol. Regul. Integr. Comp. Physiol.* 279, R255–R262.

Burkhardt, J. K., Echeverri, C. J., Nilsson, T., and Vallee, R. B. (1997). Overexpression of the dynamitin (p50) subunit of the dynactin complex disrupts dynein-dependent maintenance of membrane organelle distribution. *J. Cell Biol.* 139, 469–484. doi: 10.1083/jcb.139.2.469

Burrus, L. W., Zuber, M. E., Lueddecke, B. A., and Olwin, B. B. (1992). Identification of a cysteine-rich receptor for fibroblast growth factors. *Mol. Cell. Biol.* 12, 5600–5609. doi: 10.1128/MCB.12.12.5600

Cole, N. B., Sciaky, N., Marotta, A., Song, J., and Lippincott-Schwartz, J. (1996). Golgi dispersal during microtubule disruption: regeneration of Golgi stacks at peripheral endoplasmic reticulum exit sites. *Mol. Biol. Cell* 7, 631–650. doi: 10.1091/mbc.7.4.631

Corda, D., Barretta, M. L., Cervigni, R. I., and Colanzi, A. (2012). Golgi complex fragmentation in G2/M transition: an organelle-based cell-cycle checkpoint. *IUBMB Life* 64, 661–670. doi: 10.1002/iub.1054

Cummings, B. J., Su, J. H., and Cotman, C. W. (1993). Neuritic involvement within bFGF immunopositive plaques of Alzheimer's disease. *Exp. Neurol.* 124, 315–325. doi: 10.1006/exnr.1993.1202

Daan, S., Barnes, B. M., and Strijkstra, A. M. (1991). Warming up for sleep? Ground squirrels sleep during arousals from hibernation. *Neurosci. Lett.* 128, 265–268. doi: 10.1016/0304-3940(91)90276-Y

Dal Canto, M. C. (1996). The Golgi apparatus and the pathogenesis of Alzheimer's disease. *Am. J. Pathol.* 148, 355–360.

DeFelipe, J., and Jones, E. G. (1991). *Cajal's Degeneration and Regeneration of the Nervous System*. New York. NY: Oxford University Press.

Delobel, P., Flament, S., Hamdane, M., Mailliot, C., Sambo, A.-V., Bégard, S., et al. (2002). Abnormal Tau phosphorylation of the Alzheimer-type also occurs during mitosis. *J. Neurochem.* 83, 412–420. doi: 10.1046/j.1471-4159.2002.01143.x

Diao, A., Rahman, D., Pappin, D. J., Lucocq, J., and Lowe, M. (2003). The coiled-coil membrane protein golgin-84 is a novel rab effector required for Golgi ribbon formation. *J. Cell Biol.* 160, 201–212. doi: 10.1083/jcb.200207045

Egea, G., Lázaro-Diéguez, F., and Vilella, M. (2006). Actin dynamics at the Golgi complex in mammalian cells. *Curr. Opin. Cell Biol.* 18, 168–178. doi: 10.1016/j.ceb.2006.02.007

Eschbach, J., and Dupuis, L. (2011). Cytoplasmic dynein in neurodegeneration. *Pharmacol. Ther.* 130, 348–363. doi: 10.1016/j.pharmthera.2011.03.004

Fan, J., Hu, Z., Zeng, L., Lu, W., Tang, X., Zhang, J., et al. (2008). Golgi apparatus and neurodegenerative diseases. *Int. J. Dev. Neurosci.* 26, 523–534. doi: 10.1016/j.ijdevneu.2008.05.006

Farah, C. A., Perreault, S., Liazoghli, D., Desjardins, M., Anton, A., Lauzon, M., et al. (2006). Tau interacts with Golgi membranes and mediates their association with microtubules. *Cell Motil. Cytoskeleton* 63, 710–724. doi: 10.1002/cm.20157

Frerichs, K. U., Smith, C. B., Brenner, M., DeGracia, D. J., Krause, G. S., Marrone, L., et al. (1998). Suppression of protein synthesis in brain during hibernation involves inhibition of protein initiation and elongation. *Proc. Natl. Acad. Sci. U.S.A.* 95, 14511–14516. doi: 10.1073/pnas.95.24.14511

Fujita, Y., Ohama, E., Takatama, M., Al-Sarraj, S., and Okamoto, K. (2006). Fragmentation of Golgi apparatus of nigral neurons with alpha-synuclein-positive inclusions in patients with Parkinson's disease. *Acta Neuropathol.* 112, 261–265. doi: 10.1007/s00401-006-0114-4

Geiser, F. (2004). Metabolic rate and body temperature reduction during hibernation and daily torpor. *Annu. Rev. Physiol.* 66, 239–274. doi: 10.1146/annurev.physiol.66.032102.115105

Geiser, F. (2013). Hibernation. *Curr. Biol.* 23, R188–R193. doi: 10.1016/j.cub.2013.01.062

Geiser, F., and Martin, G. M. (2013). Torpor in the Patagonian opossum (Lestodelphys halli): implications for the evolution of daily torpor and hibernation. *Naturwissenschaften* 100, 975–981. doi: 10.1007/s00114-013-1098-2

Glick, B. S. (2002). Can the Golgi form de novo? *Nat. Rev. Mol. Cell Biol.* 3, 615–619. doi: 10.1038/nrm877

Gonatas, J. O., Chen, Y. J., Stieber, A., Mourelatos, Z., and Gonatas, N. K. (1998a). Truncations of the C-terminal cytoplasmic domain of MG160, a medial Golgi sialoglycoprotein, result in its partial transport to the plasma membrane and filopodia. *J. Cell Sci.* 111(Pt 2), 249–260.

Gonatas, J. O., Mourelatos, Z., Stieber, A., Lane, W. S., Brosius, J., and Gonatas, N. K. (1995). MG-160, a membrane sialoglycoprotein of the medial cisternae of the rat Golgi apparatus, binds basic fibroblast growth factor and exhibits a high level of sequence identity to a chicken fibroblast growth factor receptor. *J. Cell Sci.* 108(Pt 2), 457–467.

Gonatas, N. K., Gonatas, J. O., and Stieber, A. (1998b). The involvement of the Golgi apparatus in the pathogenesis of amyotrophic lateral sclerosis, Alzheimer's disease, and ricin intoxication. *Histochem. Cell Biol.* 109, 591–600.

Gonatas, N. K., Stieber, A., Mourelatos, Z., Chen, Y., Gonatas, J. O., Appel, S. H., et al. (1992). Fragmentation of the Golgi apparatus of motor neurons in amyotrophic lateral sclerosis. *Am. J. Pathol.* 140, 731–737.

Härtig, W., Oklejewicz, M., Strijkstra, A. M., Boerema, A. S., Stieler, J., and Arendt, T. (2005). Phosphorylation of the tau protein sequence 199-205 in the hippocampal CA3 region of Syrian hamsters in adulthood and during aging. *Brain Res.* 1056, 100–104. doi: 10.1016/j.brainres.2005.07.017

Härtig, W., Stieler, J., Boerema, A. S., Wolf, J., Schmidt, U., Weissfuss, J., et al. (2007). Hibernation model of tau phosphorylation in hamsters: selective vulnerability of cholinergic basal forebrain neurons - implications for Alzheimer's disease. *Eur. J. Neurosci.* 25, 69–80. doi: 10.1111/j.1460-9568.2006.05250.x

Hu, Z., Zeng, L., Huang, Z., Zhang, J., and Li, T. (2007). The study of Golgi apparatus in Alzheimer's disease. *Neurochem. Res.* 32, 1265–1277. doi: 10.1007/s11064-007-9302-4

Humphries, M. M., Thomas, D. W., and Kramer, D. L. (2003). The role of energy availability in Mammalian hibernation: a cost-benefit approach. *Physiol. Biochem. Zool.* 76, 165–179. doi: 10.1086/367950

Igelmund, P. (1996). "Hibernation and hippocampal synaptic transmission," in *Adaptation to Cold: Tenth International Hibernation Symposium,* eds H. Spangenberger, F. G. Nikmanesh, A. Gabriel, K. Lutke, Y. Q. Zhao, M. M. Bohm-Pinger, U. Heinemann, J. Hescheler, and F. W. Klubmann (Armidale: University of New England Press), 159–166.

Illenberger, S., Zheng-Fischhofer, Q., Preuss, U., Stamer, K., Baumann, K., Trinczek, B., et al. (1998). The endogenous and cell cycle-dependent phosphorylation of tau protein in living cells: implications for Alzheimer's disease. *Mol. Biol. Cell* 9, 1495–1512. doi: 10.1091/mbc.9.6.1495

Jiang, Q., Wang, L., Guan, Y., Xu, H., Niu, Y., Han, L., et al. (2014). Golgin-84-associated Golgi fragmentation triggers tau hyperphosphorylation by activation of cyclin-dependent kinase-5 and extracellular signal-regulated kinase. *Neurobiol. Aging* 35, 1352–1363. doi: 10.1016/j.neurobiolaging.2013.11.022

Képès, F., Rambourg, A., and Satiat-Jeunemaĭtre, B. (2005). Morphodynamics of the secretory pathway. *Int. Rev. Cytol.* 242, 55–120. doi: 10.1016/S0074-7696(04)42002-6

León-Espinosa, G., García, E., García-Escudero, V., Hernández, F., DeFelipe, J., and Avila, J. (2013). Changes in tau phosphorylation in hibernating rodents. *J. Neurosci. Res.* 91, 954–962. doi: 10.1002/jnr.23220

Levine, T. P., Misteli, T., Rabouille, C., and Warren, G. (1995). Mitotic disassembly and reassembly of the Golgi apparatus. *Cold Spring Harb. Symp. Quant. Biol.* 60, 549–557. doi: 10.1101/SQB.1995.060.01.058

Liazoghli, D., Perreault, S., Micheva, K. D., Desjardins, M., and Leclerc, N. (2005). Fragmentation of the Golgi apparatus induced by the overexpression of wild-type and mutant human tau forms in neurons. *Am. J. Pathol.* 166, 1499–1514. doi: 10.1016/S0002-9440(10)62366-8

Lin, W. L., Lewis, J., Yen, S. H., Hutton, M., and Dickson, D. W. (2003). Ultrastructural neuronal pathology in transgenic mice expressing mutant (P301L) human tau. *J. Neurocytol.* 32, 1091–1105. doi: 10.1023/B:NEUR.0000021904.61387.95

Lowe, M., Gonatas, N. K., and Warren, G. (2000). The mitotic phosphorylation cycle of the cis-Golgi matrix protein GM130. *J. Cell Biol.* 149, 341–356. doi: 10.1083/jcb.149.2.341

Lowe, M., Nakamura, N., and Warren, G. (1998). Golgi division and membrane traffic. *Trends Cell Biol.* 8, 40–44. doi: 10.1016/S0962-8924(97)01189-6

Lucassen, P. J., Ravid, R., Gonatas, N. K., and Swaab, D. F. (1993). Activation of human supraoptic and paraventricular nucleus neurons with aging and in Alzheimer's disease as judged from increasing size of the Golgi apparatus. *Brain Res.* 632, 1055113.

Manders, E. M. M., Verbeek, F. J., and Aten, J. A. (1993). Measurement of co-localization of objects indual-colour confocal images. *J. Microsc.* 169, 375–382. doi: 10.1111/j.1365-2818.1993.tb03313.x

Morin, L. P., and Wood, R. I. (2001). *A Stereotaxic Atlas of the Golden Hamster Brain*. San Diego, CA: Academic Press.

Nakamura, N. (2010). Emerging new roles of GM130, a cis-Golgi matrix protein, in higher order cell functions. *J. Pharmacol. Sci.* 112, 255–264. doi: 10.1254/jphs.09R03CR

Nakamura, N., Lowe, M., Levine, T. P., Rabouille, C., and Warren, G. (1997). The vesicle docking protein p115 binds GM130, a cis-Golgi matrix protein, in a mitotically regulated manner. *Cell* 89, 445–455. doi: 10.1016/S0092-8674(00)80225-1

Nakamura, N., Rabouille, C., Watson, R., Nilsson, T., Hui, N., Slusarewicz, P., et al. (1995). Characterization of a cis-Golgi matrix protein, GM130. *J. Cell Biol.* 131, 1715–1726. doi: 10.1083/jcb.131.6.1715

Pope, W. B., Lambert, M. P., Leypold, B., Seupaul, R., Sletten, L., Krafft, G., et al. (1994). Microtubule-associated protein Tau is hyperphosphorylated during mitosis in the human neuroblastoma cell line SH-SY5Y. *Exp. Neurol.* 126, 185–194 doi: 10.1006/exnr.1994.1057

Popov, V. I., and Bocharova, L. S. (1992). Hibernation-induced structural changes in synaptic contacts between mossy fibres and hippocampal pyramidal neurons. *Neuroscience* 48, 53–62.

Popov, V. I., Bocharova, L. S., and Bragin, A. G. (1992). Repeated changes of dendritic morphology in the hippocampus of ground squirrels in the course of hibernation. *Neuroscience* 48, 45–51.

Popov, V. I., Ignat'ev, D. A., and Lindemann, B. (1999). Ultrastructure of taste receptor cells in active and hibernating ground squirrels. *J. Electron Microsc. (Tokyo)* 48, 957–969. doi: 10.1093/oxfordjournals.jmicro.a023770

Preuss, U., Döring, F., Illenberger, S., and Mandelkow, E. M. (1995). Cell cycle-dependent phosphorylation and microtubule binding of tau protein stably transfected into Chinese hamster ovary cells. *Mol. Biol. Cell* 6, 1397–1410. doi: 10.1091/mbc.6.10.1397

Preuss, U., and Mandelkow, E. M. (1998). Mitotic phosphorylation of tau protein in neuronal cell lines resembles phosphorylation in Alzheimer's disease. *Eur. J. Cell Biol.* 76, 176–184. doi: 10.1016/S0171-9335(98)80032-0

Puthenveedu, M. A., Bachert, C., Puri, S., Lanni, F., and Linstedt, A. D. (2006). GM130 and GRASP65-dependent lateral cisternal fusion allows uniform Golgi-enzyme distribution. *Nat. Cell Biol.* 8, 238–248. doi: 10.1038/ncb1366

Puthenveedu, M. A., and Linstedt, A. D. (2001). Evidence that Golgi structure depends on a p115 activity that is independent of the vesicle tether components giantin and GM130. *J. Cell Biol.* 155, 227–238. doi: 10.1083/jcb.200105005

Puthenveedu, M. A., and Linstedt, A. D. (2005). Subcompartmentalizing the Golgi apparatus. *Curr. Opin. Cell Biol.* 17, 369–375. doi: 10.1016/j.ceb.2005.06.006

Rolfe, D. F., and Brown, G. C. (1997). Cellular energy utilization and molecular origin of standard metabolic rate in mammals. *Physiol. Rev.* 77, 731–758.

Sakurai, A., Okamoto, K., Fujita, Y., Nakazato, Y., Wakabayashi, K., Takahashi, H., et al. (2000). Fragmentation of the Golgi apparatus of the ballooned neurons in patients with corticobasal degeneration and Creutzfeldt-Jakob disease. *Acta Neuropathol.* 100, 270–274. doi: 10.1007/s004010000182

Sakurai, A., Okamoto, K., Yaguchi, M., Fujita, Y., Mizuno, Y., Nakazato, Y., et al. (2002). Pathology of the inferior olivary nucleus in patients with multiple system atrophy. *Acta Neuropathol.* 103, 550–554. doi: 10.1007/s00401-001-0500-x

Salehi, A., Lucassen, P. J., Pool, C. W., Gonatas, N. K., Ravid, R., and Swaab, D. F. (1994). Decreased neuronal activity in the nucleus basalis of Meynert in Alzheimer's disease as suggested by the size of the Golgi apparatus. *Neuroscience* 59, 871–880. doi: 10.1016/0306-4522(94)90291-7

Satoh, A., Wang, Y., Malsam, J., Beard, M. B., and Warren, G. (2003). Golgin-84 is a rab1 binding partner involved in Golgi structure. *Traffic* 4, 153–161. doi: 10.1034/j.1600-0854.2003.00103.x

Shorter, J., and Warren, G. (1999). A role for the vesicle tethering protein, p115, in the post-mitotic stacking of reassembling Golgi cisternae in a cell-free system. *J. Cell Biol.* 146, 57–70. doi: 10.1083/jcb.146.1.57

Sohda, M., Misumi, Y., Yamamoto, A., Nakamura, N., Ogata, S., Sakisaka, S., et al. (2010). Interaction of Golgin-84 with the COG complex mediates the intra-Golgi retrograde transport. *Traffic* 11, 1552–1566. doi: 10.1111/j.1600-0854.2010.01123.x

South, F. E. (1972). "Hibernation and hypothermia, perspectives and challenges," in *Symposium Held at Snow-mass-at-Aspen, Colorado, January 3-8, 1971* (Amsterdam, New York, NY: Elsevier Pub. Co).

Stieber, A., Mourelatos, Z., and Gonatas, N. K. (1996). In Alzheimer's disease the Golgi apparatus of a population of neurons without neurofibrillary tangles is fragmented and atrophic. *Am. J. Pathol.* 148, 415–426.

Stieler, J. T., Bullmann, T., Kohl, F., Tøien, Ø., Brückner, M. K., Härtig, W., et al. (2011). The physiological link between metabolic rate depression and tau phosphorylation in mammalian hibernation. *PLoS ONE* 6:e14530. doi: 10.1371/journal.pone.0014530

Stopa, E. G., Gonzalez, A. M., Chorsky, R., Corona, R. J., Alvarez, J., Bird, E. D., et al. (1990). Basic fibroblast growth factor in Alzheimer's disease. *Biochem. Biophys. Res. Commun.* 171, 690–696. doi: 10.1016/0006-291X(90)91201-3

Storrie, B., White, J., Röttger, S., Stelzer, E. H., Suganuma, T., and Nilsson, T. (1998). Recycling of golgi-resident glycosyltransferases through the ER reveals a novel pathway and provides an explanation for nocodazole-induced Golgi scattering. *J. Cell Biol.* 143, 1505–1521.

Storrie, B., and Yang, W. (1998). Dynamics of the interphase mammalian Golgi complex as revealed through drugs producing reversible Golgi disassembly. *Biochim. Biophys. Acta* 1404, 127–137.

Strumwasser, F. (1959). Thermoregulatory, brain and behavioral mechanisms during entrance into hibernation in the squirrel, Citellus beecheyi. *Am. J. Physiol.* 196, 15–22.

Su, B., Wang, X., Drew, K. L., Perry, G., Smith, M. A., and Zhu, X. (2008). Physiological regulation of tau phosphorylation during hibernation. *J. Neurochem.* 105, 2098–2108. doi: 10.1111/j.1471-4159.2008.05294.x

Tatebayashi, Y., Iqbal, K., and Grundke-Iqbal, I. (1999). Dynamic regulation of expression and phosphorylation of tau by fibroblast growth factor-2 in neural progenitor cells from adult rat hippocampus. *J. Neurosci.* 19, 5245–5254.

Tatebayashi, Y., Lee, M. H., Li, L., Iqbal, K., and Grundke-Iqbal, I. (2003). The dentate gyrus neurogenesis: a therapeutic target for Alzheimer's disease. *Acta Neuropathol.* 105, 225–232. doi: 10.1007/s00401-002-0636-3

van Breukelen, F., and Martin, S. L. (2001). Translational initiation is uncoupled from elongation at 18 degrees C during mammalian hibernation. *Am. J. Physiol. Regul. Integr. Comp. Physiol.* 281, R1374–R1379.

van Breukelen, F., and Martin, S. L. (2002). Reversible depression of transcription during hibernation. *J. Comp. Physiol. B.* 172, 355–361. doi: 10.1007/s00360-002-0256-1

Vincent, I., Rosado, M., and Davies, P. (1996). Mitotic mechanisms in Alzheimer's disease? *J. Cell Biol.* 132, 413–425.

von der Ohe, C. G., Darian-Smith, C., Garner, C. C., and Heller, H. C. (2006). Ubiquitous and temperature-dependent neural plasticity in hibernators. *J. Neurosci.* 26, 10590–10598. doi: 10.1523/JNEUROSCI.2874-06.2006

von der Ohe, C. G., Garner, C. C., Darian-Smith, C., and Heller, H. C. (2007). Synaptic protein dynamics in hibernation. *J. Neurosci.* 27, 84–92. doi: 10.1523/JNEUROSCI.4385-06.2007

Walker, J. M., Glotzbach, S. F., Berger, R. J., and Heller, H. C. (1977). Sleep and hibernation in ground squirrels (Citellus spp): electrophysiological observations. *Am. J. Physiol.* 233, R213–R221.

Walkley, S. U., and Suzuki, K. (2004). Consequences of NPC1 and NPC2 loss of function in mammalian neurons. *Biochim. Biophys. Acta* 1685, 48–62. doi: 10.1016/j.bbalip.2004.08.011

Wang, Y., Satoh, A., and Warren, G. (2005). Mapping the functional domains of the Golgi stacking factor GRASP65. *J. Biol. Chem.* 280, 4921–4928. doi: 10.1074/jbc.M412407200

Wang, Y., Seemann, J., Pypaert, M., Shorter, J., and Warren, G. (2003). A direct role for GRASP65 as a mitotically regulated Golgi stacking factor. *EMBO J.* 22, 3279–3290. doi: 10.1093/emboj/cdg317

Yadav, S., and Linstedt, A. D. (2011). Golgi positioning. *Cold Spring Harb. Perspect. Biol.* 3:a005322. doi: 10.1101/cshperspect.a005322

Yamaguchi, F., Morrison, R. S., Gonatas, N. K., Takahashi, H., Sugisaki, Y., and Teramoto, A. (2003). Identification of MG-160, a FGF binding medial Golgi sialoglycoprotein, in brain tumors: an index of malignancy in astrocytomas. *Int. J. Oncol.* 22, 1045–1049. doi: 10.3892/ijo.22.5.1045

Zhegunov, G. F. (1988). [Protein synthesis in cardiac cells and the ultrastructural dynamics of cardiomyocytes of hibernating animals during the hibernation cycle]. *Tsitologiia* 30, 157–162.

Zhou, F., Zhu, X., Castellani, R. J., Stimmelmayr, R., Perry, G., Smith, M. A., et al. (2001). Hibernation, a model of neuroprotection. *Am. J. Pathol.* 158, 2145–2151. doi: 10.1016/S0002-9440(10)64686-X

Zhou, Z., Zuber, M. E., Burrus, L. W., and Olwin, B. B. (1997). Identification and characterization of a fibroblast growth factor (FGF) binding domain in the cysteine-rich FGF receptor. *J. Biol. Chem.* 272, 5167–5174. doi: 10.1074/jbc.272.8.5167

Zuber, M. E., Zhou, Z., Burrus, L. W., and Olwin, B. B. (1997). Cysteine-rich FGF receptor regulates intracellular FGF-1 and FGF-2 levels. *J. Cell. Physiol.* 170, 217–227.

Conflict of Interest Statement: The authors declare that the research was conducted in the absence of any commercial or financial relationships that could be construed as a potential conflict of interest.

The handling editor Agustin González declares that, despite being affiliated to the same university as the author Alberto Muñoz, the review process was handled objectively and no conflict of interest exists.

Selective presence of a giant saccular organelle in the axon initial segment of a subpopulation of layer V pyramidal neurons

Alejandro Antón-Fernández, Pablo Rubio-Garrido, Javier DeFelipe & Alberto Muñoz

Brain Structure and Function

ISSN 1863-2653

Brain Struct Funct
DOI 10.1007/s00429-013-0689-1

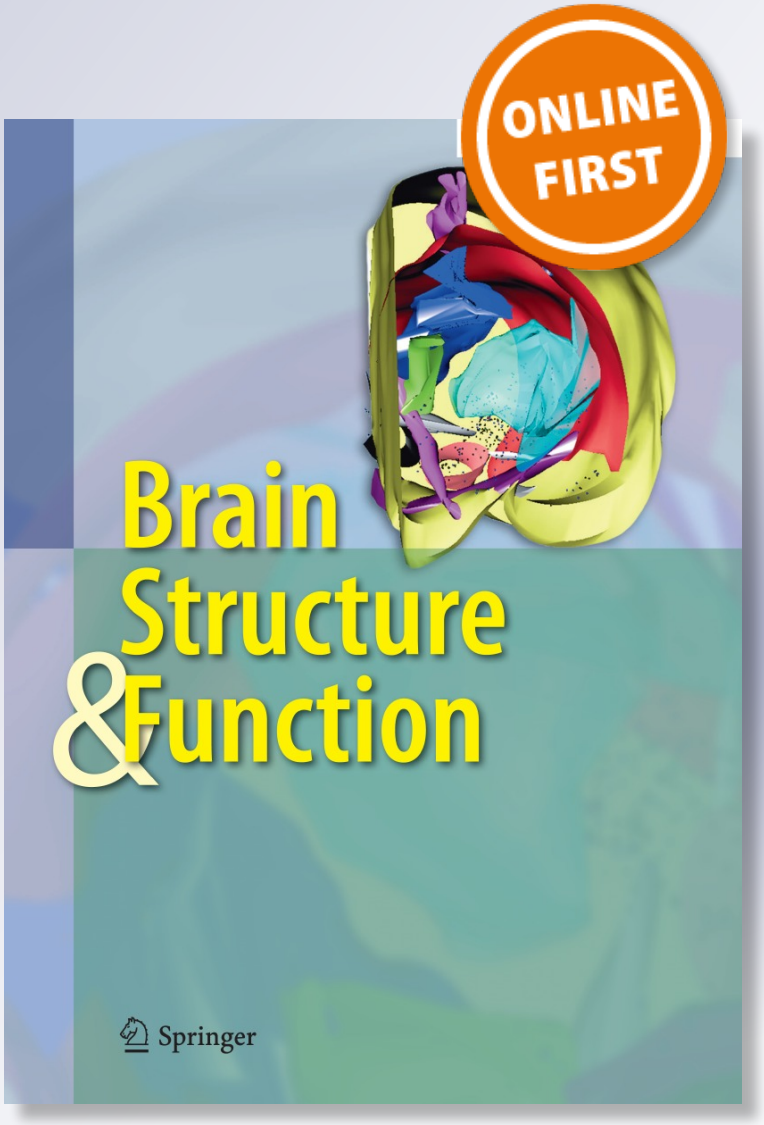

Springer

Brain Struct Funct
DOI 10.1007/s00429-013-0689-1

ORIGINAL ARTICLE

Selective presence of a giant saccular organelle in the axon initial segment of a subpopulation of layer V pyramidal neurons

Alejandro Antón-Fernández · Pablo Rubio-Garrido · Javier DeFelipe · Alberto Muñoz

Received: 12 July 2013 / Accepted: 6 December 2013

Abstract Recently it has been shown that a giant saccular organelle (GSO) of unknown function is present in the axon initial segment (AIS) of an uncharacterized population of pyramidal cells of the rodent neocortex. Using tract-tracing methods and immunocytochemistry, in the present study we show that in rodents this GSO is present in the AIS of subpopulations of layer V pyramidal neurons projecting to various subcortical, non-thalamic targets, including the spinal cord. GSO-containing neurons express SMI32 and some of them are under the control of the Thy-1 gene promoter. In addition, our results demonstrate that the GSO expresses the inositol 1,4,5-triphosphate receptor 1 (IP_3R1) and the sarco (endo) plasmic reticulum Ca^{2+} ATPase 2, both in rodent and human neocortex. These results indicate the involvement of the GSO in the regulation of Ca^{2+} levels in the AIS in a particular subpopulation of layer V neurons that give rise to subcortical non-thalamic descending projections.

Keywords Calcium · Cerebral cortex · Corticospinal tract · SERCA · Synaptopodin · IP_3R1

A. Antón-Fernández · J. DeFelipe · A. Muñoz
Instituto Cajal, CSIC, 28002 Madrid, Spain

A. Antón-Fernández · J. DeFelipe · A. Muñoz (✉)
Laboratorio Cajal de Circuitos Corticales, Centro de Tecnología Biomédica (CTB), Universidad Politécnica Madrid, Pozuelo de Alarcón, 28223 Madrid, Spain
e-mail: amunozc@bio.ucm.es

P. Rubio-Garrido
Departamento de Anatomía, Histología y Neurociencia, Facultad de Medicina, Universidad Autónoma, Madrid, Spain

J. DeFelipe
CIBERNED, Centro de Investigación Biomédica en Red de Enfermedades Neurodegenerativas, Madrid, Spain

A. Muñoz
Departamento de Biología Celular, Universidad Complutense, 28040 Madrid, Spain

Introduction

The axon initial segment (AIS) is a complex axonal domain rich in voltage-gated Na^+, K^+ and Ca^{2+} channels, and is involved in the initiation and propagation of action potentials (Rasband 2010; Debanne et al. 2011; Bender et al. 2012; Kole and Stuart 2012). During action potential generation, the activity-dependent transient elevation of AIS Ca^{2+} levels modulates the generation and timing of action potentials in the AIS (Yu et al. 2008, 2010; Bender and Trussell 2009; Bender et al. 2012). Ca^{2+} entry also influences activity-driven changes in the length and position of the AIS (Grubb and Burrone 2010; Grubb et al. 2011; Evans et al. 2013), which are thought to regulate neuronal excitability (Grubb et al. 2011; Kuba et al. 2010; Kuba 2012). In addition, the concentration of Ca^{2+} must be tightly controlled to avoid proteolysis of the AIS cytoskeleton and to prevent the loss of ion channels in the AIS (Schafer et al. 2009). In most neocortical and hippocampal principal cells, Ca^{2+} level regulation in the AIS is thought to involve the cisternal organelle (Benedeczky et al. 1994; Bas Orth et al. 2007; Sanchez-Ponce et al. 2011a), which consists of stacks of membranous cisternae derived from the smooth endoplasmic reticulum (Palay et al. 1968; Peters et al. 1968; Jones and Powell 1969; Sloper and Powell 1979; Kosaka 1980; Somogyi et al. 1983; Benedeczky et al. 1994; Jedlicka et al. 2008). The cisternal organelle is endowed with the SER Ca^{2+} ATPase

Published online: 21 December 2013

(SERCA) type Ca^{2+} pump (Benedeczky et al. 1994) and the inositol 1,4,5-trisphosphate (IP_3) receptor Ca^{2+} channel (IP_3R) type 1 (Sanchez-Ponce et al. 2011a) and expresses the acting binding proteins synaptopodin and α-actinin (Bas Orth et al. 2007; Sanchez-Ponce et al. 2011a, b).

We have recently described the presence of a conspicuous elongated organelle termed the giant saccular organelle (GSO) in the AIS of an uncharacterized subpopulation of layer V pyramidal neurons (Sanchez-Ponce et al. 2011b). This GSO can extend along the whole length of the AIS; is made up of a discrete number of long tubules and flattened sacs aligned in parallel with the long axis of the axon; and seems to be associated with microtubules and microfilaments (Sanchez-Ponce et al. 2011b). It is not yet known what the function of the GSO is in the AIS of layer V neurons. Whether or not it is involved in Ca^{2+} regulation, as proposed for the cisternal organelle in other neuronal populations (Benedeczky et al. 1994; Bas Orth et al. 2007; Sanchez-Ponce et al. 2011a), also remain unknown. In the present study, we tested—both in the rodent and human cerebral cortex—whether the saccular organelle expresses molecules such as SERCA and IP_3R1, that is, molecules involved in Ca^{2+} uptake and release.

Neocortical layer V includes a variety of pyramidal cell types, which can be divided into two main classes according to their dendritic morphology; electrical and neurochemical properties; axonal projections; the thalamocortical input they receive; and the location of their soma (Klein et al. 1986; Larkman and Mason 1990; Hallman et al. 1988; Markram et al. 1997; Voelker et al. 2004; Arlotta et al. 2005; Molnar and Cheung 2006; Molyneaux et al. 2007; Hattox and Nelson 2007). These two classes are thick-tufted (or type I) and thin-tufted (or type II) pyramidal cells. Thick-tufted pyramidal cells are characterized by the location of their somata in the lower part of layer V (Vb); their tendency to discharge a short burst of spikes at the beginning of a spike train; and their projections to subcortical targets such as the striatum, superior colliculus, brainstem and spinal cord. Thin-tufted pyramidal cells are characterized by the location of their somata in the superficial part of layer V (Va); discharge spikes with no adaptation; and projections to the contralateral cortex and the ipsilateral striatum.

In the present study, we combine tract tracing and immunocytochemistry to characterize the population of layer V pyramidal neurons containing the GSO. From the neurochemical and genetic markers available that label specific subtypes of pyramidal neurons in layer V, including GFP-positive layer V transgenic lines, here we have chosen to use antibodies to selective neurofilaments (SMI32) that are expressed in type I cells (Molnar and Cheung 2006). In addition, we have used a transgenic mouse model (Thy1-eYFP-H) in which YFP is constitutively expressed under the control of Thy-1 gene promoter (Feng et al. 2000) and label different neuronal populations in layer V, but particularly corticospinal neurons (Porrero et al. 2010). We found that the GSO is probably involved in the Ca^{2+} level regulation in the AIS of a particular subpopulation of layer V neurons that give rise to subcortical non-thalamic descending projections.

Materials and methods

For tract-tracing experiments, Wistar rats (males, aged 1–2 months) were anesthetized with isoflurane (0.5–2 % in oxygen) and were placed in a stereotaxic apparatus (David Kopf Instruments, Tujunga, CA, USA). After a small craniotomy, the retrograde tracer Fast Blue (0.2 % w/vol. solution in cacodylate buffer, 0.1 M, pH 7.3; FB, diamidino compound 253/50, Dr Illing &Co. KG, Groβ-Umstadt, Germany) was pressure injected (Picospritzer II General Valve Corporation, Fairfield, NJ, USA) through glass micropipettes (30-μm outer diameter) into the cerebral cortex ($n = 3$), the thalamus ($n = 2$), the striatum ($n = 2$), the superior colliculus ($n = 2$), the pons ($n = 2$) and the thoracic spinal cord ($n = 3$). The Paxinos and Watson atlas (Paxinos and Watson 2007) was used as reference to localize the stereotaxic injection coordinates. The pipette was left in place for 10 min before extraction. In all cases, the animals were allowed to survive for 7–15 days and were then sacrificed.

For immunocytochemical experiments, C57BL/6 mice ($n = 8$ males, aged between 30 and 32 days) and Wistar rats ($n = 5$ males, aged 30 days) were used. In all cases, animals were sacrificed by a lethal intraperitoneal injection of sodium pentobarbital (0.08 mg/g, i.p.), and were then perfused intracardially with a saline solution followed by 4 % paraformaldehyde in 0.1 M phosphate buffer (PB, pH 7.4). All experiments were performed in accordance with the guidelines established by the European Union regarding the use and care of laboratory animals (86/609/EEC). The brain of each animal was removed, postfixed by immersion in the same fixative for 24 h at 4 °C, and serial coronal sections (50-μm thick) were obtained with a Vibratome (St Louis, MO, USA). The sections from both normal and tracer-injected animals were then processed for immunocytochemical staining, and some adjacent sections to those used for immunocytochemistry were Nissl stained. In addition, sections from Thy1-eYFP line H mice (Feng et al. 2000), from Jackson labs [B6.Cg-Tg (Thy-YFP-H) 2Jrs/J], which were used in previous studies (Diaz-Alonso et al. 2012), were kindly donated by the laboratory of Dr. Guzmán and Dr. Galve-Roperh (Dept. Biochemistry, Fac. Biology, Complutense University, Madrid, Spain).

Human brain tissue was obtained by surgical resection from the anterolateral temporal cortex from one male

(H48) and one female (H136) patient diagnosed with intractable temporal lobe epilepsy. In addition, tissue from the supplementary motor cortex of a 35-year-old female patient diagnosed with supplementary motor area (SMA) epilepsy was used. Part of this material was used in previous studies (Arellano et al. 2004; Alonso-Nanclares et al. 2011) in which detailed clinical, surgical and neuropathological information from patients was reported. Presurgical evaluation of patients was carried out with scalp electroencephalography (EEG), interictal single-photon emission computer tomography, magnetic resonance imaging (MRI) 1.5 T, and video-electroencephalography using 19 scalp electrodes placed according to the international 10–20 system and foramen-ovale electrodes. Individual informed consent was obtained for all patients, following prior approval by the ethical committee of the Hospital de la Princesa (Madrid, Spain). During surgery, electrocorticography was performed with a grid of 4 × 5 electrodes embedded in Sylastic. The electrodes (1.2 mm in diameter) were placed directly over the exposed lateral temporal cortex with a 1 cm center-to-center interelectrode distance (Add-Tech, Racine, WI, USA). Recordings were taken at 400 Hz with a bandwidth of 1–70 Hz over a minimum period of 20 min., using a 32-channel Easy EEG II system (Cadwell, Kennewick, WA, USA). Spiking areas were defined as electrodes showing spikes (<80 ms) or sharp waves (80–200 ms) with a mean frequency >1 spike/min. Non-spiking areas were defined as electrodes where no spikes, sharp waves or slow activity was observed. Photographs of the placement of the electrodes were taken before grid removal, and the anatomical locations of the spiking and non-spiking areas were defined before tissue excision. In the temporal lobe epilepsy patients, tailored temporal lobectomy and amygdalohippocampectomy was performed under electrocorticography guidance (for further details see (Arion et al. 2006)). After surgery, the lateral neocortex and mesial structures were subjected to standard neuropathological assessment. The lateral neocortical biopsies were histologically normal, whereas the hippocampal formation displayed neuronal loss and gliosis (hippocampal sclerosis). In the present study, only normal non-spiking areas of the lateral neocortex were used. No neuropathological alterations were found in the neocortex from the patient with SMA. Biopsy samples were fixed in cold 4 % paraformaldehyde in 0.1 M phosphate buffer at pH 7.4 (PB) for 4–5 h at 4 °C. Vibratome sections (100-µm thick) were processed for immunocytochemistry.

In all cases, for immunofluorescence staining, the sections were first rinsed in PB and preincubated for 1 h at room temperature in a stock solution containing 3 % normal serum of the species in which the secondary antibodies were raised (Vector Laboratories, Burlingame, CA, USA) diluted in PB with Triton X-100 (0.25 %). Thereafter, the sections were incubated for 48 h at 4 °C in the same stock solution containing the following primary antibodies alone or in combination: mouse anti-ankyrin G (1:100, Neuromab 75146, Davis, CA, USA), mouse anti-SERCA (1:500 ABR Golden, CO, USA), rabbit anti-IP_3R1 (1:250, Synaptic Systems, Goettingen, Germany), rabbit anti-synaptopodin (1:250, Sigma S9442), mouse anti-synaptopodin (1:10, Acris, Herford, Germany), mouse anti-SMI32 (1:4,000, Sternberger, MA, USA), rabbit anti-vesicular GABA transporter (1:2,000, VGAT, Synaptic Systems) and rabbit anti-βIV Spectrin (1:1,000, a gift from Dr. M. N. Rasband (Dept. of Neuroscience, Baylor College of Medicine, Houston, USA)). We used mouse anti-GM130 (1: 50 BD, Franklin Lakes NJ, USA) and rabbit anti-GRP78 BiP (1: 100, Abcam, Cambridge, UK) as markers for the Golgi complex and the endoplasmic reticulum, respectively. After rinsing in PB, the sections were incubated for 2 h at room temperature in the appropriate combinations of Alexa 488-, Alexa 594- or Alexa 652-conjugated goat anti-mouse or goat anti-rabbit antibodies (1:2,000; Molecular Probes, Eugene, OR, USA). Finally, the sections were washed in PB, mounted in antifade mounting medium (Prolong Gold, Invitrogen) and studied by confocal microscopy (Zeiss, 710). Z sections were recorded at 0.2–1 µm intervals through separate channels, and ZEN 2009 software (Zeiss) was then used to construct composite images from each optical series by combining the images recorded through both channels. Adobe Photoshop (CS4) software was used to compose figures and Image J software was used to quantify, either in confocal projection images or conventional fluorescence images, the area occupied by the soma of neurons containing a synaptopodin-immunoreactive GSO or filled with Fast Blue in tract-tracing experiments. For quantification of material from tract-tracing experiments, we used tissue from one case per injection site. Statistical differences between groups of values were analyzed using SPSS16.0 software.

For DAB immunostaining, series of sections from two additional rat brains were incubated in stock solution containing rabbit anti-synaptopodin (1:250, Sigma). The sections were rinsed in PB before being incubated in biotinylated goat anti-rabbit secondary antibodies (1:200; Vector), and then processed using a Vectastain ABC immunoperoxidase kit (Vector Laboratories). Antibody labeling was visualized with 0.05 % 3,3′-diaminobenzidine tetrahydrochloride (Sigma, St Louis, MO, USA) and 0.01 % hydrogen peroxide. The sections were rinsed in PB, mounted on glass slides, dehydrated, cleared with xylene, and coverslipped.

Results

In a previous study using immunocytochemistry for synaptopodin and α-actinin (Sanchez-Ponce et al. 2011b), we

described the presence of a giant saccular organelle (GSO) in the AIS of layer V neurons. Here, to gain insight into the relative abundance and distribution patterns of GSO-containing neurons in different cortical areas, we have analyzed the whole rat brain using the Paxinos and Watson atlas (Paxinos and Watson 2007) as a reference to delineate the different cortical areas. As depicted in Fig. 1, we found that GSO-containing neurons generally represented a small number of layer V pyramidal cells in all cortical areas that were usually found in the upper part of this layer. However, some cortical areas showed a relatively large number of GSO-containing pyramidal neurons as compared to other areas. In order to perform a systematic study and to obtain quantitative data, we analyzed their distribution in 50-µm-thick coronal sections, spaced 300 µm apart throughout the right hemisphere of a rat brain immunostained for synaptopodin. The highest percent of the GSOs found corresponded to sensory-motor cortex areas, although GSO-containing layer V neurons were also occasionally found in areas of the orbitofrontal, cingulate, insular, retrosplenial, perirhinal, temporal associative, auditory and visual cortices (Fig. 1). Since GSOs were more frequently found in the AIS of layer V pyramidal neurons in somatosensory and motor cortex, we focused on these regions for the rest of the study. However, it is important to keep in mind that, even in these latter cortical areas, the number of GSOs is relatively low. Furthermore, there are some important technical limitations in performing the experiments outlined in this work. One of the greatest drawbacks is that the AISs have to extend relatively close to the surface of the sections, within the narrow depth where the penetration of the immunoreagents is optimal. In addition, in material from tract-tracing experiments, the retrogradely labeled cells in this narrow zone are relatively few. Thus, the number of AISs examined for each set of experiments described below is relatively low due to these limitations.

According to previous studies, numerous YFP-labeled neurons were found in layer V of the sensory-motor neocortex of Thy-1-eYFP mice (Porrero et al. 2010) (Fig. 2). In order to know whether they include neurons containing the GSO, we performed double immunostaining for synaptopodin and ankyrin G (as an AIS marker) in brain sections of Thy-1-eYFP mice (Fig. 3a–d). In somatosensory and motor cortical areas, we found that from a total of 129 pyramidal neurons containing a GSO (as identified by the presence of an elongated synaptopodin-ir process inside ankG-ir AIS), 43 (33.3 %) were eYFP-positive whereas the remaining 86 (66.7 %) were eYFP-negative neurons. In addition, the AISs from most (74.7 %, $n = 359$) Thy-1-positive neurons lacked a GSO. These results indicate that the expression of the Thy-1 gene seems not to be directly related to the presence of the GSO in the AIS of layer V pyramidal cells.

Immunocytochemistry using SMI32 antibodies labeled numerous cell bodies in layer V in different areas of the rat and mouse neocortex (Fig. 2c, d), as well as neurons in other cortical layers. According to previous studies (Molnar and Cheung 2006), SMI32-ir neurons in layer V correspond to type I pyramidal neurons. In SMI-32/synaptopodin double-immunostained sections (Fig. 3e–j), we found that virtually all neurons containing a GSO in the AIS were SMI32-ir (mouse 100 %, $n = 220$; rat 97.6 %,

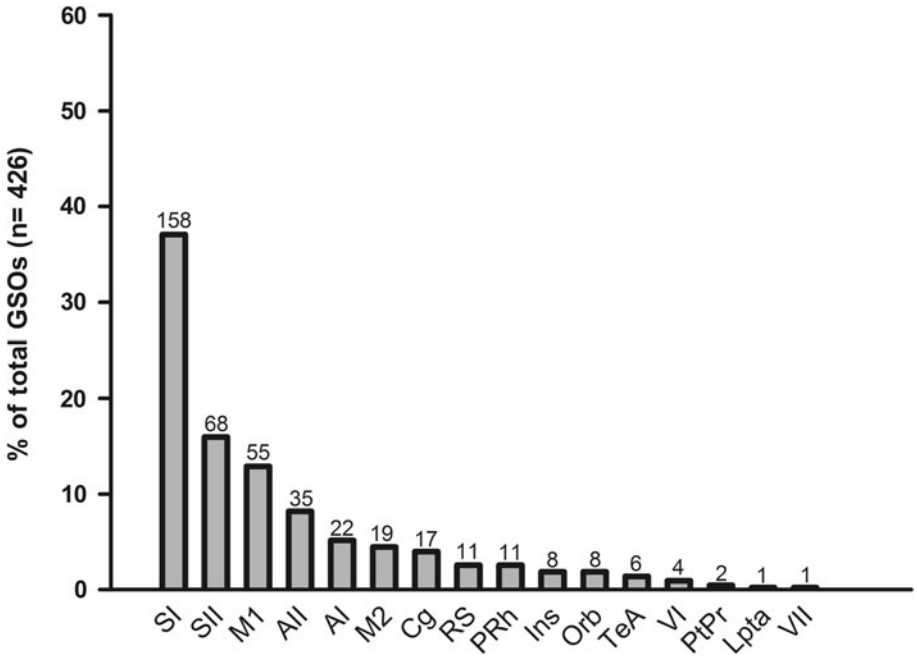

Fig. 1 Histogram showing the relative abundance (number and percentage) of synaptopodin-ir GSOs in layer V of different areas in the right hemisphere of the cerebral cortex of a rat brain. *AI* primary auditory cortex, *AII* secondary auditory cortex, *Gg* cingulate cortex, *Ins* insular cortex, *LPtA* lateral parietal associative cortex, *M1* primary motor cortex, *M2* secondary motor cortex, *Orb* orbitary cortex, *PRh* perirhinal cortex, *Rs* retrosplenial cortex, *SI* primary somatosensory cortex, *SII* secondary somatosensory cortex, *TeA* temporal associative cortex, *VI* primary visual cortex, *VII* secondary visual cortex

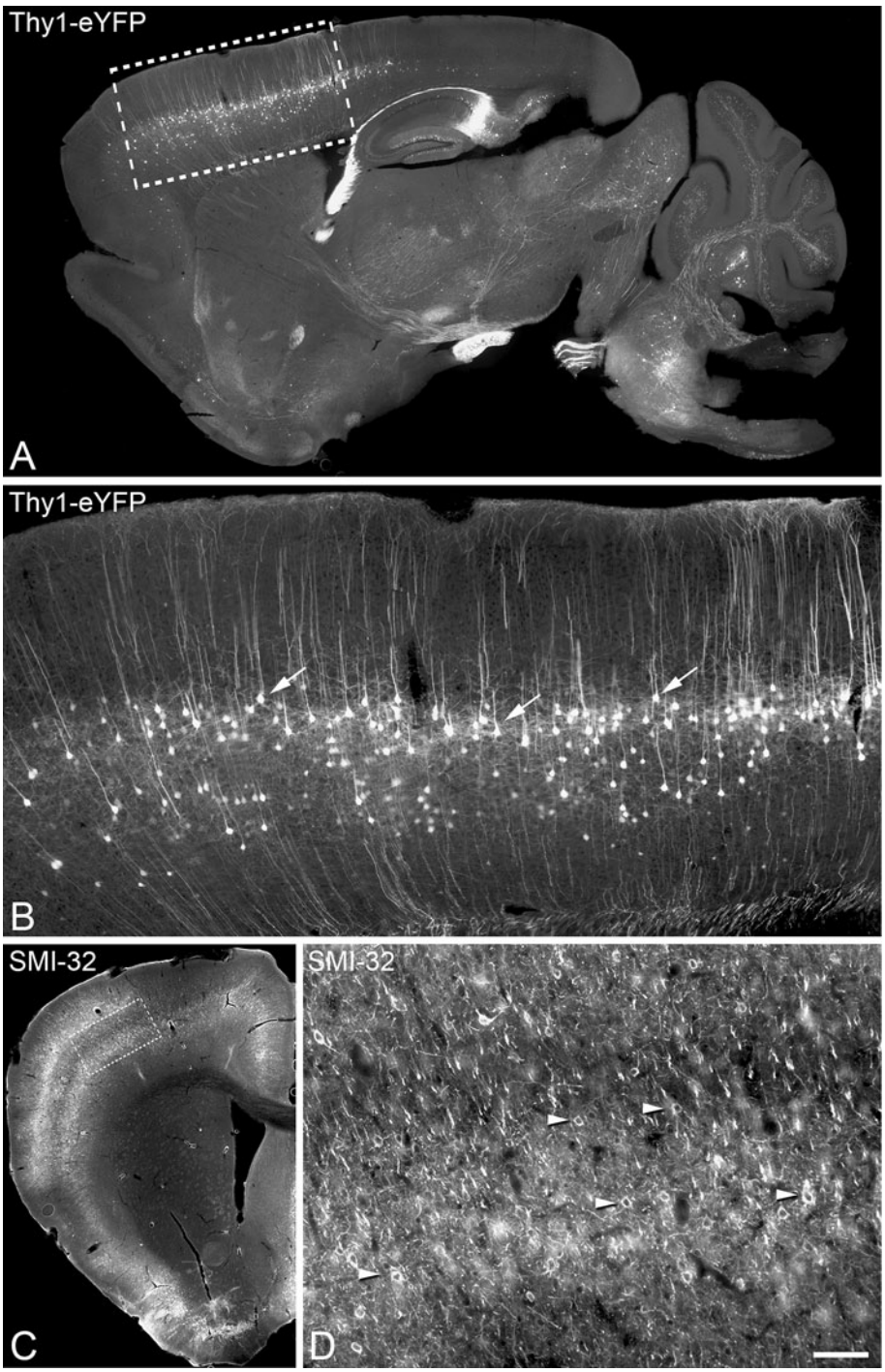

Fig. 2 Low-power photomicrographs of parasagittal (**a**, **b**) and coronal (**c**, **d**) sections from the brains of a Thy1-eYFP mouse (**a**, **b**) and from a normal mouse (**c**, **d**), showing eYFF-positive (*arrows* in **b**) and SMI32-immunoreactive (*arrowheads* in **d**) neurons in layer V. *Squared* areas in A and C are shown at higher magnification in B and D, respectively. *Scale bar* (in **d**): 710 μm in **a**; 175 μm in **b**; 715 μm in **c**; 135 μm in **d**

$n = 542$). This was corroborated in similar experiments in Thy-1-eYFP mice in which we observed that all neurons endowed with a synaptopodin-ir GSO in the AIS, regardless of whether they were eYFP-positive or -negative, were also immunoreactive for SMI-32 (Fig. 4). These results suggested that GSOs in layer V are restricted to the AIS of type I pyramidal neurons.

We performed further experiments combining immunocytochemistry for synaptopodin with retrograde tract-tracing techniques by injecting Fast Blue (FB) in different brain regions to identify the projection site of the pyramidal cells containing a GSO in their AISs, and the soma size of neurons containing a GSO and/or projecting to the different targets (Figs. 5, 6, 7). In sections immunostained for synaptopodin from animals with FB injections in the primary somatosensory cortex, we examined whether the synaptopodin-ir GSOs belonged to the AIS of contralateral projecting retrogradely labeled neurons in layer V (Fig. 5a–e).

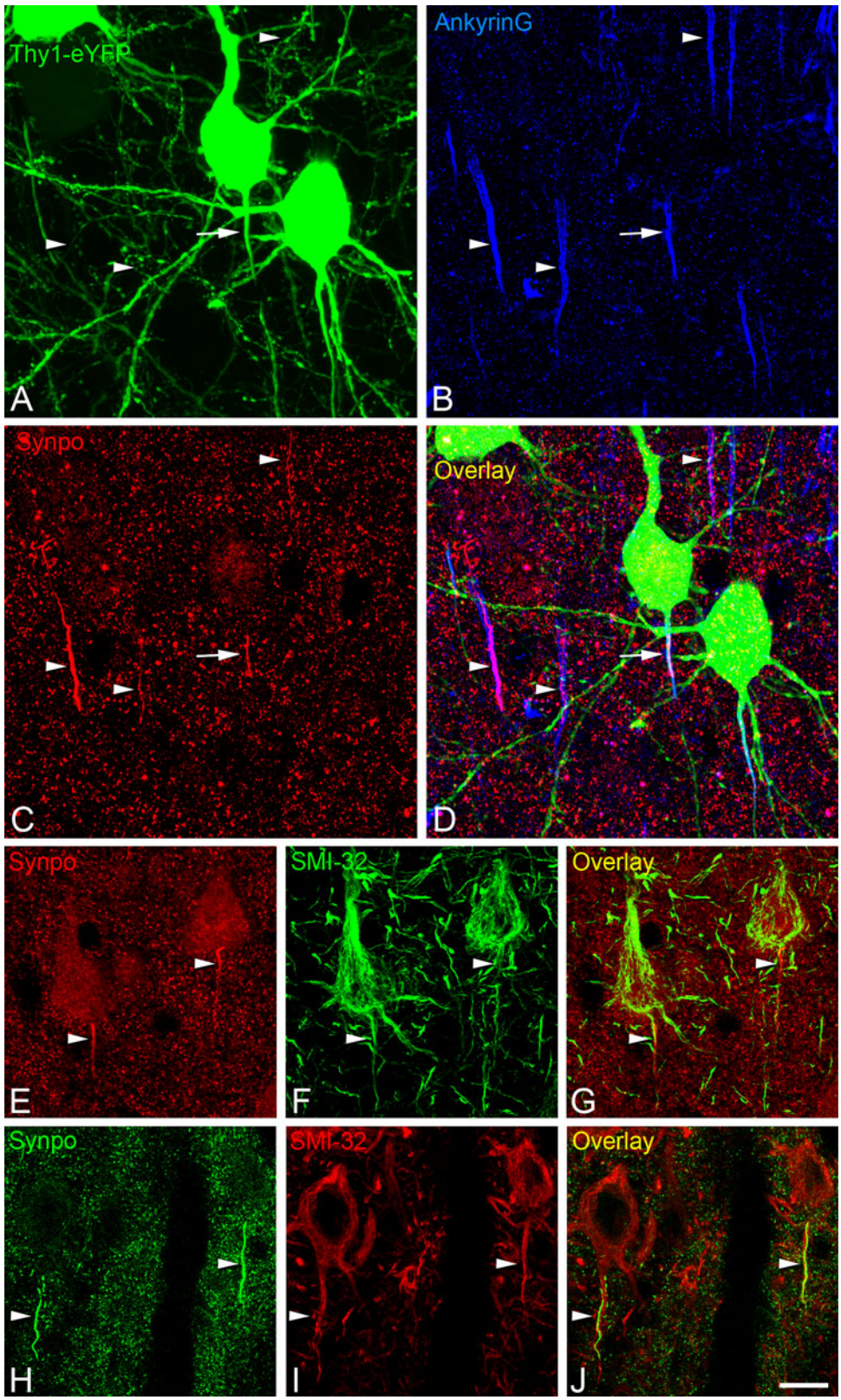

Fig. 3 **a–d** Photomicrographs from a section from a Thy1-eYFP mouse immunostained for synaptopodin (*red*) and ankyrin G (*blue*) showing the presence of synaptopodin-ir GSOs in the AIS (as identified by ankG immunostaining) of both eYFP-positive and eYFP-negative neurons shown by *arrows* and *arrowheads*, respectively. **e–j** Show that synaptopodin-ir GSOs (*arrow heads*) are present in the AIS of layer V SMI32-ir pyramidal neurons both in the mouse **e–g** and rat **h–j** neocortex. *Scale bar* (in **j**): 11 μm in **a–d**; 13 μm in **e–g**; 18 μm in **h–j**

We found that neurons containing synaptopodin-ir GSOs were intermingled with retrogradely labeled neurons. However, the cell bodies of callosal neurons in layer V were significantly smaller than those with an AIS that contained a GSO (Fig. 7f), and we observed no callosal neurons containing a GSO (Fig. 5d–e). Similarly, we

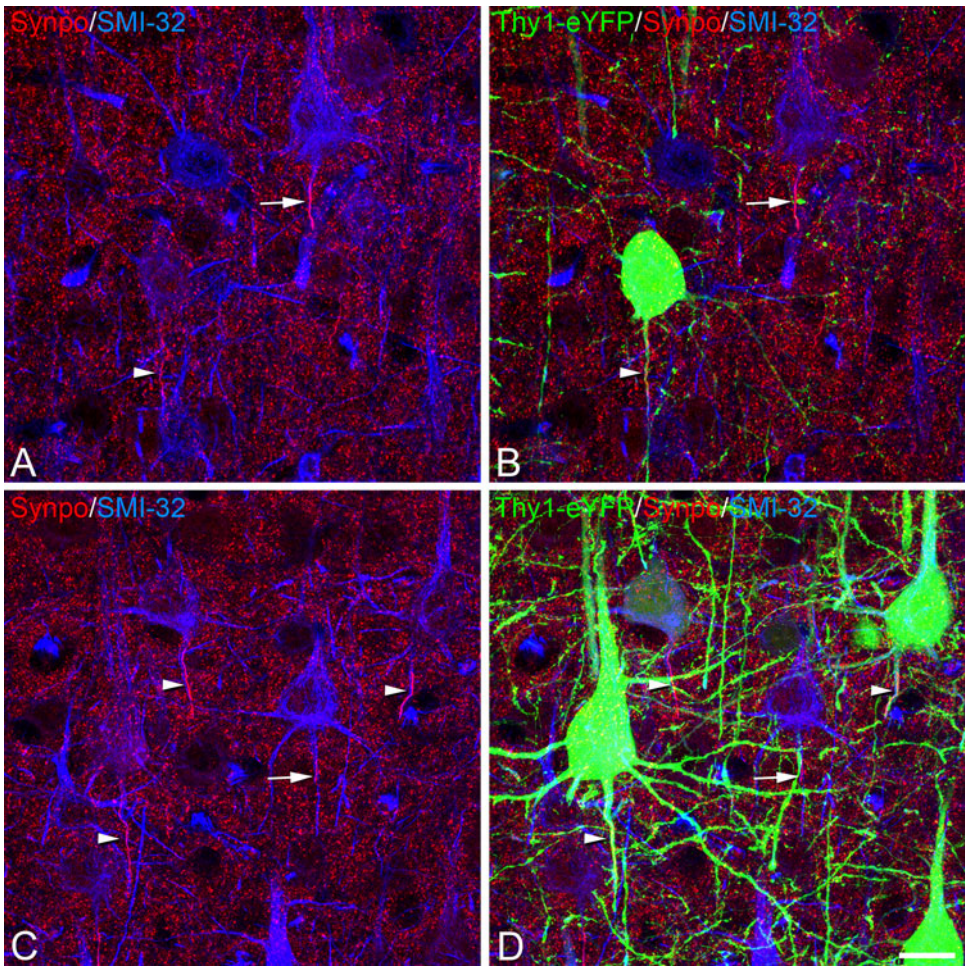

Fig. 4 Pairs **a**–**b**, **c**–**d** of photomicrographs showing examples of sections from Thy1-eYFP mouse neocortex immunostained for synaptopodin (*red*) and SMI32 G (*blue*). Note that neurons containing a synaptopodin-ir GSO are also immunoreactive for SMI32 regardless of whether they are eYFP-positive (*arrowheads*) or eYFP-negative (*arrows*). *Scale bar* (in **d**): 16 μm

performed experiments with FB applications in the ventrobasal complex of the thalamus to examine whether synaptopodin-ir GSOs were present in the AIS of retrogradely labeled corticothalamic neurons in the ipsilateral somatosensory cortex (Fig. 5f, g). Most retrogradely labeled neurons were confined to layer VI and, although some were also found at the border with layer V, no synaptopodin-ir GSOs were observed in corticothalamic neurons (Fig. 5f, g).

We then made large FB injections in a variety of subcortical non-thalamic regions, including the striatum, superior colliculus/mesencephalic tegmentum and pontine nuclei (Fig. 6a, e, i, respectively) and in the thoracic spinal cord (Fig. 7). In all these cases, in sections double immunostained for synaptopodin and for ankyrin G to identify the AIS, we found that a large subpopulation of neurons projecting to these targets contained synaptopodin-ir GSOs in their AISs (53.3 %, $n = 197$; 65.4 %, $n = 78$; 67 %, $n = 97$; 70.6 %, $n = 34$, respectively). Therefore, GSOs represent a specialization of the AIS present in a subpopulation of type I neurons that includes corticostriatal (Fig. 6c, d), corticocolicular (Fig. 6f–h), corticopontine (Fig. 6k, l) and corticospinal (Fig. 7c–e) layer V projecting neurons. We also analyzed the soma size of neurons projecting to the subcortical targets in relation to the presence or absence of a GSO at their AISs. When data from sections from four animals injected either in the striatum, superior colliculus, pontine nuclei or spinal cord was taken together (Fig. 7g), we found that the soma size of layer V neurons was significantly larger in neurons with a GSO (black bars) than in neurons with no GSO (gray bars). However, when data from each injection site (Fig. 7h) was taken separately, this difference was only significant in the case of corticostriatal and corticopontine populations but not in the case of corticocolicular and corticospinal neurons. Statistically significant differences were also found between the soma size of GSO-containing neurons projecting to the striatum and those projecting to the superior colliculus, pontine nuclei or spinal cord. In addition, GSO was absent in subpopulations of corticocolicular, corticopontine and corticospinal neurons (gray bars in Fig. 7h), which have a relatively large soma size as compared with layer V corticocortical or corticothalamic neurons (gray bars in Fig. 7f). Taking all of these results together, they

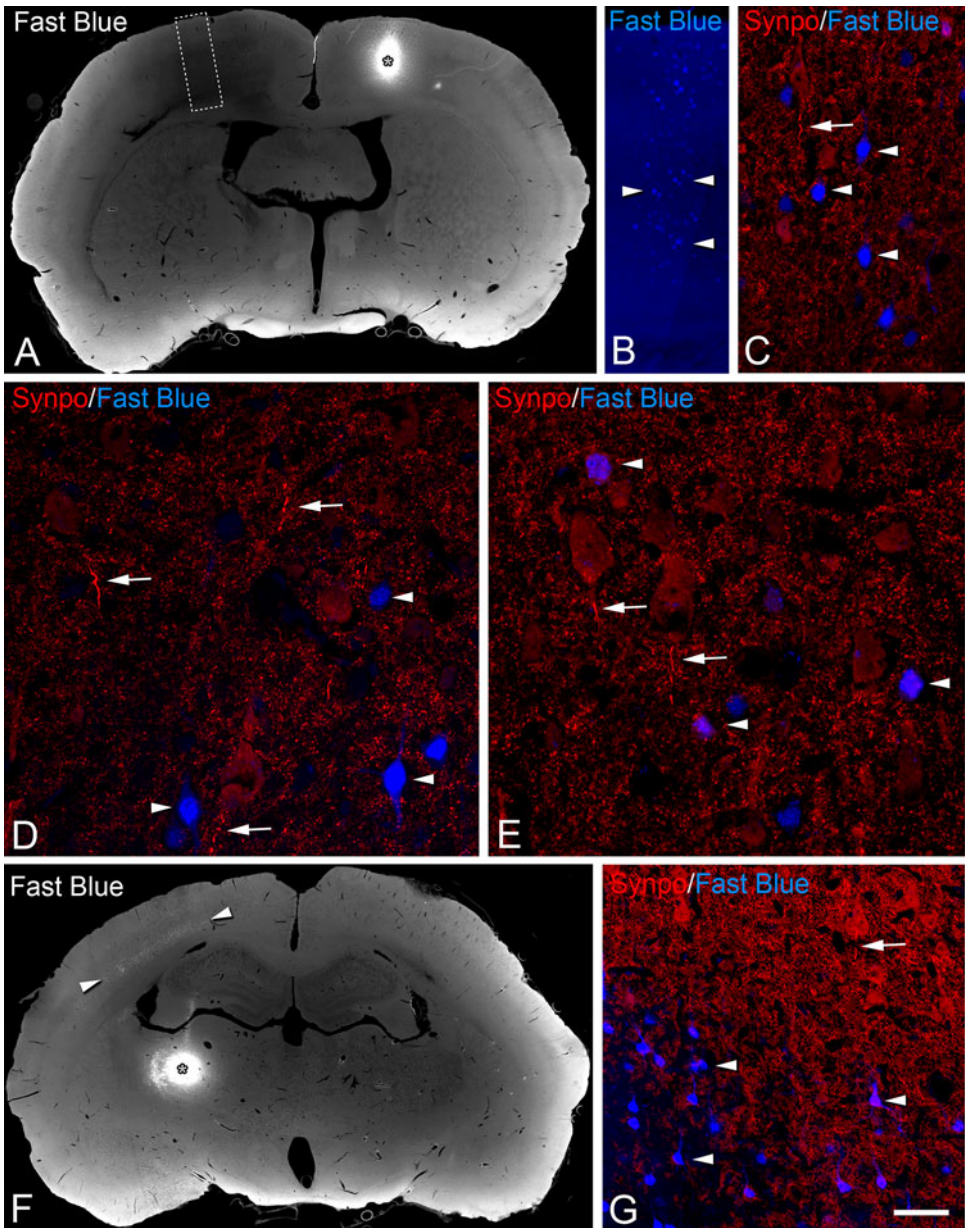

Fig. 5 Photomicrographs showing injection sites (*asterisks* in **a** and **f**) and retrogradely labeled neurons (**b**–**e** and **g**) from experiments with cortical (**a**–**e**) or thalamic (**f** and **g**) Fast Blue injections. The *squared* area in **a** is shown at higher magnification in **b**. Note that neurons with a synaptopodin-ir GSO in layer V (*arrows*) are not labeled with Fast Blue. Conversely, retrogradely labeled callosal and corticothalamic neurons (*arrows*) lack a GSO in the AIS. *Scale bar* (in **g**): 1,350 μm in **a** and **f**; 350 μm in **b**; 37 μm in **c**; 23 μm in **d** and **e**; 40 μm in **g**

indicate that in layer V, GSO is present in some—but not all—type I descending projecting neurons with a large soma size.

In order to gain insight into the possible function of the GSO in the rat and mouse neocortex, we first performed double immunostaining experiments for synaptopodin, as a GSO marker, and GM130 or GRP78 as markers for the Golgi complex (Nakamura et al. 1995) and the endoplasmic reticulum (Shim et al. 2008; Pfaffenbach and Lee 2011), respectively (Fig. 8). In this material it was observed that the GSO is negative for Golgi markers (Fig. 8a–d), whereas it expresses GRP78 indicating that the GSO is part of the endoplasmic reticulum. We then performed double labeling for SERCA or IP_3R1 with synaptopodin (Fig. 9). In this material, immunostaining for SERCA and IP_3R1 yielded diffuse, homogeneous labeling in the cell somata. In addition, SERCA and IP_3R1 antibodies labeled rod-shaped immunoreactive elements that extended along the length of the AISs of a scarce population of layer V pyramidal neurons. These elements were identified as GSOs as they largely colocalized synaptopodin (Fig. 9).

Finally, we also used human brain sections from the supplementary motor cortex (SMA) and from the lateral temporal neocortex. We also found the presence of a synaptopodin-ir GSO in the AIS, as identified by βIV spectrin immunostaining, in a subpopulation of layer V pyramidal neurons (26.6 %, $n = 387$ and 30.6 %, $n = 346$ in SMA and temporal neocortex, respectively; Fig. 10a–f). As previously noted in the rat neocortex (Sanchez-Ponce

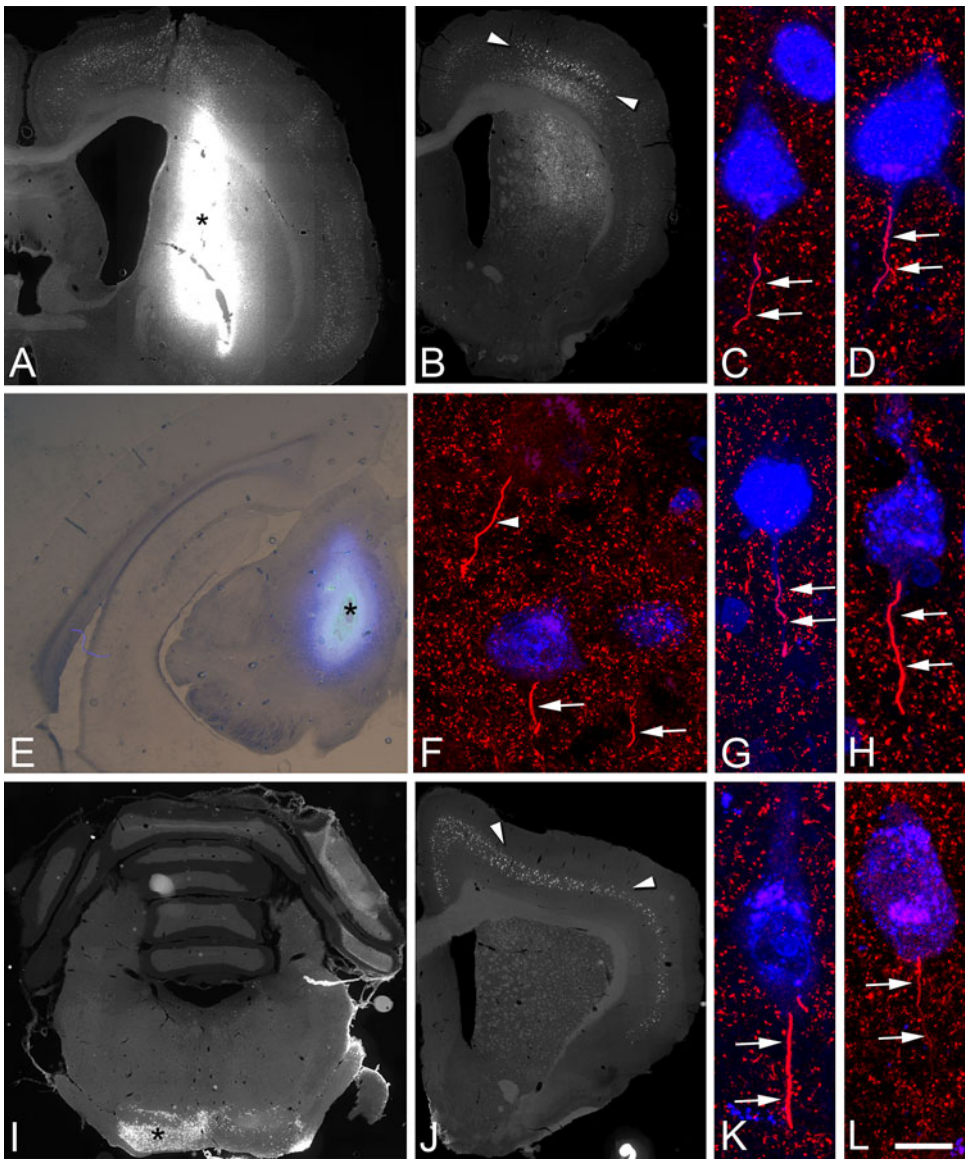

Fig. 6 Photomicrographs from experiments with Fast Blue injections at the striatum (**a**–**d**) superior colliculus (**e**–**h**) or pontine nuclei (**i**–**l**) showing the injection sites (*asterisks* in **a**, **e** and **i**) and retrogradely labeled neurons in layer V of the ipsilateral neocortex. Note the presence of synaptopodin-ir GSO (*arrows*) in corticostriatal (**c**, **d**), corticocolicular (**f**–**h**) and corticopontine (**k**, **l**) neurons. The *arrowhead* in **f** points to a synaptopodin-ir GSO in the AIS of a neuron not labeled for Fast Blue. *Scale bar* (in **l**): 980 μm in **a**, 1,200 μm in **b**; 9 μm in **c**, **h** and **k**; 10 μm in **d**, **g** and **l**; 1,020 μm in **e**; 13 μm in **f**; 1,450 μm in **i**; 1,150 μm in **j**

et al. 2011b), the GSOs were occasionally a continuation of, and probably arose from, similar elongated structures in the cytoplasm at the base of the pyramidal soma. The GSOs sometimes arose in close proximity to the cell nucleus, and switched direction to enter the axon hillock and to funnel into the AIS (see arrowhead in Fig. 10j–l). An interesting difference between the human and rodent neocortex was that, in the case of the human, some GSOs were found in the AIS of large layer III pyramidal neurons, although these pyramidal cells were observed only occasionally. In SERCA and VGAT double immunocytochemically stained sections, in which the AIS was identified by its innervation by vGAT-ir Ch-terminals (Inda et al. 2007), it was found that, in a subpopulation layer V pyramidal neurons both in SMA (Fig. 10g–i) and temporal neocortex (Fig. 10j–l), the AIS contains a GSO that expresses SERCA, as is the case in the rat cortex. These results suggest that the GSO is also involved in the regulation of Ca^{2+} levels in the AIS of a subpopulation of human pyramidal cells located mainly in layer V.

Discussion

The present study shows that the GSO is a prominent specialization of the endoplasmic reticulum that extends through the length of the AIS of a subpopulation of layer V pyramidal neurons found predominantly in sensory-motor areas of the rodent neocortex, as well as in the human supplementary motor cortex and lateral temporal cortex. Layer V pyramidal neurons are physiologically and anatomically heterogeneous and include different subtypes that are generally grouped into two main types: thick-tufted (or type I) neurons that project to subcortical targets such

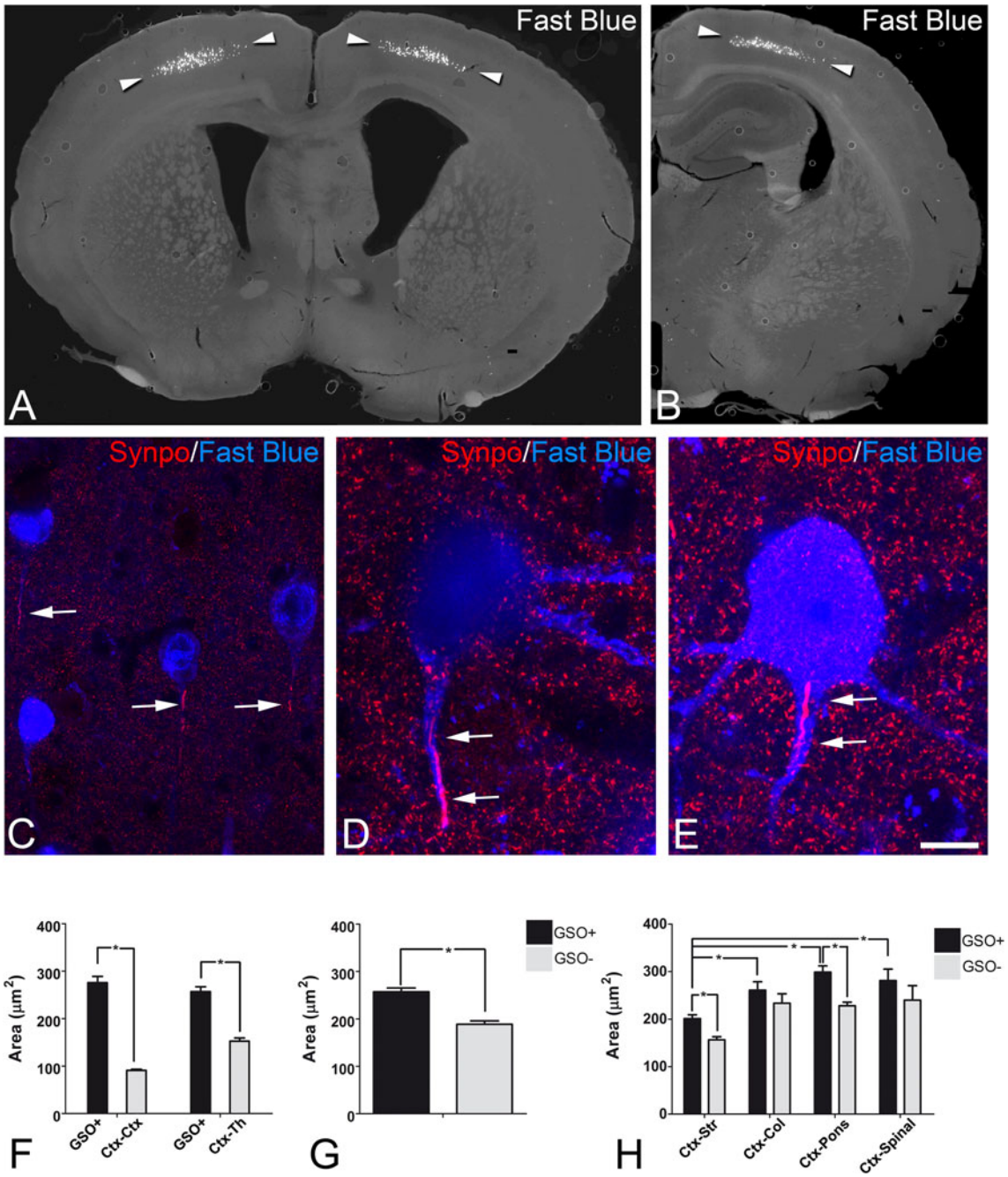

Fig. 7 Photomicrographs from an experiment with a Fast Blue bilateral injection at the dorsal spinal cord at thoracic levels showing retrogradely labeled corticospinal neurons at the motor (**a**) and somatosensory (**b**) cortex. **c**–**e** Show (at higher magnification) the presence of synaptopodin-ir GSO (*arrows*) in the AIS of corticospinal neurons. *Scale bar* (in **e**): 1,250 μm in **a**, 1,260 μm in **b**; 23 μm in **c**; 9.5 μm in **d**; 8.5 μm in **e**. **f**–**h** Histograms showing the mean ± SE values (μm^2) of the cell soma area of different neuronal populations in layer V of sensory-motor cortex. Data in **f** correspond to the experiments shown in Fig. 5 after Fast Blue injections in the cortex (*left*) or the thalamus (*right*). Note that, in both cases, the soma size GSO-containing neurons (*black bars*; $n = 50$, *left*; $n = 41$, *right*) are larger than that of FB-labeled corticocortical (Ctx-Ctx, $n = 87$) or corticothalamic (Ctx-Th, $n = 59$) neurons ($p < 0.001$, Kolmogorov–Smirnov two samples test). **g** shows data from sections from animals injected either in the striatum, superior colliculus, pontine nuclei or spinal cord taken together. The soma size of layer V neurons was significantly larger in neurons with a GSO ($n = 112$) than in neurons with no GSO ($n = 62$) ($p < 0.001$, Kolmogorov–Smirnov two samples test). **h** Illustrates data from each injection site taken separately. In this case, the soma size of layer V neurons was significantly larger in neurons with a GSO than in neurons with no GSO in corticostriatal (GSO+, $n = 38$; GSO−, $n = 33$) and corticopontine (GSO+, $n = 44$; GSO−, $n = 14$) populations, but not in corticocolicular (GSO+, $n = 20$; GSO−, $n = 10$) and corticospinal (GSO+, $n = 10$; GSO−, $n = 5$) neurons ($p < 0.001$, Kolmogorov–Smirnov two samples test). Note that GSO-containing neurons projecting to the striatum are smaller than those projecting to the superior colliculus, pontine nuclei or spinal cord ($p < 0.001$, one way ANOVA of log-transformed data with a Games–Howell Post hoc non-parametric test)

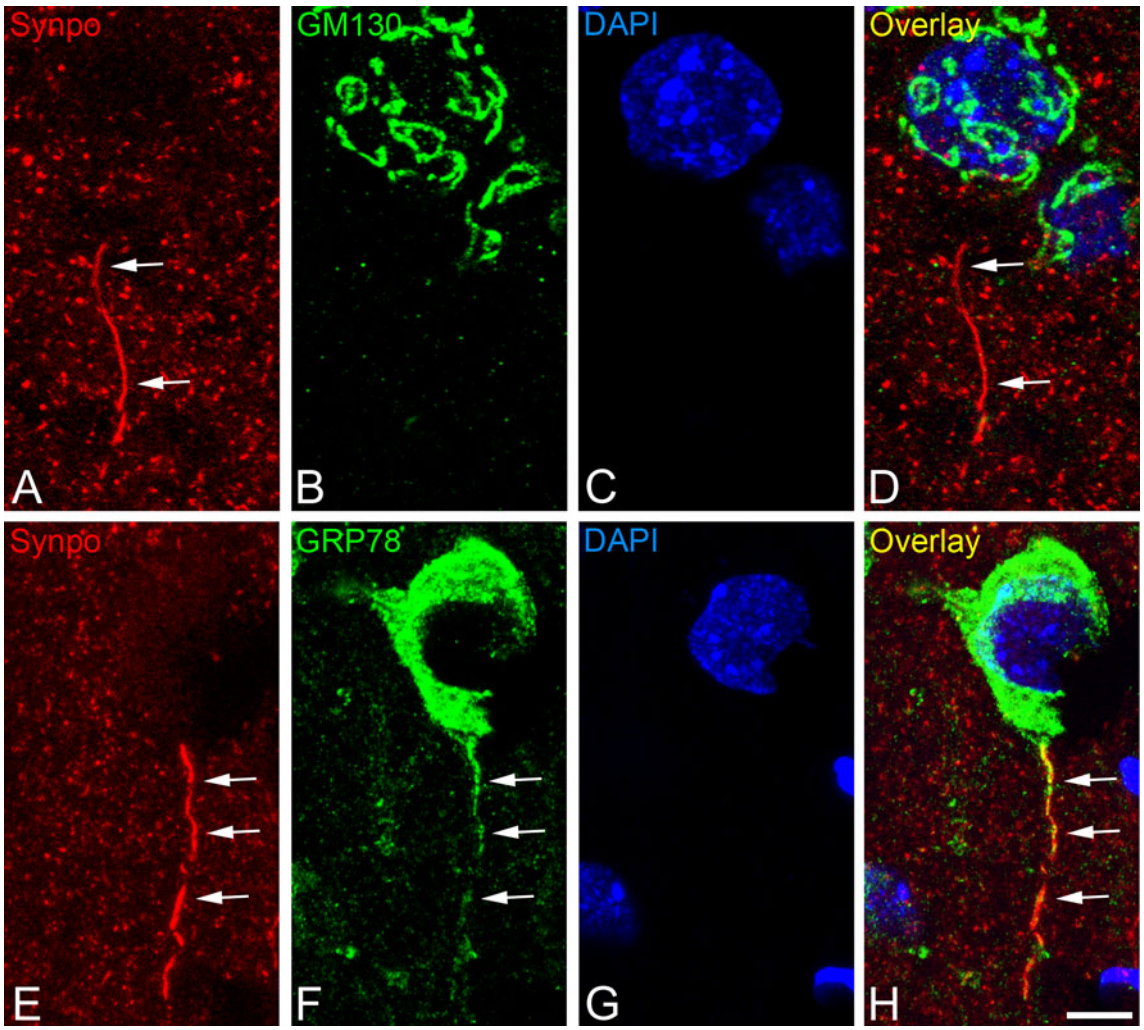

Fig. 8 Photomicrographs from sections of the rat sensory-motor cortex stained with DAPI and double immunostained for synaptopodin and the Golgi complex marker GM130 (**a**–**d**), or synaptopodin and the endoplasmic reticulum marker GRP78 (**e**–**h**). Note that the GSO, as identified by synaptopodin immunostaining (*arrows*) do not express Golgi markers, but is positive for GRP78. *Scale bar* (in **h**): 5 μm in **a**–**d**, and 6.5 μm in **e**–**h**

as the striatum, superior colliculus, brainstem and spinal cord, and tend to discharge a short burst of spikes; and thin-tufted (or type II) pyramidal cells that discharge spikes with no adaptation, and project to the contralateral cortex and the ipsilateral striatum (Molnar and Cheung 2006; Hattox and Nelson 2007; Molyneaux et al. 2007). However, this general classification is an oversimplification of the heterogeneity of layer V pyramidal neurons. For instance, different classes of tufted populations have been identified on the basis of morphological and electrophysiological characteristics, or on the basis of the expression of different combination of neuronal markers (e.g., transcription factors and neurofilaments) (Angulo et al. 2003; Tsiola et al. 2003; Molnar and Cheung 2006). In addition, in the transgenic mouse Thy1-eYFP-H used as a model to label layer V pyramidal cells (Feng et al. 2000), it has been shown that the Thy-1 gene promoter is expressed to varying degrees according to the particular subpopulations of both type I (corticospinal, and cortico-collicular) and type II (corticothalamic and callosal) neurons, identified by retrograde tract-tracing (Porrero et al. 2010). In our study, we show that GSO is present in the AIS of both Thy-1eYFP positive and Thy-1eYFP negative neurons, indicating that the presence of the GSO in the AIS is not related to the expression of the Thy-1 promoter. In contrast to this lack of specificity, we found that both in the rat and mouse neocortex, virtually all neurons containing a synaptopodin-ir GSO at the AIS systematically expressed SMI32. In line with previous studies demonstrating that SMI32 is a selective marker for type I neurons (Voelker et al. 2004; Molnar and Cheung 2006), the present results indicate that GSO-containing neurons are a subpopulation of type I (thick-tufted) layer V pyramidal neurons. However, our present tract-tracing experiments show that, concerning the

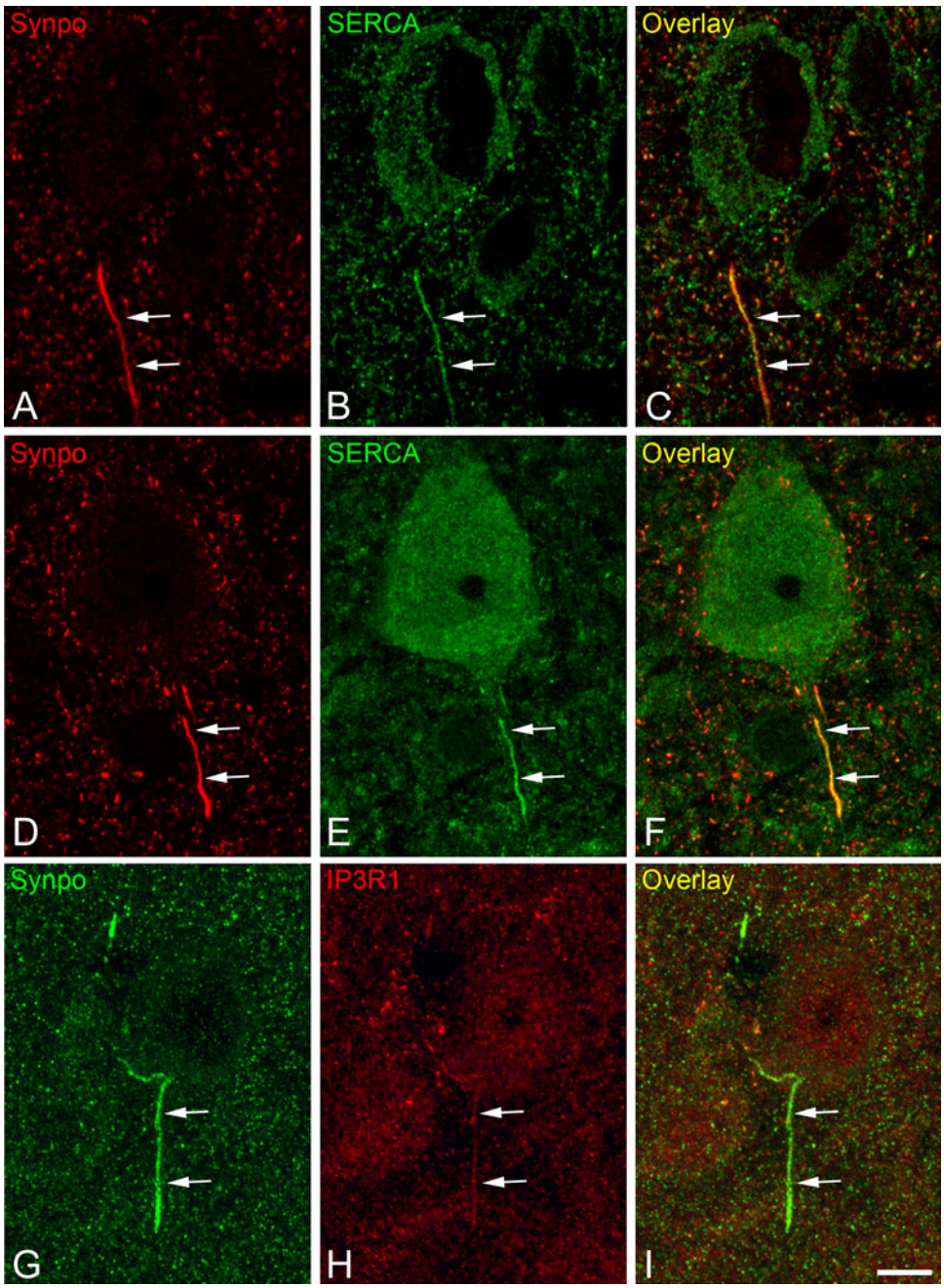

Fig. 9 Photomicrographs from sections of mouse (**a–c**, **g–i**) and rat (**d–f**) neocortex double immunostained for synaptopodin and SERCA (**a–c**, **d–f**), or synaptopodin and IP3R1 (**g–i**), showing the expression of SERCA and IP3R1 at the GSO as identified by synaptopodin immunostaining. *Scale bar* (in **i**): 6 μm in **a–c**, 7.5 μm in **d–f**; 6.5 μm in **g–i**

projection site, GSO-containing neurons are not a homogeneous neuronal population as they correspond to a variable percentage of neurons projecting to various subcortical non-thalamic targets, including the striatum, superior colliculus, pons and spinal cord. It has been previously shown that target refinement is a general feature of layer V corticofugal projection neurons; type I neurons project to different targets during early development, and may show different patterns of selective branch elimination or maintenance depending on the particular cortical area (O'Leary and Stanfield 1985, 1986; Koester and O'Leary 1993). Recent studies have reported a wide variety of pyramidal projection neurons, especially layer V neurons, based on the correlation between target specificity and gene expression patterns—such that it is possible to molecularly define functionally distinct classes of projection neurons (Sorensen et al. 2013). GSO-containing neurons are abundantly distributed in sensorimotor cortex (present study) where the restricted expression of a small number of genes has been reported in layer V neurons (Arlotta et al. 2005). Whether layer V pyramidal neurons containing a GSO at the AIS represent a subpopulation with a particular target specificity, or an axon collateralization pattern that might correlate with a specific gene expression profile are

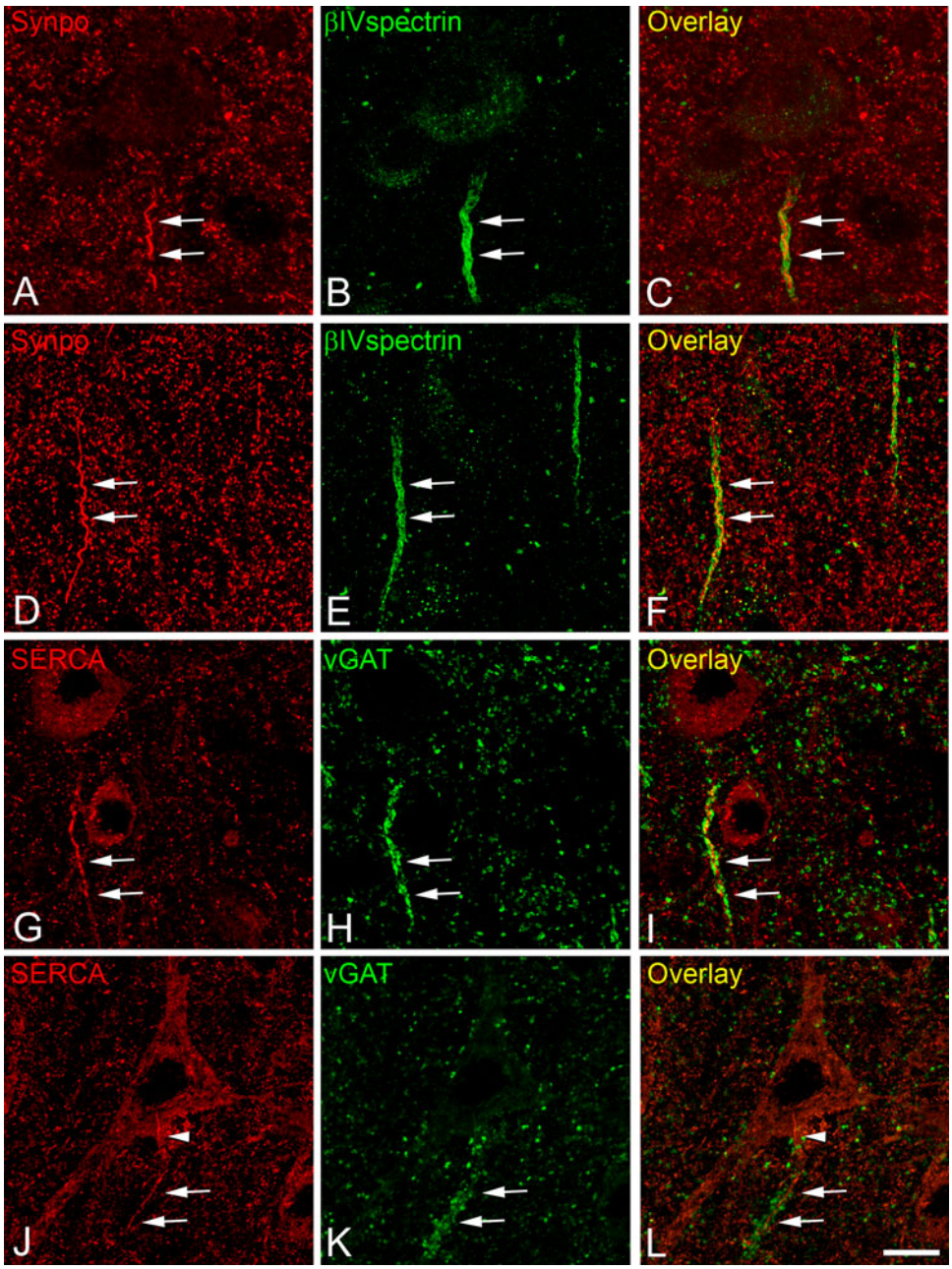

Fig. 10 Photomicrographs from human temporal (**d–f**) and supplementary motor cortex (**a–c**) showing the presence of synaptopodin-ir GSO in the AISs of layer V pyramidal neurons, as identified by spectrin βIV immunostaining. **g–l** Show the expression of SERCA at the GSO of a subpopulation of layer V AISs in the temporal (**j–l**) and supplementary motor cortex (**g–i**), identified by the vGAT immunostaining of chandelier cell axon terminals in apposition to the AISs. *Scale bar* (in **l**): 9 μm in **a–c**, 10 μm in **d–f**; 11 μm in **g–i**; 12 μm in **j–l**

both interesting possibilities that should be evaluated in future studies.

Previous studies have shown that, in various neuronal types, Ca^{2+} transiently enters the AIS through plasma membrane voltage-gated Ca^{2+} channels after depolarization of the soma and this Ca^{2+} participates in the generation and timing of action potentials in the AIS (Yu et al. 2008, 2010; Bender and Trussell 2009). The present work shows that the GSO expresses the inositol 1,4,5-triphosphate receptor 1 (IP_3R1) and the sarcoplasmic reticulum Ca^{2+} ATPase (SERCA) 2—both in rodent and human neocortex. Thus, the GSO seems to be an organelle with similar characteristics in both rodents and humans. However, while GSOs were not found in layer III of rodents, occasional GSOs were found in layer III of the supplementary motor cortex and lateral temporal cortex in human. Whether these GSOs are found in other human cortical areas and species remains to be elucidated.

It is known that different domains of the neuronal ER are responsible for a range of morphological and functional specializations (Park and Blackstone 2010) and that the distribution of IP_3Rs, ryanodine receptors and other ER proteins such as calsequestrin and calreticulin is heterogeneous within the ER (Copray et al. 1996; Gatti et al. 2001; Bannai et al. 2004). Therefore, the expression in the GSO of IP_3R1 and SERCA (through which Ca^{2+}

mobilization and uptake is likely to occur, respectively), suggests that the GSO may be involved in recruiting these proteins in the AIS, and also suggests the involvement of the GSO in AIS spatiotemporal Ca^{2+} level regulation in a subpopulation of layer V pyramidal neurons with extrathalamic descending projections. The GSO seems to be an IP_3-sensitive store that may serve as a pool of releasable Ca^{2+}. However, the signals that promote IP_3R1-mediated Ca^{2+} signaling in the AIS of this neuronal population are not known. Other questions also remain, such as how these signals might coordinate with other possible mechanisms of Ca^{2+} entry and extrusion across the plasma membrane, or how they may coordinate with Ca^{2+} release and resequestration from the ER stores, as described for other neuronal regions and cell types (Bootman et al. 2001; Blaustein and Golovina 2001).

In the AIS of most populations of cortical pyramidal neurons, in which a GSO is lacking, a specialization of the ER—the cisternal organelle—also expresses IP_3R1, SERCA and synaptopodin, and it is thought that these organelles participate in AIS Ca^{2+} level regulation (Kosaka 1980; Benedeczky et al. 1994; Bas Orth et al. 2007; Jedlicka et al. 2008; Sanchez-Ponce et al. 2011a). Despite these neurochemical similarities, there are important differences between the organization of the GSO and cisternal organelles. According to previous studies (Sanchez-Ponce et al. 2011b), the GSO is located in a central position along the length of the AIS with only occasional contacts with the AIS plasma membrane. The GSO is made up of a discrete number of long tubules and flattened sacs aligned in parallel with the long axis of the axon, and it is in continuation with similar elongated structures found in the cytoplasm at the base of the pyramidal soma that switch direction to enter the axon hillock and to funnel into the AIS. By contrast, the cisternal organelle consists of stacks of flat membranous cisternae with a narrow lumen, alternating with electron dense material, and the outermost cisternae are attached to the inner side of the axonal plasma membrane. Furthermore, the cisternal organelles are positioned at different points along the AIS, and are often associated with regions of the AIS that receive synaptic contacts (Palay et al. 1968; Peters et al. 1968; Jones and Powell 1969; Sloper and Powell 1979; Kosaka 1980; Somogyi et al. 1983; Benedeczky et al. 1994; Jedlicka et al. 2008). Although three-dimensional reconstructions of the AIS at the ultrastructural level would be necessary to fully address the possible coexistence of the GSO and the cisternal organelle in the subpopulation of GSO-containing pyramidal neurons, the present light microscopy observations strongly suggest that this is not the case. Therefore, the present results indicate the existence of differences in AIS organization which may have important implications in the Ca^{2+} level regulation between GSO-containing layer V pyramidal neurons with extrathalamic descending projections (including some corticospinal neurons) and other populations of pyramidal cells. Different studies have suggested that neuronal Ca^{2+} levels must be tightly regulated, since AIS Ca^{2+}-dependent plasticity processes including activity-dependent changes in AIS length and position (Grubb and Burrone 2010; Grubb et al. 2011; Kuba et al. 2010) and injury-related proteolysis provoke structural changes in the AIS cytoskeleton (Schafer et al. 2009) that affect, for instance, the distribution of voltage-gated Na^+ channels. The organization of the neuronal ER in different morphological and functional domains is highly dynamic (Park and Blackstone 2010). Similarly, the morphological and neurochemical integrity of the cisternal organelle in hippocampal neurons, which is likely to have an impact on AIS Ca^{2+} regulation, depend on the integrity of the actin cytoskeleton (Sanchez-Ponce et al. 2011a) and on the presence of synaptopodin (Bas Orth et al. 2007). The precise functions of the GSO in the AIS are presently unknown. However, the present observations suggest that the GSO is involved in AIS Ca^{2+} level regulation, which might be relevant to proper functioning and maintenance of the AIS in descending projecting pyramidal neurons. These are interesting possibilities that should be addressed in future studies.

Acknowledgments The authors declare no conflict of interest. This work was supported by grants from the following entities: SAF 2010-18218 to AM and BFU2012-34963 to JD from the Ministerio de Economía y Competitividad; CIBERNED (CB06/05/0066; Spain); and from the Cajal Blue Brain Project (Spanish partner of the Blue Brain Project initiative from EPFL). We thank Dr. Rasband (Dept. of Neuroscience, Baylor College of Medicine, Houston, USA) for providing antibodies to βIV spectrin. We also thank Dr. Guzmán and Dr. Galve-Roperh (Dept. Biochemistry, Fac. Biology, Complutense University, Madrid, Spain) for providing brain sections from Thy1-eYFP-H mice.

References

Alonso-Nanclares L, Kastanauskaite A, Rodriguez JR, Gonzalez-Soriano J, Defelipe J (2011) A stereological study of synapse number in the epileptic human hippocampus. Front Neuroanat 5:8

Angulo MC, Staiger JF, Rossier J, Audinat E (2003) Distinct local circuits between neocortical pyramidal cells and fast-spiking interneurons in young adult rats. J Neurophysiol 89(2):943–953

Arellano JI, Munoz A, Ballesteros-Yanez I, Sola RG, DeFelipe J (2004) Histopathology and reorganization of chandelier cells in the human epileptic sclerotic hippocampus. Brain 127(Pt 1):45–64

Arion D, Sabatini M, Unger T, Pastor J, Alonso-Nanclares L, Ballesteros-Yanez I, Garcia Sola R, Munoz A, Mirnics K, DeFelipe J (2006) Correlation of transcriptome profile with electrical activity in temporal lobe epilepsy. Neurobiol Dis 22(2):374–387

Arlotta P, Molyneaux BJ, Chen J, Inoue J, Kominami R, Macklis JD (2005) Neuronal subtype-specific genes that control corticospinal motor neuron development in vivo. Neuron 45(2):207–221

Bannai H, Inoue T, Nakayama T, Hattori M, Mikoshiba K (2004) Kinesin dependent, rapid, bi-directional transport of ER sub-compartment in dendrites of hippocampal neurons. J Cell Sci 117(Pt 2):163–175

Bas Orth C, Schultz C, Muller CM, Frotscher M, Deller T (2007) Loss of the cisternal organelle in the axon initial segment of cortical neurons in synaptopodin-deficient mice. J Comp Neurol 504(5):441–449

Bender KJ, Trussell LO (2009) Axon initial segment Ca2 + channels influence action potential generation and timing. Neuron 61(2):259–271

Bender KJ, Uebele VN, Renger JJ, Trussell LO (2012) Control of firing patterns through modulation of axon initial segment T-type calcium channels. J Physiol 590(Pt 1):109–118

Benedeczky I, Molnar E, Somogyi P (1994) The cisternal organelle as a Ca(2+)-storing compartment associated with GABAergic synapses in the axon initial segment of hippocampal pyramidal neurones. Exp Brain Res 101(2):216–230

Blaustein MP, Golovina VA (2001) Structural complexity and functional diversity of endoplasmic reticulum Ca(2+) stores. Trends Neurosci 24(10):602–608

Bootman MD, Collins TJ, Peppiatt CM, Prothero LS, MacKenzie L, De Smet P, Travers M, Tovey SC, Seo JT, Berridge MJ, Ciccolini F, Lipp P (2001) Calcium signalling–an overview. Semin Cell Dev Biol 12(1):3–10

Copray JC, Liem RS, Kernell D (1996) Calreticulin expression in spinal motoneurons of the rat. J Chem Neuroanat 11(1):57–65

Debanne D, Campanac E, Bialowas A, Carlier E, Alcaraz G (2011) Axon physiology. Physiol Rev 91(2):555–602

Diaz-Alonso J, Aguado T, Wu CS, Palazuelos J, Hofmann C, Garcez P, Guillemot F, Lu HC, Lutz B, Guzman M, Galve-Roperh I (2012) The CB(1) cannabinoid receptor drives corticospinal motor neuron differentiation through the Ctip2/Satb2 transcriptional regulation axis. J Neurosci 32(47):16651–16665

Evans MD, Sammons RP, Lebron S, Dumitrescu AS, Watkins TB, Uebele VN, Renger JJ, Grubb MS (2013) Calcineurin signaling mediates activity-dependent relocation of the axon initial segment. J Neurosci 33(16):6950–6963

Feng G, Mellor RH, Bernstein M, Keller-Peck C, Nguyen QT, Wallace M, Nerbonne JM, Lichtman JW, Sanes JR (2000) Imaging neuronal subsets in transgenic mice expressing multiple spectral variants of GFP. Neuron 28(1):41–51

Gatti G, Trifari S, Mesaeli N, Parker JM, Michalak M, Meldolesi J (2001) Head-to-tail oligomerization of calsequestrin: a novel mechanism for heterogeneous distribution of endoplasmic reticulum luminal proteins. J Cell Biol 154(3):525–534

Grubb MS, Burrone J (2010) Activity-dependent relocation of the axon initial segment fine-tunes neuronal excitability. Nature 465(7301):1070–1074

Grubb MS, Shu Y, Kuba H, Rasband MN, Wimmer VC, Bender KJ (2011) Short- and long-term plasticity at the axon initial segment. J Neurosci 31(45):16049–16055

Hallman LE, Schofield BR, Lin CS (1988) Dendritic morphology and axon collaterals of corticotectal, corticopontine, and callosal neurons in layer V of primary visual cortex of the hooded rat. J Comp Neurol 272(1):149–160

Hattox AM, Nelson SB (2007) Layer V neurons in mouse cortex projecting to different targets have distinct physiological properties. J Neurophysiol 98(6):3330–3340

Inda MC, Defelipe J, Munoz A (2007) The distribution of chandelier cell axon terminals that express the GABA plasma membrane transporter GAT-1 in the human neocortex. Cereb Cortex 17(9):2060–2071

Jedlicka P, Vlachos A, Schwarzacher SW, Deller T (2008) A role for the spine apparatus in LTP and spatial learning. Behav Brain Res 192(1):12–19

Jones EG, Powell TP (1969) Synapses on the axon hillocks and initial segments of pyramidal cell axons in the cerebral cortex. J Cell Sci 5(2):495–507

Klein BG, Mooney RD, Fish SE, Rhoades RW (1986) The structural and functional characteristics of striate cortical neurons that innervate the superior colliculus and lateral posterior nucleus in hamster. Neuroscience 17(1):57–78

Koester SE, O'Leary DD (1993) Connectional distinction between callosal and subcortically projecting cortical neurons is determined prior to axon extension. Dev Biol 160(1):1–14

Kole MH, Stuart GJ (2012) Signal processing in the axon initial segment. Neuron 73(2):235–247

Kosaka T (1980) The axon initial segment as a synaptic site: ultrastructure and synaptology of the initial segment of the pyramidal cell in the rat hippocampus (CA3 region). J Neurocytol 9(6):861–882

Kuba H (2012) Structural tuning and plasticity of the axon initial segment in auditory neurons. J Physiol 590(Pt 22):5571–5579

Kuba H, Oichi Y, Ohmori H (2010) Presynaptic activity regulates Na(+) channel distribution at the axon initial segment. Nature 465(7301):1075–1078

Larkman A, Mason A (1990) Correlations between morphology and electrophysiology of pyramidal neurons in slices of rat visual cortex. I. Establishment of cell classes. J Neurosci 10(5):1407–1414

Markram H, Lubke J, Frotscher M, Roth A, Sakmann B (1997) Physiology and anatomy of synaptic connections between thick tufted pyramidal neurones in the developing rat neocortex. J Physiol 500(Pt 2):409–440

Molnar Z, Cheung AF (2006) Towards the classification of subpopulations of layer V pyramidal projection neurons. Neurosci Res 55(2):105–115

Molyneaux BJ, Arlotta P, Menezes JR, Macklis JD (2007) Neuronal subtype specification in the cerebral cortex. Nat Rev Neurosci 8(6):427–437

Nakamura N, Rabouille C, Watson R, Nilsson T, Hui N, Slusarewicz P, Kreis TE, Warren G (1995) Characterization of a cis-Golgi matrix protein, GM130. J Cell Biol 131(6 Pt 2):1715–1726

O'Leary DD, Stanfield BB (1985) Occipital cortical neurons with transient pyramidal tract axons extend and maintain collaterals to subcortical but not intracortical targets. Brain Res 336(2):326–333

O'Leary DD, Stanfield BB (1986) A transient pyramidal tract projection from the visual cortex in the hamster and its removal by selective collateral elimination. Brain Res 392(1–2):87–99

Palay SL, Sotelo C, Peters A, Orkand PM (1968) The axon hillock and the initial segment. J Cell Biol 38(1):193–201

Park SH, Blackstone C (2010) Further assembly required: construction and dynamics of the endoplasmic reticulum network. EMBO Rep 11(7):515–521

Paxinos G, Watson C (2007) The rat brain in stereotaxic coordinates, 6th edn. Academic Press/Elsevier, Amsterdam

Peters A, Proskauer CC, Kaiserman-Abramof IR (1968) The small pyramidal neuron of the rat cerebral cortex. The axon hillock and initial segment. J Cell Biol 39(3):604–619

Pfaffenbach KT, Lee AS (2011) The critical role of GRP78 in physiologic and pathologic stress. Curr Opin Cell Biol 23(2):150–156

Porrero C, Rubio-Garrido P, Avendano C, Clasca F (2010) Mapping of fluorescent protein-expressing neurons and axon pathways in adult and developing Thy1-eYFP-H transgenic mice. Brain Res 1345:59–72

Rasband MN (2010) The axon initial segment and the maintenance of neuronal polarity. Nat Rev Neurosci 11(8):552–562

Sanchez-Ponce D, Blazquez-Llorca L, Defelipe J, Garrido JJ, Munoz A (2011a) Colocalization of {alpha}-actinin and synaptopodin in the pyramidal cell axon initial segment. Cereb Cortex 22(7):1648–1661

Sanchez-Ponce D, DeFelipe J, Garrido JJ, Munoz A (2011b) In vitro maturation of the cisternal organelle in the hippocampal neuron's axon initial segment. Mol Cell Neurosci 48(1):104–116

Schafer DP, Jha S, Liu F, Akella T, McCullough LD, Rasband MN (2009) Disruption of the axon initial segment cytoskeleton is a new mechanism for neuronal injury. J Neurosci 29(42):13242–13254

Shim SY, Wang J, Asada N, Neumayer G, Tran HC, Ishiguro K, Sanada K, Nakatani Y, Nguyen MD (2008) Protein 600 is a microtubule/endoplasmic reticulum-associated protein in CNS neurons. J Neurosci 28(14):3604–3614

Sloper JJ, Powell TP (1979) A study of the axon initial segment and proximal axon of neurons in the primate motor and somatic sensory cortices. Philos Trans R Soc Lond B Biol Sci 285(1006):173–197

Somogyi P, Nunzi MG, Gorio A, Smith AD (1983) A new type of specific interneuron in the monkey hippocampus forming synapses exclusively with the axon initial segments of pyramidal cells. Brain Res 259(1):137–142

Sorensen SA, Bernard A, Menon V, Royall JJ, Glattfelder KJ, Hirokawa K, Mortrud M, Miller JA, Zeng H, Hohmann JG, Jones AR, Lein ES (2013) Correlated gene expression and target specificity demonstrate excitatory projection neuron diversity. Cereb Cortex. doi:10.1093/cercor/bht243

Tsiola A, Hamzei-Sichani F, Peterlin Z, Yuste R (2003) Quantitative morphologic classification of layer 5 neurons from mouse primary visual cortex. J Comp Neurol 461(4):415–428

Voelker CC, Garin N, Taylor JS, Gahwiler BH, Hornung JP, Molnar Z (2004) Selective neurofilament (SMI-32, FNP-7 and N200) expression in subpopulations of layer V pyramidal neurons in vivo and in vitro. Cereb Cortex 14(11):1276–1286

Yu Y, Shu Y, McCormick DA (2008) Cortical action potential backpropagation explains spike threshold variability and rapid-onset kinetics. J Neurosci 28(29):7260–7272

Yu Y, Maureira C, Liu X, McCormick D (2010) P/Q and N channels control baseline and spike-triggered calcium levels in neocortical axons and synaptic boutons. J Neurosci 30(35):11858–11869

Phospho-tau accumulation and the structural alterations of the pyramidal cell axon initial segment in Alzheimer´s disease

Alejandro Antón-Fernández[1,2], Gonzalo León-Espinosa[1,2,5], Javier DeFelipe[1,2,3], and Alberto Muñoz[1,2,3,4]

1 Instituto Cajal, CSIC, Madrid, Spain.

2 Laboratorio Cajal de Circuitos Corticales (CTB), Universidad Politécnica de Madrid, Madrid, Spain.

3 CIBERNED, Centro de Investigación Biomédica en Red de Enfermedades Neurodegenerativas, Spain.

4 Departamento de Biología Celular, Universidad Complutense de Madrid, Spain.

5 Facultad de Farmacia, Universidad San Pablo CEU, Madrid, Spain

Running title: AIS alteration in neuron with hyperphohphorylated tau

Keywords: βIV-Spectrin, temporal neocortex, aging, AIS plasticity

Correspondence: Alberto Muñoz, Ph.D.,
Laboratorio Cajal de circuitos corticales
Centro de Tecnología Biomédica
Universidad Politécnica, Madrid
Pozuelo de Alarcón
Madrid 28223, SPAIN.
Tel: +34 4524900 (ext1943)
e-mail: amunozc@bio.ucm.es

Abstract

The axon initial segment (AIS) is a critical region of the neuron for action potential generation as well as for the regulation of neural activity. This specialized structure — characterized by the expression of different types of ion channels and adhesion, scaffolding and cytoskeleton proteins— is subjected to morpho-functional plastic changes in length and position upon variations in neural activity or in pathological conditions. In the present study, using immunocytochemistry with AT8 antibodies (phospho-tau S202/T205) and 3D confocal microscopy reconstruction techniques in brain tissue from Alzheimer´s disease patients, we found that the majority of neurons with hyperphosphorylated tau showed changes in AIS length and position in comparison with AT8-negative neurons from the same cortical layers. We observed a wide variety of AIS alterations in neurons with hyperphosphorylated tau although the most common changes were either a proximal shift or a lengthening of the AISs. Similar results were found in neocortical tissue from a non-demented patient with neurons with hyperphosphorylated tau and from the neocortex of P301S mouse model of tauopathy. These findings support the idea that the accumulation of phospho-tau is associated with structural alterations of the AIS that are likely to impact the normal neuronal activity, which might contribute to neuronal dysfunction in AD.

Introduction

The axon initial segment (AIS) is the cellular domain in neurons which is characterized for a unique architecture, molecular and functional specializations and that occupies about 20–60 μm of the proximal axon length (Jones and Svitkina 2016), . Therefore, it represents a small, intermediate region of the axon between the somatodendritic and "distal" axonal compartments. Due to the contribution of the AIS in the generation and modulation of action potential, owing to the high concentration of ion channels situated there (Kole et al. 2008; Lorincz and Nusser 2010), AIS structural changes could have relevant consequences on network excitability (Kole et al. 2007; Kole et al. 2008). In fact, it has been shown that plastic changes in the AIS microanatomy occurs in response to under or over-stimulation of neurons, adjusting the excitability of a neuron in response to its inputs, what contributes to the homeostasis of neuronal circuits (Grubb and Burrone 2010; Kuba et al. 2010). Specifically, properties of the AIS such as length or position (i.e., point where the AIS is originated in the axon hillock, at the base of the cell body or a main dendrite) can determine the firing properties of neurons (Kole et al. 2007; Boiko et al. 2003). For example, it has been reported an increase in the AIS length after loss of auditory input due to the cochlea removal in chickens (Kuba et al. 2010). Also, it has been shown that the depolarization of dentate granule cells shortens their AIS (Evans et al. 2015) whereas in CA1 pyramidal neurons promoted a distal AIS shift (Wefelmeyer et al. 2015), decreasing in both cases the neuronal excitability.

The importance of the AIS has also been demonstrated by the involvement of its alterations in distinct pathological conditions such as demyelination, traumatic brain injury, Angelman syndrome, stroke, schizophrenia, autism, epilepsy and channelopathies (Schafer et al. 2009; Buffington and Rasband 2011; Kaphzan et al. 2011; Hinman et al. 2013; Harty et al. 2013; Baalman et al. 2013; Stoler and Fleidervish 2016; Hamada and Kole 2015). Alzheimer´s disease (AD) has been studied less in spite that is the most common neurodegenerative disorder, characterized clinically by a progressive memory impairment followed by global cognitive deficits and pathologically by the presence of senile plaques made of extracellular deposits of amyloid- β peptides and intracellular neurofibrillary tangles of hyperphosphorylated tau. The involvement of AIS alterations in the physiopathology of AD was suggested (Buffington and Rasband 2011). Later studies using the APP (amyloid precursor

protein) transgenic mouse model of AD, found that the presence of Aβ plaques induced an impairment in GABAergic innervation of the AIS (Leon-Espinosa et al. 2012) and also leads to a reduction in AIS length and βIV-spectrin expression, which is an essential structural protein of AIS (Marin et al. 2016).

Regarding tau hyperphosphorylation, previous studies described that alterations of the barrier functions of the AIS —that restrict various isoforms of tau to specific neuronal domains (Binder et al. 1985; Kosik and Finch 1987; Migheli et al. 1988; Mandell and Banker 1996)— are disrupted in AD mouse models resulting in the missorting of hyperphosphorylated tau that accumulates in the somatodendritic domain (Li et al. 2011). *In vitro* studies have shown that tau phosphorylation or the downregulation of AIS proteins like Ankyrin G or EB1, induce the missorting of tau by disruption of the AIS diffusion barrier, what was suggested to participate in the pathogenesis of AD (Li et al. 2011; Zempel et al. 2017; Sun et al. 2014). The presence of phosphorylated tau in the somatodendritic compartment has also been shown *in vitro* to decrease neuronal activity (Thies and Mandelkow 2007; Hoover et al. 2010) which was correlated with an AIS distal shift along the axon (Hatch et al. 2017). The expression of AIS cytoskeletal proteins such as AnkyrinG or βIV-spectrin, which are essential for AIS integrity maintenance (Hedstrom et al. 2008; Jenkins and Bennett 2001), has been found downregulated in AD brains (Sohn et al. 2016) what conceivably could be related to plastic changes or pathological alterations of the AIS. However, the possible structural alterations of the AIS in cortical neurons from AD patients, and their possible relationship with phospho-tau accumulation and have not been directly explored. In the present study, we address the potential impact that the presence of phospho-tau aggregates might have on AIS integrity in neocortical tissue from AD patients and from the P301 mouse model of tauopathy. The results indicate that the presence of somatodendritic phospho-tau deposits is associated with a variety alterations in the length and/or the position of the AIS that might contribute to changes in the activity of neuronal circuits in tauopathies.

Materials and methods

In the present study we have used brain tissue from AD patients obtained from the *Instituto de Neuropatología* (Dr. I. Ferrer, *Servicio de Anatomía Patológica*, IDIBELL-*Hospital Universitario de Bellvitge*, and Neurological Tissue Bank Biobanc-Hospital Clínic-IDIBAPS, Barcelona, Spain IF1, IF4, IF6, IF8, IF10, IF11, IF12, IF13, Bcn5, Bcn7, Bcn8, Bcn13 cases), from the *Banco de Tejidos Fundación* CIEN (Dr. A. Rábano, *Área de Neuropatología, Centro Alzheimer, Fundación Reina Sofia*, Madrid, Spain; Vk11, Vk22 cases). Control human brain was obtained from Dr. Ricardo Insausti (*Facultad de Medicina, Universidad* UCLM, Albacete; AB1). Some of this material has been used in previous studies from our laboratory in which the clinical data from patients were thoroughly described (Anton-Fernandez et al. 2017a). Following neuropathological examination, the AD stages were defined according to the Consortium to Establish a Registry for Alzheimer's Disease (CERAD; (Mirra et al. 1991)) and the Braak and Braak criteria (Braak and Braak 1995).

The postmortem delay in tissue obtained at autopsy, between death and tissue processing was below 6h (Table 1), and the brain samples were obtained following the guidelines of the Institutional Ethical Committees, which also granted approval. Upon removal, the brains were immediately fixed in cold 4% paraformaldehyde in phosphate buffer (PB 0.1M, pH7.4), and after 2 h, the tissue was cut into small blocks and post-fixed in the same fixative for 24– 48 h at 4 °C. However, one human patient (AB1) was intraarterially perfused through the internal carotid artery 1 h after death with a saline solution followed by 4% paraformaldehyde in PB. The brain was then removed and post-fixed as mentioned above. After fixation, it was immersed in graded sucrose solutions and stored in a cryoprotectant solution at −20 °C. Serial sections (50 μm) of the cortical tissue were obtained using a vibratome (St. Louis, MO, USA), and the sections from each region and case were batch-processed for immunohistochemical staining. The sections immediately adjacent to those stained immunohistochemically were Nissl-stained in order to identify the cortical areas and the laminar boundaries.
Unfortunately, the combination of antibodies used for this study (see below) only rendered satisfactory results in tissue from 4 out of the 14 patients (see Table 1): three

patients with AD (aged 75-91) and one control human brain tissue (aged 45) free of any known neurological or psychiatric illness.

In addition, we have used brain tissue from transgenic mice P301S for the human tau gene and wildtype control littermates. This material has been used in a previous study (Anton-Fernandez et al. 2017b). The P301S mouse model, obtained from Jackson laboratory (B6;C3-Tg (Prnp- MAPT*P301S)PS19Vle/J), carries a mutant (P301S) human MAPT gene encoding T34-tau isoform (1N4R) driven by the mouse prion-protein promoter (Prnp) on a B6C3H/F1 genetic background. The 3 animals analyzed were 36 weeks old, when these animals show learning and motor deficits and hyperphosphorylated tau aggregates similar to those of AD patients, in some cortical neurons (Yoshiyama et al. 2007). A total of 3 P301S transgenic mice aged 36 weeks were analyzed. All mice were housed at the "*Centro de Biología Molecular Severo Ochoa*" animal facility. Mice were housed four per cage with food and water available ad libitum and maintained in a temperature-controlled environment on a 12/12 h light-dark cycle with light onset at 07:00 h. Animal housing and maintenance protocols followed the guidelines of Council of Europe Convention ETS123, recently revised as indicated in Directive 86/609/EEC. Animal experiments were performed under protocols (P15/P16/P18/P22) approved by the Institutional Animal Care and Utilization Committee (*Comité de Ética de Experimentación Animal del* CBM, CEEA-CBM, Madrid, Spain). Animals were sacrificed by a lethal intraperitoneal injection of sodium pentobarbital (200 mg/kg b.w.) and were then perfused intracardially with a saline solution followed by 4% paraformaldehyde in PB. The brain of each animal was removed and post-fixed by immersion in the same fixative for 24 h at 4◦C. After rinsing in PB, brains were cut in the sagital plane using a vibratome (Leica VT2100S). Serial parasagital sections (50 µm thick) were cryoprotected in 30% sucrose solution in PB and stored in ethylenglicol/glycerol at –20◦C until they were used.

Immunofluorescence

For immunofluorescence, free floating serial sections (50-µm thick) from human tissue were first rinsed in PB and then pre-treated in 1.66% H_2O_2 for 30 min to inactivate the endogenous peroxidase activity and were then preincubated for 1 h in PB with 0.25% Triton-X100 and 3% normal serum of the species in which the secondary antibodies

were raised (Vector Laboratories, Burlingame, CA, USA). Regarding tissue from P301S mice, free floating serial sections were first rinsed in PB and then preincubated for 1 h in PB with 0.25% Triton-X100 and 3% normal serum of the species in which the secondary antibodies were raised (Vector Laboratories, Burlingame, CA, USA). In all cases the sections were incubated for 48 h at 4◦C in the same stock solution containing the following primary antibodies: rabbit anti-βIV Spectrin (1:1000, a gift from Dr. M. N. Rasband; Dept. of Neuroscience, Baylor College of Medicine, Houston, USA), guinea-pig anti-NeuN (Millipore, 1:2000) and mouse anti-phospho-PHF-tau pSer202+Thr205 antibody (AT8, 1:2000, Pierce Endogen). After rinsing in PB, the sections were first incubated for 2 h at room temperature in biotinylated goat anti-rabbit antibody (1:200) to amplify the AIS immunoreactivity signal. Sections were then rinsed in PB and incubated for 2 h at room temperature in streptavidin-coupled Alexa 488 (1:200; Molecular Probes, Eugene, OR, USA), Alexa 594- conjugated goat anti-mouse and in Alexa 647- conjugated goat anti-guinea pig antibodies (1:1000; Molecular Probes, Eugene, OR, USA). After rinsing in PB, the sections were treated with Autofluorescence Eliminator Reagent (Chemicon; only human sections) to reduce autofluorescence and were then mounted in antifade mounting medium (Prolong Gold, Invitrogen) and studied by confocal microscopy (Zeiss, 710).

Image processing

Confocal image stacks taken from the somatomotor neocortex of P301S mice and from the human temporal neocortex (areas 20/21/38 of Brodmann), were recorded at 0.14 µm intervals through separate channels with a 63x oil-immersion lens (NA, 1.40, refraction index, 1.45). ZEN 2012 software (Zeiss) was used to construct composite images from each optical series by combining the images recorded through the different channels (image resolution: 1024×1024 pixels; pixel size: 0.08 µm). Finally we used a commercial software package (Imaris 6.4.0 Bitplane AG, Zurich, Switzerland) to measure in 3D the AIS length (measurement point tool) on the basis of βIV-Spectrin immunofluorescence. To establish AIS position, the distance from the AIS start point and from the AIS end point from the edge of the soma (defined by NeuN immunofluorescence) was measured. To ensure that we selected complete AIS, we only considered only those AIS which complete immunostaining was separated in all

dimensions from the edges of the image stacks by at least 5 µm. Adobe Photoshop (CS4) software was used to compose figures.

Results

In order to study the possible relationship between the accumulation of hyperphosphorylated tau in neurons and the structural alterations of the AIS we performed experiments with triple immunocytochemical staining of neocortical tissue from three sources: 1) from autopsies of AD patients, some of them previously used in other studies from our laboratory, 2) from autopsy of a 45-year-old male adult who was free of any neurological or psychiatric disease (AB1, not diagnosed with AD),and 3) from the P301S transgenic mouse model of tauopathy (Fig 1). In all cases, we combined antibodies against βIV spectrin and NeuN, to label the AIS and neuronal cell body respectively, and AT8 antibodies to label neurons that accumulate hyperphosphorylated tau (phospho-Ser202 and phosho-Thr205) (Figure 1). Imaris software (3D measurement point tool) was used to measure the distance to the base of the pyramidal cell somata of the AIS start point and AIS end point. AIS length was calculated as the difference between AIS-start and AIS-end point distance values.

Alterations of the AIS in neurons from Alzheimer disease patients

A limitation of the present study is the relatively low number of AIS analyzed. Several factors contribute to this limitation. To our knowledge, the rabbit anti- βIV-spectrin antibodies used is among the best options to label AIS in human tissue in combination to mouse AT8 antibody which detects phosphorylated -tau at positions S205 and T205. However, among the AD cases available in our laboratory, some of them used in previous studies using different antibodies (Anton-Fernandez et al. 2017a), βIV-spectrin antibodies only labeled AISs in tissue from three patients (IF6, IF8 and IF13) and in one non-demented human case (AB1). In addition, in two (IF6 and IF8) out of these patients, the presence of neurons immunostained with AT8 antibodies was relatively low (Figure 1), reducing the potential number of AISs to study. It is also known that the contact with or the close proximity of β-amyloid plaques, which presence is a hallmark of AD tissue, induce structural alterations in the AIS (Leon-Espinosa et al. 2012; Marin

et al. 2016). Therefore, in order to investigate the possible effects on the AIS induced by the presence of the aggregation of hyperphosphorylated tau (minimizing the effects induced by the proximity of β-amyloid plaques), we have focused only in AISs from neurons non-adjacent to β-amyloid plaques, which can be detected by the AT8 immunostaining or by the characteristic scarcity of neuronal cell bodies in plaques. In these regions, distant from β-amyloid plaques, we only considered for analysis the AIS from these neocortical pyramidal neurons whose cell bodies and AISs were completely included within the tissue thickness in which both AT8 and βIV-spectrin antibodies penetrated rendering patterns of AIS βIV spectrin immunoreactivity (Fig 2), apparently similar to that found in human control tissue in previous studies from our laboratory (Anton-Fernandez et al. 2015).

Patients	**Age (years)**	**Gender**	**Postmortem delay (hours)**	**Neurologic diagnosis**	**Cause of death**
P5 (IF6)	85	Male	2	AD III-A	Unknown
P7 (IF8)	91	Male	2.5	AD III-A	Unknown
P11 (IF13)	75	Male	2	AD III - B	Lymphoproliferative disorder
AB1	45	Male	<1	-	Pleural *mesothelioma*
P1 (IF1)	80	Female	2	AD IV-B	Unknown
P4 (IF5)	80	Female	3	AD III	Unknown
IF7	88	Female	2	AD III	Unknown
P14 (Vk11)	87	Female	1.5	AD III/IV - A	Respiratory infection
Vk22	86	Female	2	AD V	Unknown
Bcn3	81	Female	5.30	AD V-C	Unknown
Bcn5	83	Female	4	AD V/VI-C	Unknown
Bcn8	64	Female	<6	AD VI-C	Unknown

Table 1: Summary of clinical data and neurologic diagnosis according to Braak and Braak criteria (Braak and Braak 1995), defined by different stages (from I to VI) and to CERAD criteria (Consortium to Establish a Registry for Alzheimer's Disease) (Mirra et al. 1991), which use a semiquantitative score of the density of neuritic plaques in the most severely affected region of the isocortex (A= mild presence of plaques, B= moderate presence of plaques, C= severe presence of plaques). In red are indicated those cases in which antibodies to βIV spectrin labeled the AISs.

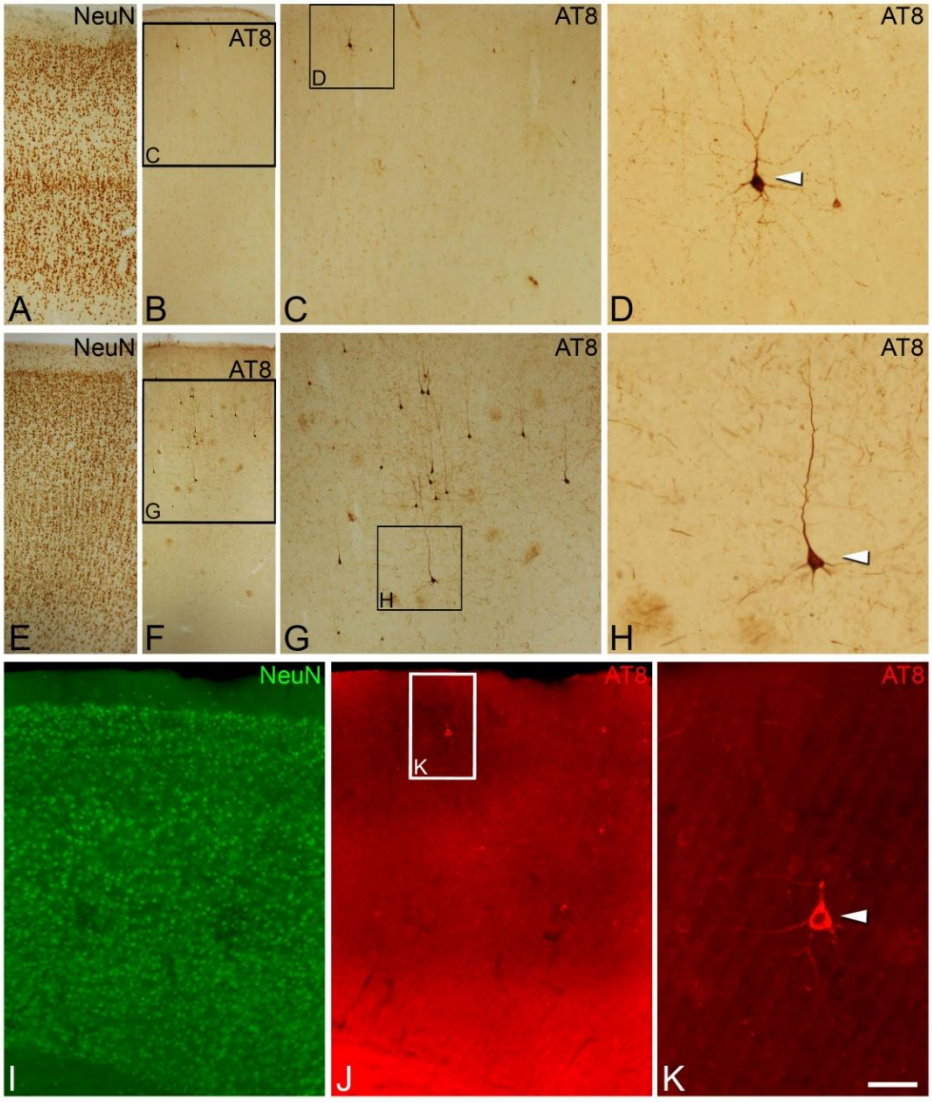

Figure 1: Photomicrographs taken from brain sections of the temporal neocortex from an AD patient (IF8, A-D) and in a non-demented human case (AB1, E-H) showing the distribution of neurons with hyperphosphorylated tau revealed by DAB immunostaining with AT8 antibodies (B and F) in different cortical layers identified by NeuN immunostaining of adjacent sections (A and E, respectively). I-J pair of microphotographs taken from a NeuN (green)/AT8 (red) double-immunostained section from the somatosensory cortex of a P301S transgenic mouse. Squared areas in B, C, F, G and J are shown at higher magnification in C, D, G, H and K, respectively. Arrowheads indicate AT8 positive neurons. Scale bar in K: 106 µm in A, B, E, F, 47 µm in C and G, 21µm in D and H, 167 µm in I and J, and 38 µm in K.

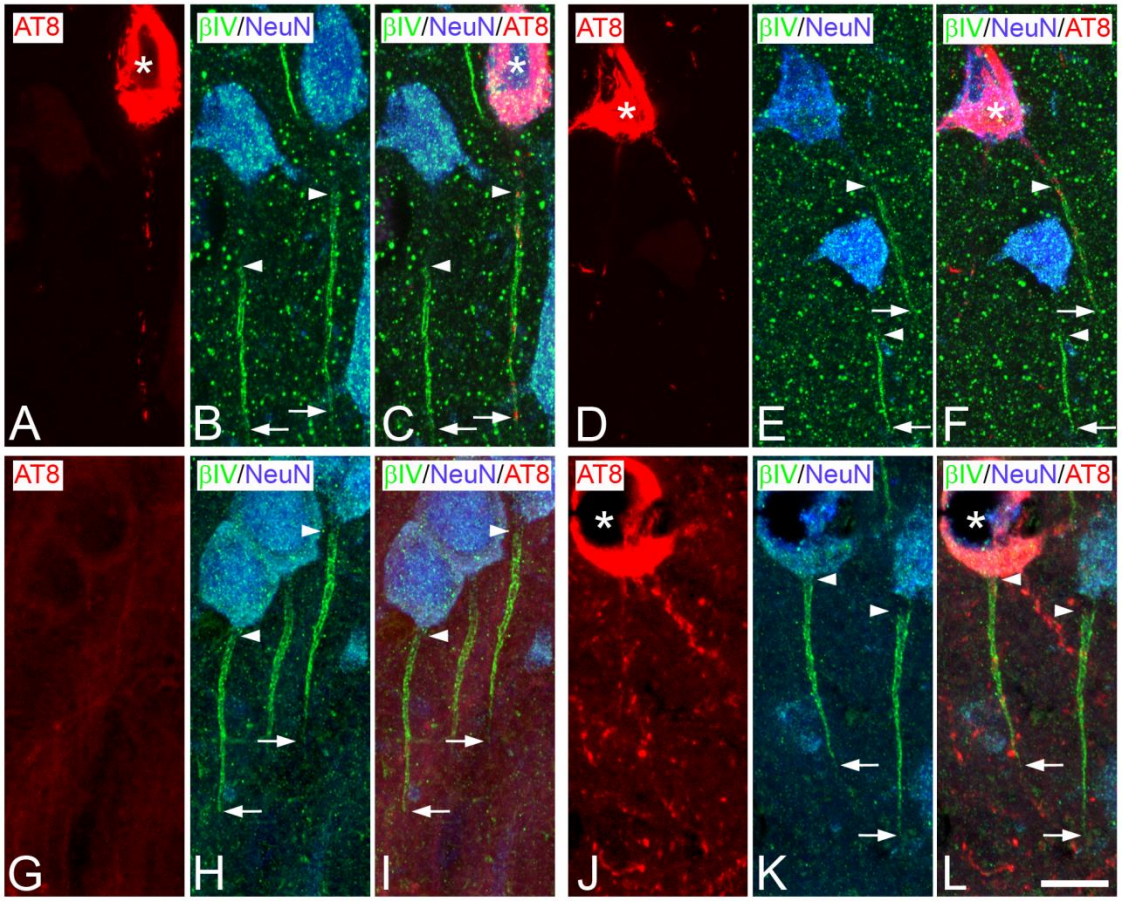

Figure 2: Trios of confocal stack Z projection microphotographs taken from AT8 (red)/βIV-spectrin (green)/NeuN (blue) triple-immunostained sections from Temporal neocortex of AD patient (IF13, A-C) and non-demented case (AB1, D-F), and from somatosensory cortex of wild-type (G-I) and P301 (J-L) animals aged 36 weeks. Arrowheads and arrows respectively indicate the start point and the end point of AISs labeled by βIV-spectrin immunostaining. Neurons containing neurofibrillary tangles are indicated by asterisks. Scale bar in L: 11 µm in A-F, 9.29 µm in G-L.

It is known the existence of a considerable variability on AIS length between neurons in different cortical layers and between different neuronal populations (Hofflin et al. 2017; Inda et al. 2009). In addition, in the tissue analyzed from each of the three patients we found a differential abundance in the number of AT8-positive neurons through cortical layers (table 2). An important limitation when addressing the AIS structural alterations caused by the accumulation of hyperphosphorylated tau consists in that, with the present methodology, it is not possible to know the AIS length and position in AT8+ neurons prior the phospho-tau accumulation.

Therefore, and in order to avoid inter-individual and inter-layer variability, we compared, for each patient separately, AIS length and position data from every AT8+ neuron with mean±standard deviation values obtained from all AT8- neurons in the

same cortical layer. For the measurements performed, we only considered that AIS values from any AT8+ neuron were different from mean values from AT8- neurons when the differences exceeded the standard deviation.

	IF13	IF8	IF6	All patients	AB1	P301S
AT8+ neurons in Layer II (n/AIS length/AIS distance to soma)	12/27.4/7.3	3/22.2/4.8	1/16.6/2.9	16/25.8/6.6	3/21.7/5.3	15/26/0.5
AT8+ neurons in Layer III (n/AIS length/AIS distance to soma)	12/26.4/5.9	1/19/2.8	0	13/25.8/5.6	7/22.5/4.3	6/24.2/0.2
AT8+ neurons in Layer IV (n/AIS length/AIS distance to soma)	6/30.4/7.4	1/22.9/5.6	0	7/29.2/7.2	3/20.8/7.2	0
AT8+ neurons in Layer V (n/AIS length/AIS distance to soma)	3/24.3/4.3	6/20.6/3.7	5/20.6/3.8	14/21.4/3.9	28/25.7/6.8	5/23/1.1
Total number of AT8+ neurons / AT8- neurons examined	33 / 57	11 / 19	6/ 12	50 / 87	41/ 51	26/40
Total number of neurons (AT8+ & AT8- neurons)	90	30	18	137	92	66
AIS mean length in AT8+ neurons	27.2	21.1	19.9	25.02	24.4	25.2
AIS mean length in AT8-	23.3	22.4	18.5	22.51	24	25.7
AIS mean distance to soma in AT8+	6.5	4.1	3.6	5.68	6.4	0.6
AIS mean distance to soma in AT8-	7.1	7.6	6.9	7.23	8.7	1.3

Table 2: Table showing the number of neurons and mean values for AIS length and AIS distance to soma in AT8+ or AT8- in the different cortical layers in each human case and in tissue from P301S mice model (somatosensory neocortex). Length and distance are expressed in µm.

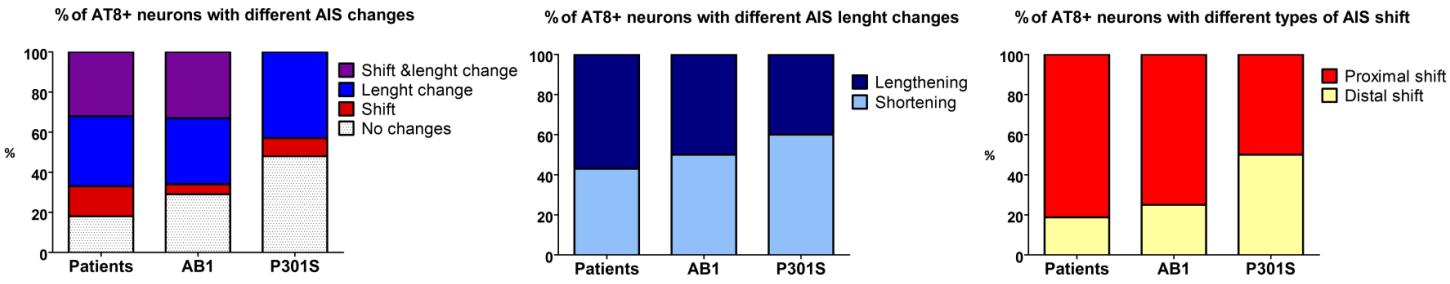

Figure 3: Histograms showing in AD patients (left column), in the non-demented case (AB1, middle column) and in P301S mice (right column) the percentages of AT8+ neocortical neurons with different AIS changes (A), with different AIS length changes (B) and with different types of AIS shift (C).

Taking data from the three patients and layers together (Fig 3) we found that, in the vast majority (82%, 28 out of 34) of AT8+ neurons, AIS length and/or position (start-point) values (25.02±5.4 / 5.6±2.3µm respectively, n=50) changed as compared to AT8-

neurons (22.51±5.9 /7.23 ±2.3 respectively, n=87) (Fig 3A). AIS length and position was unaltered in the remaining 17% of AT8+ neurons despite of the presence of tau hyperphosphorylation (Figs 3A, 4). In the AT8-positive neurons analyzed, we found a important heterogeneity in the AIS length and position changes finding examples of many of the theoretically potential combinations indicated in Fig.4.We found that in 56.5% (13 out of 23) of the AT8+ neurons with a change in AIS length, the AIS was longer (8.94 ±2.7 μm) that in AT8- neurons whereas it was shorter (4.14 ±2.57 μm) in the remaining 43.5% (Figs 3B, 4). We also found that in 81.2% (13 out of 16) of the AT8+ neurons with a change in AIS position, the AIS start point was located closer to the soma (proximal shift of 4.39 ± 2.36 μm) that in AT8- neurons, whereas it was located further down the axon (distal shift of 4.5 ±2.87 μm) in the remaining 19.8% (Figs, 3C, 4). Finally, some (32.3%, 11 out of 34) of the AT8+ neurons showed simultaneous changes in AIS length and position (Fig 4).

Therefore, a variety of AIS changes occurred although the most frequently found were AIS lengthening and AIS proximal shift. Furthermore, these events were only scarcely found to occur simultaneously in the same neuron (see Fig 4).

Alterations of the AIS in neurons with hyperphosphorylated tau in a non-demented case

To test in human tissue the potential effects induced by the sole presence of aggregates of hyperphosphorylated tau, presumably without any other potential pathologic factor such as β-amyloid pathology, we performed the same type of AIS analysis in temporal cortex from a non-demented patient (AB1), used in a previous study from the laboratory (Anton-Fernandez et al. 2017a), in which we found a relatively large number of neurons immunoreactive for hyperphosphorylated tau (AT8 antibodies) in the temporal cortex (Fig 1) in the absence of β-amyloid plaques. Taking data from all layers together we found that, in the majority (71.4%, 15 out of 21) of AT8+ neurons, AIS length and/or position (start-point) values (24.4± 4.9 /6.4±2.5 μm respectively, n=41) changed as compared to AT8- neurons (24 ± 4.8 / 8.7 ±2.9 μm respectively, n=51). AIS length and position was unaltered in the remaining 28.6% of AT8+ neurons despite of the presence of hyperphosphorylated tau (Figs 3A, 4). We found that in 50% (7 out of 14) of the AT8+ neurons with a change in AIS length, the AIS was longer (7.8 ± 3.7 μm) than in AT8- neurons whereas it was shorter (6.2 ± 2.1 μm) in the remaining 50% (Figs 3B, 4). We also found that in 75% (6 out of 8) of the AT8+ neurons with a change in AIS

position, the AIS start point was located closer to the soma (proximal shift of 5.1 ± 1.6 μm) than in AT8- neurons whereas it was located further down the axon (distal shift of 4 ± 0.5 μm) in the remaining 25% (Figs 3C, 4). Finally, some (33.4%, 7 out of 21) of the AT8+ neurons showed simultaneous changes in AIS length and position (see Fig 4). Therefore, as it was the case in tissue from AD patients, a variety of AIS changes were observed although the most frequently found AIS changes were AIS lengthening and AIS proximal shift.

Alterations of the AIS in neurons with hyperphosphorylated tau in the P301S mouse model of tauopathy

We finally studied the morphological features of the AIS of pyramidal neurons from the somatosensory cortex in relation to the accumulation of hyperphosphorylated tau, in P301S transgenic and control animals aged 36 weeks. In line with previous descriptions of this mouse model (Yoshiyama et al. 2007; Anton-Fernandez et al. 2017b), we found an abundant subpopulation of phospho-tau accumulating AT8+ neurons in the somatosensory cortex (Fig 1). No apparent general changes in the overall distribution of βIV spectrin immunostaining was found between wild-type and P301S 36-week-old mice (not shown). However, the analysis of confocal image stacks at higher magnification revealed alterations in the morphological characteristics of the AIS in some phospho tau accumulating neurons. Taking data from all layers together we found that, in about half (52.2%, 12 out of 23) of AT8+ neurons, AIS length and/or position (start-point) values changed (25.2± 2.98/ 0.6 ±1.05 μm respectively, n=26) as compared to AT8- neurons (25.7±3.7 /1.3 ±1.7 μm respectively, n=40). AIS length and position was unaltered in the remaining 47.8% of AT8+ neurons despite of the presence of hyperphosphorylated tau (Figs 3A, 4). We found that in 40% (4 out of 10) of the AT8+ neurons with a change in AIS length, the AIS was longer (5.53 ±4.3 μm) than in AT8- neurons whereas it was shorter (5.45 ±1.99 μm) in the remaining 60% (Figs 3B, 4). We also found that in 1 out of 2 of the AT8+ neurons with a change in AIS position, the AIS start point was located closer to the soma (proximal shift of 2.31 μm) than in AT8- neurons whereas it was located further down the axon (distal shift of 1.77 μm) in the remaining other AIS (Figs 3C, 4). Finally, simultaneous changes in AIS length and

position were only scarcely found (8.7%, 2 out of 23) of the AT8+ neurons showed (Figs 3C, 4).

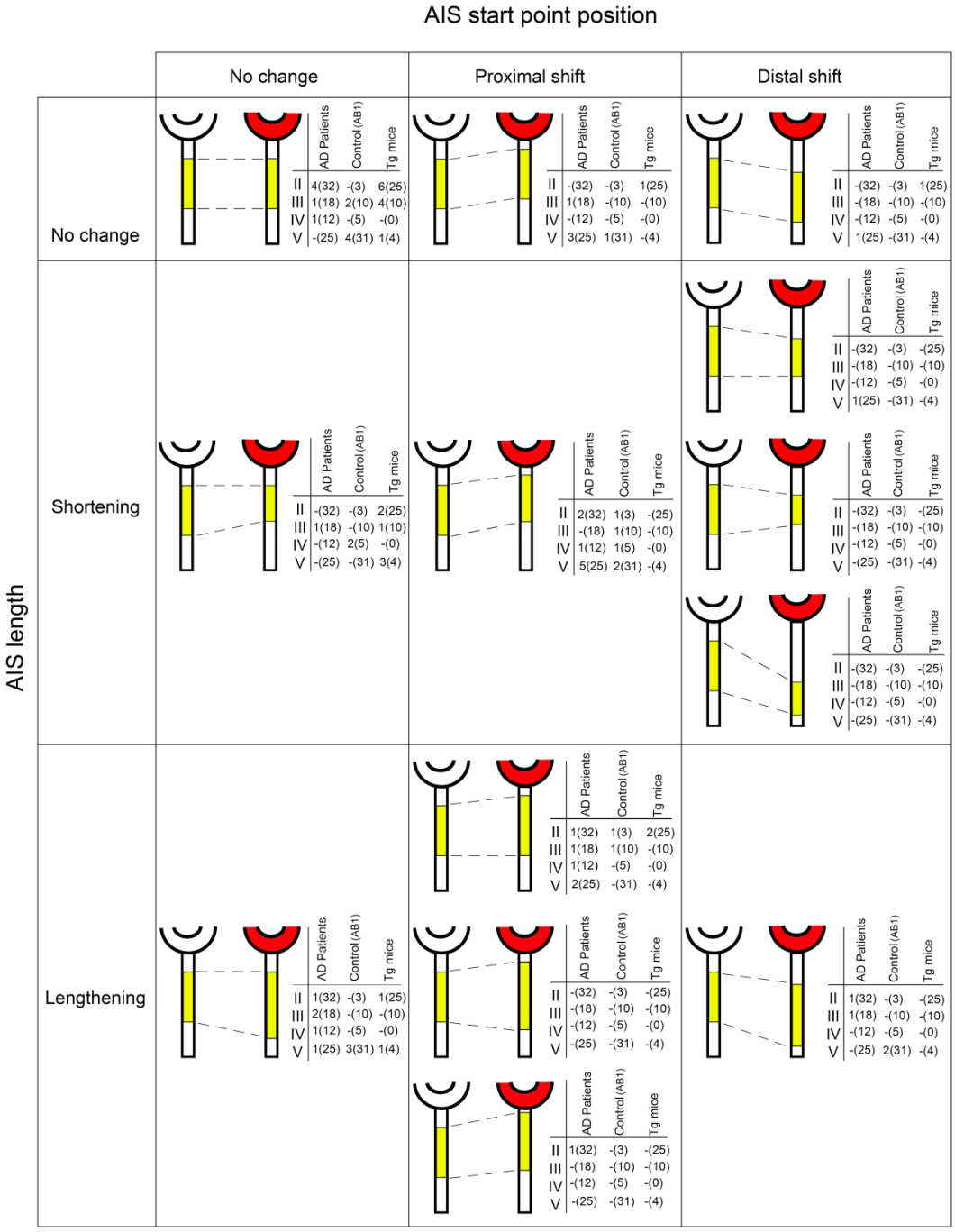

Figure 4: Summarizing diagram showing all possible changes and the heterogeneity of alterations in AIS length and/or position observed in AT8+ neocortical neurons from AD patients, a non-demented case with tau pathology (Control AB1) and in P301S tauopathy mouse model. For each case, AIS (yellow) length and position in AT8- neurons (based in mean values obtained from all AT8-cells analyzed in each cortical layer) is indicated on the left side (white colored neuronal somatas) whereas AIS features from AT8+ neurons is shown on the right side (red colored somatas). The number of AT8+ neurons in which the different types of AIS change in length and/or position was found is indicated in relation to the number (between brackets) of AT8- neurons analyzed .

Discussion

The importance of AIS structural alterations by their potential involvement in many psychiatric and neurological disorders has been previously recognized (see (Buffington and Rasband 2011). In the case of AD, a down regulation of the AIS proteins AnkyrinG or βIV-spectrin, which are essential for the maintenance of AIS integrity (Jenkins and Bennett 2001; Komada and Soriano 2002; Hedstrom et al. 2008) was found in AD patients at late- (V-VI) as compared to early (I-II)-Braak stages (Sohn et al. 2016). In line with the study by Sohn et al., (Sohn et al. 2016), in the present study we found that βIV-spectrin immunostaining of the AIS was preserved in cortical tissue from only AD patients at relatively early stages of the disease (stage III). In contrast, no βIV-spectrin AIS immunostaining was found in tissue from eight AD patients that, except two cases, were at more advanced stages of the disease (see table 1).

In addition to ante-mortem factors (age, use of toxic substances and drugs, duration of agonal state, etc.), it is known that a major limitation in studies using brain tissue from autopsy consist in the fact that various post mortem factors affect histological stainings. These factors include post-mortem time (PT) and tissue fixation, embedding and staining procedures (Gonzalez-Riano et al. 2017). As in the present study there were no differences in these post-mortem parameters between patients, and the postmortem delay time was in most (all except one) cases below 5h, known to be optimal for histological stainings (Gonzalez-Riano et al. 2017), the differences observed in βIV-spectrin immunostaining of the AIS might be considered to relate with the evolution of the disease. The lack of βIV-spectrin immunostaining in tissue from the eight AD patients with advanced stages could be partially due to the presence of Aβ plaques, one the two pathological hallmarks of AD. It has been shown a decrease in AIS length and βIV-spectrin expression in APP-PS1 mouse model of amyloidosis (Marin et al. 2016), in addition to alterations in AIS GABAergic innervation (Leon-Espinosa et al. 2012). However, our results indicate that the plaque load probably is not the factor responsible for the decrease in AIS βIV-spectrin immunostaining in AD, as this staining was preserved in a patient with a relatively high plaque load (IF13).

Tau hyperphosphorylation, AIS alterations and neuronal activity

The main results of the present study demonstrate for the first time the existence of a relationship, in tissue from AD patients, between the neuronal content of hyperphosphorylated tau and alterations in AIS length and position. Similar results were found in neocortical tissue from a non-demented patient with AT8 positive neurons and from the P301S mouse model of tauopathy which support the idea that the accumulation of phospho-tau is associated with structural alterations of the AIS. In present study is that we have examined relatively few labeled cells and only using AT8 antibodies to detect hyperphosphorylated tau that recognized tau phosphorylation in Ser202/Thr205 residues. Therefore, the significance of the proportion of neurons showing changes should be considered only an approximation and we cannot discard the possibility that among the AT8 negative neurons, some neurons with tau hyperphosphorylated at residues other than Ser202/Thr205 could be included. Further studies using antibodies directed to AIS markers in combination with antibodies that recognize tau phosphorylated at additional residues should be carried out to get a deeper insight in the AIS vulnerability to the progression of tau hyperphosphorylation during the course of AD.

Studies in AD mouse models have shown that the barrier functions of the AIS —that control the traffic of tau and help in the restriction of various isoforms of tau to specific neuronal domains — are disrupted in AD mouse models in the presence of phosphorylated tau and disorganized microtubules, or by the downexpression of AIS proteins like AnkyrinG or EB1, resulting in the missorting of hyperphosphorylated tau that accumulates in the somatodendritic domain (Zempel et al. 2017; Li et al. 2011; Sun et al. 2014).

In a previous study, a distal shift of the AIS was reported in hippocampal neurons from the tauopathy mouse model rTg4510 (Hatch et al. 2017) although the neuronal content in phosphorylated tau of the neurons with an altered AIS was not directly evaluated. In the present study, it is important to emphasize that we found in AD patients a heterogeneity in AIS alterations in AT8-immunostained neurons, being the most common changes the proximal shift and the lengthening of the AIS. Various studies have demonstrated that the AIS is an efficient site to regulate neuronal activity as it has been shown to be subjected to plastic changes in response to neural activity (Grubb and

Burrone 2010; Kuba et al. 2010; Grundemann and Hausser 2010). Among the variety of AIS plasticity phenomena reported to date, it has been shown in the chicken auditory system that the loss of neuronal activity induced by the disruption of presynaptic sensory inputs leads to an increase in AIS length in brainstem auditory nuclei (Kuba et al. 2010; Yamada and Kuba 2016). Visual information deprivation during the critical period of plasticity of visual cortical neurons prevents the shortening of the AIS and maintains a longer immature AIS (Gutzmann et al. 2014).

Alterations in neuronal excitability have been acknowledged as important features in AD (Palop and Mucke 2009). Various studies in AD models have suggested important, although heterogeneous roles of tau in the modulation of neuronal excitability. For example, reduction of tau using antisense gene therapy or the removal of tau in knock our mice was reported to reduce hyperexcitability (Roberson et al. 2007; DeVos et al. 2013; Holth et al. 2013). In addition, the presence of phosphorylated tau in the somatodendritic compartment has also been shown *in vitro* to decrease neuronal activity (Thies and Mandelkow 2007; Hoover et al. 2010). Furthermore, it has been shown in the P301L tauopathy mouse model that the effects induced by tau pathology on neuronal activity are heterogeneous and vary among different cortical regions. For instance, an increased firing rate was reported in neocortical neurons from frontal cortex (Rocher et al. 2010) whereas a reduced action potential firing rate was reported in hippocampal neurons (Hatch et al. 2017) and no changes were reported in the activity of neurons in the visual cortex (Kuchibhotla et al. 2014).

It is known that changes in neuronal activity differentially affect the AIS of different neuronal populations. For example, neuronal chronic depolarization induces AIS shortening in dentate granule cells (Evans et al. 2015) and an AIS distal shift in hippocampal CA1 pyramidal neurons (Wefelmeyer et al. 2015). Therefore, it is tempting to speculate that the heterogeneity in AIS changes found in the present study could be derived from differential changes in neuronal activity that the presence of hyperphosphorylated tau might induce in different neuronal populations. Further research is necessary to test this possibility. Finally, AIS relative position and length have been shown to modulate neuronal excitability (Grubb and Burrone 2010; Kuba et al. 2010) with a negative linear relationship between action potential firing with the AIS distance to the soma (Hatch et al. 2017). Therefore, the heterogeneous changes on the AIS of different AT8 positive neurons found in the present study are likely to have a

relevant impact on the excitability of these cells and could help to explain the different effects that the presence of pathological tau might induce in different neuronal populations. In summary, our results show that neurons with hyperphosphorylated tau aggregates undergo alterations in the length and/or the position of the AIS which are likely to alter the normal neuronal excitability which might contribute to neuronal dysfunction and to changes in the activity of neuronal circuits contributing to the pathophysiology of AD. The various and complex causal relationships that might exist between phosphorylated tau accumulation, neuronal activity changes and AIS structural alterations along with their potential variability between different populations are interesting questions that remain to be clarified and warrant further research.

Acknowledgments

This work was supported by grants from the following entities: SAF 2015-66603-P from the Ministerio de Economía y Competitividad; Centro de Investigación en Red sobre Enfermedades Neurodegenerativas (CIBERNED, CB06/05/0066, Spain); and a grant from the Alzheimer's Association (ZEN-15-321663). The authors thank Biobanco-Hospital Clínico-IDIBAPS for the human tissue supplied. The authors declare that they have no conflict of interest.

References

Anton-Fernandez A, Aparicio-Torres G, Tapia S, DeFelipe J, Munoz A (2017a) Morphometric alterations of Golgi apparatus in Alzheimer's disease are related to tau hyperphosphorylation. Neurobiol Dis 97 (Pt A):11-23.

Anton-Fernandez A, Merchan-Rubira J, Avila J, Hernandez F, DeFelipe J, Munoz A (2017b) Phospho-Tau Accumulation and Structural Alterations of the Golgi Apparatus of Cortical Pyramidal Neurons in the P301S Tauopathy Mouse Model. J Alzheimers Dis 60 (2):651-661.

Anton-Fernandez A, Rubio-Garrido P, DeFelipe J, Munoz A (2015) Selective presence of a giant saccular organelle in the axon initial segment of a subpopulation of layer V pyramidal neurons. Brain Struct Funct 220 (2):869-884.

Baalman KL, Cotton RJ, Rasband SN, Rasband MN (2013) Blast wave exposure impairs memory and decreases axon initial segment length. J Neurotrauma 30 (9):741-751.

Binder LI, Frankfurter A, Rebhun LI (1985) The distribution of tau in the mammalian central nervous system. J Cell Biol 101 (4):1371-1378

Boiko T, Van Wart A, Caldwell JH, Levinson SR, Trimmer JS, Matthews G (2003) Functional specialization of the axon initial segment by isoform-specific sodium channel targeting. J Neurosci 23 (6):2306-2313.

Braak H, Braak E (1995) Staging of Alzheimer's disease-related neurofibrillary changes. Neurobiol Aging 16 (3):271-278; discussion 278-284.

Buffington SA, Rasband MN (2011) The axon initial segment in nervous system disease and injury. Eur J Neurosci 34 (10):1609-1619.

DeVos SL, Goncharoff DK, Chen G, Kebodeaux CS, Yamada K, Stewart FR, Schuler DR, Maloney SE, Wozniak DF, Rigo F, Bennett CF, Cirrito JR, Holtzman DM, Miller TM (2013) Antisense reduction of tau in adult mice protects against seizures. J Neurosci 33 (31):12887-12897.

Evans MD, Dumitrescu AS, Kruijssen DL, Taylor SE, Grubb MS (2015a) Rapid Modulation of Axon Initial Segment Length Influences Repetitive Spike Firing. Cell Rep 13 (6):1233-1245.

Gonzalez-Riano C, Tapia-Gonzalez S, Garcia A, Munoz A, DeFelipe J, Barbas C (2017) Metabolomics and neuroanatomical evaluation of post-mortem changes in the hippocampus. Brain Struct Funct 222 (6):2831-2853.

Grubb MS, Burrone J (2010) Activity-dependent relocation of the axon initial segment fine-tunes neuronal excitability. Nature 465 (7301):1070-1074.

Grundemann J, Hausser M (2010) Neuroscience: A plastic axonal hotspot. Nature 465 (7301):1022-1023.

Gutzmann A, Ergul N, Grossmann R, Schultz C, Wahle P, Engelhardt M (2014) A period of structural plasticity at the axon initial segment in developing visual cortex. Front Neuroanat 8:11.

Hamada MS, Kole MH (2015) Myelin loss and axonal ion channel adaptations associated with gray matter neuronal hyperexcitability. J Neurosci 35 (18):7272-7286.

Harty RC, Kim TH, Thomas EA, Cardamone L, Jones NC, Petrou S, Wimmer VC (2013) Axon initial segment structural plasticity in animal models of genetic and acquired epilepsy. Epilepsy Res 105 (3):272-279.

Hatch RJ, Wei Y, Xia D, Gotz J (2017) Hyperphosphorylated tau causes reduced hippocampal CA1 excitability by relocating the axon initial segment. Acta Neuropathol 133 (5):717-730.

Hedstrom KL, Ogawa Y, Rasband MN (2008) AnkyrinG is required for maintenance of the axon initial segment and neuronal polarity. J Cell Biol 183 (4):635-640.

Hinman JD, Rasband MN, Carmichael ST (2013) Remodeling of the axon initial segment after focal cortical and white matter stroke. Stroke 44 (1):182-189.
Hofflin F, Jack A, Riedel C, Mack-Bucher J, Roos J, Corcelli C, Schultz C, Wahle P, Engelhardt M (2017) Heterogeneity of the Axon Initial Segment in Interneurons and Pyramidal Cells of Rodent Visual Cortex. Front Cell Neurosci 11:332.
Holth JK, Bomben VC, Reed JG, Inoue T, Younkin L, Younkin SG, Pautler RG, Botas J, Noebels JL (2013) Tau loss attenuates neuronal network hyperexcitability in mouse and Drosophila genetic models of epilepsy. J Neurosci 33 (4):1651-1659.
Hoover BR, Reed MN, Su J, Penrod RD, Kotilinek LA, Grant MK, Pitstick R, Carlson GA, Lanier LM, Yuan LL, Ashe KH, Liao D (2010) Tau mislocalization to dendritic spines mediates synaptic dysfunction independently of neurodegeneration. Neuron 68 (6):1067-1081.
Inda MC, DeFelipe J, Munoz A (2009) Morphology and distribution of chandelier cell axon terminals in the mouse cerebral cortex and claustroamygdaloid complex. Cereb Cortex 19 (1):41-54.
Jenkins SM, Bennett V (2001) Ankyrin-G coordinates assembly of the spectrin-based membrane skeleton, voltage-gated sodium channels, and L1 CAMs at Purkinje neuron initial segments. J Cell Biol 155 (5):739-746.
Jones SL, Svitkina TM (2016) Axon Initial Segment Cytoskeleton: Architecture, Development, and Role in Neuron Polarity. Neural Plast 2016:6808293.
Kaphzan H, Buffington SA, Jung JI, Rasband MN, Klann E (2011) Alterations in intrinsic membrane properties and the axon initial segment in a mouse model of Angelman syndrome. J Neurosci 31 (48):17637-17648.
Kole MH, Ilschner SU, Kampa BM, Williams SR, Ruben PC, Stuart GJ (2008) Action potential generation requires a high sodium channel density in the axon initial segment. Nat Neurosci 11 (2):178-186.
Kole MH, Letzkus JJ, Stuart GJ (2007) Axon initial segment Kv1 channels control axonal action potential waveform and synaptic efficacy. Neuron 55 (4):633-647.
Komada M, Soriano P (2002) [Beta]IV-spectrin regulates sodium channel clustering through ankyrin-G at axon initial segments and nodes of Ranvier. J Cell Biol 156 (2):337-348.
Kosik KS, Finch EA (1987) MAP2 and tau segregate into dendritic and axonal domains after the elaboration of morphologically distinct neurites: an immunocytochemical study of cultured rat cerebrum. J Neurosci 7 (10):3142-3153
Kuba H, Oichi Y, Ohmori H (2010) Presynaptic activity regulates Na(+) channel distribution at the axon initial segment. Nature 465 (7301):1075-1078.
Kuchibhotla KV, Wegmann S, Kopeikina KJ, Hawkes J, Rudinskiy N, Andermann ML, Spires-Jones TL, Bacskai BJ, Hyman BT (2014) Neurofibrillary tangle-bearing neurons are functionally integrated in cortical circuits in vivo. Proc Natl Acad Sci U S A 111 (1):510-514.
Leon-Espinosa G, DeFelipe J, Munoz A (2012) Effects of amyloid-beta plaque proximity on the axon initial segment of pyramidal cells. J Alzheimers Dis 29 (4):841-852.
Li X, Kumar Y, Zempel H, Mandelkow EM, Biernat J, Mandelkow E (2011) Novel diffusion barrier for axonal retention of Tau in neurons and its failure in neurodegeneration. EMBO J 30 (23):4825-4837.
Lorincz A, Nusser Z (2010) Molecular identity of dendritic voltage-gated sodium channels. Science 328 (5980):906-909.
Mandell JW, Banker GA (1996) A spatial gradient of tau protein phosphorylation in nascent axons. J Neurosci 16 (18):5727-5740
Marin MA, Ziburkus J, Jankowsky J, Rasband MN (2016) Amyloid-beta plaques disrupt axon initial segments. Exp Neurol 281:93-98.
Migheli A, Butler M, Brown K, Shelanski ML (1988) Light and electron microscope localization of the microtubule-associated tau protein in rat brain. J Neurosci 8 (6):1846-1851
Mirra SS, Heyman A, McKeel D, Sumi SM, Crain BJ, Brownlee LM, Vogel FS, Hughes JP, van Belle G, Berg L (1991) The Consortium to Establish a Registry for Alzheimer's

Disease (CERAD). Part II. Standardization of the neuropathologic assessment of Alzheimer's disease. Neurology 41 (4):479-486

Palop JJ, Mucke L (2009) Epilepsy and cognitive impairments in Alzheimer disease. Arch Neurol 66 (4):435-440.

Roberson ED, Scearce-Levie K, Palop JJ, Yan F, Cheng IH, Wu T, Gerstein H, Yu GQ, Mucke L (2007) Reducing endogenous tau ameliorates amyloid beta-induced deficits in an Alzheimer's disease mouse model. Science 316 (5825):750-754.

Rocher AB, Crimins JL, Amatrudo JM, Kinson MS, Todd-Brown MA, Lewis J, Luebke JI (2010) Structural and functional changes in tau mutant mice neurons are not linked to the presence of NFTs. Exp Neurol 223 (2):385-393.

Schafer DP, Jha S, Liu F, Akella T, McCullough LD, Rasband MN (2009) Disruption of the axon initial segment cytoskeleton is a new mechanism for neuronal injury. J Neurosci 29 (42):13242-13254.

Sohn PD, Tracy TE, Son HI, Zhou Y, Leite RE, Miller BL, Seeley WW, Grinberg LT, Gan L (2016) Acetylated tau destabilizes the cytoskeleton in the axon initial segment and is mislocalized to the somatodendritic compartment. Mol Neurodegener 11 (1):47.

Stoler O, Fleidervish IA (2016) Functional implications of axon initial segment cytoskeletal disruption in stroke. Acta Pharmacol Sin 37 (1):75-81.

Sun X, Wu Y, Gu M, Liu Z, Ma Y, Li J, Zhang Y (2014) Selective filtering defect at the axon initial segment in Alzheimer's disease mouse models. Proc Natl Acad Sci U S A 111 (39):14271-14276.

Thies E, Mandelkow EM (2007) Missorting of tau in neurons causes degeneration of synapses that can be rescued by the kinase MARK2/Par-1. J Neurosci 27 (11):2896-2907.

Wefelmeyer W, Cattaert D, Burrone J (2015) Activity-dependent mismatch between axo-axonic synapses and the axon initial segment controls neuronal output. Proc Natl Acad Sci U S A 112 (31):9757-9762.

Yamada R, Kuba H (2016) Structural and Functional Plasticity at the Axon Initial Segment. Front Cell Neurosci 10:250.

Yoshiyama Y, Higuchi M, Zhang B, Huang SM, Iwata N, Saido TC, Maeda J, Suhara T, Trojanowski JQ, Lee VM (2007) Synapse loss and microglial activation precede tangles in a P301S tauopathy mouse model. Neuron 53 (3):337-351.

Zempel H, Dennissen FJA, Kumar Y, Luedtke J, Biernat J, Mandelkow EM, Mandelkow E (2017) Axodendritic sorting and pathological missorting of Tau are isoform-specific and determined by axon initial segment architecture. J Biol Chem 292 (29):12192-12207.

Brain Structure and Function

Modifications of the axon initial segment during the hibernation of the Syrian hamster

--Manuscript Draft--

Manuscript Number:	
Full Title:	Modifications of the axon initial segment during the hibernation of the Syrian hamster
Article Type:	Original Article
Keywords:	Hibernation; Ankyrin G; cortex; hippocampus; hypothermia
Corresponding Author:	Alberto Munoz, Ph.D. Politecnica University Pozuelo de Alarcón, Madrid SPAIN
Corresponding Author Secondary Information:	
Corresponding Author's Institution:	Politecnica University
Corresponding Author's Secondary Institution:	
First Author:	Alberto Munoz, Ph.D.
First Author Secondary Information:	
Order of Authors:	Alberto Munoz, Ph.D. Gonzalo León-Espinosa, PhD Silvia Tapia-González, PhD Alejandro Antón-Fernández, PhD student Javier DeFelipe, PhD
Order of Authors Secondary Information:	
Funding Information:	Ministerio de Economía y Competitividad (SAF 2015-66603-P) — Dr Javier DeFelipe CIBERNED (CB06/05/0066) — Dr Javier DeFelipe Alzheimer´s Association (ZEN-15-321663) — Dr Javier DeFelipe
Abstract:	Mammalian hibernation is a natural process in which the brain undergoes profound adaptive changes that appear to protect the brain from extreme hypoxia and hypothermia. In addition to a virtual cessation of neural and metabolic activity, these changes include a decrease in adult neurogenesis; the retraction of neuronal dendritic trees; changes in dendritic spines and synaptic connections; fragmentation of the Golgi apparatus; and the phosphorylation of the microtubule-associated protein tau. Furthermore, alterations of microglial cells also occur in torpor. Importantly, all of these changes are rapidly and fully reversed when the animals arouse from torpor state, with no apparent brain damage occurring. Thus, hibernating animals are excellent natural models to study different aspects of brain plasticity. The axon initial segment (AIS) is critical for the initiation of action potentials in neurons and is an efficient site for the regulation of neural activity. This specialized structure —characterized by the expression of different types of ion channels and adhesion, scaffolding and cytoskeleton proteins— is subjected to morpho-functional plastic changes upon variations in neural activity or in pathological conditions. Here, we used immunocytochemistry and 3D confocal microscopy reconstruction techniques to measure the possible morphological differences in the AIS of cortical (layers IIIII and V) and hippocampal (CA1) neurons during the hibernation of the Syrian hamster. Our results indicate that the general integrity of the AIS is resistant to the ischemia/hypoxia conditions that are characteristic of the torpor phase of hibernation. In addition, the length of the AIS significantly increased in all the regions studied — by about 1620% in torpor animals compared to controls, suggesting the existence of compensatory

	mechanisms in response to a decrease in neuronal activity during the torpor phase of hibernation. Furthermore, in double-labeling experiment, we found that the AIS in layer V of torpid animals was longer in neurons expressing phospho-tau than in those not labeled for phospho-tau. This suggests that AIS plastic changes were more marked in phospho-tau accumulating neurons. Overall, the results further emphasize that mammalian hibernation is a good physiological model to study AIS plasticity mechanisms in non-pathological conditions.
Suggested Reviewers:	Marteen Kole Koninklijke Nederlandse Academie van Wetenschappen m.kole@nin.knaw.nl
	Thomas Arendt Paul Flechsig Institute of Brain Research, Unive, Leipzig aret@medizin.uni-leipzig.de
	H Crair Heller Prof, Stanford University hcheller@stanford.edu
	Eckhard Mandelkow, Proffesor German Center for Neurodegenerative Diseases eckhard.mandelkow@dzne.de
Opposed Reviewers:	

Modifications of the axon initial segment during the hibernation of the Syrian hamster

Gonzalo León-Espinosa[*1,2,5], Alejandro Antón-Fernández[,*1,2], Silvia Tapia-González [1,2], Javier DeFelipe[1,2,3], and Alberto Muñoz[1,2,4]

1 Instituto Cajal, CSIC, Madrid, Spain.

2 Laboratorio Cajal de Circuitos Corticales (CTB), Universidad Politécnica de Madrid, Madrid, Spain.

3 CIBERNED, Centro de Investigación Biomédica en Red de Enfermedades Neurodegenerativas, Spain.

4 Departamento de Biología Celular, Universidad Complutense, Madrid, Spain.

5 Facultad de Farmacia, Universidad San Pablo CEU, Madrid, Spain

[*] Equal contribution

Abbreviated title: AIS plasticity during hibernation

Orcid codes:

Gonzalo León-Espinosa: 0000-0002-9921-2614

Javier DeFelipe: 0000-0001-5484-0660

Alberto Muñoz: 0000-0003-4607-3398

Alejandro Antón-Fernández: 0000-0001-8029-4288

- **Corresponding Author:** Alberto Muñoz, Ph.D., Laboratorio Cajal de circuitos corticales. Centro de Tecnología Biomédica. Universidad Politécnica de Madrid. Pozuelo de Alarcón, Madrid 28223, SPAIN. Tel: +34 91 4524900 (ext. 1943).e-mail: amunozc@bio.ucm.es

Abstract

Mammalian hibernation is a natural process in which the brain undergoes profound adaptive changes that appear to protect the brain from extreme hypoxia and hypothermia. In addition to a virtual cessation of neural and metabolic activity, these changes include a decrease in adult neurogenesis; the retraction of neuronal dendritic trees; changes in dendritic spines and synaptic connections; fragmentation of the Golgi apparatus; and the phosphorylation of the microtubule-associated protein tau. Furthermore, alterations of microglial cells also occur in torpor. Importantly, all of these changes are rapidly and fully reversed when the animals arouse from torpor state, with no apparent brain damage occurring. Thus, hibernating animals are excellent natural models to study different aspects of brain plasticity. The axon initial segment (AIS) is critical for the initiation of action potentials in neurons and is an efficient site for the regulation of neural activity. This specialized structure —characterized by the expression of different types of ion channels and adhesion, scaffolding and cytoskeleton proteins— is subjected to morpho-functional plastic changes upon variations in neural activity or in pathological conditions. Here, we used immunocytochemistry and 3D confocal microscopy reconstruction techniques to measure the possible morphological differences in the AIS of cortical (layers II–III and V) and hippocampal (CA1) neurons during the hibernation of the Syrian hamster. Our results indicate that the general integrity of the AIS is resistant to the ischemia/hypoxia conditions that are characteristic of the torpor phase of hibernation. In addition, the length of the AIS significantly increased in all the regions studied — by about 16–20% in torpor animals compared to controls, suggesting the existence of compensatory mechanisms in response to a decrease in neuronal activity during the torpor phase of hibernation. Furthermore, in double-labeling experiment, we found that the AIS in layer V of torpid animals was longer in neurons expressing phospho-tau than in those not labeled for phospho-tau. This suggests that AIS plastic changes were more marked in phospho-tau accumulating neurons. Overall, the results further emphasize that mammalian hibernation is a good physiological model to study AIS plasticity mechanisms in non-pathological conditions.

Keywords: Hibernation, Ankyrin G, cortex, hippocampus, hypothermia

Introduction

The axon initial segment (AIS) is a short, non-myelinated specialized region of the axon that separates the axonal and somato-dendritic compartments. The AIS contributes to the generation and modulation of action potentials in neurons due to the high density of voltage-gated Na^+, K^+ and Ca^{2+} channels associated with cytoskeletal and membrane scaffold proteins and cell adhesion molecules (Kordeli et al. 1990; Kordeli et al. 1995; Srinivasan et al. 1988; Srinivasan et al. 1992). Ankyrin G is an adaptor protein that is concentrated at the AIS and plays a pivotal role in the recruitment of ion channels and in the assembly and maintenance of AIS structure and function (Jenkins et al. 2015). The AIS is an efficient site to regulate neuronal activity as it is a dynamic structure that may undergo plastic changes to modulate neuronal responses after changes in input activity — a process that may have a role in adaptive responses of the nervous system (Grubb and Burrone 2010; Kuba et al. 2010; Turrigiano and Nelson 2000, 2004). These modifications include variations in AIS length and/or distance from the soma that will attenuate or enhance the excitability of the neuron. For example, it has been shown that loss of auditory input leads to an increase in the length of Na^+ channel clusters at the AIS, compensating for the loss of auditory nerve activity and leading to an increase in neuronal excitability (Kuba et al. 2010). Furthermore, neuronal depolarization has been shown to shorten the AIS of hippocampal dentate granule cells (Evans et al. 2015) and to promote a distal shift of the AIS in hippocampal CA1 pyramidal neurons (Wefelmeyer et al. 2015). In both of these cases, these changes promote a decrease in the excitability of neurons to maintain homeostasis of neuronal circuits.

The importance of AIS structural plasticity mechanisms, occurring with a variety of alterations in the concentration and/or location of the proteins within the AIS, has also been demonstrated by their involvement in different pathological conditions. Disruption of the AIS integrity has been proposed to play a role in different neurological disorders such as channelopathies, autism, schizophrenia, autoimmune disorders and Alzheimer's disease (Buffington and Rasband 2011). AIS shortening has been reported after demyelination (Hamada and Kole 2015), traumatic brain injury (Baalman et al. 2013) or in animal models of stroke (Hinman et al. 2013; Schafer et al. 2009; Stoler and Fleidervish 2016). AIS elongation was reported in an Angelman syndrome mouse model (Kaphzan et al. 2011). A distal shift in AIS position in a mouse model of genetic epilepsy and a rat model of acquired epilepsy have been proposed to result in a change in action potential firing threshold (Harty et al. 2013).

However, hibernation is a non-pathological adaptive biological process that allows animals to survive periods of reduced food availability with minimum energy expenditure (Ruf and Geiser 2015). The Syrian hamster (*Mesocricetus auratus*) is a common laboratory rodent that may enter hibernation in response to low temperatures and prolonged short photoperiod, leading to a decrease in body and brain temperature, blood flow reduction, as well as suppression of the immune system and a reduced metabolism (Bouma et al. 2010a; Bouma et al. 2010b; Drew et al. 2001; Zhou et al. 2001). This biological state is called torpor and can last for 3–4 days. However, these torpor bouts are alternated with short arousal periods of activity and normothermia (Geiser 2004, 2013). Remarkable adaptive and reversible structural changes have been shown to occur in the brain during torpor states such as a decrease in adult neurogenesis; the fragmentation and reduction of the neuronal Golgi apparatus; alterations in dendritic trees including dendritic spine retraction; and a decrease in synaptic connections (Leon-Espinosa et al. 2016; Anton-Fernandez et al. 2015; Popov and Bocharova 1992b; Popov et al. 1992a; Popov et al. 2007; von der Ohe et al. 2006; von der Ohe et al. 2007; Popov et al. 2011; Bullmann et al. 2016). These changes occur in parallel with a virtual cessation in neuronal activity (Strumwasser 1959b, c; Igelmund 1995; South 1972; Walker et al. 1977).

As the AIS has been shown to undergo structural plasticity processes after in vitro or pathological manipulation of neuronal input activity, in the present study we analyze whether the entrance in torpor of hibernating hamsters would induce plastic changes in the morphological features or the position of the AIS. For this purpose, we have compared the length and position of the AIS of pyramidal neurons from layers II–III and V of the somatosensory cortex and from the CA1 hippocampal field between Syrian hamster in euthermia conditions and at the torpor phase of hibernation.

In addition, various studies have described alterations of the AIS in animal models of Alzheimer's disease (AD), which is characterized by two main pathological hallmarks: accumulation of amyloid β (Aβ) and hyperphosphorylated microtubule-associated protein tau. Regarding Aβ plaques, it has been reported that their presence induces alterations in the GABAergic innervation of the AIS (Leon-Espinosa et al. 2012) and also leads to decreases in AIS length and βIV spectrin expression (Marin et al. 2016) in APP mouse models of AD. Regarding tau phosphorylation, previous studies reported that the barrier functions of the AIS —that restrict tau protein to the axonal compartment (Binder et al. 1985; Kosik and Finch 1987; Migheli et al. 1988; Mandell and Banker 1996)— are disrupted in AD mouse models resulting in the missorting of hyperphosphorylated tau that accumulates in the somatodendritic domain (Li et al. 2011). In this regard, mammalian hibernation has been proposed as a model to study

the neuroprotection mechanisms in the early stages of AD since, during the torpor state, tau shows a transitory PHF (Paired Helical Filament)-like hyperphosphorylation with some similarities to that found in AD patients at early stages of the disease (e.g., the neuronal pretangle stage). This phospho-tau is observed during torpor in various brain regions, including large subpopulations of neocortical and hippocampal neurons (Zhou et al. 2001; Arendt et al. 2003; Avila et al. 2004; Hartig et al. 2005; Hartig et al. 2007; Leon-Espinosa et al. 2013; Anton-Fernandez et al. 2015; Stieler et al. 2011; Su et al. 2008). Therefore, in the present study, we have also analyzed whether possible morphological plastic changes of the AIS can be influenced by the accumulation of hyperphosphorylated tau, by comparing AIS length measurements from layer V neurons from hamsters at torpor with or without phospho (Ser202/Thr205) tau accumulation.

Materials and methods

All experimental procedures were carried out at the animal facility of San Pablo CEU University of Madrid (SVA-CEU.USP, registration number ES 28022 0000015) and were approved by the institutional Animal Experiment Ethics Committee. A total of 21 male one-month-old Syrian hamsters (*Mesocricetus auratus*) were purchased from Janvier Labs (*Le Genest-Saint-Isle*, France). The animals had free access to food and water and were kept at 23°C with an 8:16 h light/dark cycle for a four- to six-week acclimatization period in our animal facility. After the acclimatization period, some of these hamsters were transferred to a hibernaculum or hibernation chamber to induce torpor as previously described (Anton-Fernandez et al. 2015). Nine hamsters were sacrificed during the torpor state and, in order to establish a control (euthermic) group, a further 12 animals were left in normal conditions (not forced to hibernate) and were sacrificed at the same age as the torpid animals (approximately 3 months).

For immunofluorescence experiments, we used 21 hamsters (9 control and 12 torpor). Animals were sacrificed by an intraperitoneal overdose (40 mg/kg) of sodium pentobarbital and perfused with a saline solution (together with heparin) followed by 4% paraformaldehyde. Brains were then removed and postfixed by immersion in 4% paraformaldehyde for 24 h at 4°C. The brains were cut into 50 µm-thick coronal sections with a Vibratome (St Louis, MO, USA).

In addition, we used brain sections from one euthermic hamster subjected to a focal cerebral ischemia induced by the permanent occlusion of the frontal branch of the middle cerebral artery making use of tissue that was available from a previous study carried out at our laboratory (Leon-Espinosa et al. 2017). Briefly, the animal was anesthetized, the right lateral aspect of the skull was drilled, the dura mater was cut and retracted and the frontal branch of the middle cerebral artery was ligated with a suture nylon monofilament. A sharp decrease in blood flow was confirmed by laser Doppler flowmetry (Järfalla, Sweden). Following surgery, the animal was returned to its cage, kept at room temperature and allowed free access to food and water for one week after which it was euthanized.

In addition, for the characterization of the immunocytochemical labeling of the AIS, we used additional brain tissue from mouse and human brains. We examined the brain of two 8-week-old male C57BL/6J mice obtained from the animal facility at the Cajal Institute (CSIC). These animals were sacrificed and the brain extracted and processed as described above for hamsters. For the human brain tissue, we used neocortical tissue from the anterolateral temporal cortex obtained by surgical resection from a 20-year-old female patient (H136) diagnosed with intractable temporal lobe epilepsy with a mesial origin. This material has been used in previous studies from our laboratory (Arellano et al. 2004; Anton-Fernandez et al. 2017a) in which medical history details were described. Informed consent was obtained from this patient, and procedures were previously approved by the ethical committee of the ''Hospital de la Princesa'' (Madrid). During surgery, electrocorticography allowed the spiking and non-spiking areas to be distinguished before tissue excision by tailored temporal lobectomy and amygdalohippocampectomy under electrocorticography guidance. After surgery, the lateral neocortex and mesial structures were subjected to standard neuropathological assessment. The lateral neocortical biopsy sample from this patient was histologically normal, whereas the hippocampal formation displayed neuronal loss and gliosis (hippocampal sclerosis). In the present study, only normal nonspiking areas of the lateral neocortex were used. Biopsy samples were fixed in cold 4% paraformaldehyde in 0.1 M phosphate buffer at pH 7.4 (PB) for 12 h at 4°C. Vibratome sections (100 µm thick) were processed for immunostaining.

Immunocytochemistry

For immunofluorescence experiments, sections were first rinsed in PB and preincubated for 1 h at room temperature in a stock solution containing 3% normal serum of the species in which the secondary antibodies were raised (Vector Laboratories, Burlingame, CA, USA) diluted in PB

with Triton X-100 (0.25 %). Thereafter, the sections were incubated for 48 h at 4°C in the same stock solution containing the following primary antibodies alone or in the indicated combinations: Mouse IgG2a anti-Ankyrin G (clone N106/36, UC Davis/NIH NeuroMab Facility, CA, USA), c-20 goat anti-Grasp 65 (SC-19481; Santa Cruz, CA, USA), rabbit anti-Grasp65 (ab30315; Abcam, Cambridge, UK), mouse IgG1-anti-phospho-tau, clone AT8 (Thermo Fisher Scientific Cat# MN1020).

For Grasp65 immunostaining, the sections were rinsed and then incubated for 2 h at room temperature with Alexa 488-donkey anti-goat antibodies (1:1000; Molecular Probes, Eugene, OR, USA). For AnkG, NeuN and Grasp65 (c-20) triple immunostaining, sections were incubated with biotinilated horse anti-mouse antibody (1:200), followed by streptavidin 594 (1:1000) and Alexa 488-anti-goat and Alexa 594-anti-rabbit antibodies (1:1000; Molecular Probes). For phospho-tau (AT8) immunostaining, we used biotinilated horse anti-mouse antibodies (1:200), followed by streptavidin 594 (1:1000). All sections were also stained with the nuclear stain DAPI (4,6 diamino-2-phenylindol; Sigma, St. Louis, MO, EEUU). Finally, these sections were washed in PB, mounted with Prolong gold antifade reagant (P36930; Invitrogen) and studied by confocal microscopy (Zeiss, 710).

Image analysis and statistics

We obtained stacks of images recorded at 0.35 µm intervals through separate channels with a 63x oil-immersion lens (NA, 1.40, refraction index, 1.45). ZEN 2012 software (Zeiss) was used to construct composite images from each optical series by combining the images recorded through the different channels, and the same software was used to obtain Z projection images (image resolution: 1024 × 1024 pixels; pixel size: 0.11 µm). Adobe Photoshop (CS4) software was used to compose figures. We used a commercial software package (Imaris 6.4.0 Bitplane AG, Zurich, Switzerland) to measure in 3D the AIS lengths (measurement point tool). To ensure that we selected complete AIS, we only considered those AIS that had complete immunostaining, which was separated in all dimensions from the edges of the stack by at least 5 µm.

The AIS length differences (mean values) between the control and torpor animal groups were compared by a U Mann-Whitney test with the aid of GraphPadPrism (version 5). The differences in AIS length between AT8+ and AT8- cells from layer V (Fig. 4) and the differences in AIS length between the Grasp65 versus AnkG antibodies (Fig. 2) were analyzed using a Wilcoxon test (GraphPadPrism, version 5). Finally, the possible differences in AIS length

between CA1, layer II and layer V from the neocortex were analyzed using a one-way ANOVA (Bonferroni posthoc test).

Immunoprecipitation

The left brain hemisphere was dissected from 1 mouse and homogenized in 1.5 ml RIPA buffer (Sigma-Aldrich, R0278) containing an anti-protease cocktail (Complete mini, Protease inhibitor cocktail tablets, Roche Diagnostics, 1836153), 1mM Phenylmethylsulfonyl Fluoride PMSF, (Calbiochem, 52332). The homogenate was centrifuged twice at 9200 × g for 10 min at 4°C, with the supernatant being transferred to a new tube after each centrifugation. 1.2 ml of lysate was preabsorbed with 100 µl of protein A-Sepharose beads (Sigma-Aldrich, P3296-1ML) and incubated for 30 min at 4°C on a rotator, and was then centrifuged at 1000 × g for 30 sec at 4°C. The supernatant was transferred and distributed into 2 new tubes — one for a negative control (without antibody) and the other for incubation with anti-GRASP65 (C-20) antibody (Santa Cruz Biotechnology, Inc., sc-19481). In the case of the negative control, 20 µl of ascetic liquid was added, whereas in the other tube 500 µg anti-GRASP65 antibody per 1 µg total cellular protein was added, and both tubes were incubated overnight at 4°C on a rotator. The following day, 20 µl of protein A-Sepharose beads were added to each tube and incubated for 2 h at 4°C on a rotator. The mixture was centrifuged at 1000 × g for 30 sec at 4°C, and the supernatants were carefully aspirated and discarded. The pellets with the beads were washed 2–4 times with 1ml RIPA buffer, each time repeating centrifugation at 1000 × g for 30 sec at 4°C. After the final wash, the supernatants were carefully removed and the pellets were resuspended in 75 µl Laemmli Lysis-buffer 1X (Sigma-Aldrich, 38733). The precipitated proteins were detected by SDS-PAGE and LC-MS analysis. The samples were dissolved in simple buffer, denatured and loaded in a 10% SDS-gel and the gel was then stained with Colloidal Coomassie. The protein band was horizontally divided into two similar portions and each one was excised in small pieces and the trypsin digestion protocol was performed (Cristobo et al. 2011).

LC-MS analysis

All peptide separations were carried out on an Easy-nLC 1000 nano system (Thermo Scientific). For each analysis, the sample was loaded into a precolumn Acclaim PepMap 100 (Thermo Scientific) and eluted in an RSLC PepMap C18 (15 cm long, 75 µm inner diameter and 3 µm particle size; Thermo Scientific). The mobile phase flow rate was 300 nL/min using 0.1% formic acid in water (solvent A), and 0.1% formic acid and 100% acetonitrile (solvent B). The gradient profile was set as follows: 0–35% solvent B for 90 min, 35–100% solvent B for 4 min, 100%

solvent B for 8min. Four microliters of each sample were injected. MS analysis was performed using a Q-Exactive mass spectrometer (Thermo Scientific). For ionization, 1800 V of liquid junction voltage and a capillary temperature of 270°C was used. The full scan method employed an m/z 400–1500 mass selection, an Orbitrap resolution of 70,000 (at m/z 200), a target automatic gain control (AGC) value of 3e6, and maximum injection times of 100 ms. After the survey scan, the 10 most intense precursor ions were selected for MS/MS fragmentation. Fragmentation was performed with a normalized collision energy of 27 eV and MS/MS scans were acquired with a starting mass of m/z 100, AGC target of 2e5, resolution of 17,500 (at m/z 200), intensity threshold of 8e3, isolation window of 2 m/z units and maximum IT of 100 ms. Charge state screening was enabled to reject unassigned, singly charged, and seven or more protonated ions. A dynamic exclusion time of 20s was used to discriminate against previously selected ions.

MS data analysis

MS data were analyzed with Proteome Discoverer (version 1.4.1.14) (Thermo) using standardized workflows. Mass spectra *.raw files were searched against the Uniprot *Mus musculus* database (178667 protein sequence entries) using SEQUEST search engine. Precursor and fragment mass tolerance were set to 10 ppm and 0.02 Da, respectively, allowing 2 missed cleavages, carbamidomethylation of cysteines as a fixed modification, methionine oxidation and acetylation N-terminal as a variable modification. Identified peptides were filtered using Percolator algorithm 9 (2) with a q-value threshold of 0.01.

Results

AIS labeling with polyclonal c-20 antibodies (sc-19481)

In studies focusing on the relationship between the hyperphosphorylation of the microtubule-associated protein tau and the structural alterations of the Golgi apparatus (GA) in neurons from AD patients and from animal models of the disease (Anton-Fernandez et al. 2017a; Anton-Fernandez et al. 2015; Anton-Fernandez et al. 2017b), we used several antibodies to identify the GA. Among them, we noted that goat IgG policlonal antibodies raised against a peptide corresponding to human Grasp65 (c-20 antibody, Santa Cruz sc-19481) —which selectively labeled the neuronal GA in human brain tissue (Fig. 1A)— stained the GA with a much lower intensity in mouse and hamster brain tissue and, instead, in these animals, there

was intense staining of eyelash-like processes extending distally from the base of the soma of pyramidal neurons, reminiscent of the AIS (Fig. 1B, C). To determine whether they were in fact AISs, we performed double labeling experiments combining c-20 antibodies with commercially available antibodies to Ankyrin G (neuromab) — the main structural component of AIS. In neurons from layer II of the neocortex from control (euthermic) hamsters, we found c-20 immunostaining in 660 out of 667 AISs (99% colocalization), as identified by Ankyrin G immunostaining (neuromab antibodies) (Fig. 1 D–F). In addition, using Imaris software (measurement point tool) we measured the length of the AISs (n=24) stained with both antibodies and found that both immunostainings yielded virtually the same AIS length (24.09 ± 3.36 µm with c-20 and 24.42 ± 3.08 µm with Neuromab antibodies) (Fig. 2). These results revealed that c-20 goat antibodies represent a reliable AIS marker in mouse and hamster brain tissue. Although the manufacturer company did not provide the precise sequence or the position of the immunogen peptide, they indicated that c-20 antibodies were raised against a 15–25 amino acid peptide in the C terminal region (between positions 350 and 400) of the Grasp65 GA protein of human origin (NCBI AAH75854.1). In an attempt to find out which component of the AIS c-20 antibodies might bind to, we sequenced the blocking peptide provided by the company (Santa Cruz, sc-19481 P) used to raise the c-20 antibodies. Nano-scale liquid chromatography tandem mass spectrometry (nLC MS/MS) was performed (Proteomics and genomics service, CIB, CSIC). This analysis revealed that "EFEVSFLDSPGA" was the peptide sequence most frequently detected by the spectrometer (17 PSM), thus making it the most likely immunogenic peptide (Fig. 1 G). Blast analysis (Basic Local Alignment Search Tool, NIH, U.S National Library of Medicine database) and Clustal Omega analysis (a new multiple sequence alignment program developed by The European Bioinformatics Institute, EMBL-EBI) of this immunogen peptide sequence with the sequences of known protein constituents of the AIS revealed a 60% homology with positions 3133 to 3144 of the 480-kDa isoform of AnkirinG (Fig. 1 H), which is known to be a major component that is highly concentrated in the AIS (Hedstrom et al. 2008; Jenkins et al. 2015; Kordeli et al. 1995). To gain insight into the reasons underlying the above-mentioned interspecies differences in the immunostaining with c-20 antibodies, we compared the region corresponding to the immunogen peptide between the Grasp65 sequences in rodents and humans. We found that, in rodents, there is a proline in position 374 instead of the leucine present in humans (Fig. 1I). The presence of this proline in rodents is likely to modify (Piela et al. 1987; Yun et al. 1991) the protein structure of Grasp-65, making it different from that seen in humans. Structural simulation of this protein region in both species (Phyre2 software (Kelley et al. 2015)) revealed a probable alpha helix secondary structure in human Grasp65 that is absent in rodents (Fig. 1I).

This might help to explain the lower efficacy of the binding of c-20 antibodies to Grasp65 in rodents and the resulting low intensity of staining in the GA. This lower affinity would favor the binding of c-20 antibodies to Ankyrin G in rodents with intense immunostaining of the AIS as a consequence

Finally, to explore whether c-20 antibodies bind to AnkG or to any other known AIS component, we performed immunoprecipitation and mass spectrometry analysis (Proteomics and Genomics Service, CIB, CSIC). A mouse brain homogenate sample was immunoprecipitated with c-20 antibodies and the precipitated proteins were separated by SDS-PAGE. Bands with the adequate molecular weight were excised, trypsin-digested and analyzed by LC-MS analysis. Mass spectrometry data were searched against the Uniprot *Mus musculus* database (178667 protein sequence entries) using SEQUEST search engine. This analysis showed multiple peptides produced by protein digestion corresponding to 97 different proteins. AnkG was the only known AIS component among them and showed the third highest PSM and Score (reliability factor) and the highest percentage of coverage (% of protein sequence recognized) (see supplementary material). In addition, one of the digestion peptides was detected as AnkG "unique peptide". Taken together, these data indicate that c-20 antibodies recognize AnkG in mouse brain, therefore justifying their use as a reliable AIS marker. Finally, the use of polyclonal c-20 antibodies to stain the AIS in the hamster tissue was extremely useful as it efficiently labeled the AIS and allowed the use of mouse monoclonal antibodies for double labeling experiments (see below).

AIS lengthens during hibernation

To characterize possible changes of the AIS of neurons during the hibernation cycle of Syrian hamsters and the possible relationship with tau hyperphosphorylation, we performed experiments with DAPI staining and double immunocytochemical staining combining c-20 antibodies, as an AIS marker, and AT8 antibodies. We first measured in confocal image stacks the length in 3D of the AIS from neurons in layers II–III and V from primary sensory (visual and somatosensory) neocortex and from the CA1 region of the hippocampus in control (euthermic) animals (n=3) (Fig. 3A–C). In the neocortex, the AIS length from neurons in layers II–III and V in control animals was 22.23 ± 1.39 µm (n=154 measured AIS in 9 different animals) and 23.79 ± 2.01 µm (n=141 measured AIS in 9 different animals), respectively, whereas in hippocampal CA1 neurons, they were significantly (ANOVA with Bonferroni correction) longer (31.76 ± 3.00 µm; n=192 measured AIS in 9 different animals) than in the somatosensory cortex.

We next analyzed the possible variations in AIS length during the hibernation cycle by measuring the AIS in animals at torpor (Fig. 3D–F). In torpid animals, AIS length was significantly longer than in euthermic animals in both the neocortex and hippocampus, particularly in the latter region (Fig. 3 G–I). In neurons of layers II–III, this length was 26.53 ± 1.86 µm (n=210 measured AIS in 12 different animals), whereas in layer V it was 27.41 ± 2.19 µm (n=273 measured AIS in 11 different animals). In CA1 hippocampal neurons, the AIS length was 37.93 ± 3.30 µm (n=113 measured AIS in 6 different animals). The analysis revealed that, in neurons from the neocortex (both layers II–III and V) and CA1 regions, AIS were significantly longer in torpid animals than in euthermic animals (p=0.0039, p=0.0273 and p=0.0313 in neurons from layer II–III, layer V of the neocortex, and in CA1, respectively). AIS lengths in neurons from torpid animals were 19.48% longer than in euthermic hamsters in layer II (4.30 µm), 13.20% longer in layer V neurons (3.62 µm) and 19.42% longer in CA1 (6.17 µm).

In addition, to study whether the AIS increase in length during torpor was accompanied by a shift in AIS position, we compared the starting or origin point of the AISs between neurons from control and torpor animals. In neurons from control animals, we found that the c-20-ir AISs started directly from the base of the soma in the large majority of neurons (173 out of 189) (Fig 1D-F). In the 16 remaining neurons (8.5%), the AIS was located slightly more distally in the axon, with a lag between the base of the soma and the AIS starting point (mean ± 1.3 ± 0.7 µm). Similarly, in neurons from animals in torpor, we found that in only 10 out of 121 neurons (8.2%) the starting point of the AIS was located at a distal position (1.84 ± 0.55 µm), whereas in most neurons the AIS started right from the base of the neuronal somata. Therefore, these results indicate that the increase in the length of the AIS during torpor is in general not accompanied by a shift in AIS position.

AIS changes in neurons with hyperphosphorylated tau during torpor

It is well known that, during the torpor phase of hibernation, the microtubule-associated protein tau is highly phosphorylated in various subpopulations of neocortical and hippocampal neurons, whereas after arousal and return to euthermia, this tau phosphorylation decreases to normal levels (Arendt et al. 2003; Hartig et al. 2005; Hartig et al. 2007; Stieler et al. 2011; Leon-Espinosa et al. 2013; Anton-Fernandez et al. 2015). Accordingly, in brain sections immunocytochemically stained with AT8 antibody, which recognizes phospho Ser202 and phospho Thr205 sites in tau protein, we found high levels of tau hyperphosphorylation in the

cell body of a subpopulation of layer V pyramidal neurons in the neocortex (Fig. 4A–C). No AT8 immunostaining was observed at the AIS of these AT8-ir neurons (Fig. 4A–C). We then studied whether neurons with hyperphosphorylated tau were more or less prone to undergoing morphological alterations in the AIS during the hibernation cycle.

For this purpose, in confocal image stacks taken from sections of somatosensory cortex from torpid animals, double immunostained for AT8 and AnKG (c-20 antibodies), we analyzed whether alterations in AIS length were more or less pronounced in neurons with tau hyperphosphorylation (AT8-ir) than in AT8-negative neurons. We measured the AIS length of 133 AT8-ir pyramidal neurons and of 129 surrounding AT8-negative neurons from 10 different animals. We found that, in torpid hamsters, the AIS length from AT8-ir layer V neurons was longer (28.54 ± 2.29 µm) than that of nearby AT8-negative neurons (27.47 ± 2.163 µm) (Fig. 4D). Although the mean difference in AIS length between AT8-ir and AT8-negative neurons was only 1.07 µm (3.9%), these differences were statistically significant (p=0.0488).

AIS disorganization after stroke-induce ischemia during normothermia

Previous studies have reported that, in non-hibernating rodents, the AIS of neocortical neurons is disrupted after ischemic conditions (induced by middle cerebral artery occlusion) by the proteolysis of AIS cytoskeleton components, including AnkG (Schafer et al. 2009). Hibernation is accompanied by ischemia-like conditions due to a reduction in cardiac output and blood flow that conceivably should induce general damage of the AIS of cortical neurons. The above results showing no AnkG degradation in AISs of cortical neurons during torpor suggest the existence of neuroprotective mechanisms that preserve AIS AnkG expression in Syrian hamsters during that phase. To test whether these AIS neuroprotective mechanisms preserve the AIS, as judged by AnkG expression, in hypoxia/ischemia conditions in the normothermia phase of the hibernation cycle, we studied AnkG/iba-1/NeuN triple immunostained sections from an animal subjected to a focal ischemia by the permanent occlusion of the frontal branch of the middle cerebral artery. As expected, iba-1 immunostaining revealed —in the ipsilateral neocortex— an infarct region that primarily affected the primary somatosensory neocortex (Fig. 5A, B). In this infarct region, iba-1-ir microglial cells where very abundant, intensely immunostained and showed a non-ramified hypertrophic phenotype (reactive) as compared with resting microglial cells in the contralateral somatosensory and motor cortical regions (Fig. 5A, C). In contrast to various regions of the contralateral hemisphere that were not affected by the artery occlusion and

that showed normal patterns of AnkG immunostaining, in the infarct region, AnkG AIS immunostaining (with either c-20 or Nm antibodies) was either severely reduced or absent in the base of many pyramidal neurons (Fig. 5D–I). These results indicated that, in the Syrian hamster, AnkG accumulation at the AIS and therefore AIS integrity is disrupted after exposure to ischemia/hypoxia conditions in normothermia. This contrasts with the preservation of the AnkG expression at the AIS during the ischemia/hypoxia conditions associated with the torpor phase of hibernation.

Discussion

In the present study, the main findings are threefold: First, we showed that the use of goat c-20 antibodies —originally raised against a synthetic peptide corresponding to the human Golgi reassembly stacking protein— is an excellent tool to label the AIS of rodent neurons. This allowed the measurement of AIS length in Syrian hamsters during the hibernation cycle in combination with the simultaneous detection of phosphorylated tau with monoclonal AT8 antibodies raised in mouse. Second, the length of the AIS significantly increases in the somatosensory cortex and CA1 field of the hippocampus in torpor animals compared to controls. Third, the AIS of layer V of torpid animals were longer in neurons that expressed phospho-tau than in those not labeled with AT8 antibodies, suggesting that AIS plastic changes were more marked in phospho-tau accumulating neurons.

Our results indicate that, while in humans c-20 antibodies label the neuronal GA, in rodents they label the AIS — most likely by recognizing the 480kD isoform of Ankyrin G. This protein is a specific scaffolding protein that, together with spectrin βIV, has a pivotal role in the maintenance of the structure and function of the AIS, as it is responsible for the tethering of different types of ion voltage-gated channels to the axonal cytoskeleton (Rasband 2010; Leterrier 2016; Jenkins et al. 2015), with such channels determining the biophysical properties of the AIS, including action potential generation. The use of c-20 antibodies allowed us to measure the AIS length in Syrian hamsters during the hibernation cycle in combination with the simultaneous detection of phosphorylated tau with monoclonal AT8 antibodies raised in mouse. This is of particular interest given the scarcity of suitable or specifically designed reagents to label the AIS in Syrian hamsters.

AIS plasticity during hibernation

The main results of the present study demonstrate —through the use of double immunofluorescence as well as 3D reconstruction and measurement techniques— that the length of the AIS of neurons in layers II–III and V and in the CA1 region of the hippocampus changes during the hibernation cycle of the Syrian hamster. AIS length during torpor was 19.48% longer than in euthermic hamsters in layer II (4.30 µm), 13.20% longer in layer V neurons (3.62 µm) and 19.42% longer in CA1 (6.17 µm). Since this AIS increase in length during torpor was not paralleled by a distal shift in the AIS starting point position, it is likely related to the distal shift of the AIS endpoint, a boundary established between axonal territories expressing AnkG and AnkB (Galiano et al. 2012). Although the overexpression of AnkG was shown to lead to an increase in AIS length (Galiano et al. 2012), the molecular mechanisms leading to AIS lengthening during torpor remain to be explored.

Various studies have demonstrated that the AIS is an efficient site to regulate neuronal activity as it has been shown to be subjected to plastic changes in response to neural activity, which may play a role in the homeostasis of neuronal circuits and adaptive responses of the nervous system (Grubb and Burrone 2010; Kuba et al. 2010; Grundemann and Hausser 2010). Among the variety of AIS plasticity phenomena reported to date, it was shown in the chicken auditory system that the loss of neuronal activity induced by the disruption of presynaptic sensory inputs leads to an increase in AIS length in brainstem auditory nuclei (Kuba et al. 2010; Yamada and Kuba 2016). Visual information deprivation during the critical period of plasticity of visual cortical neurons prevents the shortening of the AIS and maintains a longer immature AIS (Gutzmann et al. 2014). During the torpor phase of hibernation, a virtual cessation of neuronal activity in cortical and midbrain areas has been reported (Strumwasser 1959b, c, a; Igelmund 1995; Igelmund and Heinemann 1995; South 1972; Walker et al. 1977). Therefore, we hypothesized that AIS lengthening observed in the present study might be a consequence of this cessation of neuronal activity during torpor. Changes in neuronal activity have been reported to differentially affect the AIS of different neuronal populations. For example, neuronal depolarization induces AIS shortening in dentate granule cells (Evans et al. 2015) and an AIS distal shift in hippocampal CA1 pyramidal neurons (Wefelmeyer et al. 2015). Therefore, it is conceivable that cessation or a significant decrease in neuronal activity might also differentially affect the AIS of various neuronal populations. As we have quantitatively examined neurons only in the somatosensory cortex and CA1 region of the hippocampus, further quantitative studies should be performed in other brain regions to ascertain whether AIS lengthening during torpor is a general brain process or a region-specific phenomenon,

which is more or less accentuated in different regions or even in different neuronal populations.

Although the AIS distal lengthening concomitant to the onset of the torpor state is relatively small (13–19%), this change might exert pronounced effects on neuronal excitability, especially considering that the action potential trigger zone is located in the distal part of the AIS (Baranauskas et al. 2013; Kole et al. 2007). In the chicken auditory system, AIS lengthening induced by input deprivation leads to an increase in AIS Nav channel clusters concomitant to a lowering in the neuronal threshold for excitability (Kuba et al. 2010). Although the biological outcome of AIS lengthening during torpor and the direct effects that it might impose on neuronal excitability and action potential characteristics require further study, they are likely related to the widening of action potentials reported in previous studies during the torpor phase of hibernation (Krilowicz et al. 1989), characterized by a general decrease in brain electrical activity (Mihailovic 1972; Strumwasser 1959c; South et al. 1968). In addition, AIS lengthening during torpor may have indirect consequences for pyramidal neuron excitability by changing the spatial relationship between AIS and its axoaxonic GABAergic inputs by Chandelier cells (Muir and Kittler 2014; Wefelmeyer et al. 2015). All these possible consequences of AIS changes during torpor may be relevant to promote arousal events, or the seasonal exit from the torpor phase, in which hibernators return to a 'normal' situation in a short period of time. Therefore, the results obtained in the present study propose hibernators as a natural model to study AIS adaptive plasticity mechanisms in non-pathological conditions and the compensatory changes in neuronal excitability in response to changes in neuronal activity.

AIS plasticity and tau phosphorylation during the torpor phase of hibernation

According to previous studies (Arendt et al. 2003; Hartig et al. 2005; Hartig et al. 2007; Stieler et al. 2011; Leon-Espinosa et al. 2013; Anton-Fernandez et al. 2015; Avila et al. 2004), during the torpor state of hibernation, the microtubule-associated protein tau is phosphorylated and accumulates in the somatodendritic compartment of layer V pyramidal neurons. We analyzed whether neurons with hyperphosphorylated tau —that therefore have microtubule alterations, which tau hyperphosphorylation itself might induce— undergo morphological alterations in the AIS during torpor. We found that the AIS length of AT8-ir neurons in cortical layer V from torpor hamsters was significantly longer than the AIS length of AT8-negative neurons. One possible explanation for these results is that AIS plastic changes during torpor are more marked in neurons with an accumulation of hyperphosphorylated tau. The presence

of phosphorylated tau in the somatodendritic domain has been shown to decrease neuronal activity (Thies and Mandelkow 2007; Hoover et al. 2010). Therefore, this activity reduction would be more pronounced in AT8-ir than in AT8-negative neurons during torpor, which would conceivably induce a more marked AIS lengthening in AT8-ir neurons. Alternatively, AIS plasticity mechanisms may affect AT8-ir and AT8-negative neurons equally. It is known that layer V pyramidal neurons are physiologically and anatomically heterogeneous and include different subtypes on the basis of morphological and electrophysiological characteristics, or on the basis of the expression of different combinations of neuronal markers and gene expression patterns (Angulo et al. 2003; Tsiola et al. 2003; Molnar and Cheung 2006; Sorensen et al. 2013). The identity of the layer V pyramidal neurons which accumulate phospho-tau during torpor remains unknown and, therefore, given that a wide range of AIS morphological properties among cortical neuronal populations has been reported (Hofflin et al. 2017), the possibility of them representing a neuronal subpopulation with particularly long AISs during euthermia in addition to torpor cannot be ruled out. These are both interesting possibilities that should be evaluated in future studies.

Despite the similarities of the somatodendritic accumulation of hyperphosphorylated tau between hibernating mammals at torpor and neurons in the initial phases of AD, there are clear differences that might be related to AIS integrity preservation. It has been reported that the AIS diffusion barrier, that maintains the differential distribution of the various isoforms of tau to specific neuronal domains, is disrupted in AD models in which tau is hyperphosphorylated and missorted from the axon into the somatodendritic domain (Li et al. 2011). In vitro studies have shown that tau phosphorylation or the knock down of AnkG disrupts the AIS diffusion barrier inducing the missorting of tau (Zempel et al. 2017). By contrast, regarding AT8-ir neurons from hamsters in torpor, in which AIS general integrity is maintained (as judged by the preservation of AnkG immunostaining), AT8 immunostaining was restricted to the somatodendritic domain and was never found in axons, including the AIS (present data). This suggests that tau phosphorylation is not the only requirement for the disruption of the AIS diffusion barrier. Tau phosphorylation is a consequence of the balance between the activity of a variety of kinases and phosphatases, some of which are restricted to the somatodendritic or axonal neuronal domains (Bertrand et al. 2010). Therefore, in addition to the differences between the human and Syrian hamster tau sequence that could affect tau phosphorylation (Leon-Espinosa et al. 2013), the present data suggest that, unlike with AD, somatodendritic phospho-tau accumulation in neurons from torpid hamsters could be related to somatodendritic kinase activation and/or phosphatase inactivation, rather than to an AIS

barrier disruption. However, further research is needed to distinguish between these intriguing possibilities.

AIS neuroprotection during the torpor phase of hibernation

Mammalian hibernation includes general adaptive responses to extreme environments. The torpor phase of hibernation is accompanied by a depression in the immune system, a reduced metabolism, a decrease in body temperature and a reduction in cardiac output and blood flow, which would result in brain ischemia under normal conditions (Drew et al. 2001; Zhou et al. 2001; Bouma et al. 2010a; Frerichs et al. 1994). Previous studies showed that neuroprotective adaptive changes that may prevent neuronal damage during torpor include changes in microglial cells and structural changes in neurons such as the fragmentation and reduction of the Golgi apparatus, changes in synaptic connectivity and the retraction of dendritic spines (Popov and Bocharova 1992; Popov et al. 2007; von der Ohe et al. 2006; Anton-Fernandez et al. 2015; Bouma et al. 2010a; Bouma et al. 2010b; Cogut et al. 2017; von der Ohe et al. 2007; Leon-Espinosa et al. 2017). The present study adds the AIS to the list of neuronal structures that might benefit from neuroprotective mechanisms during hibernation.

Previous studies have shown that different cerebral ischemic insults in non-hibernating mammals including humans resulted in tissue damage leading to AIS disassembly (Schafer et al. 2009; Hinman et al. 2013; Coban et al. 2017; Del Puerto et al. 2015). It was shown that ischemia after a middle cerebral artery occlusion model of stroke leads to alterations in the AIS cytoskeleton including calcium-dependent calpain-mediated proteolysis of the AIS essential proteins AnkG and spectrin βIV (Schafer et al. 2009). Similarly, it has recently been shown that oxidative stress drives a calcium-dependent calpain-mediated loss of AIS protein clustering *in vitro* related to inflammatory mediated pathological insults that alter AIS stability, such as Multiple Sclerosis and lipopolysaccharide peripheral injections (Benusa et al. 2017; Clark et al. 2017; Clark et al. 2016). In line with these studies, the present study shows that the AIS of cortical neurons of Syrian hamsters during euthermia is targeted for disruption as it lacks AnkG in the cortical ischemic region after middle cerebral artery occlusion. However, AIS AnkG expression is not disrupted during torpor and AIS general integrity is maintained, despite the reduction of blood flow characteristic of this phase of hibernation.

It is known that the torpor phase is associated with and confers tolerance to hypoxia and aglycemia (Frerichs et al. 1998), as antioxidant defense systems increase allowing a higher

tolerance to cerebral damage in comparison to non-hibernating animals (Buzadzic et al. 1990; Drew et al. 2001; Zhou et al. 2001; Buzadzic et al. 1997; Vucetic et al. 2013; Ross and Drew 2006; Yin et al. 2016; Dave et al. 2012; Osborne and Hashimoto 2006; Carey et al. 2003; Drew et al. 2007). The lack of AnkG disruption during torpor suggests that neuroprotective mechanisms that are yet to be resolved participate in the attenuation of oxidative stress-driven calpain-mediated loss of AIS protein that accounts for the maintenance of AIS general integrity during the hibernation cycle. Since the torpor phase of hibernation is accompanied by hypothermia, it is also tempting to speculate that some of these mechanisms could also contribute to neuroprotection against ischemic insults of therapeutic hypothermia, in which the lowering of the metabolic rate is concomitant with a reduction in the formation of reactive oxygen species (Karibe et al. 1994; Katz et al. 2004; Yenari and Han 2012; Yenari and Hemmen 2010; Dietrich and Bramlett 2010; Piironen et al. 2014; Wu et al. 2017). The confirmation of this hypothesis awaits further research for which hibernating animals represent a viable model to study potential therapeutic mechanisms that would confer tolerance to ischemia during hibernation and preclude AIS degeneration after severe brain damage, including ischemic stroke.

Acknowledgments

This work was supported by grants from the following entities: SAF 2015-66603-P from the Ministerio de Economía y Competitividad; Centro de Investigación en Red sobre Enfermedades Neurodegenerativas (CIBERNED, CB06/05/0066, Spain); and a grant from the Alzheimer's Association (ZEN-15-321663). We thank Soledad Martínez for technical help with the surgical procedures in the middle cerebral artery occlusion experiments and María Albillos and Andrea González for their technical help.

Compliance with Ethical Standards

The authors declare that the research was conducted in the absence of any commercial or financial relationships that should be construed as a potential conflict of interest.

All experimental procedures were carried out at the animal facility in the San Pablo CEU University of Madrid (SVA-CEU.USP, registration number ES 28022 0000015) and were approved by the institutional Animal Experiment Ethics Committee.

References

Angulo MC, Staiger JF, Rossier J, Audinat E (2003) Distinct local circuits between neocortical pyramidal cells and fast-spiking interneurons in young adult rats. J Neurophysiol 89 (2):943-953. doi:10.1152/jn.00750.2002

Anton-Fernandez A, Aparicio-Torres G, Tapia S, DeFelipe J, Munoz A (2017a) Morphometric alterations of Golgi apparatus in Alzheimer's disease are related to tau hyperphosphorylation. Neurobiol Dis 97 (Pt A):11-23. doi:S0969-9961(16)30245-5 [pii]
10.1016/j.nbd.2016.10.005

Anton-Fernandez A, Leon-Espinosa G, DeFelipe J, Munoz A (2015) Changes in the Golgi Apparatus of Neocortical and Hippocampal Neurons in the Hibernating Hamster. Front Neuroanat 9:157. doi:10.3389/fnana.2015.00157

Anton-Fernandez A, Merchan-Rubira J, Avila J, Hernandez F, DeFelipe J, Munoz A (2017b) Phospho-Tau Accumulation and Structural Alterations of the Golgi Apparatus of Cortical Pyramidal Neurons in the P301S Tauopathy Mouse Model. J Alzheimers Dis 60 (2):651-661. doi:JAD170332 [pii]
10.3233/JAD-170332

Arellano JI, Munoz A, Ballesteros-Yanez I, Sola RG, DeFelipe J (2004) Histopathology and reorganization of chandelier cells in the human epileptic sclerotic hippocampus. Brain 127 (Pt 1):45-64. doi:10.1093/brain/awh004
awh004 [pii]

Arendt T, Stieler J, Strijkstra AM, Hut RA, Rudiger J, Van der Zee EA, Harkany T, Holzer M, Hartig W (2003) Reversible paired helical filament-like phosphorylation of tau is an adaptive process associated with neuronal plasticity in hibernating animals. J Neurosci 23 (18):6972-6981. doi:23/18/6972 [pii]

Avila J, Lucas JJ, Perez M, Hernandez F (2004) Role of tau protein in both physiological and pathological conditions. Physiol Rev 84 (2):361-384. doi:10.1152/physrev.00024.2003
84/2/361 [pii]

Baalman KL, Cotton RJ, Rasband SN, Rasband MN (2013) Blast wave exposure impairs memory and decreases axon initial segment length. J Neurotrauma 30 (9):741-751. doi:10.1089/neu.2012.2478

Baranauskas G, David Y, Fleidervish IA (2013) Spatial mismatch between the Na+ flux and spike initiation in axon initial segment. Proc Natl Acad Sci U S A 110 (10):4051-4056. doi:1215125110 [pii]
10.1073/pnas.1215125110

Benusa SD, George NM, Sword BA, DeVries GH, Dupree JL (2017) Acute neuroinflammation induces AIS structural plasticity in a NOX2-dependent manner. J Neuroinflammation 14 (1):116. doi:10.1186/s12974-017-0889-3
10.1186/s12974-017-0889-3 [pii]

Bertrand J, Senechal P, Zummo-Soucy M, Plouffe V, Leclerc N (2010) The formation of tau pathological phospho-epitopes in the axon is prevented by the dephosphorylation of selective sites in primary hippocampal neurons over-expressing human tau. J Neurochem 114 (5):1353-1367. doi:JNC6855 [pii]
10.1111/j.1471-4159.2010.06855.x

Binder LI, Frankfurter A, Rebhun LI (1985) The distribution of tau in the mammalian central nervous system. J Cell Biol 101 (4):1371-1378

Bouma HR, Carey HV, Kroese FG (2010a) Hibernation: the immune system at rest? J Leukoc Biol 88 (4):619-624. doi:jlb.0310174 [pii]
10.1189/jlb.0310174

Bouma HR, Strijkstra AM, Boerema AS, Deelman LE, Epema AH, Hut RA, Kroese FG, Henning RH (2010b) Blood cell dynamics during hibernation in the European Ground Squirrel. Vet Immunol Immunopathol 136 (3-4):319-323. doi:S0165-2427(10)00088-7 [pii]
10.1016/j.vetimm.2010.03.016

Buffington SA, Rasband MN (2011) The axon initial segment in nervous system disease and injury. Eur J Neurosci 34 (10):1609-1619. doi:10.1111/j.1460-9568.2011.07875.x

Bullmann T, Seeger G, Stieler J, Hanics J, Reimann K, Kretzschmann TP, Hilbrich I, Holzer M, Alpar A, Arendt T (2016) Tau phosphorylation-associated spine regression does not impair hippocampal-dependent memory in hibernating golden hamsters. Hippocampus 26 (3):301-318. doi:10.1002/hipo.22522

Buzadzic B, Blagojevic D, Korac B, Saicic ZS, Spasic MB, Petrovic VM (1997) Seasonal variation in the antioxidant defense system of the brain of the ground squirrel (Citellus citellus) and response to low temperature compared with rat. Comp Biochem Physiol C Pharmacol Toxicol Endocrinol 117 (2):141-149

Buzadzic B, Spasic M, Saicic ZS, Radojicic R, Petrovic VM, Halliwell B (1990) Antioxidant defenses in the ground squirrel Citellus citellus. 2. The effect of hibernation. Free Radic Biol Med 9 (5):407-413

Carey HV, Rhoads CA, Aw TY (2003) Hibernation induces glutathione redox imbalance in ground squirrel intestine. J Comp Physiol B 173 (4):269-276. doi:10.1007/s00360-003-0330-3

Clark K, Sword BA, Dupree JL (2017) Oxidative Stress Induces Disruption of the Axon Initial Segment. ASN Neuro 9 (6):1759091417745426. doi:10.1177/1759091417745426

Clark KC, Josephson A, Benusa SD, Hartley RK, Baer M, Thummala S, Joslyn M, Sword BA, Elford H, Oh U, Dilsizoglu-Senol A, Lubetzki C, Davenne M, DeVries GH, Dupree JL (2016) Compromised axon initial segment integrity in EAE is preceded by microglial reactivity and contact. Glia 64 (7):1190-1209. doi:10.1002/glia.22991

Coban H, Tung S, Yoo B, Vinters HV, Hinman JD (2017) Molecular Disorganization of Axons Adjacent to Human Cortical Microinfarcts. Front Neurol 8:405. doi:10.3389/fneur.2017.00405

Cogut V, Bruintjes JJ, Eggen BJL, van der Zee EA, Henning RH (2017) Brain inflammatory cytokines and microglia morphology changes throughout hibernation phases in Syrian hamster. Brain Behav Immun. doi:S0889-1591(17)30465-8 [pii]
10.1016/j.bbi.2017.10.009

Cristobo I, Larriba MJ, de los Rios V, Garcia F, Munoz A, Casal JI (2011) Proteomic analysis of 1alpha,25-dihydroxyvitamin D3 action on human colon cancer cells reveals a link to splicing regulation. J Proteomics 75 (2):384-397. doi:S1874-3919(11)00390-3 [pii]
10.1016/j.jprot.2011.08.003

Dave KR, Christian SL, Perez-Pinzon MA, Drew KL (2012) Neuroprotection: lessons from hibernators. Comp Biochem Physiol B Biochem Mol Biol 162 (1-3):1-9. doi:S1096-4959(12)00024-3 [pii]
10.1016/j.cbpb.2012.01.008

Del Puerto A, Fronzaroli-Molinieres L, Perez-Alvarez MJ, Giraud P, Carlier E, Wandosell F, Debanne D, Garrido JJ (2015) ATP-P2X7 Receptor Modulates Axon Initial Segment Composition and Function in Physiological Conditions and Brain Injury. Cereb Cortex 25 (8):2282-2294. doi:bhu035 [pii]
10.1093/cercor/bhu035

Dietrich WD, Bramlett HM (2010) The evidence for hypothermia as a neuroprotectant in traumatic brain injury. Neurotherapeutics 7 (1):43-50. doi:S1933-7213(09)00216-5 [pii]
10.1016/j.nurt.2009.10.015

Drew KL, Buck CL, Barnes BM, Christian SL, Rasley BT, Harris MB (2007) Central nervous system regulation of mammalian hibernation: implications for metabolic suppression and ischemia tolerance. J Neurochem 102 (6):1713-1726. doi:JNC4675 [pii]

10.1111/j.1471-4159.2007.04675.x
Drew KL, Rice ME, Kuhn TB, Smith MA (2001) Neuroprotective adaptations in hibernation: therapeutic implications for ischemia-reperfusion, traumatic brain injury and neurodegenerative diseases. Free Radic Biol Med 31 (5):563-573. doi:S0891584901006281 [pii]
Evans MD, Dumitrescu AS, Kruijssen DL, Taylor SE, Grubb MS (2015) Rapid Modulation of Axon Initial Segment Length Influences Repetitive Spike Firing. Cell Rep 13 (6):1233-1245. doi:S2211-1247(15)01108-0 [pii]
10.1016/j.celrep.2015.09.066
Frerichs KU, Kennedy C, Sokoloff L, Hallenbeck JM (1994) Local cerebral blood flow during hibernation, a model of natural tolerance to "cerebral ischemia". J Cereb Blood Flow Metab 14 (2):193-205. doi:10.1038/jcbfm.1994.26
Frerichs KU, Smith CB, Brenner M, DeGracia DJ, Krause GS, Marrone L, Dever TE, Hallenbeck JM (1998) Suppression of protein synthesis in brain during hibernation involves inhibition of protein initiation and elongation. Proc Natl Acad Sci U S A 95 (24):14511-14516
Galiano MR, Jha S, Ho TS, Zhang C, Ogawa Y, Chang KJ, Stankewich MC, Mohler PJ, Rasband MN (2012) A distal axonal cytoskeleton forms an intra-axonal boundary that controls axon initial segment assembly. Cell 149 (5):1125-1139. doi:S0092-8674(12)00473-4 [pii]
10.1016/j.cell.2012.03.039
Geiser F (2004) Metabolic rate and body temperature reduction during hibernation and daily torpor. Annu Rev Physiol 66:239-274. doi:10.1146/annurev.physiol.66.032102.115105
Geiser F (2013) Hibernation. Curr Biol 23 (5):R188-193. doi:S0960-9822(13)00131-0 [pii]
10.1016/j.cub.2013.01.062
Grubb MS, Burrone J (2010) Activity-dependent relocation of the axon initial segment fine-tunes neuronal excitability. Nature 465 (7301):1070-1074. doi:nature09160 [pii]
10.1038/nature09160
Grundemann J, Hausser M (2010) Neuroscience: A plastic axonal hotspot. Nature 465 (7301):1022-1023. doi:4651022a [pii]
10.1038/4651022a
Gutzmann A, Ergul N, Grossmann R, Schultz C, Wahle P, Engelhardt M (2014) A period of structural plasticity at the axon initial segment in developing visual cortex. Front Neuroanat 8:11. doi:10.3389/fnana.2014.00011
Hamada MS, Kole MH (2015) Myelin loss and axonal ion channel adaptations associated with gray matter neuronal hyperexcitability. J Neurosci 35 (18):7272-7286. doi:35/18/7272 [pii]
10.1523/JNEUROSCI.4747-14.2015
Hartig W, Oklejewicz M, Strijkstra AM, Boerema AS, Stieler J, Arendt T (2005) Phosphorylation of the tau protein sequence 199-205 in the hippocampal CA3 region of Syrian hamsters in adulthood and during aging. Brain Res 1056 (1):100-104. doi:S0006-8993(05)01060-7 [pii]
10.1016/j.brainres.2005.07.017
Hartig W, Stieler J, Boerema AS, Wolf J, Schmidt U, Weissfuss J, Bullmann T, Strijkstra AM, Arendt T (2007) Hibernation model of tau phosphorylation in hamsters: selective vulnerability of cholinergic basal forebrain neurons - implications for Alzheimer's disease. Eur J Neurosci 25 (1):69-80. doi:EJN5250 [pii]
10.1111/j.1460-9568.2006.05250.x
Harty RC, Kim TH, Thomas EA, Cardamone L, Jones NC, Petrou S, Wimmer VC (2013) Axon initial segment structural plasticity in animal models of genetic and acquired epilepsy. Epilepsy Res 105 (3):272-279. doi:S0920-1211(13)00089-2 [pii]
10.1016/j.eplepsyres.2013.03.004

Hedstrom KL, Ogawa Y, Rasband MN (2008) AnkyrinG is required for maintenance of the axon initial segment and neuronal polarity. J Cell Biol 183 (4):635-640. doi:jcb.200806112 [pii]
10.1083/jcb.200806112
Hinman JD, Rasband MN, Carmichael ST (2013) Remodeling of the axon initial segment after focal cortical and white matter stroke. Stroke 44 (1):182-189. doi:STROKEAHA.112.668749 [pii]
10.1161/STROKEAHA.112.668749
Hofflin F, Jack A, Riedel C, Mack-Bucher J, Roos J, Corcelli C, Schultz C, Wahle P, Engelhardt M (2017) Heterogeneity of the Axon Initial Segment in Interneurons and Pyramidal Cells of Rodent Visual Cortex. Front Cell Neurosci 11:332. doi:10.3389/fncel.2017.00332
Hoover BR, Reed MN, Su J, Penrod RD, Kotilinek LA, Grant MK, Pitstick R, Carlson GA, Lanier LM, Yuan LL, Ashe KH, Liao D (2010) Tau mislocalization to dendritic spines mediates synaptic dysfunction independently of neurodegeneration. Neuron 68 (6):1067-1081. doi:S0896-6273(10)00972-4 [pii]
10.1016/j.neuron.2010.11.030
Igelmund P (1995) Modulation of synaptic transmission at low temperatures by hibernation-related changes in ionic microenvironment in hippocampal slices of golden hamsters. Cryobiology 32 (4):334-343. doi:S0011-2240(85)71034-6 [pii]
10.1006/cryo.1995.1034
Igelmund P, Heinemann U (1995) Synaptic transmission and paired-pulse behaviour of CA1 pyramidal cells in hippocampal slices from a hibernator at low temperature: importance of ionic environment. Brain Res 689 (1):9-20. doi:0006-8993(95)00524-T [pii]
Jenkins PM, Kim N, Jones SL, Tseng WC, Svitkina TM, Yin HH, Bennett V (2015) Giant ankyrin-G: a critical innovation in vertebrate evolution of fast and integrated neuronal signaling. Proc Natl Acad Sci U S A 112 (4):957-964. doi:1416544112 [pii]
10.1073/pnas.1416544112
Kaphzan H, Buffington SA, Jung JI, Rasband MN, Klann E (2011) Alterations in intrinsic membrane properties and the axon initial segment in a mouse model of Angelman syndrome. J Neurosci 31 (48):17637-17648. doi:31/48/17637 [pii]
10.1523/JNEUROSCI.4162-11.2011
Karibe H, Chen SF, Zarow GJ, Gafni J, Graham SH, Chan PH, Weinstein PR (1994) Mild intraischemic hypothermia suppresses consumption of endogenous antioxidants after temporary focal ischemia in rats. Brain Res 649 (1-2):12-18. doi:0006-8993(94)91043-X [pii]
Katz LM, Young AS, Frank JE, Wang Y, Park K (2004) Regulated hypothermia reduces brain oxidative stress after hypoxic-ischemia. Brain Res 1017 (1-2):85-91. doi:10.1016/j.brainres.2004.05.020
S0006899304007504 [pii]
Kelley LA, Mezulis S, Yates CM, Wass MN, Sternberg MJE (2015) The Phyre2 web portal for protein modeling, prediction and analysis. Nature Protocols 10:845. doi:10.1038/nprot.2015.053
Kole MH, Letzkus JJ, Stuart GJ (2007) Axon initial segment Kv1 channels control axonal action potential waveform and synaptic efficacy. Neuron 55 (4):633-647. doi:S0896-6273(07)00576-4 [pii]
10.1016/j.neuron.2007.07.031
Kordeli E, Davis J, Trapp B, Bennett V (1990) An isoform of ankyrin is localized at nodes of Ranvier in myelinated axons of central and peripheral nerves. J Cell Biol 110 (4):1341-1352

Kordeli E, Lambert S, Bennett V (1995) AnkyrinG. A new ankyrin gene with neural-specific isoforms localized at the axonal initial segment and node of Ranvier. J Biol Chem 270 (5):2352-2359

Kosik KS, Finch EA (1987) MAP2 and tau segregate into dendritic and axonal domains after the elaboration of morphologically distinct neurites: an immunocytochemical study of cultured rat cerebrum. J Neurosci 7 (10):3142-3153

Krilowicz BL, Edgar DM, Heller HC (1989) Action potential duration increases as body temperature decreases during hibernation. Brain Res 498 (1):73-80. doi:0006-8993(89)90400-9 [pii]

Kuba H, Oichi Y, Ohmori H (2010) Presynaptic activity regulates Na(+) channel distribution at the axon initial segment. Nature 465 (7301):1075-1078. doi:nature09087 [pii]

10.1038/nature09087

Leon-Espinosa G, DeFelipe J, Munoz A (2012) Effects of amyloid-beta plaque proximity on the axon initial segment of pyramidal cells. J Alzheimers Dis 29 (4):841-852. doi:J73624871X1R134N [pii]

10.3233/JAD-2012-112036

Leon-Espinosa G, Garcia E, Garcia-Escudero V, Hernandez F, Defelipe J, Avila J (2013) Changes in tau phosphorylation in hibernating rodents. J Neurosci Res 91 (7):954-962. doi:10.1002/jnr.23220

Leon-Espinosa G, Garcia E, Gomez-Pinedo U, Hernandez F, DeFelipe J, Avila J (2016) Decreased adult neurogenesis in hibernating Syrian hamster. Neuroscience 333:181-192. doi:S0306-4522(16)30321-9 [pii]

10.1016/j.neuroscience.2016.07.016

Leon-Espinosa G, Regalado-Reyes M, DeFelipe J, Munoz A (2017) Changes in neocortical and hippocampal microglial cells during hibernation. Brain Struct Funct. doi:10.1007/s00429-017-1596-7

10.1007/s00429-017-1596-7 [pii]

Leterrier C (2016) The Axon Initial Segment, 50Years Later: A Nexus for Neuronal Organization and Function. Curr Top Membr 77:185-233. doi:S1063-5823(15)00069-1 [pii]

10.1016/bs.ctm.2015.10.005

Li X, Kumar Y, Zempel H, Mandelkow EM, Biernat J, Mandelkow E (2011) Novel diffusion barrier for axonal retention of Tau in neurons and its failure in neurodegeneration. EMBO J 30 (23):4825-4837. doi:emboj2011376 [pii]

10.1038/emboj.2011.376

Mandell JW, Banker GA (1996) A spatial gradient of tau protein phosphorylation in nascent axons. J Neurosci 16 (18):5727-5740

Marin MA, Ziburkus J, Jankowsky J, Rasband MN (2016) Amyloid-beta plaques disrupt axon initial segments. Exp Neurol 281:93-98. doi:S0014-4886(16)30098-X [pii]

10.1016/j.expneurol.2016.04.018

Migheli A, Butler M, Brown K, Shelanski ML (1988) Light and electron microscope localization of the microtubule-associated tau protein in rat brain. J Neurosci 8 (6):1846-1851

Mihailovic LJT (1972) Cortical and subcortical electrical activity in hibernation and hypothermia. In: South FE, Hannon JP, J.R. W, E.T. P, N.R. A (eds) Hibernation and Hypothermia, Perspectives and Challenges. Elsevier, Amsterdam, pp 487-534

Molnar Z, Cheung AF (2006) Towards the classification of subpopulations of layer V pyramidal projection neurons. Neurosci Res 55 (2):105-115. doi:S0168-0102(06)00044-7 [pii]

10.1016/j.neures.2006.02.008

Muir J, Kittler JT (2014) Plasticity of GABAA receptor diffusion dynamics at the axon initial segment. Front Cell Neurosci 8:151. doi:10.3389/fncel.2014.00151

Osborne PG, Hashimoto M (2006) Brain antioxidant levels in hamsters during hibernation, arousal and cenothermia. Behav Brain Res 168 (2):208-214. doi:S0166-4328(05)00475-4 [pii]

10.1016/j.bbr.2005.11.007
Piela L, Nemethy G, Scheraga HA (1987) Proline-induced constraints in alpha-helices. Biopolymers 26 (9):1587-1600. doi:10.1002/bip.360260910
Piironen K, Tiainen M, Mustanoja S, Kaukonen KM, Meretoja A, Tatlisumak T, Kaste M (2014) Mild hypothermia after intravenous thrombolysis in patients with acute stroke: a randomized controlled trial. Stroke 45 (2):486-491. doi:STROKEAHA.113.003180 [pii]
10.1161/STROKEAHA.113.003180
Popov VI, Bocharova LS (1992) Hibernation-induced structural changes in synaptic contacts between mossy fibres and hippocampal pyramidal neurons. Neuroscience 48 (1):53-62. doi:0306-4522(92)90337-2 [pii]
Popov VI, Bocharova LS (1992b) Hibernation-induced structural changes in synaptic contacts between mossy fibres and hippocampal pyramidal neurons. Neuroscience 48 (1):53-62. doi:0306-4522(92)90337-2 [pii]
Popov VI, Bocharova LS, Bragin AG (1992a) Repeated changes of dendritic morphology in the hippocampus of ground squirrels in the course of hibernation. Neuroscience 48 (1):45-51. doi:0306-4522(92)90336-Z [pii]
Popov VI, Kraev IV, Ignat'ev DA, Stewart MG (2011) Suspension of mitotic activity in dentate gyrus of the hibernating ground squirrel. Neural Plast 2011:867525. doi:10.1155/2011/867525
Popov VI, Medvedev NI, Patrushev IV, Ignat'ev DA, Morenkov ED, Stewart MG (2007) Reversible reduction in dendritic spines in CA1 of rat and ground squirrel subjected to hypothermia-normothermia in vivo: A three-dimensional electron microscope study. Neuroscience 149 (3):549-560. doi:S0306-4522(07)00906-2 [pii]
10.1016/j.neuroscience.2007.07.059
Rasband MN (2010) The axon initial segment and the maintenance of neuronal polarity. Nat Rev Neurosci 11 (8):552-562. doi:nrn2852 [pii]
10.1038/nrn2852
Ross AP, Drew KL (2006) Potential for discovery of neuroprotective factors in serum and tissue from hibernating species. Mini Rev Med Chem 6 (8):875-884
Ruf T, Geiser F (2015) Daily torpor and hibernation in birds and mammals. Biol Rev Camb Philos Soc 90 (3):891-926. doi:10.1111/brv.12137
Schafer DP, Jha S, Liu F, Akella T, McCullough LD, Rasband MN (2009) Disruption of the axon initial segment cytoskeleton is a new mechanism for neuronal injury. J Neurosci 29 (42):13242-13254. doi:29/42/13242 [pii]
10.1523/JNEUROSCI.3376-09.2009
Sorensen SA, Bernard A, Menon V, Royall JJ, Glattfelder KJ, Hirokawa K, Mortrud M, Miller JA, Zeng H, Hohmann JG, Jones AR, Lein ES (2013) Correlated Gene Expression and Target Specificity Demonstrate Excitatory Projection Neuron Diversity. Cereb Cortex. doi:bht243 [pii]
10.1093/cercor/bht243
South FE (1972) Hibernation and hypothermia, perspectives and challenges. Symposium held at Snow-mass-at-Aspen, Colorado, January 3-8, 1971. Elsevier Pub. Co., Amsterdam, New York,
South FE, J.E. B, H.D. D, A.D. E (1968) Sleep, hibernation, and hypothermia in the yellow-bellied marmot (M.flaviventris). In: Musacchia XJ, J.F.Saunders (eds) Depressed Metabolism. Elsevier, New york, pp 277-312
Srinivasan Y, Elmer L, Davis J, Bennett V, Angelides K (1988) Ankyrin and spectrin associate with voltage-dependent sodium channels in brain. Nature 333 (6169):177-180. doi:10.1038/333177a0
Srinivasan Y, Lewallen M, Angelides KJ (1992) Mapping the binding site on ankyrin for the voltage-dependent sodium channel from brain. J Biol Chem 267 (11):7483-7489

Stieler JT, Bullmann T, Kohl F, Toien O, Bruckner MK, Hartig W, Barnes BM, Arendt T (2011) The physiological link between metabolic rate depression and tau phosphorylation in mammalian hibernation. PLoS One 6 (1):e14530. doi:10.1371/journal.pone.0014530

Stoler O, Fleidervish IA (2016) Functional implications of axon initial segment cytoskeletal disruption in stroke. Acta Pharmacol Sin 37 (1):75-81. doi:aps2015107 [pii]

10.1038/aps.2015.107

Strumwasser F (1959a) Factors in the pattern, timing and predictability of hibernation in the squirrel, Citellus beecheyi. Am J Physiol 196 (1):8-14

Strumwasser F (1959b) Regulatory mechanisms, brain activity and behavior during deep hibernation in the squirrel, Citellus beecheyi. Am J Physiol 196 (1):23-30

Strumwasser F (1959c) Thermoregulatory, brain and behavioral mechanisms during entrance into hibernation in the squirrel, Citellus beecheyi. Am J Physiol 196 (1):15-22

Su B, Wang X, Drew KL, Perry G, Smith MA, Zhu X (2008) Physiological regulation of tau phosphorylation during hibernation. J Neurochem 105 (6):2098-2108. doi:JNC5294 [pii]

10.1111/j.1471-4159.2008.05294.x

Thies E, Mandelkow EM (2007) Missorting of tau in neurons causes degeneration of synapses that can be rescued by the kinase MARK2/Par-1. J Neurosci 27 (11):2896-2907. doi:27/11/2896 [pii]

10.1523/JNEUROSCI.4674-06.2007

Tsiola A, Hamzei-Sichani F, Peterlin Z, Yuste R (2003) Quantitative morphologic classification of layer 5 neurons from mouse primary visual cortex. J Comp Neurol 461 (4):415-428. doi:10.1002/cne.10628

Turrigiano GG, Nelson SB (2000) Hebb and homeostasis in neuronal plasticity. Curr Opin Neurobiol 10 (3):358-364. doi:S0959-4388(00)00091-X [pii]

Turrigiano GG, Nelson SB (2004) Homeostatic plasticity in the developing nervous system. Nat Rev Neurosci 5 (2):97-107. doi:10.1038/nrn1327

nrn1327 [pii]

von der Ohe CG, Darian-Smith C, Garner CC, Heller HC (2006) Ubiquitous and temperature-dependent neural plasticity in hibernators. J Neurosci 26 (41):10590-10598. doi:26/41/10590 [pii]

10.1523/JNEUROSCI.2874-06.2006

von der Ohe CG, Garner CC, Darian-Smith C, Heller HC (2007) Synaptic protein dynamics in hibernation. J Neurosci 27 (1):84-92. doi:27/1/84 [pii]

10.1523/JNEUROSCI.4385-06.2007

Vucetic M, Stancic A, Otasevic V, Jankovic A, Korac A, Markelic M, Velickovic K, Golic I, Buzadzic B, Storey KB, Korac B (2013) The impact of cold acclimation and hibernation on antioxidant defenses in the ground squirrel (Spermophilus citellus): an update. Free Radic Biol Med 65:916-924. doi:S0891-5849(13)00591-1 [pii]

10.1016/j.freeradbiomed.2013.08.188

Walker JM, Glotzbach SF, Berger RJ, Heller HC (1977) Sleep and hibernation in ground squirrels (Citellus spp): electrophysiological observations. Am J Physiol 233 (5):R213-221

Wefelmeyer W, Cattaert D, Burrone J (2015) Activity-dependent mismatch between axo-axonic synapses and the axon initial segment controls neuronal output. Proc Natl Acad Sci U S A 112 (31):9757-9762. doi:1502902112 [pii]

10.1073/pnas.1502902112

Wu D, Shi J, Elmadhoun O, Duan Y, An H, Zhang J, He X, Meng R, Liu X, Ji X, Ding Y (2017) Dihydrocapsaicin (DHC) enhances the hypothermia-induced neuroprotection following ischemic stroke via PI3K/Akt regulation in rat. Brain Res 1671:18-25. doi:S0006-8993(17)30277-9 [pii]

10.1016/j.brainres.2017.06.029

Yamada R, Kuba H (2016) Structural and Functional Plasticity at the Axon Initial Segment. Front Cell Neurosci 10:250. doi:10.3389/fncel.2016.00250

Yenari MA, Han HS (2012) Neuroprotective mechanisms of hypothermia in brain ischaemia. Nat Rev Neurosci 13 (4):267-278. doi:nrn3174 [pii]
10.1038/nrn3174

Yenari MA, Hemmen TM (2010) Therapeutic hypothermia for brain ischemia: where have we come and where do we go? Stroke 41 (10 Suppl):S72-74. doi:41/10_suppl_1/S72 [pii]
10.1161/STROKEAHA.110.595371

Yin Q, Ge H, Liao CC, Liu D, Zhang S, Pan YH (2016) Antioxidant Defenses in the Brains of Bats during Hibernation. PLoS One 11 (3):e0152135. doi:10.1371/journal.pone.0152135
PONE-D-15-48216 [pii]

Yun RH, Anderson A, Hermans J (1991) Proline in alpha-helix: stability and conformation studied by dynamics simulation. Proteins 10 (3):219-228. doi:10.1002/prot.340100306

Zempel H, Dennissen FJA, Kumar Y, Luedtke J, Biernat J, Mandelkow EM, Mandelkow E (2017) Axodendritic sorting and pathological missorting of Tau are isoform-specific and determined by axon initial segment architecture. J Biol Chem 292 (29):12192-12207. doi:M117.784702 [pii]
10.1074/jbc.M117.784702

Zhou F, Zhu X, Castellani RJ, Stimmelmayr R, Perry G, Smith MA, Drew KL (2001) Hibernation, a model of neuroprotection. Am J Pathol 158 (6):2145-2151. doi:S0002-9440(10)64686-X [pii]
10.1016/S0002-9440(10)64686-X

Figure legends

Figure 1. AIS immunostaining using c-20 antibodies. A–C: images taken from the human temporal neocortex (A) and the somatosensory cortex of hamster (B) and mouse (C), to illustrate the patterns of DAB immunostaining using c-20 antibodies raised against the GA protein GRASP65. Note that c-20 antibodies intensely stain the GA of pyramidal neurons in human tissue (arrows in A), whereas in rodents (B and C) they intensely stained eyelash-like processes oriented perpendicularly to the pial surface (arrow heads), which are typical of the AIS of neurons. Triple immunostaining with c-20 antibodies and antibodies directed to AnKG and the neuronal marker NeuN from hamsters (D–F) allowed verification that these c-20-ir processes were indeed AIS in both hamsters and mice (not shown). Scale bar (in F): 15 µm in A–C; 13 µm in D–F. G shows the sequence of human Grasp65 protein. Red highlights the region (350–400 positions) that, according to the manufacturer company, included the immunizing peptide used to raise c-20 antibodies. Mass spectrometry analysis of the blocking peptide provided by the company revealed that EFEVSFLDSPGA (squared) was the peptide sequence most frequently detected by the spectrometer (17 PSM) and therefore the most likely used to raise c-20 antibodies. H: Blast and clustalW analysis showing the homology between the putative immunogen peptide sequence with positions 3133 to 3144 of the 480-kDa isoform of AnkirinG sequence. I: Interspecies comparison of GRASP65 sequence targeted by c-20 antibodies. Note the presence of a proline in position 374 in rodents, instead of leucine that is present in humans. Note in this region, according to Phyre2 software simulation, the presence of a probable alpha helix in the secondary structure of human Grasp65 that is absent in rodents.

Figure 2. A–C: Trios of confocal stack Z projection photomicrographs taken from a section from the somatosensory cortex of a euthermic Syrian hamster double immunostained with c-20 (green) antibodies and commercial antibodies (Nm) to AnkG (red). C shows the extensive colocalization of both immunostainings at the AIS of pyramidal neurons (some indicated by arrows), in addition to the immunostaining of the GA with c-20 antibodies (arrowheads). D and E show examples of the measurement (Imaris software, measurement point tool) of the length of the same AISs on the basis of immunostaining with c-20 or Nm antibodies. Scale bar (in E): 20 µm. F: Box-and-whisker graphs showing that both immunostainings yielded virtually the same AIS length (n=29).

Figure 3. Changes in AIS length between control and torpid hamsters. A–F: Z projection photomicrographs taken from confocal stacks showing c-20-ir AISs in layer II–III (A, D), layer V (B, E) of the somatosensory cortex and the stratum pyramidale from the CA1 hippocampal region (C, F) from control (A–C) and torpid (D–F) hamsters. Scale (in F): 22.5 µm in A–F. G–I: Box-and-whisker graphs showing the increase in the length of the AIS from layer II–III (G), layer V (H) or CA1 (I) pyramidal cells from hamsters at torpor as compared to euthermic (control) animals. Wilcoxon, *$p \leq 0.05$.

Figure 4. Analysis of Tau phosphorylation effect on the AIS plasticity. A–C: Trio of confocal stack Z projection photomicrographs taken from a section from layer V of the somatosensory cortex of a Syrian hamster at torpor, double immunostained with c-20 (green) and AT8 (red) antibodies to label the AIS and the neurons with hyperphosphorylated tau, respectively. Arrows point to the AISs from AT8-ir neurons (asterisks), whereas arrowheads point to the AIS from AT8- neurons. Scale bar (in C): 10 µm. D shows that AIS length is longer in AT8+ (28.54 ± 2.292 µm) than in AT8- (27.47 ± 2.163 µm) neurons. Wilcoxon, *$p \leq 0.05$.

Figure 5. AIS alterations after focal ischemia. A: photomicrograph from a coronal brain section immunostained for iba-1 from a Syrian hamster subjected to a focal ischemia by the occlusion of the frontal branch of the middle cerebral artery showing (squared zones) the increase in the intensity of iba-1 immunostaining of the infarct zone as compared to the contralateral neocortex, respectively shown at higher magnification in B and C. D–G: Images from sections triple immunostained for NeuN/iba-1/AnkG (Nm) (D–E) or NeuN/iba-1/AnkG (c-20) (F–G) showing (in green) the alterations of AIS AnkG immunostaining with Nm (D) or c-20 (F) antibodies in the infarct zone, as compared to the normal AIS immunostaining in the contralateral neocortex (E, G). Insets show images from the same microscopic fields with merged immunostainings for iba-1 (red) and Neu-N (white) to reveal the presence of cell bodies from microglial and neuronal cells, respectively. Scale (in G): 980 µm in A, 440 µm in B–C and 11.5 µm in D–G.

Figure 1

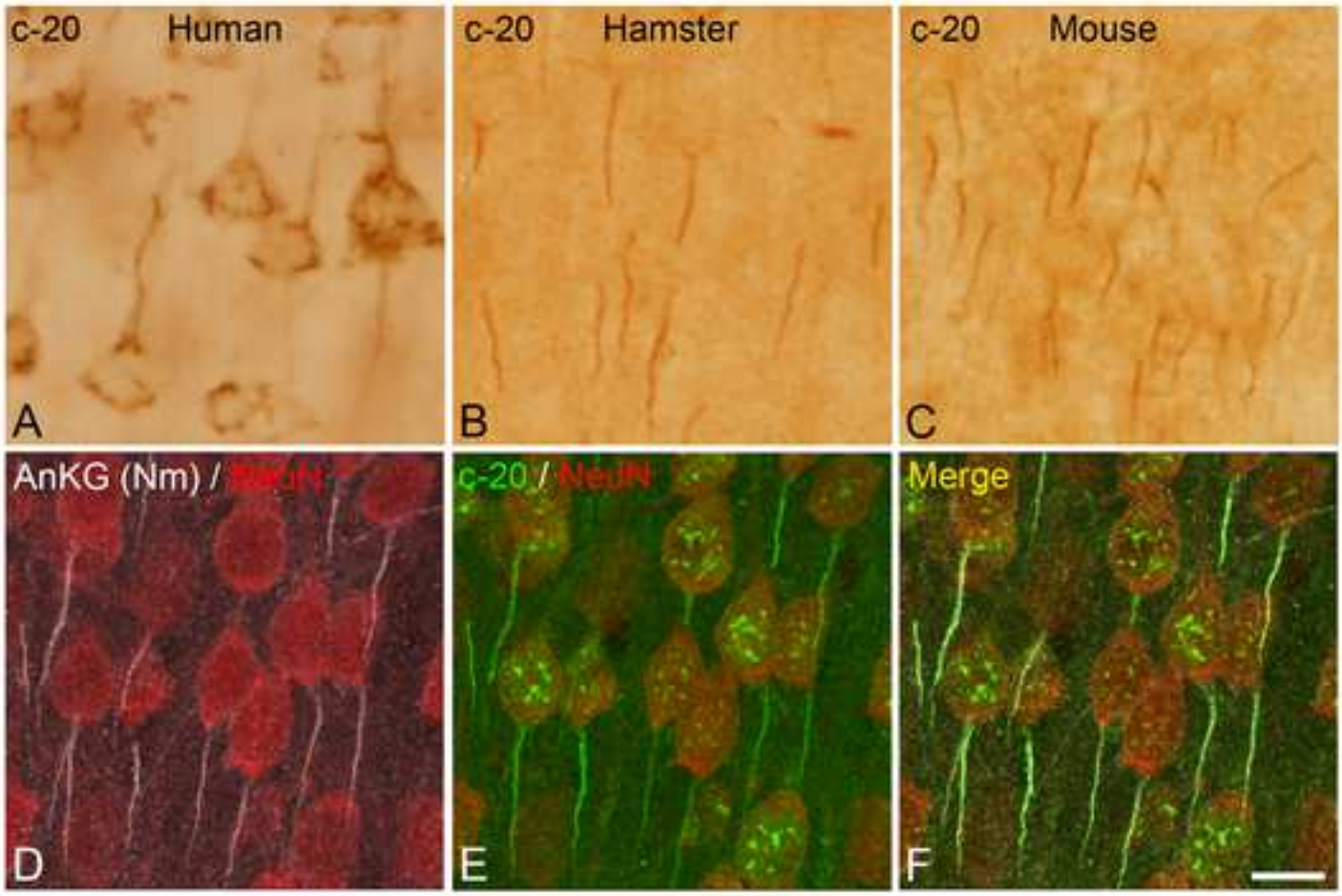

G

Golgi reassembly stacking protein 1, 65kDa [Homo sapiens]
GeneBank: AAH75854.1

```
1   mglgvsaeqp aggaegfhll gvqenspaqq aglepyfdfi itighsrlnk endtlkallk
61  anvekpvkle vfnmktmrvr evevvpsnmw ggqgllgasv rfcsfrrase qvwhvldvep
121 sspaalaglr pytdyvvgsd qilqesedff tlieshegkp lklmvynsks dscrevtvtp
181 naawggegsl gcgigygylh riptqppsyh kkppgtppps alplgapppd alppgptped
241 spsletgsrq sdymeallqa pgssmedplp gpgspshsap dpdglphfme tplqppppvq
301 rvmdpgfldv sgislldnsn asvwpslpss teltttavst sgpedicsss ssherggeat
361 wsgsefevsf ldspgaqaqa dhlpqltlpd sltsaasped glsaelleaq aeeepasteg
421 ldtgteaegl dsqaqistte
```

H

Comparison between human GRASP65 sequence targeted by c-20 antibodies and Ank G sequence

```
EFEVSFLDSPGA
lEQVSFLDSSGK
***** *
```

I

Interspecies comparison of GRASP65 sequence targeted by c-20 antibodies

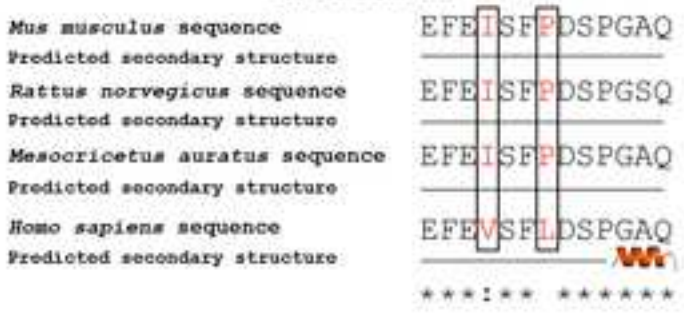

Figure 2

Click here to download Figure FIgure 2.tif

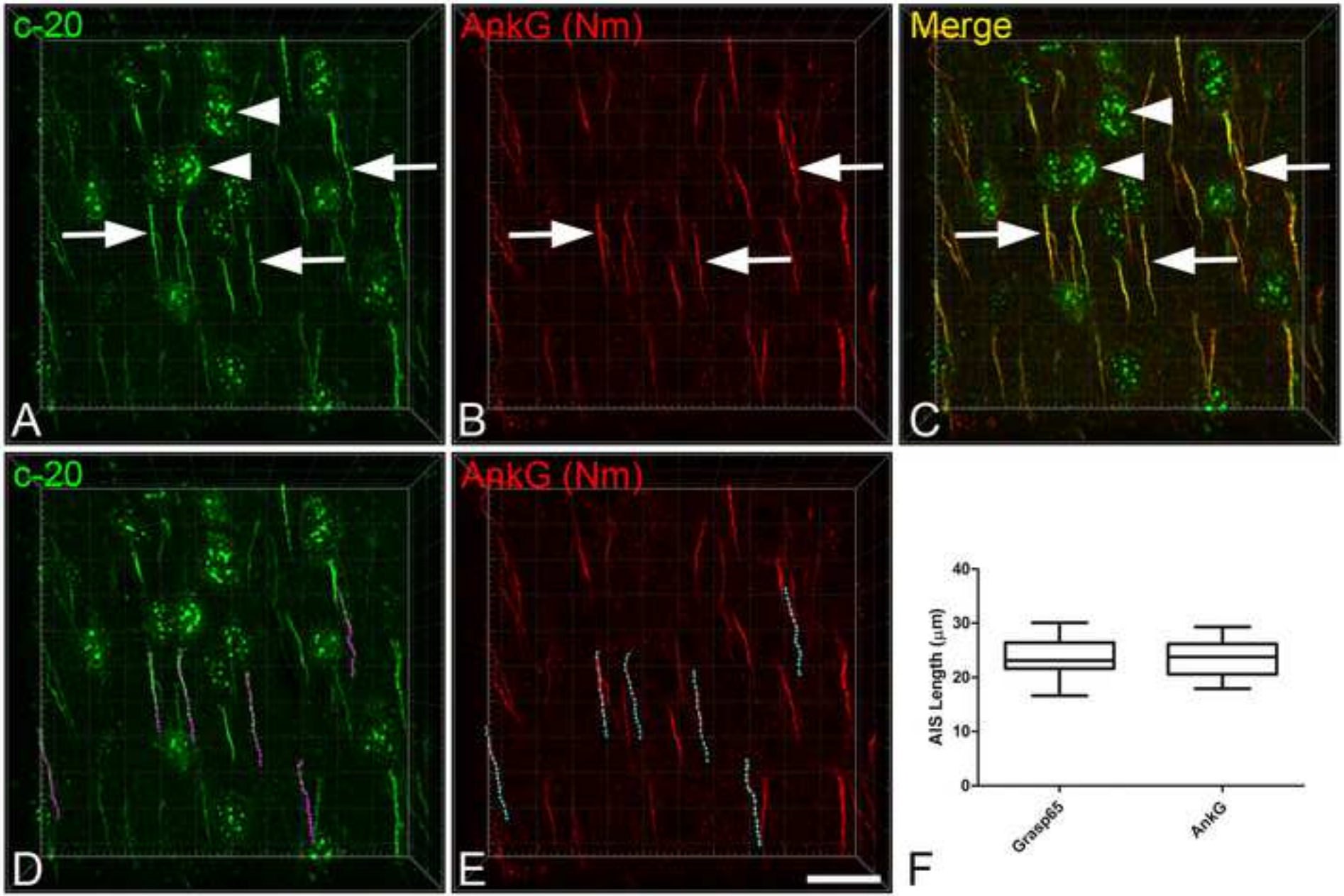

Figure 3

Click here to download Figure Figure 3.tif

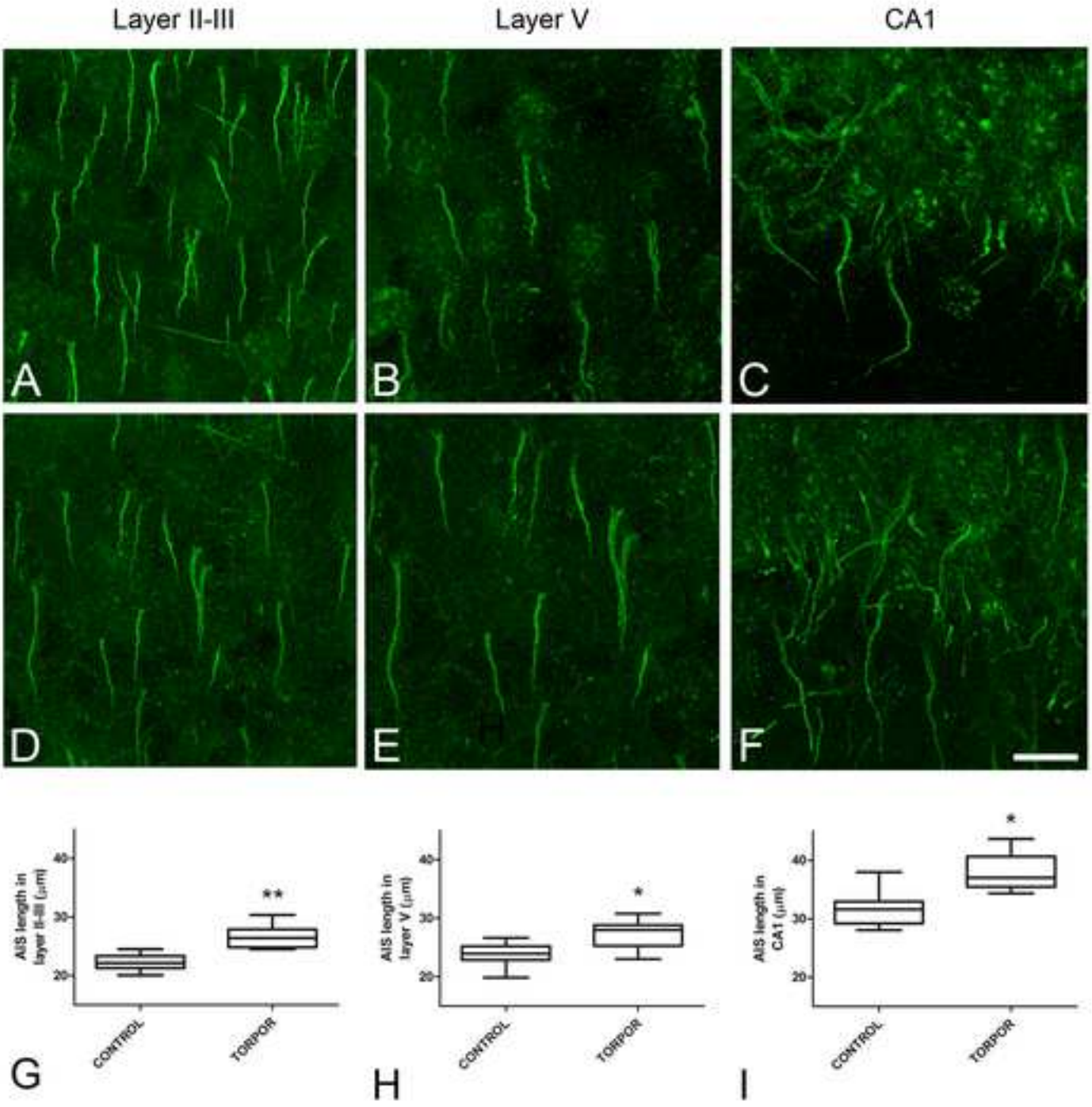

Figure 4

Click here to download Figure Figure 4.tif

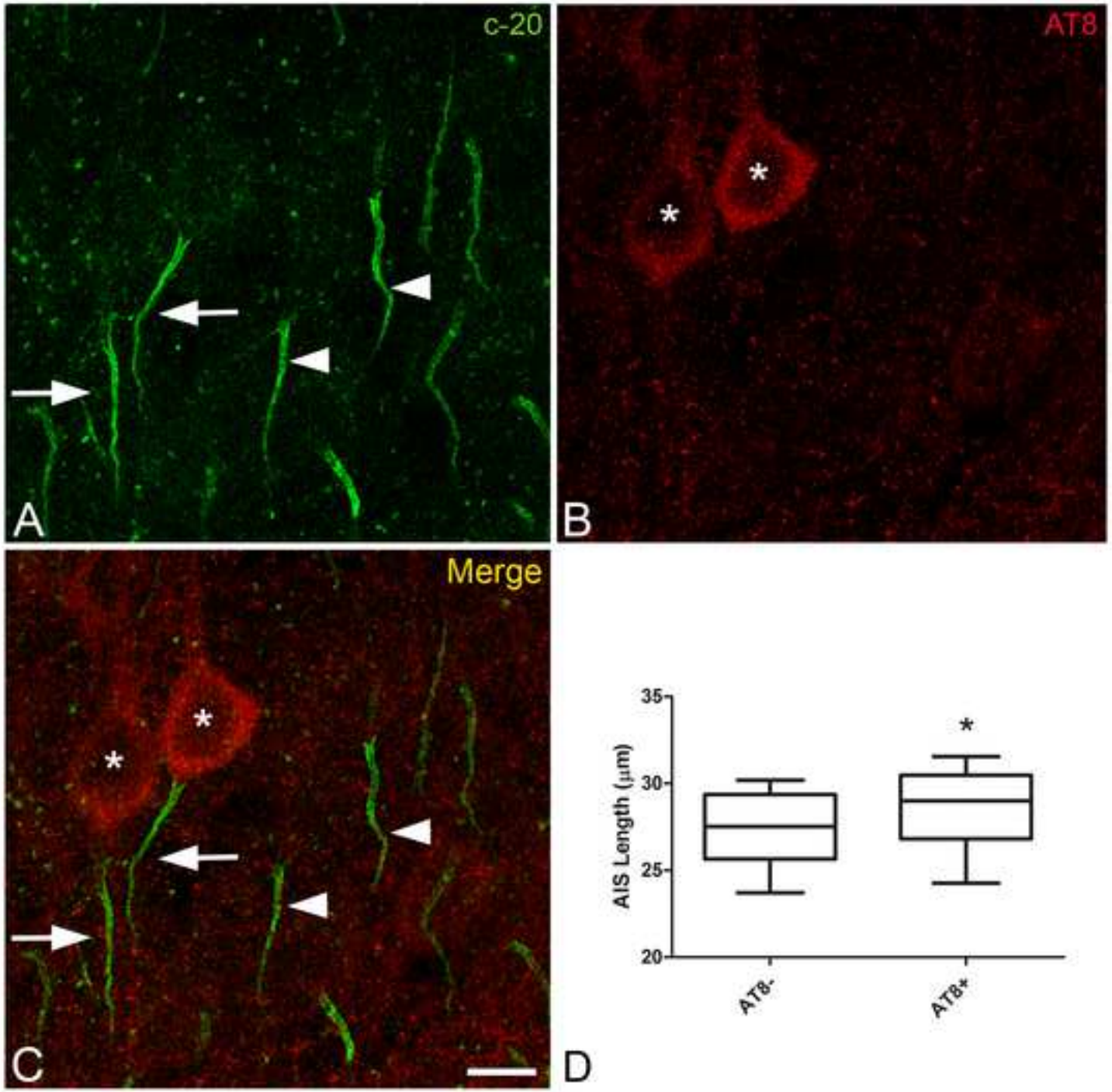

Figure 5

Click here to download Figure Figure 5.tif

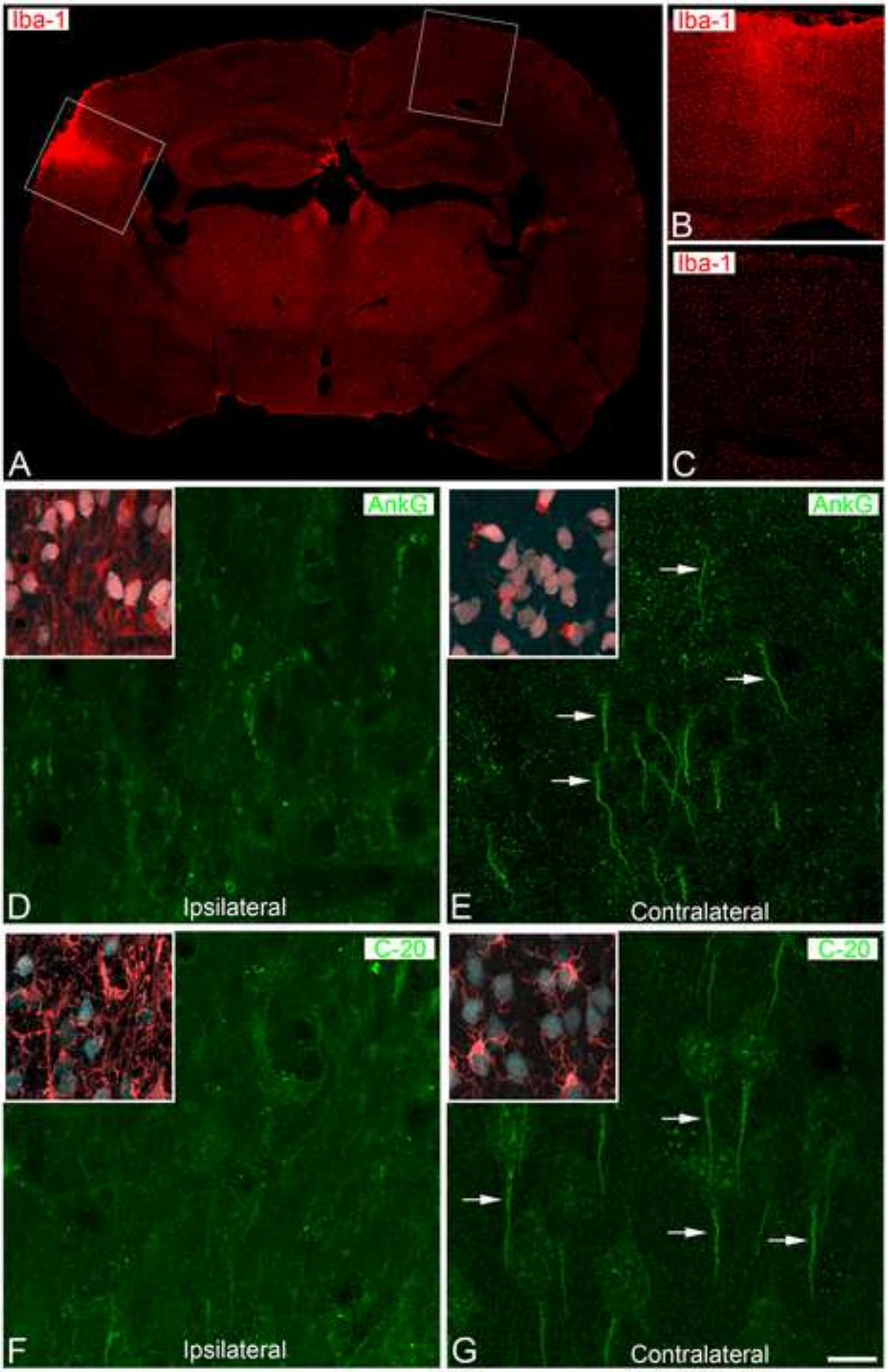

En Madrid, a 4 de Abril del 2018